Technische Universität München
Max-Planck-Institut für Quantenoptik

Quantum Simulation of Topological States of Matter

Leonardo Mazza

Vollständiger Abdruck der von der Fakultät für Physik
der Technischen Universität München
zur Erlangung des akademischen Grades eines

Doktors der Naturwissenschaften (Dr. rer. nat.)

genehmigten Dissertation.

Vorsitzende : Univ.-Prof. Dr. rer. nat. K. Krischer

Prüfer der Dissertation : 1. Hon.-Prof. J. I. Cirac, Ph.D.
2. Univ.-Prof. Dr. rer. nat. W. Zwerger

Die Dissertation wurde am 13.06.2012 bei der
Technischen Universität München eingereicht und
durch die Fakultät für Physik am 18.07.2012 angenommen.

Contents

Abstract

This thesis is a contribution to the research field of quantum simulations of topological phases of matter, i.e. quantum states characterized by a non-local order parameter. The aim of the research on quantum simulations is to overcome the difficulties encountered in the study of quantum mechanical models with conventional numerical methods. The proposed way to accomplish this task is the direct exploitation of controllable quantum systems whose properties, for instance low-energy physics, mimic those of the model to be studied. We study several problems connected to the objective of creating a quantum simulator of topological phases of matter. In particular, we discuss how to engineer the Hamiltonian of topological models, how to measure quantities which unravel topological orders, and how to quantify the reliability of topological quantum memories.

The first direction of investigation considered in this thesis regards the development of new techniques to simulate topological states of matter with cold atoms in optical lattices. We propose a scheme based on an unconventional use of a bi-chromatic optical lattice to engineer the Hamiltonians of several topological insulators and of the related non-interacting relativistic models. We also focus on the Pfaffian wavefunction, a topological state supporting non-Abelian quasi-excitations arising in the presence of three-body interactions. We present a proposal for the realization with optical lattices of systems characterized by such interactions and discuss the possibility of using such a scheme to create a topological state, such as the mentioned wavefunction.

The second line of research considered in this thesis concerns the detection of a string operator in optical lattices. We report on an experiment, to which we provided theoretical support, aimed at the measurement of the non-local order parameter of a one-dimensional Mott insulator; we support the discussion with the relevant theoretical background. Although the Mott insulator is not a topological phase, the measurement of string observables is crucial to reveal the non-local order of several topological states, and the developed experimental protocol is expected to be relevant in future experiments.

The third contribution of this thesis is related to the use of topological phases to build a quantum computer, which is a specific example of a quantum simulator. We focus on the important problem of understanding whether it is possible to reliably store quantum information in topological states. We consider one specific class of topological quantum memories, namely those based on a fermionic topological superconductor with zero-energy Majorana modes. At the end of the storage period, we take into account the possibility of applying an operation aimed at the recovery of the information initially encoded into the system and then diminished by the time evolution. In particular, we

develop several theoretical tools that quantify the fidelity of the best recovery operation. We apply such tools to understand the effect of various experimentally relevant decoherence processes which could act on the fermionic quantum memory. We show that this class of quantum memories is extremely susceptible to the presence of an environment whose action can be described with a master equation. We also consider another decoherence process, namely the convex combination of several Hamiltonian time evolutions, and show that in this case the topological properties of the model protect the encoded information.

Zusammenfassung

Diese Doktorarbeit ist ein Beitrag zu Quantensimulationen topologischer Materiezustände, das heißt von Quantenzuständen, die durch einen nicht-lokalen Ordnungsparameter beschrieben werden. Das Ziel der Forschung über Quantensimulatoren ist es Schwierigkeiten zu überwinden, die auftreten, wenn quantenmechanische Modelle mithilfe herkömmlicher numerischer Methoden untersucht werden. Der anvisierte Weg, um diese Aufgabe zu bewerkstelligen, nutzt direkt den hohen Grad an Kontrolle einiger Quantensysteme aus, deren Eigenschaften, zum Beispiel ihr Verhalten bei niedrigen Energien, denen des zu untersuchenden Systems entsprechen. Wir betrachten einige Problemstellungen, die miteinander durch das Ziel einen Quantensimulator topologischer Materiezustände zu realisieren, verbunden sind. Insbesondere diskutieren wir wie Hamiltonoperatoren topologischer Modelle beschrieben werden können, wie Größen, die topologische Ordnung anzeigen, gemessen werden können und wie die Verlässlichkeit topologischer Quantenspeicher quantifiziert werden kann.

Die erste Forschungslinie, die in dieser Arbeit verfolgt wird, betrifft die Entwicklung neuer Methoden, um topologische Materiezustände mit Hilfe kalter Atome in optischen Gittern zu simulieren. Basierend auf einer unkonventionellen Verwendung bichromatischer optischer Gitter, schlagen wir ein Schema vor, um die Hamiltonoperatoren einiger topologischer Isolatoren und mit ihnen verwandte nicht-wechselwirkende relativistische Modelle zu simulieren. Ein weiterer Fokus liegt auf der Pfaffschen Wellenfunktion, einem topologischen Zustand, der nicht-Abelsche Quasi-Anregungen, die sich bei Anwesenheit von Drei-Körper-Wechselwirkungen ausbilden, beschreibt. Wir stellen einen Vorschlag zur Realisierung von Systemen, die durch derartige Wechselwirkungen beschrieben werden, mithilfe optischer Gitter, vor. Darüber hinaus diskutieren wir die Möglichkeit dieses Schema zur Präparation topologischer Zustände, zum Beispiel der oben erwähnten Wellenfunktion, zu benutzen.

Die zweite Richtung unserer Untersuchungen geht um den Nachweis eines String-Operators in optischen Gittern. Wir beschreiben ein Experiment, zu dem wir durch die Beschreibung der theoretischer Grundlagen und die Entwicklung theoretischer Modelle beigetragen haben. Ziel dieses Experimentes ist es den nicht-lokalen Ordnungsparameter eines ein-dimensionalen Mott-Isolators zu beschreiben. Obwohl der Mott-Isolator keine topologische Phase ist, ist die Detektion von String-Observablen essenziell, um die nichtlokale Ordnung mehrerer topologischer Zustände zu beschreiben. Dies rechtfertigt die Erwartung, dass das hier entwickelte Protokoll relevant in zukünftigen Experimenten sein wird.

Im dritten Teil dieser Arbeit geht es um die Verwendung topologischer Phasen, um einen Quantencomputer zu konstruieren, der ein spezifisches Beispiel eines Quantensimulators darstellt. Im Besonderen untersuchen wir das wich-

tige Problem, zu verstehen, ob es möglich ist Quanteninformation verlässlich in topologischen Zuständen zu speichern. Wir betrachten eine spezifische Klasse topologischer Quantenspeicher, nämlich Zustände, die auf einem fermionischen Supraleiter mit null-Energie Majorana-Moden basieren. Die Möglichkeit am Ende der Speicherperiode eine Operation anzuwenden, die die ursprünglich im System codierte Information wiederherstellt, wird betrachtet. Im Speziellen entwickeln wir mehrere theoretische Methoden, die die Fidelität der besten Operation zur Wiederherstellung der Information quantifizieren. Wir verwenden diese Methoden, um die Wirkung unterschiedlicher experimentell relevanter Dekohärenz-Prozesse, die auf den fermionischen Quantenspeicher wirken können, zu verstehen. Wir zeigen, dass diese Klasse Quantenspeicher sehr anfällig auf die Anwesenheit einer Umgebung, deren Wirkung durch eine Master-Gleichung beschrieben wird, reagiert. Darüber hinaus untersuchen wir eine andere Art von Dekohärenz-Prozess, genauer gesagt eine konvexe Kombination mehrerer Hamiltonscher Zeitentwicklungen. In diesem Fall zeigen wir, dass die topologischen Eigenschaften des Modells die codierte Information schützen.

Publications Related to this Thesis

1. L. Mazza, M. Rizzi, M. Lewestein and J. I. Cirac
   Emerging bosons with three-body interactions from spin-1 atoms in optical lattices
   Phys. Rev. A **82** (2010), 043629.
   See chapter 4

2. A. Bermudez, L. Mazza, M. Rizzi, N. Goldman, M. Lewenstein, M. A. Martin-Delgado
   Wilson fermions and axion electrodynamics in optical lattices
   Phys. Rev. Lett. **105** (2010), 190404.
   See chapters 2 and 3

3. M. Endres, M. Cheneau, T. Fukuhara, C. Weitenberg, P. Schauß, C. Gross, L. Mazza, M. C. Bañuls, L. Pollet, I. Bloch, S. Kuhr
   Observation of correlated particle-hole pairs and string order in low-dimensional Mott insulators
   Science **334** (2011), 200.
   See chapter 5

4. L. Mazza, A. Bermudez, N. Goldman, M. Rizzi, M. A. Martin-Delgado, M. Lewenstein
   An optical-lattice-based quantum simulator for relativistic field theories and topological insulators
   New J. Phys. **14** (2012), 015007.
   See chapters 2 and 3

5. L. Mazza, M. Rizzi, M. Lukin, J. I. Cirac
   On the stability of a quantum memory encoded with Majorana fermions subject to external perturbations
   in preparation, (2012)
   See chapters 6 and 7

Introduction

Quantunque il simular sia le più volte
ripreso, e dia di mala mente indici,
si trova pur in molte cose e molte
aver fatti evidenti benefici, [1]

Ludovico Ariosto, *Orlando Furioso*, IV 1-4

Quantum mechanics is the theory which describes the behaviour of atoms, electrons and all constituents of matter on atomic length scales. Unfortunately, the theoretical study of quantum mechanical systems whose number of elementary components scales as the Avogadro number is almost always challenging. Indeed, several many-body models, originating both from very abstract problems and from attempts to understand experimental observations, are still to be solved. One of the most severe obstacles to obtain a full understanding of their properties is the fact that the required computational resources scale exponentially with the size of the system, so that only small ones have been studied exactly. Several attempts have been made to circumvent this issue. Algorithms which do not treat the problem exactly have been proposed and efficiently applied to solve selected models. To name the most important ones, let us cite quantum Monte Carlo (QMC) methods [CA80], the density matrix renormalization group (DMRG) technique [Sch11], the algorithms based on matrix product states (MPS) [PGVWC07] and on projected entangled pair states (PEPS) [VC04]. All these methods have been designed to work on conventional computers, and in what follows we refer to them as *classical simulations*.

A *quantum simulator* is an alternative solving tool which has been proposed in 1982 by R. P. Feynman [Fey82] and is currently at the focus of a broad area of research. The key idea is to engineer a technological instrument which actively exploits quantum mechanics to solve quantum mechanical problems. Researchers have been since interested in understanding the computational power of such an approach. In 1996, a milestone theorem was demonstrated: it was shown by S. Lloyd that the complicated many-body dynamics of a local Hamiltonian can be efficiently simulated inducing on a controllable quantum system a reduced number of elementary time-evolutions to be engineered from outside [Llo96]. This *digital* quantum simulator is said to be *universal* because

[1] *Though an ill mind appear in simulation,/ And, for the most, such quality offends;/ 'Tis plain that this in many a situation/ Is found to further beneficial ends,* - Translation by *William S. Rose* (1823-1831); source *Wikipedia*.

once reprogrammed it can simulate every local Hamiltonian and it is indeed equivalent to a quantum computer [NC04].

The difficulty of building such a device leads to the formulation of a less demanding but still ambitious concept, namely that of *analog* quantum simulations [BN09, HCT$^+$11]. The idea here is to construct purpose-built setups, able to simulate only a restricted range of models. The quantum simulator simply emulates the system of interest, in the same fashion as fermionic atoms in a lattice structure emulate electrons in a crystal: the Hamiltonian to be simulated is mapped into the Hamiltonian of the simulator.

Not every genuine quantum system is a good candidate for a quantum simulator. Even if no generally accepted criteria have been formulated, some scientists are trying to identify the relevant properties that a system should fulfill [HCT$^+$11, CZ12]. We list here some of them:

1. the *microscopic theoretical knowledge* of such a system must be satisfactory, in order to be able to understand the simulation with an *ab-initio* approach.

2. Since we are interested in going beyond single-particle physics, which is relatively well understood with present computers, the simulator must contain *many elementary constituents* (fermions or bosons, both if possible) and must be scalable.

3. From a general point of view, a simulation requires the *manipulation of the system*, which must thus be extremely controllable. In general, it must be possible to engineer couplings between the different components of the system.

4. It is also desirable to be able to *initialize* the system in a range of different initial states and to change the parameters of the setup in real time.

5. Finally, the desired information is to be obtained via a *measurement* of the system, which must be carried out with high fidelity.

Some of the most studied experimental candidates are: cold atoms in optical lattices, trapped ions, photons, superconducting circuits, and arrays of quantum dots [BN09]. In this thesis we concentrate only on cold atoms in *optical lattices*, which are especially suited for analog simulations[2].

In general, quantum simulators have not yet managed to provide some significant information that is not obtainable with analytical approaches or classical simulations. On the one hand, the need for quantifying the accuracy of a quantum simulation is forcing each research community to benchmark the developed setups with classical simulations. On the other one, the experimental control of large many-body quantum systems is still challenging. However, the pace at which the recent progresses have been obtained motivates the expectation that important milestone experiments will be carried out in the next future.

This thesis is a contribution to the research field of quantum simulations of topological phases of matter, i.e. quantum states which cannot be fully characterized by local order parameters. In this case, the paradigm introduced

[2] A general discussion of cold gases oriented towards the topic of quantum simulations is given in references [JZ05, LSA$^+$07, BDZ08, BDN12].

by Landau, which describes quantum phase transitions via the breaking of local symmetries, fails. Instead, the concept of *topological order* arises, which reflects the presence of non-local order parameters and concerns global properties of the system [Wen04]. The interplay between concepts from topology, the branch of mathematics devoted to the study of global properties preserved by continuous transformations, and quantum physics is old and well-established [Nak03a]; in this thesis, we focus on two recent developments: *topological insulators* and *anyons*.

Apart from posing a number of still open questions, topological states feature intriguing properties, whose experimental observation would be extremely interesting, even if theoretically well understood. At this point it can be useful to stress that the topic of quantum simulations closely relates to the problem of quantum Hamiltonian engineering. As the relevant scientific literature does not get involved with the subtlety of separating the two research fields, we refrain from it as well, and also include within the area of quantum simulations studies that are not strictly aimed at solving a not yet understood model.

In part I of this thesis we consider the use of cold atoms in optical lattices as analog quantum simulators. After devoting chapter 1 to a review of optical lattices, we consider the problem of engineering the Hamiltonians of topological models in such systems. We begin chapter 2 with a review of the tools developed by the research community to push optical lattices beyond the bosonic and fermionic Hubbard model, which, depending on the atomic statistics, describe naturally the system, but are unfortunately non-topological. To achieve this goal, unconventional optical lattices, dressed, for instance, with additional light fields, are necessary [JZ03, GD10, AAN+11, Coo11]. The first original contribution of this thesis is the theoretical development of one such simulation scheme [MBG+12]. The setup consists of a spin-independent optical lattice that traps a collection of hyperfine states of the same alkaline atom, to which the different degrees of freedom of the field theory to be simulated are mapped. We show that dressing a bi-chromatic optical lattice (or superlattice) with Raman transitions can allow the engineering of a spin-dependent tunneling of the atoms between neighboring lattice sites.

The applications of this scheme are extensively presented in chapter 3. We argue that the mentioned assisted-hopping processes can be used for the quantum simulation of topological insulators, i.e. fermionic models which display a gapped (insulating) bulk and gapless (conducting) boundary modes [HK10, QZ11]. We devote section 3.2 to a brief review of the topic. Considerations borrowed from mathematical topology can be applied to the single-particle band-structure of these models and with their help some global properties of the system can be related to integer numbers (or to subsets of the integer numbers) [Nak03a]. Since the aforementioned topological arguments are insensitive to Hamiltonian perturbations which do not close any band gap, there exist macroscopic properties of the topological insulators which feature an extreme robustness.

We present a toolbox for the realization of different types of relativistic lattice fermions, which can then be exploited to synthesize the majority of the phases of the periodic table of topological insulators [BMR+10, MBG+12]. The exotic phenomenology makes the experimental observation of these models interesting *per se*. Moreover, some peculiar transport properties, such as spin-polarized currents [KM05], make the realization of some topological insulators extremely

attractive also from the applicative point of view. However, solid state samples hosting some of the topological phases we propose to engineer have already been produced [vK86, KBM$^+$07, HQW$^+$08]. We justify the need for an experiment based on cold atoms by proposing a use in the spirit of a quantum simulation. The measurement versatility and the possibility of directly relating such outputs to a specific theoretical model are expected to be an advantage in this respect. For example, we cite the problem of understanding the fate of topological insulators in presence of interactions, which in cold gases can be tuned with high confidence [WQZ10, RT10, FK11, TPB11, Gur11].

In chapter 4 we present a scheme aimed at the engineering of many-body Hamiltonians characterized by a three-body infinite contact repulsion; in order to do that, we exploit an optical lattice with spin-1 atoms realizing a Mott insulator with the filling of one particle per site [MRLC10]. The idea, reminiscent of the connection between spin-1/2 particles and hardcore bosons [Gia04], prescribes the local mapping of the spin degrees of freedom into the occupation numbers of emerging quantum particles interacting via three-body repulsion. As many-body interactions are at the heart of unconventional phenomena, three-body interactions are a fundamental ingredient for the realization of the so-called Pfaffian wavefunction, a topological state which is known to support anyonic quasi-excitations [MR91, GWW92].

Anyons are particle-like quasi-excitations satisfying an unconventional statistics [LM77, Wil82], i.e. neither bosonic nor fermionic; they can only exist in two dimensions [NSS$^+$08]. The experimental investigation of anyons is one of the challenges of modern physics and no unquestionable observation has been performed yet [WPW09, WPW10, MZF$^+$12]. It is therefore reasonable to raise the question of whether optical lattices can host such an interesting phenomenon. Among the several states characterized by anyonic quasi-excitations, we focus on the Pfaffian one. We first provide numerical evidence that corroborates the possibility of realizing such wavefunction, usually studied in the continuum space, in a spatially discrete structure, such as an optical lattice. Unfortunately, the Pfaffian wavefunction is not in the class of models which can be realized with the proposed spin-1 atoms scheme, and we finally elaborate on the difficulties encountered.

We then leave the problem of Hamiltonian engineering and move to the problem of measuring topological order in cold atomic gases. Because topological phases lie outside the Landau paradigm, their characterization requires to probe a non-local observable. In chapter 5, we focus on the measurement of a string operator in an optical lattice, which is a well-defined non-local order parameter of the one-dimensional Mott insulator [DTBA06, BDTGA08]. We report on an experiment, to which we provided theoretical support, in which such measurement was carried out in practice [ECF$^+$11]. Although a Mott insulator is not a topological phase, the developed experimental protocol will become of crucial importance to characterize genuine one-dimensional topological phases, such as the Haldane phase, in cold-atoms experiments [Hal83, dNR89].

In part II, we switch our attention to the use of topological phases for quantum-information purposes. Indeed, some models of anyons have been proven to support fault-tolerant universal quantum computation [Kit97]. In such a *topological quantum computer*, which is a particular instance of a digital quantum simulator, the information is processed via the creation, braiding and annihilation of the anyons. An intermediate goal which might require less con-

trol on the setup is represented by the use of these topologically ordered models only to store quantum information [DKLP02]. A complete characterization of these *topological quantum memories*, focussing on questions such as the stability against thermal effects and other forms of noise and decoherence, is extremely important, because much of the experimental and theoretical work in the field of anyons regards such applications as a long term goal and motivation. Let us indeed stress that the robustness of many properties of topological models, such as the degeneracy of the ground space, has long convinced the researchers that these were ideal systems for storing quantum information. Unfortunately, recent studies, to which our work belongs, are showing that the action of an external environment can have severe consequences on the performances of the quantum memory [AFH09, CLBT10, PKSC10, Yos11, GC11].

The concepts of topological insulators and of anyonic systems are different and not mutually exclusive. There are classes of quasi one-dimensional and two-dimensional systems, named *topological superconductors*, which have both properties [Kit01, RG00]. On the one side, they have a gapped bulk and gapless boundary modes; on the other one, such edge modes are zero-energy Majorana fermions which can be interchanged, or braided, and display non-Abelian statistics [Iva01, AOR$^+$11]. Such models are currently raising interest also because their experimental realization seems to be possible in the near future [MZF$^+$12]. In chapter 6 we review the most natural formalism for dealing with these systems, and in general with quadratic fermionic Hamiltonians, namely that of fermionic Gaussian states [BR04, Bra05].

In chapter 7, we consider these topological superconducting model and answer the question of how long quantum information can be stored reliably in such systems. The information is encoded with the zero-energy Majorana modes mentioned above. We develop the theoretical tools needed to quantify the amount of information which is spoiled by a non-Hamiltonian time evolution, describing the storage time. In particular, we consider the possibility of performing an operation after the storage period aimed at recovering the largest amount of information from the system and moreover discuss what is the maximal achievable fidelity of such operation. The complete characterization of recovery operations is one of the most original contributions of the discussion presented in chapter 7.

Equipped with these tools, we characterize several perturbations which can hinder the possibility of storing quantum information in these memories. We show in a rigorous way that the topological properties of the Hamiltonian cannot protect the information from the action of perturbations described by a large class of physically relevant master equations.

We subsequently depart from the assumptions needed to use master equations, and consider time evolutions which can even be unitary, even if we ignore the details of the Hamiltonian ruling such dynamics. In this case we find a rather intriguing phenomenology. On the one side, we show that the Hamiltonian is able to protect the information stored in the system, namely, considering larger systems improves the storage time of the memory. On the other one, the recovery operation needed to extract such information from the memory is not of the most simple class, i.e. a Gaussian operation.

In general, topological superconductors are the focus of the attention of both the solid-state community and the quantum information one. The discussion we present is mainly reminiscent of the methods used by the latter. Nonetheless, it

is abstract and as such can be applied not only to solid-state implementations, but also to alternative ones, based for example on cold atoms.

* * *

Summarizing, this thesis is organized as follows. In chapter 1 we review some selected topics about optical lattices which are used in the thesis. In chapter 2 we present the superlattice scheme proposal for an unconventional optical lattice which permits to realize hopping processes changing the internal state of the atom. Some possible applications of this quantum simulator, ranging from non-interacting relativistic theories to fermionic models, are discussed in chapter 3. In chapter 4 we introduce a method for engineering three-body interactions with optical lattices and elaborate on the possibility of realizing the topological Pfaffian wavefunction. In chapter 5 we discuss the experimental measurement of a string operator, crucial for the characterization of topological phases of matter. Chapter 6 is devoted to the review of the properties of fermionic Gaussian states. We use them in chapter 7 to characterize a quantum memory encoding the information in zero-energy Majorana modes.

Part I

Quantum Simulation of Topological States of Matter with Cold Atoms in Optical Lattices

Chapter 1

Optical Lattices

This chapter reviews some selected topics about optical lattices, chosen because of their relevance in this thesis. Consequently, it is not intended to be a comprehensive review; the interested reader is referred to references [JZ05, LSA+07, BDZ08] for a more exhaustive discussion.

1.1 Optical Potentials

Various experimental methods for trapping and storing ultracold gases have been developed in the last decades[1]. All these methods have to cope with the fact that atoms are charge neutral, and thus the Coulomb force cannot be exploited. We focus here on optical dipole traps, where atoms interact with light via their induced dipole moment and, depending on the specific light frequency, experience a force pushing them towards high or low intensity regions [GWO00].

An atom in the presence of an external oscillating electro-magnetic field is subjected to a potential $U_{\rm dip}(\mathbf{r})$ due to the interaction of the electric field $\mathbf{E}(\mathbf{r}) = \hat{\boldsymbol{\epsilon}}\tilde{E}(\mathbf{r})e^{-i\omega t} + c.c.$ (we consider here only one frequency ω) with the induced atomic dipole moment $\mathbf{p}$:

$$U_{\rm dip}(\mathbf{r}) = -\frac{1}{2}\langle \mathbf{p}\cdot\mathbf{E}(\mathbf{r})\rangle_{\rm time} = -\Re(\alpha(\omega))\, E^2(\mathbf{r}); \tag{1.1}$$

where $\alpha(\omega)$ is the dynamical atomic polarizability.

The polarizability $\alpha(\omega)$ is a complex quantity and its imaginary part describes absorption effects. Indeed, it can be associated to the absorbed power via:

$$P_{\rm abs}(\mathbf{r}) = \langle \dot{\mathbf{p}}\cdot\mathbf{E}(\mathbf{r})\rangle_{\rm time} = 2\omega\Im(\alpha(\omega))\, E^2(\mathbf{r}); \tag{1.2}$$

or, equivalently, to an absorption scattering rate:

$$\Gamma_{\rm sc}(\mathbf{r}) = \frac{2}{\hbar}\Im(\alpha)E^2(\mathbf{r}). \tag{1.3}$$

A quantum mechanical expression for the real part of $\alpha(\omega)$ of a multi-level atom in the ground state can be obtained via a perturbative treatment of the

[1] A general overview can be found in chapter 4 of [PS01] and references therein.

atom-light interaction:

$$\alpha(\omega) = \sum_{n\neq 0} |\langle n|\hat{\mathbf{d}}\cdot\hat{\boldsymbol{e}}|0\rangle|^2 \left(\frac{1}{E_n - E_0 - \hbar\omega} + \frac{1}{E_n - E_0 + \hbar\omega}\right); \tag{1.4}$$

where $\{|n\rangle, E_n\}$ are the atomic states and energies, and $\hat{\mathbf{d}}$ is the atomic dipole operator. It is reasonable to keep only the most relevant terms of the sum in equation (1.4); thus, we consider the states $\bar{n}$ such that $E_{\bar{n}} - E_0 \sim \hbar\omega$ and discard the term $\propto (E_{\bar{n}} - E_0 + \hbar\omega)^{-1}$, which is small.

The imaginary part of the polarizability, whose *ab-initio* derivation would require to take into account the infinite modes of the electromagnetic field [CTDRG98], can be effectively evaluated by substituting the real atomic energies with a complex number, whose imaginary part represents the state lifetime: $E_n \mapsto E_n - i\hbar\Gamma_n/2$. Following this procedure, we get a fully complex polarizability:

$$\alpha(\omega) = \sum_{\bar{n}} \frac{|\langle\bar{n}|\hat{\mathbf{d}}\cdot\hat{\boldsymbol{e}}|0\rangle|^2}{E_{\bar{n}} - i\hbar\Gamma_{\bar{n}}/2 - E_0 - \hbar\omega}. \tag{1.5}$$

The used approximation requires that the state $|\bar{n}\rangle$ can be regarded as a well-defined state, i.e. $\hbar\Gamma_{\bar{n}} \ll E_{\bar{n}}$, and that the light is not on-resonance, i.e. $\hbar\Gamma_{\bar{n}} \ll |E_{\bar{n}} - E_0 - \hbar\omega|$, which is a more stringent condition.

Let us use formula (1.5) to obtain an explicit expression for $U_{\rm dip}(\mathbf{r})$ and $\Gamma_{\rm sc}(\mathbf{r})$; we consider for simplicity only one relevant state $\bar{n}$. We obtain:

$$U_{\rm dip}(\mathbf{r}) \sim -\frac{1}{2}\frac{|\langle\bar{n}|\hat{\mathbf{d}}\cdot\hat{\boldsymbol{e}}|0\rangle|^2}{E_{\bar{n}} - E_0 - \hbar\omega}|\tilde{E}(\mathbf{r})|^2; \tag{1.6a}$$

$$\Gamma_{\rm sc}(\mathbf{r}) \sim -\frac{(\Gamma_{\bar{n}}/2)\,|\langle\bar{n}|\hat{\mathbf{d}}\cdot\hat{\boldsymbol{e}}|0\rangle|^2}{(E_{\bar{n}} - E_0 - \hbar\omega)^2}|\tilde{E}(\mathbf{r})|^2. \tag{1.6b}$$

These equations show the different scaling of the optical trapping, $\propto \tilde{E}^2/(E_{\bar{n}} - E_0 - \hbar\omega)$, and of the scattering rate, $\propto \tilde{E}^2/(E_{\bar{n}} - E_0 - \hbar\omega)^2$; this explains why experiments, which need a small $\Gamma_{\rm sc}$, work preferentially in the far-detuned regime, with $E_{\bar{n}} - E_0 - \hbar\omega$ as large as possible.

Moreover, the sign of $E_{\bar{n}} - E_0 - \hbar\omega$ defines the sign of $U_{\rm dip}$. In the case of *red-detuning*, $\hbar\omega < E_{\bar{n}} - E_0$, the minima of the potential coincide with the maxima of the light intensity; and viceversa for the *blue-detuning* case, $\hbar\omega > E_{\bar{n}} - E_0$.

The potential $U_{\rm dip}(\mathbf{r})$ has the same *space-dependence* of the squared electric field $\propto |\tilde{E}(\mathbf{r})|^2$. A periodic potential can be generated with two counter-propagating laser beams of wavelength λ, which create a standing wave along the propagation direction, say $\hat{z}$, with periodicity $\lambda/2$: $|\tilde{E}(\mathbf{r})|^2 \propto \sin^2(2\pi z/\lambda)$. This is the core idea at the basis of experiments with *optical lattices*; the last decade has seen a flourishing of innovations on top of this simple concept. For example, periodic potentials can be generated in one, two and three dimensions. Moreover, non-square geometries have also been created, the most prominent examples being the two-dimensional honeycomb and triangular lattices [SPSH$^+$11, TGU$^+$12]. Finally, it is also possible to realize optical superlattices, i.e. bi-chromatic optical lattices [FTC$^+$07, GDF$^+$08].

Another important experimental line of research has focussed on the development of trapping schemes which depend on the *internal atomic states*. For alkali atoms, the typical atoms employed in these experiments, the electronic

ground state splits into a number of hyperfine states originating from the interaction of the nuclear spin with the electronic spin [BJ83]. In order to have a different potential for each state, the frequency of the trapping light must be almost resonant with the first atomic excitation line, so that the internal structure of the first electronic excited state can become relevant. In this situation, specific combinations of light polarizations and carefully selected detunings can create periodic potentials which are completely out of phase for two different internal states. The explicit theoretical derivation of this fact, worked out through polarization selection rules, for alkaline and earth-alkaline-like atoms, is reviewed in references [JZ05, GD10]. Experiments have demonstrated the possibility of using this technique to realize entangling gates via controlled collisions [MGW$^+$03a, MGW$^+$03b], quantum walks [KFC$^+$09], and to do thermometry of strongly correlated phases [MD10].

Still, the vicinity of a resonance can significantly increase the probability of a scattering event, i.e. the absorption of one photon. This drawback becomes particularly severe for some atoms, e.g. potassium, for which the atomic properties do not allow for a stable implementation of the method sketched above. This motivated the work presented in chapter 2, where we show that a spin-independent, and thus potentially long-lived, optical superlattice can be used to address the different hyperfine states of the atom, like in a spin-dependent optical lattice.

1.2 Theoretical Description of Bosonic Atoms in Optical Lattices

Atoms trapped in a three-dimensional optical lattice are quantum objects subject to a potential:

$$V(\mathbf{r}) = -V_0 \sum_j \sin^2(k_0\, x_j); \quad k_0 = \frac{2\pi}{\lambda}. \tag{1.7}$$

The corresponding single-particle Schrödinger equation with periodic boundary conditions can be solved working in momentum space, see e.g. [AM76]. The spectrum displays a band structure $E_m(\mathbf{k})$, and the eigenfunctions $\psi_{m,\mathbf{k}}(\mathbf{r})$ are usually called Bloch wavefunctions (see figure 1.1).

Rather than working in this basis, it is sometimes more convenient to use another orthonormal basis, the so-called Wannier wavefunctions:

$$w_{m,\mathbf{R}}(\mathbf{r}) = \sum_{\mathbf{k}} e^{-i\mathbf{k}\cdot\mathbf{R}} \psi_{m,\mathbf{k}}(\mathbf{r}); \tag{1.8}$$

which can be chosen to be exponentially localized around the lattice site $\mathbf{R}$, as shown in figure 1.1 and reference [Koh59]. Notice that they are not anymore eigenstates of the Hamiltonian. Indeed, we introduce the notation $|m, \mathbf{R}\rangle$ for the Wannier wavefunction $w_{m,\mathbf{R}}(\mathbf{r})$ and write the single-particle Hamiltonian in this basis:

$$\hat{H} = \sum_m \sum_{\mathbf{R},\mathbf{R}'} J_m(\mathbf{R}-\mathbf{R}')|m,\mathbf{R}\rangle\langle m,\mathbf{R}'|; \tag{1.9}$$

where:

$$J_m(\mathbf{R}-\mathbf{R}') = \int d\mathbf{r}\, w^*_{m,\mathbf{R}}(\mathbf{r}) \left[-\frac{\hbar^2}{2m}\nabla^2 + V(\mathbf{r})\right] w_{m,\mathbf{R}'}(\mathbf{r}). \tag{1.10}$$

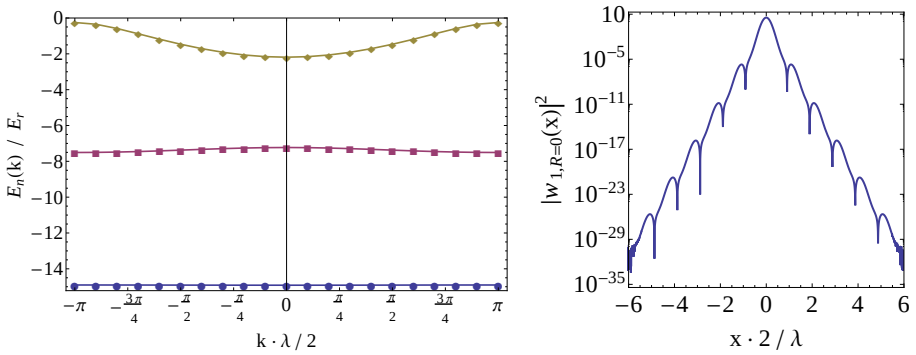

Figure 1.1: (Left) Band structure $E_m(\mathbf{k})$, $m \leq 3$, for a one-dimensional optical lattice with $V_0 = 19.0\, E_r$. Notice that the lowest band is almost flat: this reflects the fact that $J_1(\mathbf{R} - \mathbf{R}') \sim 0$ even for neighboring lattice sites. (Right) Plot of $|w_{1,\mathbf{R}=0}(x)|^2$ for an exponentially localized Wannier wavefunction of the first lattice band, $m = 1$.

The notation introduced in (1.9) is particularly useful if one is interested in the low-energy properties of the model, and thus truncates the sum over the bands to the first ones. Due to the localization of $w_{m,\mathbf{R}}(\mathbf{r})$ around $\mathbf{R}$, usually $J(\mathbf{R}-\mathbf{R}')$ is significantly different from zero only for neighboring $\mathbf{R}$ and $\mathbf{R}'$. The natural energy scale for this problem is the so-called *recoil energy*: $E_r = \hbar^2 k_0^2/(2M)$, with M the mass of the atom and $k_0 = 2\pi/\lambda$, whose typical order of magnitude for alkali atoms is the kHz.

In order to study many-body effects and interactions, it is more convenient to use a the second-quantization formalism. Statistics is relevant, and we consider bosons [PS03]. We denote $\hat{\Psi}(\mathbf{r})$ the bosonic field operator annihilating one particle at $\mathbf{r}$; it satisfies the canonical anticommutaion relation $\left[\hat{\Psi}(\mathbf{r}), \hat{\Psi}(\mathbf{r}')\right] = 0$ and $\left[\hat{\Psi}(\mathbf{r}), \hat{\Psi}^\dagger(\mathbf{r}')\right] = \delta(\mathbf{r}-\mathbf{r}')$. We introduce the bosonic operators $\hat{a}_{m,\mathbf{R}}$, which annihilate one boson in the state $|m, \mathbf{k}\rangle$, and expand $\hat{\Psi}(\mathbf{r})$ as:

$$\hat{\Psi}(\mathbf{r}) = \sum_{m,\mathbf{R}} w_{m,\mathbf{R}}(\mathbf{r})\, \hat{a}_{m,\mathbf{R}}. \tag{1.11}$$

Neutral atoms at long distance interact via van der Waals attraction, which scale as r^{-6}, whereas at short distances the interaction is due to the overlap of the electronic clouds and is usually modelled as a hard-core repulsion. Low-energy interactions happen only in the s-wave channel (higher angular momenta are frozen by a centrifugal barrier) and are described by one single parameter, the scattering length a_s. Such collisions are completely characterized by a contact pseudopotential. Within this pseudopotential approximation, the many-body interaction Hamiltonian reads [BDZ08]:

$$\hat{H}_{\text{int}} = \frac{g}{2} \int d\mathbf{r}\, \hat{\Psi}^\dagger(\mathbf{r}) \hat{\Psi}^\dagger(\mathbf{r}) \hat{\Psi}(\mathbf{r}) \hat{\Psi}(\mathbf{r}). \tag{1.12}$$

In the limit of a strong optical lattice, i.e. of atoms confined to the lowest

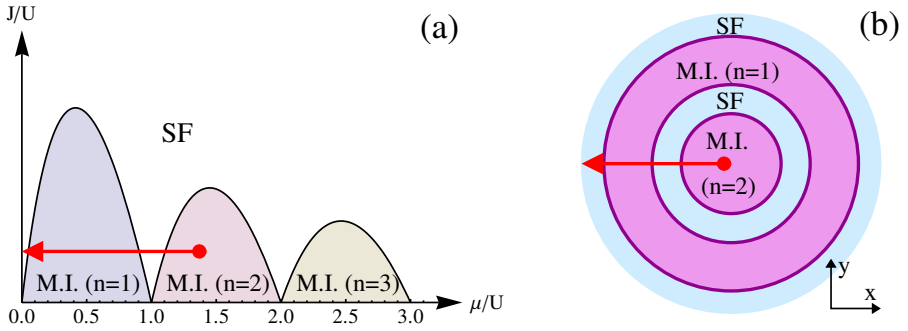

Figure 1.2: Phase diagram of the Bose-Hubbard model at zero temperature. (a) The phase diagram comprises two phases: the Mott insulator (MI), appearing for large interactions and at commensurate lattice filling; and the superfluid (SF), appearing at low interaction. (b) Within the local density approximation, the presence of an external trap can be regarded as a space-dependent chemical potential term. The gas shows an alternating sequence of insulating and superfluid phases, known as *wedding-cake structure*.

band, the final Hamiltonian for a bosonic gas is ($\hat{a}_i \equiv \hat{a}_{1,\mathbf{R}_i}$; $\hat{n}_i \equiv \hat{a}_i^\dagger \hat{a}_i$):

$$\hat{H} = -J \sum_{<i,j>} \left(\hat{a}_i^\dagger \hat{a}_j + H.c. \right) + \frac{U}{2} \sum_j \hat{n}_j (\hat{n}_j - 1) - \mu \sum_j \hat{n}_j \tag{1.13}$$

where $< i, j >$ denotes the summation over neighboring sites, $J = J(\mathbf{R}_i - \mathbf{R}_j)$ is the hopping parameter, $U = g \int d\mathbf{r} |w_{1,\mathbf{R}}(\mathbf{r})|^4$ is the interaction energy and μ is the chemical potential [JBC+98].

Hamiltonian (1.13) is known as the Bose-Hubbard model [FWGF89], whose phase diagram has been widely studied. It comprises two phases, the *Mott insulator* for large interactions $U \gg J$, and the *superfluid* for $J \gg U$ (see figure 1.2a). The two phases differ, for example, in the excitation spectrum, as the insulating phase is gapped, and the superfluid phase is gapless. Moreover, they can also be characterized via the diverse scaling of the correlation function $\langle \hat{a}_i^\dagger \hat{a}_j \rangle$. For the insulating phase, it is decaying exponentially:

$$\langle \hat{a}_i^\dagger \hat{a}_j \rangle \propto e^{-|\mathbf{R}_i - \mathbf{R}_j|/\xi}; \tag{1.14}$$

with a correlation length ξ diverging at the phase transition. The superfluid phase displays long range order:

$$\langle \hat{a}_i^\dagger \hat{a}_j \rangle \xrightarrow{|\mathbf{R}_i - \mathbf{R}_j| \to \infty} \Lambda_0 \tag{1.15}$$

and the limit value Λ_0 defines the condensate fraction of the system. The fact that Λ_0 can be different from 0 is related to the spontaneous symmetry breaking of the $U(1)$ symmetry of the phase of the condensate. As the Mermin-Wagner theorem forbids any such symmetry breaking in low dimensions, Λ_0 is equal to 0 in one dimension and also in two dimensions at finite temperature. The superfluid in such cases is characterized only by the algebraic scaling of the correlation function $\langle \hat{a}_i^\dagger \hat{a}_j \rangle$ and one speaks of quasi long range order [PS03].

So far, we have completely neglected the contribution due to the parabolic trapping: $V_{\text{trap}} = \frac{1}{2}m\omega_{\text{trap}}^2|\mathbf{x}|^2$. The corresponding field Hamiltonian is:

$$\hat{H}_{\text{trap}} = \frac{1}{2}m\omega_{\text{trap}}^2 \left(\frac{\lambda}{2}\right)^2 \sum_j j^2 \hat{n}_j \tag{1.16}$$

Within the local density approximation, the trap potential can be regarded as a space dependent chemical potential $\mu_{\text{eff}} = \mu - \frac{1}{2}m\omega_{\text{trap}}^2 \left(\frac{\lambda}{2}\right)^2 j^2$. The trapped gas does not realize a single point of the phase diagram, but rather a cut at fixed J/U for chemical potential smaller than the initial μ. For $U \ll J$ it is possible to create an alternance of insulating and superfluid shells, as shown in figure 1.2b [JBC+98].

A distinguishing feature of optical lattices is the fact that both J and U depend on the externally tunable parameter V_0 via the dependence of $w_{1,\mathbf{R}}(\mathbf{r})$ on it. If the optical lattice is deep enough to suppress the intersite tunneling, the limit $U \gg J$ is achieved. Viceversa, in a more shallow optical lattice, interaction effects are less pronounced and $J \gg U$. The variation of the lattice depth, V_0, can therefore induce a quantum phase transition from superfluid to Mott insulator. Both phases have been observed; the used measurement techniques are explained in the next section.

Let us mention that it is also possible to study the limit of a weak optical lattice, for which the assumption of occupation of only the lowest band is not true [BBZ03]. Remarkably, it is shown that the Mott insulator can appear also in this limit, as soon as the number of particles is an integer multiple of the number of sites. The theoretical model in the limit of weak optical lattice is the sine-Gordon model [Gia04], which we briefly discuss in chapter 5.

We conclude this section with a brief paragraph on the fermionic case. The description of fermions in optical lattices is analogous to the bosonic case. In the limit of atoms confined to the lowest energy band and of only two possible internal atomic states, briefly denoted as $|\uparrow\rangle$ and $|\downarrow\rangle$, we obtain the Hubbard model:

$$\hat{H} = -J \sum_{<i,j>,\sigma} \left(\hat{c}_{i,\sigma}^\dagger \hat{c}_{j,\sigma} + H.c.\right) + U \sum_i \hat{n}_{i,\uparrow}\hat{n}_{i,\downarrow} - \mu \sum_{i,\sigma} \hat{n}_{i,\sigma} \tag{1.17}$$

The field operators are fermionic and satisfy canonical anticommutation relations: $\{\hat{c}_{i,\sigma}, \hat{c}_{j,\tau}\} = 0$ and $\left\{\hat{c}_{i,\sigma}, \hat{c}_{j,\tau}^\dagger\right\} = \delta_{\sigma,\tau}\delta_{i,j}$. The model highlights the fact that the dominant interaction is still described by a contact pseudopotential, but only between species with different spin. In the case of atoms with the same spin, the Pauli exclusion principle forbids s-wave interactions, so that in the experimentally relevant limit of a dilute and cold gas, the negligence of interactions between atoms with the same spin is a good approximation.

1.3 Measurement Techniques

In order to characterize the phase transition from Mott-insulator to superfluid, it is crucial to have access to the quantum correlations of the gas, like $\langle \hat{a}_i^\dagger \hat{a}_j \rangle$. As we have seen, the two quantum phases are characterized by two different scalings, summarized by equations (1.14) and (1.15).

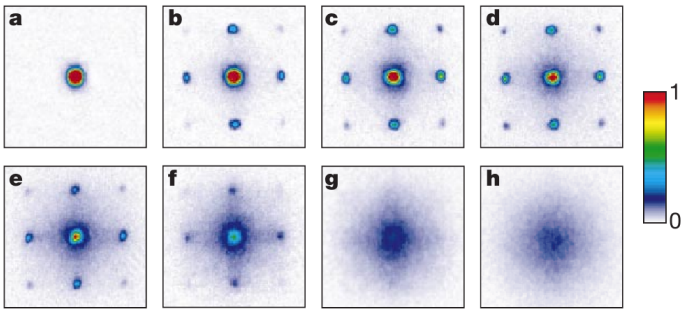

Figure 1.3: Experimental observation of the quantum phase transition from a superfluid to a Mott insulator in three -dimensional optical lattices. The images represent $\int n_{\mathrm{TOF}}(\mathbf{x})dz$ for V_0 equal to (a) $0E_r$, (b) $3E_r$, (c) $7E_r$, (d) $10E_r$, (e) $13E_r$, (f) $14E_r$, (g) $16E_r$ and (h) $20E_r$. In (a), the Bose-Einstein condensate shows a peaked momentum distribution. Raising an optical lattice, which destroys full translational invariance, leads to the creation of secondary peaks (b)-(e); this is a signature of the superfluid phase. For higher intensities (f)-(h), the Mott insulating phase sets in and the absence of long range order is reflected by a featureless momentum distribution. Reproduction from [GME$^+$02].

In this respect, an established measurement technique is the so-called *time-of-flight*, which consists in suddenly releasing the gas from the trap [BDZ08]. After a fall of time t, usually some ms, the gas is described by a three-dimensional density distribution $n_{\mathrm{TOF}}(\mathbf{x})$ which carries information about the in-trap momentum distribution. Let us consider the mapping $\mathbf{k} = m\mathbf{x}/(\hbar t)$, which describes a ballistic expansion (m is the atomic mass); one obtains:

$$\langle n_{\mathrm{TOF}}(\mathbf{x})\rangle = \left(\frac{m}{\hbar t}\right)^3 |\tilde{w}(\mathbf{k})|^2 \mathcal{G}(\mathbf{k}); \quad \mathcal{G}(\mathbf{k}) = \sum_{\mathbf{R},\mathbf{R}'} e^{i\mathbf{k}\cdot(\mathbf{R}-\mathbf{R}')}\langle a^\dagger_{\mathbf{R}} a_{\mathbf{R}'}\rangle; \qquad (1.18)$$

where $\mathcal{G}(\mathbf{k})$ is the in-trap momentum distribution and $\tilde{w}(\mathbf{k})$ is the Fourier transform of the Wannier wavefunction. This measurement technique has been used, for example, to distinguish the Mott insulator from the superfluid (see figure 1.3).

Another possibility for measuring the superfluid-Mott transition, is to look at the *excitation spectrum* of the cloud. In reference [GME$^+$02] this quantity is probed by applying a potential gradient to the system. If the system is gapped, a small potential gradient is not able to perturb the quantum state and after the removal of the perturbation it returns to the initial state. Experimental measurements in the Mott phase clearly identify both the gap and the excitation energy to the second excited state. Moreover, the superfluid phase shows a higher sensibility to such external perturbation.

The last years have seen the development of a completely new technique, called *in-situ microscopy*, which combines the standard experimental setup with high-quality lenses, allowing to observe and to actively manipulate the gas with single-site precision. This tool can also be used to characterize the Mott insulator. In this section we limit the discussion to the description of the measurement technique, whereas in chapter 5 we elaborate on the relation between the phases

of the Bose-Hubbard model and the quantities measurable by this setup, i.e. all the functions of the parity of the number of atoms in each site.

The technique has been developed independently by two research groups and so far applied only to bosons in one- or two-dimensional optical lattices [BGP$^+$09, SWE$^+$10]. After the quantum state of interest has been prepared, the lattice depth is abruptly raised to an extremely high value $V_0 \sim 10^3 E_r$ and the gas is illuminated with high intensity laser beams. This procedure realizes a measurement of the parity of the number of atoms for each site and the initial many-body state is projected to a Fock state. The experimental sequence does not perform a measurement of the number of atoms for each site because pairs of atoms are lost due to inelastic light-induced collisions. The atomic fluorescence, i.e. the set of photons absorbed and then spontaneously re-emitted by the atom, is detected and carries information about the presence of the atom. Therefore, one can observe either one atom left in the site, which means that the initial number of atoms was odd, or an empty site, corresponding to an even initial number. The repetition of this procedure can lead to the experimental evaluation of the expectation values of operators which are functions of the local parity.

The described setup can also be used for the manipulation of atoms sitting in specific lattice sites. Roughly speaking, the imaging apparatus can be used in the opposite direction to focus a laser beam on a specific site and selectively modify the internal state of the atom positioned there. This possibility has been demonstrated experimentally [WES$^+$11].

1.4 Optical Lattices as Quantum Simulators

In this section we list the properties of optical lattices which make them a promising candidate as an analogue quantum simulator.

- The *microscopic theoretical knowledge* of optical lattices is detailed. First, atomic physics is advanced enough to be able to identify and classify the atomic states which are relevant for these experiments [BJ83]. Second, the light-atom interaction, which is at the heart of any trapping and manipulation technique, has been extensively investigated, both theoretically and experimentally [CTDRG98]. Although the experimental setup always introduces some forms of uncertainty, it is not exaggerated to state that given an experiment it is possible to write down the equations of its dynamics with a high fidelity.

- Optical lattices can access the *many-body* strongly-correlated regime. The paradigmatic example is the experimental study of the quantum phase transition from the Mott to the superfluid phase [GME$^+$02]. Moreover, the research community has extensively focussed on the possibility of engineering different many-body Hamiltonians via the extreme versatility of optical lattices. We discuss these ideas in the next subsection.

- The usual *initial state* for experiments with optical lattices is a thermal state with temperature of the order of some nK. Moreover, optical superlattices have been successfully exploited for initializing states appearing less naturally, like: a density wave [TCF$^+$12], a three-dimensional array

of plaquette resonating valence bond states [NCA+12], and excited states of a Bose-Hubbard chain [CBP+12].

- Finally, optical lattices allow for *high-fidelity experiments*, from the initialization to the final measurement. The fully quantitative comparison between theory and experiments done in reference [TPG+10] validated the use of optical lattices as quantum simulators of the three-dimensional Bose-Hubbard model. A quantum Monte Carlo (QMC) simulation of such a model is compared to the experimental data for a three-dimensional optical lattice, and the thermal properties of the phase diagram are studied. This kind of analysis is necessary in order to put experiments accessing models which cannot be numerically investigated on the most solid ground and should be further pursued.

On the other side, the study of the effects of noise, inhomogeneities and other disturbances on the outcome of the quantum simulation has recently started [HCT+11]. The authors propose the analysis of the effects of disorder on a measurable quantity, the two-body correlations, for the Ising model in a transverse magnetic field. This is a research program which should receive attention in the future.

At the present stage, an experiment in which an optical lattice addresses a physical regime theoretically unaccessible is still missing. Some work in this direction has been carried out in the study of the interplay of disorder with interactions [GDF+08, DZR+10, DLM+11], but the golden age of optical lattices as quantum simulators is yet still to come.

1.4.1 Versatility of Optical Lattices

We now discuss the versatility of optical lattices, i.e. we list the parameters which can be controlled from outside and which make optical lattices an appealing candidate for an analogue quantum simulator.

- *Quantum statistics.* Optical lattices have been loaded both with bosons, fermions, and Bose-Fermi mixtures. This has allowed, for example, the study of both the Bose-Hubbard and the finite-temperature Hubbard model [SHW+08, JSG+08].

- *Spin and multi-level physics.* The study of the ground state of atomic gases whose internal degrees of freedom, usually called spins, has not been frozen is one of the present experimental challenges. Whereas condensation phenomena demonstrate the cooling of the spatial degrees of freedom, the cooling of the spin degrees of freedom has still not been accomplished. This prevents, for example, the possibility of studying the spin-order of the ground state of the Hubbard model. In chapter 4 we will discuss an idea to study effective three-body interactions via spin physics.

- *Lattice geometry and dimensionality.* Optical lattices have been realized in one, two and three spatial dimensions. As argued in section 1.1, different laser configuration can also lead to non-square lattices. A new technique exploits the described microscope to project with holographic methods any lattice geometry on the atomic cloud [BGP+09].

- *Intersite tunneling.* The easiest way to change the hopping parameter J is to vary the depth of the optical lattices (see section 1.2). The need for the simulation of gases coupled to static gauge fields, e.g. magnetic fields, has lead to the development of methods which can create, for instance, complex hopping constants. Proposals can be grouped into three areas: methods implementing laser-assisted tunnelling, methods exploiting a dynamical shaking and methods taking advantage of the orbital physics of higher lattice bands. We extensively describe these techniques in section 2.1

- *On-site interactions.* Feshbach resonances allow the tuning of the scattering length a_s, i.e. of the strength of on-site interactions, via application of external magnetic fields or intense optical fields [CGJT10].

- *Long-range interactions.* There are some ways, all of them still under development, to overcome the fact that usual gases display a contact interaction. On one side, there are atoms with strong magnetic dipole moments, such as ^{52}Cr, which naturally interact with r^{-3} and which have been recently loaded in optical lattices [PBM$^+$11, MBH$^+$11]. On the other one, the experimental community is also working on Rydberg atoms, i.e. atoms excited to electronic state with a high principal quantum number [VBR$^+$11], characterized by a strong electric dipole moment.

- *Disorder.* The construction of bi-chromatic optical lattices with wavelengths which are not commensurate creates a quasi-random periodic potential, where the depth of each site is quasi-randomly shifted [GDF$^+$08]. This configuration has been used for the study of the interplay of disorder and interactions.

Chapter 2

An Optical Superlattice Scheme

In this chapter, we suggest to use a spin-independent bi-chromatic optical lattice dressed with suitable Raman transitions as a platform for quantum simulations [MRLC10, MBG$^+$12]. We present a concrete proposal to create a three-dimensional optical lattice trapping a multi-species atomic gas, and to tailor arbitrary spin-dependent hopping processes. We show how this setup can break the SU(2) invariance of the hopping rates of the atomic hyperfine states with a spin-independent lattice, and that a slight complication can even allow for the realization of hopping processes which modify the atomic hyperfine state. Possible applications of such a scheme will be discussed in chapters 3 and 4. The idea was conceived in a discussion with Dr. U. Schneider, whose contribution is gratefully acknowledged.

This chapter is organized as follows: we start with a brief review of experimental approaches appeared in the literature for realizing non-standard optical lattices. In section 2.2, we describe qualitatively our proposal. Further analysis and technical details are given in section 2.3, where we also present some numerical results to support our study. Final remarks on the proposal are presented in section 2.4.

2.1 Beyond Standard Hopping Processes

After the experimental observation of the controlled Mott insulator - superfluid phase transition of the Bose-Hubbard model in optical lattices [GME$^+$02], much effort has been devoted to the development of new ideas and schemes for the engineering of more exotic models. We briefly review some of the main ideas appeared in the literature to develop unconventional optical lattices which can address key-problems of many-body quantum physics, high-energy physics and statistical mechanics. Because of the amplitude of the subject, a complete review goes beyond the purpose of this thesis; we concentrate only on non-trivial hopping processes, selecting some pioneering ideas with a strong experimental focus.

2.1.1 Laser-Assisted Tunneling

One of the most apparent drawbacks of using cold atoms as quantum simulators is the difficulty of coupling their spatial degrees of freedom to external magnetic fields, preventing e.g. the direct simulation of the quantum Hall physics [Eza00]. It was early pointed out that dressing the optical lattice with momentum-transferring Raman couplings leads to a complex space-dependent hopping parameter [JZ03] which corresponds exactly to the discrete version of the kinetic energy of particles coupled to a magnetic field. The proposal was recently revisited and adapted to earth-alkaline atoms, as bosonic Yb [GD10]. These works inspired the first experimental observation of a strong staggered magnetic field in an optical lattice [AAN$^+$11]. Methods for rectifying the magnetic fields are discussed in [GD10].

Simulating a magnetic field in optical lattices can be regarded as a special case of simulation of a background gauge field coupled to the cold gas. Much effort has been devoted to the generalization of these schemes from the Abelian case (magnetic field) to non-Abelian ones. Reference [OBS$^+$05] accomplishes this by considering many internal atomic sublevels. The idea has been further elaborated in [GSN$^+$10] combining optical potentials and atom chips, where the simulation of time-reversal invariant topological insulators (Spin-Hall effect) has suggested.

Recently, the new concept of *optical flux lattices* has been introduced [Coo11]. A two-level atom is considered and the desired gauge field is engineered via adiabatic following of one internal state. The idea, already well known in the literature [DGJO11], is here specified to atomic clouds dressed with periodic space-dependent laser fields. Atoms adiabatically move either in space-periodic potentials (lattices) and experience either an effective magnetic field with a strong flux density [Coo11], or in a band structure with nontrivial $\mathbb{Z}_2$ topological order [BC11].

From an historical perspective, the possibility of using laser-assisted tunneling has already been envisaged in 2002 in [RDJ02] for a different purpose, i.e. the study of particle number fractionalization in a one-dimensional optical lattice.

2.1.2 Dynamical Shaking

The hopping parameter of an optical lattice can also be tuned via dynamical shaking of the setup. It has been theoretically and experimentally shown that this technique can lead not only to the suppression of the inter-site tunneling, but even to the change of sign of the hopping parameter [EWH05, LSC$^+$07]. The shaking of the lattice is expected to create a Floquet quasi-energy spectrum in which the tunneling matrix element is renormalized to a new value.

The simplicity and versatility of the technique make it especially appealing for the study of frustrated two-dimensional systems. In triangular lattices, for instance, its application only along a selected direction produces a lattice with hopping parameters whose sign depends on the tunnelling direction. The technique has been successfully exploited in both experiments and theoretical proposals to study classical and quantum models with highly non-trivial properties [EHSP$^+$10, SOLT$^+$11].

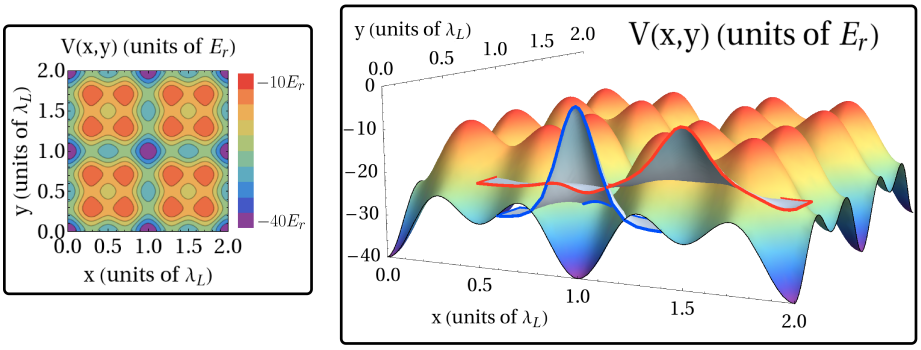

Figure 2.1: Optical superlattice potential of equation (2.1) in the two-dimensional case, with parameters $V_0 = 10E_r$ and $\xi = 1$. Left: the potential is characterized by a square geometry of main minima; in the middle of each link an intermediate minimum is also present. Right: if the lattice is deep enough, the spectrum of the system features two energy bands whose Wannier functions are localized in the main minima and in the secondary minima, as plotted in the figure. Reproduced from [MBG+12].

2.1.3 Orbital Physics

Finally, optical lattices with atoms populating higher-lattice bands automatically display anisotropies and non-trivial effects in the hopping parameters. This is essentially due to the orbital degeneracy and to the symmetries of the various Wannier wavefunctions. Experiments are now moving the first steps in this direction, with the first observations of multiorbital superfluidity in different optical lattices [WOH11, SPLS+12]. It was suggested that this unconventional properties could be exploited for the study of nearly flatbands with nontrivial topology [SGKDS11].

2.2 The Setup and the Idea

Let us now discuss in some details the scheme that we propose, which can allow the realization of non-trivial hopping matrices via laser-assisted methods.

We consider the following atomic three-dimensional optical potential

$$V(\mathbf{x}) = -V_0 \sum_{j\in\{1,2,3\}} \left[\cos^2(qx_j) + \xi\cos^2(2qx_j)\right], \tag{2.1}$$

where $\mathbf{x} = (x_1, x_2, x_3)$, $q = 2\pi/\lambda_L$ (λ_L is the wavelength of the laser), and where $V_0, \xi > 0$ represent the potential amplitudes. The low-energy structure of this potential is a cubic array of main minima separated by "secondary" minima located in the middle of each lattice link (see figure 2.1). We note that additional higher-order minima are also present, but will not play any role in the phenomena discussed in the following. Due to the specific form of the potential in equation (2.1), the Hamiltonian can be divided into three independent terms, each one depending on one of the three couples of conjugate operators, $\{x_i, p_i\}_{i\in 1,2,3}$. Consequently, the Bloch functions of the n-th band

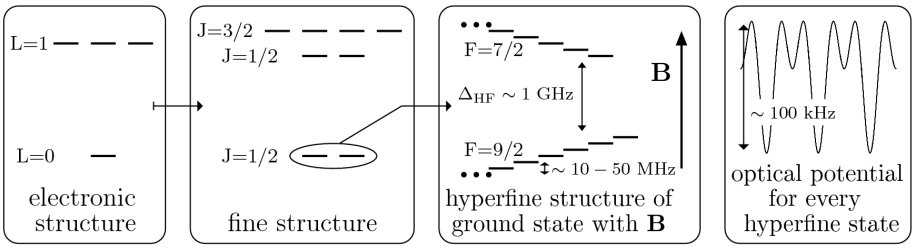

Figure 2.2: Sketch of the atomic structure of ^{40}K: from the electronic structure ($\mathbf{L}$ is the electronic angular momentum) to the fine structure ($\mathbf{J} = \mathbf{L} + \mathbf{S}$, where $\mathbf{S}$ is the electronic spin) to the hyperfine structure ($\mathbf{F} = \mathbf{J} + \mathbf{I}$, where $\mathbf{I}$ is the nuclear spin). The latter is drawn in the specific case of an external magnetic field present. The last box shows the optical spin-independent potential which traps equally all the hyperfine levels. Reproduced from [MBG$^+$12].

with energy $E_n(\mathbf{p})$, can be written as $\psi_{n,\mathbf{p}}(\mathbf{x}) = \prod_j \psi_{n,p_j}(x_j)$. In order to discuss the effects occurring on the scale of one lattice site, Wannier functions can be introduced for each band (see also section 1.2):

$$w_{n,\mathbf{R}}(\mathbf{x}) = \frac{1}{V} \int e^{-i\mathbf{R}\cdot\mathbf{p}} \psi_{n,\mathbf{p}}(\mathbf{x}) d\mathbf{p} = w_{n,R_1}(x_1)\, w_{n,R_2}(x_2)\, w_{n,R_3}(x_3).$$

This setup can be used for the simulation of a lattice field theory, where the field operators are identified with the atomic creation and annihilation operators written in the Wannier basis and restricted to the lowest energy band. These states are localized in the main minima of the lattice. Conversely, higher energy bands provide auxiliary levels that shall be used as a resource to tailor the tunneling processes. The main result of this chapter is the claim that a complicated though not unfeasible combination of current technologies can lead to the realization of the following Hamiltonian:

$$\hat{H}_{\rm sys} = \sum_{\mathbf{r}\boldsymbol{\nu}} \sum_{\tau\tau'} t_\nu\, \hat{a}^\dagger_{\mathbf{r}+\boldsymbol{\nu}\tau'} [U_{\boldsymbol{\nu}}]_{\tau'\tau} \hat{a}_{\mathbf{r}\tau} + \sum_{\mathbf{r}} \sum_{\tau\tau'} \Omega\, \hat{a}^\dagger_{\mathbf{r}\tau'} [\Lambda]_{\tau'\tau} \hat{a}_{\mathbf{r}\tau} + \text{H.c.} \qquad (2.2)$$

where $\hat{a}^{(\dagger)}_{\mathbf{r},\tau}$ are fermionic operators satisfying canonical anticommutation relations. Here, we are considering a multi-species fermionic scenario with many hyperfine levels of the same atom: $\hat{a}^{(\dagger)}_{\mathbf{r}\tau}$ annihilates (creates) one fermion with hyperfine spin τ localized in the main minima of the superlattice at $\mathbf{r} = m_1\mathbf{a}_1 + m_2\mathbf{a}_2 + m_3\mathbf{a}_3$, where $m_j \in \{1...L_j\}$, L_j stands for the number of lattice sites along the x_j axis, and $\mathbf{a}_j$ is the lattice spacing in the j-th direction. The parameter t_ν stands for the strength of the laser-assisted tunneling in the $\hat{\boldsymbol{\nu}}$ direction, with $\boldsymbol{\nu} \in \{\mathbf{a}_1, \mathbf{a}_2, \mathbf{a}_3\}$, which shall be described below. The operators $U_{\boldsymbol{\nu}}$ describe the tunneling from $\mathbf{r}$ to $\mathbf{r} + \boldsymbol{\nu}$, and are a common feature in lattice gauge theories. We have also included an on-site Raman term Λ, of strength Ω, that induces a certain transition between the hyperfine states. In this chapter we use Gaussian units and $\hbar = 1$.

Let us note that the control of the homogeneous tunneling for a single-species atomic gas is straightforward, and would not even require the superlattice ($\xi = 0$) [KMS$^+$05]. Moving to a many-species case, one runs into the

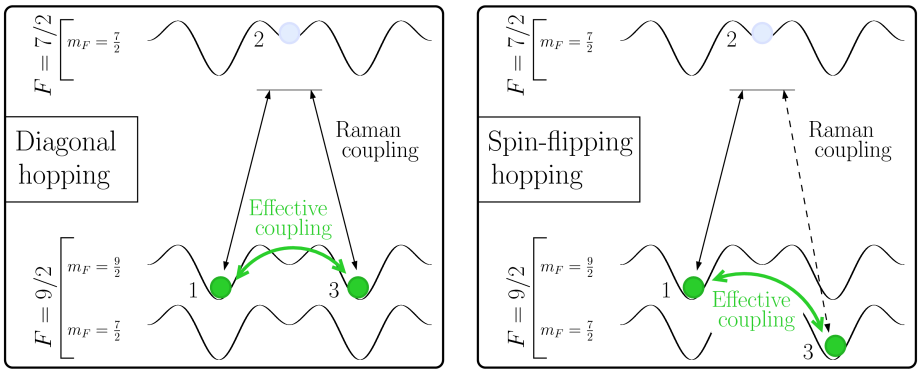

Figure 2.3: Sketch of a laser-assisted tunneling induced in the presence of a superlattice. Two physical hyperfine states belonging to the $F = 9/2$ manifold are connected via Raman couplings with the intermediate level of an auxiliary state belonging to the $F = 7/2$ manifold. If the coupling is detuned enough, the $F = 7/2$ level can be adiabatically eliminated: no population is left there and an effective coupling is engineered between neighboring sites. Left: scheme for a spin-preserving (i.e. diagonal) hopping. Right: scheme for a spin-flipping hopping. Reproduced from [MBG+12].

problem that a general hopping matrix also entails terms flipping the atomic hyperfine spin (simply referred as *spin* in the following), which are not easily engineered. Here, we propose to realize such couplings by combining Raman transfers and a bi-chromatic superlattice ($\xi \neq 0$ in equation (2.1)). The proposal can be applied to all the alkalis notwithstanding their bosonic or fermionic nature. In the following, however, we shall focus in the fermionic scenario, which is best explained with the following practical example.

Let us consider an ultra-cold cloud of non-interacting ^{40}K atoms in the presence of a magnetic field of intensity B. Such field lifts the spin degeneracy within the two atomic hyperfine manifolds of the ground state, $F = 9/2$ and $F = 7/2$, according to the following relations (see also figure 2.2):

$$E_{9/2,m_F} = +g_F\,\mu_B\,B\,m_F \qquad E_{7/2,m_F} = \Delta_{\mathrm{HF}} - g_F\,\mu_B\,B\,m_F \tag{2.3}$$

where m_F is the projection of the hyperfine spin along the quantization axis defined by the magnetic field, μ_B is the Bohr magneton, g_F is the hyperfine Landé Factor, and Δ_{HF} stands for the hyperfine splitting. These hyperfine levels are all trapped into the same spin-independent optical potential (2.1). Depending on the lattice theory we want to simulate, we select a subset of these hyperfine levels described theoretically by creation-annihilation operators in the lattice sites. We then identify such fields with the components of the lattice field theory to be simulated. This leads us to divide the hyperfine levels into two subsets: the subset of "physically meaningful" states, which belong to the hyperfine manifold $F = 9/2$, and the usually larger subset of auxiliary levels that shall be used to assist the tunneling and create the desired hopping matrix.

Regarding the hopping matrix in equation (2.2), we address each of its matrix elements $[U_{\boldsymbol{\nu}}]_{\tau'\tau}$ separately. Given a matrix element – i.e. identified the initial and final hyperfine levels τ and τ' – we choose an auxiliary level be-

λ_L	~ 738 nm	$E_r = \frac{h^2}{2m\lambda_L}$	9.17 kHz
V_0	10 E_r	ξ	1
$\langle E_1 \rangle$	$-13.909 * 3$ E_r	$\langle E_2 \rangle$	$-13.909 * 2 - 6.364$ E_r
ΔE_1	0.024 E_r	ΔE_2	0.995 E_r
ΔE_1	216.7 Hz	ΔE_2	9120.1 Hz
Δ_{HF}	1.286 GHz	$g_F \mu_B$	$0.22 * 1.34$ MHz/G
$\langle E_2 - E_1 \rangle$	69.160 kHz	Staggering	10 kHz

Table 2.1: Numerical values of a possible three-dimensional optical bi-chromatic superlattice (2.1) for ^{40}K used in section 2.3 for numerical simulations. We characterize the properties of the two energy bands, which exhibit Wannier functions localized respectively in the main and secondary minima, by listing the energy expectation value $\langle E_i \rangle$ of the most localized Wannier function and the bandwidth ΔE_i. Finally, we argue that atoms trapped in optical lattices show a hierarchy of typical energies which can be actively exploited for engineering non-trivial hopping processes.

longing to the hyperfine manifold $F = 7/2$ trapped in the middle of the link. These levels provide intermediate "bus" states that shall be used as a resource to assist the tunneling as follows. The couplings between the atoms in the main sites, $\mathbf{R}_1$, and the "bus" states, $\mathbf{R}_2$, are realized via optical two-photon Raman processes transferring a net momentum $\mathbf{q}_t$. They have a mathematical expression proportional to the overlap integral of the initial and final Wannier functions: $\int w^*_{n_2,\mathbf{R}_2}(\mathbf{x}) e^{i\mathbf{q}_t\cdot\mathbf{x}} w_{n_1,\mathbf{R}_1}(\mathbf{x}) d\mathbf{x}$. This integral is not zero because of the term $e^{i\mathbf{q}_t\cdot\mathbf{x}}$, which is of course relevant only if $2\pi/|\mathbf{q}_t|$ is of the order of the lattice spacing. Since this regime cannot be achieved with microwave transitions, one is motivated to employ two-photon Raman transitions. It is possible to eliminate adiabatically the intermediate level and obtain an effective four-photon coupling between neighboring sites (see figure 2.3). We stress that different matrix elements can be engineered at the same time thanks to the magnetic-field splitting of the hyperfine levels (2.3): the involved atomic transitions become non-degenerate and can be individually addressed with different Raman couplings. Furthermore, the use of coherent laser light for the Raman transitions entails the additional advantage of being able to deal with complex phases, and thus to realize complex gauge structures at will. The realization of the non-diagonal matrix elements requires the lattice to be slightly staggered, a technique discussed also in reference [GD10]. The on-site term Λ in equation (2.2) can be performed with technology based on microwave transitions, or Raman transitions carrying negligible momentum. Furthermore, these terms can also be exploited to correct spurious on-site couplings which may be induced by the laser scheme. Summarizing, this proposal tries to exploit a hierarchy of energies characterizing atomic gases in optical lattices in order to assist the tunneling between neighboring sites with controlled adiabatic eliminations (see table 2.1).

We stress here that the proposal does not exploit any selection rule on the polarization properties of the light, but rather relies only on energy-based selection rules, i.e. on the detuned atomic transitions induced by the magnetic field. Even though in low-dimensional setups the specific experimental imple-

mentation could benefit from polarization selection rules, they are not necessary and there is no fundamental limitation to the extension of the setup to more dimensions.

2.3 Realization of Spin-Dependent Hopping Processes

In this technical section, we theoretically and numerically confirm the qualitative scheme presented above. We study two simple but important cases: the realization of diagonal and non-diagonal hopping matrices for a two-species atomic gas. These can be considered as the main building blocks needed to realize any tunneling process even in situations with more than two atomic species.

2.3.1 Coupling Between Different Hyperfine Manifolds

We start discussing the explicit expression of the coupling realised with an optical Raman transition between two different hyperfine levels of the ground state $L = 0$ via elimination of the manifold of excited states $L = 1$, where L is the electronic angular momentum. Atomic levels are addressed with the notation $|L, \alpha, k\rangle$, where α labels the hyperfine degrees of freedom (see also figure 2.2 for some insights on the internal structure of ^{40}K) and k are the quantum numbers of the center-of-mass wavefunction. The Raman coupling between two states $|0\,\alpha\,k\rangle$ and $|0\,\alpha'\,k'\rangle$ is:

$$\begin{aligned}\tilde{\Omega}_{\alpha' k';\alpha k}(t) &= -\frac{1}{2}\sum_{|1\,\beta\,q\rangle} \langle k'|e^{-i\mathbf{p}_2\cdot\mathbf{x}}|q\rangle\langle q|e^{i\mathbf{p}_1\cdot\mathbf{x}}|k\rangle \cdot \\ &\quad \cdot c^*_{2\alpha'\beta}\,\|\mu\|^*_2\,E^*_2\,E_1\,\|\mu\|_1\,c_{1\alpha\beta}\;\cdot\; e^{-i(\omega_1-\omega_2)t}\;\cdot \\ &\quad \cdot\left(\frac{1}{E_{1\beta q}-E_{0\alpha k}-\hbar\omega_1}+\frac{1}{E_{1\beta q}-E_{0\alpha' k'}-\hbar\omega_2}\right) \qquad (2.4)\end{aligned}$$

where $E_{L\alpha k}$ is the energy of the level $|L, \alpha, k\rangle$ and ω_i and $\mathbf{p}_i$ are the energy and momentum of the i-th laser. The coupling realized by the i-th laser between the internal atomic states $|0\alpha\rangle$ and $|1\beta\rangle$ is described by $\|\mu\|_i$, E_i and $c_{i\alpha\beta}$ according to the notation of reference [GWO00]. The sum over the excited states is limited to the first excited manifold because we consider lasers far-detuned from higher excited levels. In the case of a spin-independent lattice, lasers can be detuned from the first excited manifold $L = 1$ of even some tens of THz: in this case the expression in equation (2.4) can be simplified. Indeed, the energy differences at the denominators depend only slightly on the internal structure of the levels (they can differ at most for some GHz): once $E_{1\beta q} - E_{0\alpha' k'}$ is substituted with the 0-th order energy difference between excited and ground states ΔE_{10}, we can write:

$$\begin{aligned}\tilde{\Omega}_{\alpha' k';\alpha k}(t) &= -\frac{1}{2}\left(\frac{\langle k'|e^{-i(\mathbf{p}_2-\mathbf{p}_1)\cdot\mathbf{x}}|k\rangle}{\Delta E_{10}-\hbar\omega_1}+\frac{\langle k'|e^{-i(\mathbf{p}_2-\mathbf{p}_1)\cdot\mathbf{x}}|k\rangle}{\Delta E_{10}-\hbar\omega_2}\right)\cdot \\ &\quad \cdot\sum_{\beta} c^*_{2\alpha'\beta}\,\|\mu\|^*_2\,E^*_2\,E_1\,\|\mu\|_1\,c_{1\alpha\beta}\;\; e^{-i(\omega_1-\omega_2)t} = \\ &= S_{k'k}\,\Omega_{\alpha'\alpha}\,e^{-i\omega t} \qquad (2.5)\end{aligned}$$

This expression clearly factorizes the following contributions:

- the time-dependence of the effective coupling and its effective frequency, which is the difference between the frequencies of the two lasers $\omega = \omega_1 - \omega_2$.
- The dependence on the center-of-mass degrees of freedom:

  $$S_{k'k} = \langle k'|e^{-i(\mathbf{p}_2-\mathbf{p}_1)\cdot\mathbf{x}}|k\rangle,$$

  where $\mathbf{p}_1$ and $\mathbf{p}_2$ are the momenta of the two lasers. The very simplified expression for the center-of-mass part of the coupling $S_{k'k}$ comes from the substitution of $\sum_q |q\rangle\langle q|$ with the identity on the center-of-mass Hilbert space.
- The dependence on the initial and final internal states and on the polarization properties of light, $\Omega_{\alpha'\alpha}$, which is a function of the dipole matrix elements between the initial (final) state and the excited levels.

Next, we specify (2.5) to the superlattice setup of section 2.2, i.e. we will consider Raman transitions in presence of lattices characterized by a Wannier function trapped in the middle of each link.

2.3.2 Developing an Effective "6-Level Model"

Let us address the simulation a theory characterized by two-component fields. Following the discussion of section 2.2, we take two states of the $F = 9/2$ manifold of ^{40}K, for instance $|9/2; m_F = 7/2\rangle$ and $|9/2; m_F = 9/2\rangle$, and map them into the theory to be simulated. Here and in the following subsections, we discuss the laser-assisted hopping in the diagonal case (m_F preserved while hopping) and non-diagonal case (m_F flipped while hopping).

For the diagonal case, we develop the "6-level model" depicted in figure 2.4. We consider one physically meaningful state, say $|F = 9/2, m_F = 9/2\rangle$, and one auxiliary state, say $|F = 7/2, m_F = 7/2\rangle$. Moreover, we consider different Wannier states for each of them, two localized in main sites ($k = 1$ and 3) and one in the intermediate link ($k = 2$). The model includes the effects of undesired couplings and additional levels, and its limitations, together with the approximations on which it relies, will be discussed at the end of the paragraph. We can identify the states with the short notation $|F, k\rangle$ rather than with the longer previous one $|0\,\alpha\,k\rangle$. Below, we give an analytical estimate of the population transfer rate, whereas in the next subsections we present the numerical time-evolution for physically interesting cases.

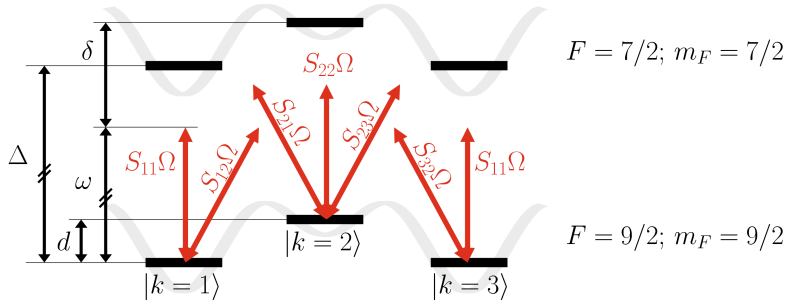

Figure 2.4: The "6-level model" used to model the spin-preserving (diagonal) hopping of $F = 9/2, m_F = 9/2$. The auxiliary state $F = 7/2, m_F = 7/2$ has been chosen. The center-of-mass quantum number is k. Energies are not to scale; the orders of magnitude of the parameters are the following: $d \sim 10 \div 100$ kHz, $\delta \sim 100 \div 300$ kHz and $\Delta \sim 1 \div 10$ GHz. We propose to adiabatically eliminate the upper manifold and to study the dynamics of the lowest one with an effective Hamiltonian H_{pert} (2.10). Reproduced from [MBG+12].

The model is parametrized by six relevant couplings between the different Wannier functions $S_{k'k}$ (see figure 2.4), whose properties are listed below. We exploit the existence of theorems which assure the possibility, in our case, of considering three real and exponentially localized Wannier functions $w_j(\mathbf{x}), j \in \{1, 2, 3\}$ [Koh59]. We write the parameters $S_{k'k}$ factorizing out the space dependence of the coupling $e^{i\mathbf{q}_t\cdot\mathbf{x}_j}$, where $\mathbf{x}_j$ is the position of the point around which the Wannier function $w_j(\mathbf{x})$ is localized,

$$S_{k'k} = e^{i\mathbf{q}_t\cdot\mathbf{x}_k}\int w^*_{k'}(\mathbf{x}-\mathbf{x}_{k'}+\mathbf{x}_k)e^{i\mathbf{q}_t\cdot\mathbf{x}}w_k(\mathbf{x})d\mathbf{x}; \tag{2.6}$$

$$S_{1,1} = S_{3,3} \neq S_{2,2}; \qquad S_{1,3},\ S_{3,1} \sim 0. \tag{2.7}$$

The parameters $S_{1,1}$ and $S_{2,2}$ describe two on-site couplings, whereas $S_{1,2}$ is the coupling between a main site and an intermediately trapped state (see figure 2.4). The last relation states that couplings between neighboring main sites are negligible. The relation between the other four overlap factors depends on the particular experimental situation. In the simplest case of a single Raman transition inducing all the couplings, we get

$$S_{1,2} = S_{2,1} = e^{2i\mathbf{q}_t\cdot\mathbf{x}_1}e^{i\mathbf{q}_t\cdot(\mathbf{x}_3-\mathbf{x}_1)}S^*_{3,2} = e^{2i\mathbf{q}_t\cdot\mathbf{x}_1}e^{i\mathbf{q}_t\cdot(\mathbf{x}_3-\mathbf{x}_1)}S^*_{2,3}. \tag{2.8}$$

In order to make this scheme simpler, we assume $\mathbf{q}_t = 2\mathbf{q}_L$, and thus $e^{i\mathbf{q}_t\cdot(\mathbf{x}_2-\mathbf{x}_1)} = 1$. As we will argue below, transferring a momentum which does not fulfill this requirement is not a problem since the resulting phase can be gauged away. The phase $2\mathbf{q}_t\cdot\mathbf{x}_1$ can also be put to zero for the moment, since its role only becomes important when one needs to give a phase to different matrix elements. In the following, we will also consider situations where the coupling between the lattice sites 2 and 3 could be induced by lasers propagating in the opposite direction due to staggering of the second site, so that one can assume $S_{1,2} = S_{2,1} = S_{3,2} = S_{2,3}$. Taking these considerations into account, the

Hamiltonian reads as follows (see figure 2.4 for the definitions of δ, Δ and ω):

$$\begin{aligned} H &= d\,|9/2,2\rangle\langle 9/2,2| + (\Delta+d)|7/2,2\rangle\langle 7/2,2| + \\ &\quad +\Delta\,(|7/2,1\rangle\langle 7/2,1| + |7/2,3\rangle\langle 7/2,3|) + \\ &\quad +\Omega e^{-i\omega t}\,[\,S_{1,2}\,(|7/2,2\rangle\langle 9/2,1| + |7/2,1\rangle\langle 9/2,2|) + \\ &\qquad + S^*_{1,2}\,(|7/2,2\rangle\langle 9/2,3| + |7/2,3\rangle\langle 9/2,2|) + \\ &\qquad + S_{1,1}\,(|7/2,1\rangle\langle 9/2,1| + |7/2,3\rangle\langle 9/2,3|) + \\ &\qquad + S_{2,2}\,|7/2,2\rangle\langle 9/2,2|\,] \;+\; \text{H.c.} \end{aligned} \tag{2.9}$$

Once we apply the unitary transformation

$$\Gamma(t) = \exp[i\,d\,(|9/2,2\rangle\langle 9/2,2| + |7/2,2\rangle\langle 7/2,2|)\,t],$$

the three levels $|9/2,k\rangle$ become degenerate. In case the three inequalities $|S_{i,j}\Omega|/(\delta-d) \ll 1$ are fulfilled, it is possible to use second-order perturbation theory in order to develop an effective Hamiltonian describing the dynamics within the sub-manifold we are interested in, namely

$$\begin{aligned} H_{pert}/\Omega^2 &= -\left(\frac{|S_{1,1}|^2}{\delta-d} + \frac{|S_{1,2}|^2}{\delta}\right)[|9/2,1\rangle\langle 9/2,1| + |9/2,3\rangle\langle 9/2,3|] + \\ &\quad -\left(\frac{|S_{2,2}|^2}{\delta-d} + 2\frac{|S_{1,2}|^2}{\delta-2d}\right)|9/2,2\rangle\langle 9/2,2| + \\ &\quad -\frac{S^2_{1,2}}{\delta}|9/2,3\rangle\langle 9/2,1| \;+\; H.c. + \\ &\quad -\left[\frac{S^*_{1,2}\,S_{1,1}}{2}\left(\frac{1}{\delta-d}+\frac{1}{\delta-2d}\right)e^{idt} + \frac{S^*_{2,2}\,S_{1,2}}{2}\left(\frac{1}{\delta-d}+\frac{1}{\delta}\right)e^{idt}\right]\cdot \\ &\quad \cdot\,[|9/2,2\rangle\langle 9/2,1| + |9/2,2\rangle\langle 9/2,3|] \;+\; H.c. \end{aligned} \tag{2.10}$$

Remarkably enough, this Hamiltonian leads to the desired transfer rate of population from level $|9/2,1\rangle$ to $|9/2,3\rangle$, and viceversa. The main contribution is the direct coupling

$$-\,J^{(1)}_{13}e^{i2\phi} = -\frac{|S_{1,2}|^2\Omega^2}{\delta}e^{i2\phi}; \qquad \phi = \arg S_{1,2}. \tag{2.11}$$

A second contribution, which in our system will prove to be not-negligible, comes from a sort of "adiabatic elimination" of the level $|9/2,2\rangle$, namely

$$-\,J^{(2)}_{13} = -\frac{\langle 9/2,3|H_{pert}|9/2,2\rangle\,\langle 9/2,2|H_{pert}|9/2,1\rangle}{\langle 9/2,2|H_{pert}|9/2,2\rangle - \langle 9/2,1|H_{pert}|9/2,1\rangle + d}. \tag{2.12}$$

Accordingly, we have derived the desired effective Hamiltonian where the Raman lasers assist the hopping of the physically meaningful $F = 9/2$ levels, after the auxiliary $F = 7/2$ bus states have been adiabatically eliminated. In the following sections, we shall address the range of validity of the approximations leading to this Hamiltonian, and compare it with the exact numerical investigation of the initial Hamiltonian (2.9).

We want to stress here that even if the integrals in the definition (2.6) of the $S_{kk'}$ can be complex numbers, this does not have any physical influence on this proposal. Indeed, even if the effective coupling between neighboring main

sites $-J$ was complex, its spatially uniform phase can be gauged away with a space-dependent unitary transformation (even in the case of periodic boundary conditions). Conversely, the non-uniform phase coming from the $e^{i\mathbf{q}_t\cdot\mathbf{x}_k}$ factor, which arises when $\mathbf{q}_t$ is not parallel to the direction of the hopping it assists, cannot be gauged away even in presence of open boundary conditions. Such a phase, which is not related to the fact that the integrals in (2.6) are complex, can be used to simulate an external uniform magnetic field [JZ03, GD10]. Finally, we underline that in our setup, where the tunneling along each axis is induced by lasers propagating parallel to the axis itself, both complex phases can be gauged away. In order to simulate a magnetic field, therefore, one should move slightly away from this configuration and engineer a Raman coupling whose effective transmitted momentum does not run parallel to the links of the lattice.

2.3.3 Range of Validity of the "6-Level Model"

The presented "6-level model" strongly relies on two approximations:

1. considering the bands of the lattice as being flat;
2. neglecting delocalized higher-energy free states.

If these approximations are not justified for a given experimental configuration, spurious population transfers to next-neighboring sites would arise.

The approximation (1) is required to fulfill the core idea of the proposal, namely the adiabatic elimination of the intermediate level. This is demonstrated with a model which considers only a subset of the Hilbert space spanned by the real eigenstates of the Hamiltonian (Bloch functions), considering just three of their linear combinations (the Wannier functions $w_{k=1}(\mathbf{x})$, $w_2(\mathbf{x})$ and $w_3(\mathbf{x})$). This is equivalent to approximating the dispersion laws of the band as being flat, neglecting thus possible curvature effects, and is legitimated as long as the width of the band is much smaller than the detuning of the transition $\delta - d$. In case the degeneracy of the Bloch functions cannot be assumed, all the Bloch functions should be considered in order to quantitatively estimate the spurious effects cited above. In general, this issue sets a trade-off for the relative depth ξ of the secondary lattice in (2.1): on one hand, a shallow lattice ($\xi < 1$) is desirable because the Wannier function of the intermediate minimum $w_{k=2}(\mathbf{x})$ is not strongly localized and laser-induced transitions are favored ($|S_{1,2}| \sim |S_{1,1}|$). On the other hand, the more the wavefunction is delocalized, the more the band bends, eventually becoming parabolic at $\mathbf{k} = 0$ with a bandwidth comparable to the detuning. In our numerical simulations we consider $\xi = 1$, which is a reasonable middle-way.

Regarding the issue (2), higher-energy bands could become important in the presence of intense Raman transitions Ω and large detunings $\delta - d$, which couple them to the lowest-band states. The presented analytical and numerical studies do not take into account these effects since they consider only three Wannier functions and effectively only two bands, even though including bands with localized Wannier functions would just imply a renormalization of the numerical coefficients $S_{k,k'}$. A different problem is the case of high-energy strongly parabolic bands, whose Wannier functions are not strongly localized. The effect of such states is not considered by our model, which is that of spreading population among many next- and further-neighboring main sites. From an

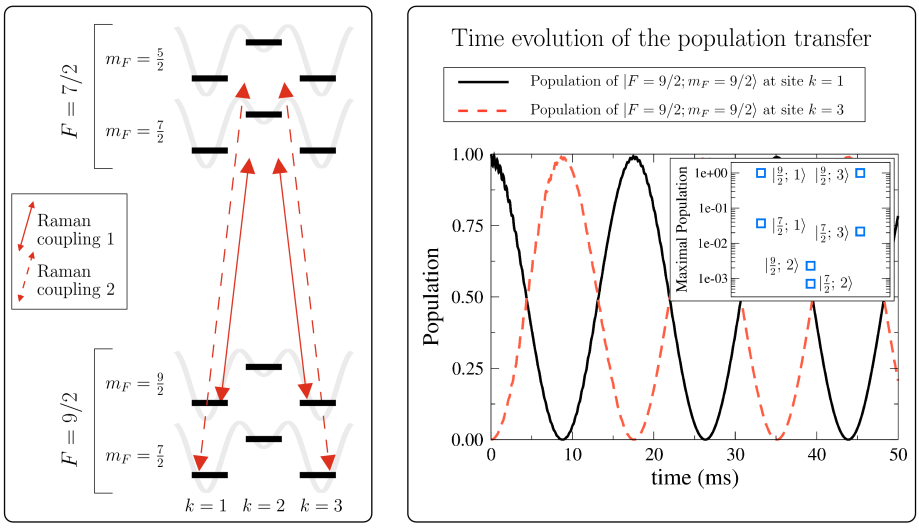

Figure 2.5: Left: sketch of the scheme proposed for the realization of a diagonal hopping matrix (Energies are not to scale). Raman coupling 1 (2) connects the $|F = 9/2, m_F = 9/2\rangle$ ($|F = 9/2, m_F = 7/2\rangle$) states to their auxiliary state. Detuning allows independent control of the hopping rates. Right: exact time-evolution of the "6-levels model" (2.9), showing the coherent population transfer between sites 1 and 3 of the spin state $|F = 9/2, m_F = 9/2\rangle$. The parameters used are listed in table 2.2. The inset shows the maximal populations of the six considered levels labeled $|F, k\rangle$ as in (2.9) and shows that only a small fraction of the population is lost in auxiliary levels. Reproduced from [MBG+12].

experimental point of view, we expect a trade-off to arise between a large detuning regime, allowing powerful lasers and strong effective couplings with noisy spurious population transfers, and a small detuning one, with clean but small couplings.

2.3.4 Diagonal Hopping Matrix

We now explicitly study the possibility of realizing a diagonal tunneling matrix. We numerically simulate the Hamiltonian (2.9) with a simple Runge-Kutta algorithm. We did not include in the simulation hyperfine states different from $|F = 9/2, m_F = 9/2\rangle$ and $|F = 7/2, m_F = 7/2\rangle$ because they are strongly detuned from those we are considering. However, for completeness, we include the presence of a second Raman coupling which would be needed to induce the hopping of $|F = 9/2;\ m_F = 7/2\rangle$ and check that it is unimportant.

We show in figure 2.5 the numerical results. The realistic parameters used in this simulation are listed in table 2.2. The population is coherently transferred between two neighboring levels and only a negligible fraction is lost in auxiliary states. Regarding the validity of the "6-levels model", for the lattice considered here, the bandwidths of the two bands are respectively 0.2 kHz and 9.1 kHz, which should be compared with the considered detuning of 300 kHz. In these and the following simulations, the employed numerical values have only

Level: $\lvert F, m_F, k\rangle$	Energy	Parameters	
$\lvert 9/2; 9/2; 1\rangle$	$g_F\mu_B B m_F$	Δ_{HF}	1.285 GHz
$\lvert 9/2; 9/2; 2\rangle$	$g_F\mu_B B m_F + d$	$\mu_F B$	40 MHz
$\lvert 9/2; 9/2; 3\rangle$	$g_F\mu_B B m_F$	d	69.160 kHz
$\lvert 7/2; 7/2; 1\rangle$	$\Delta_{\mathrm{HF}} - g_F\mu_B B m_F$	$S_{1,1}$	0.46
$\lvert 7/2; 7/2; 2\rangle$	$\Delta_{\mathrm{HF}} - g_F\mu_B B m_F + d$	$S_{1,2}$	$0.07 + i0.13$
$\lvert 7/2; 7/2; 3\rangle$	$\Delta_{\mathrm{HF}} - g_F\mu_B B m_F$	$S_{2,2}$	0.16

# Raman	Ω	ω
1	49.5 kHz	$E_{\lvert 7/2;7/2;2\rangle} - E_{\lvert 9/2;9/2;1\rangle} - 300$ kHz
2	49.5 kHz	$E_{\lvert 7/2;5/2;2\rangle} - E_{\lvert 9/2;7/2;2\rangle} - 300$ kHz

$J_{13}^{(1)}$	$J_{13}^{(2)}$	Estimated T	Numerical T
176 Hz	17 Hz	0.018 s	0.017 s

Table 2.2: Parameters used for the numerical simulation of the diagonal hopping in subsection 2.3.4. We list the numerical values of all the main parameters characterizing the atomic transitions and the Raman couplings. The first Raman coupling induces the hopping of the $F = 9/2$, $m_F = 9/2$ whereas the second one addresses the $F = 9/2$, $m_F = 7/2$ (such states were however not considered in the simulation).

Level: $\lvert F, m_F, k\rangle$		Energy	Parameters	
$\lvert 9/2; 9/2; 1\rangle$,	$\lvert 9/2; 7/2; 1\rangle$	$g_F\mu_B B m_F$	Δ_{HF}	1.285 GHz
$\lvert 9/2; 9/2; 2\rangle$,	$\lvert 9/2; 7/2; 2\rangle$	$g_F\mu_B B m_F + d$	$\mu_F B$	40 MHz
$\lvert 9/2; 9/2; 3\rangle$,	$\lvert 9/2; 7/2; 3\rangle$	$g_F\mu_B B m_F + 15$ kHz	d	69.160 kHz
$\lvert 7/2; 7/2; 1\rangle$,	$\lvert 7/2; 5/2; 1\rangle$	$\Delta_{\mathrm{HF}} - g_F\mu_B B m_F$	$S_{1,1}$	0.46
$\lvert 7/2; 7/2; 2\rangle$,	$\lvert 7/2; 5/2; 1\rangle$	$\Delta_{\mathrm{HF}} - g_F\mu_B B m_F + d$	$S_{1,2}$	$0.07 + i0.13$
$\lvert 7/2; 7/2; 3\rangle$,	$\lvert 7/2; 5/2; 1\rangle$	$\Delta_{\mathrm{HF}} - g_F\mu_B B m_F + 15$ kHz	$S_{2,2}$	0.16

# Raman	Ω	ω
1	49.5 kHz	$\sim E_{\lvert 7/2;7/2;2\rangle} - E_{\lvert 9/2;9/2;1\rangle} - 300$ kHz
2	49.5 kHz	$\sim E_{\lvert 7/2;5/2;2\rangle} - E_{\lvert 9/2;7/2;1\rangle} - 300$ kHz
3	49.5 kHz	$\sim E_{\lvert 7/2;7/2;2\rangle} - E_{\lvert 9/2;7/2;3\rangle} - 300$ kHz

Table 2.3: Parameters used for the numerical simulation of the non-diagonal hopping in subsection 2.3.5. We list the numerical values of the main parameters characterizing atomic transitions and Raman couplings. The reported frequencies of the Raman couplings are approximate because some additional tuning is needed to compensate the different Stark shift for states with $k = 1$ and $k = 3$ arising due to Raman dressing in presence of staggering. Perfect matching the atomic transition becomes difficult and imperfections are responsible for the not clean population transfer in figure 2.7. Larger staggering values would help.

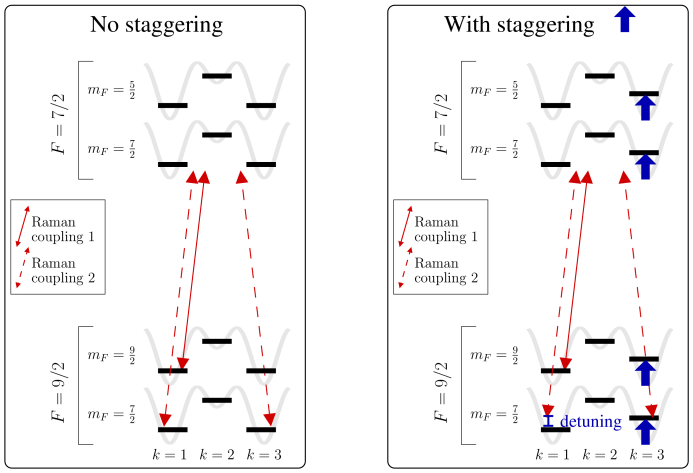

Figure 2.6: Left: the realization of a spin-flipping hopping matrix suffers from the problem that undesired on-site spin-flipping processes could spontaneously arise. Right: the solution to this problem comes from the introduction of a staggered lattice. The on-site spin-flipping process is detuned from the atomic transition and its contribution is negligible with respect to the hopping process, which is resonant with the atomic transition. Reproduced from [MBG+12].

an illustrative purpose and other regimes could be considered.

To estimate for the accuracy of the assisted hopping matrix, we compute the fidelity of generating a particular target spin state at site $k = 3$ in the internal state $\{F_t, m_{F,t}\}$, i.e. $|\psi_t\rangle = |3, F_t, m_{F,t}\rangle$, for an atom that is initially populating the site $k = 1$ in the internal state $\{F_i, m_{F,i}\}$, i.e. $|\psi_i\rangle|1, F_i, m_{F,i}\rangle$. Such fidelity can be quantified defining

$$\mathcal{F}^2 = \max_{\tau} |\langle\psi_t|\psi(\tau)\rangle|^2, \tag{2.13}$$

with $|\psi(\tau)\rangle$ the time evolved state, which is the amplitude of the oscillations between the sites between which the hopping acts. For the presented simulation the fidelity of the stimulated hopping process is $\mathcal{F}^2 > 97\%$. Therefore, these results confirm the plausibility of our scheme to induce a laser-assisted tunneling between the atoms sitting in the main minima of the optical lattice. To make the simulation toolbox reacher, we now address the possibility to control a spin-dependent hopping process.

2.3.5 Non-Diagonal Hopping Matrix

In order to study the realization of the non-diagonal hopping matrix, we consider an enlarged 12-levels model, which is a generalization of the previous one taking into account more hyperfine states. We want now to transfer population between the manifolds $|F = 9/2, m_F = 9/2\rangle$ and $|F = 9/2, m_F = 7/2\rangle$ and consider as auxiliary states $|F = 7/2, m_F = 7/2\rangle$ and $|F = 7/2, m_F = 5/2\rangle$.

A big issue which must be solved to engineer such a hopping is the appearance of undesired spin-flipping terms induced by the laser (see figure 2.6). In

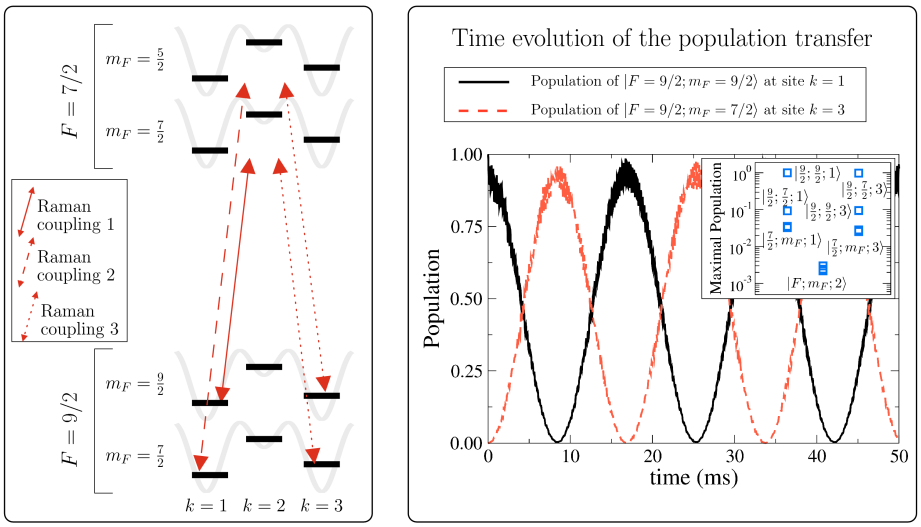

Figure 2.7: Left: sketch of the scheme proposed for the realization of a non-diagonal hopping matrix (Energies are not to scale). Raman couplings 1, 2 and 3 connect the $|F = 9/2, m_F = 9/2\rangle$ and $|F = 9/2, m_F = 7/2\rangle$ states to the auxiliary states. Detuning allows independent control of the hopping rates. Right: exact time-evolution of the "12-levels model" introduced in subsection 2.3.5 and generalizing (2.9). We show the coherent population transfer between sites 1 and 3 of the spin state $|F = 9/2, m_F = 9/2\rangle$ and $|F = 9/2, m_F = 7/2\rangle$. The parameters used are listed in table 2.2. The inset shows the maximal populations of the twelve considered levels labeled $|F, m_F, k\rangle$ and shows that only a fraction of the population is lost in auxiliary levels. Reproduced from [MBG+12].

this paper we consider the possibility of staggering the lattice with an additional optical field, in order to lift the degeneracy between the different sites of the optical lattice, in the same fashion of [GD10]. Such a staggering can be done also in three dimensions since the cubic lattice is bipartite, and we consider staggering values of $10 - 15$ kHz.

Figure 2.7 sketches the experimental scheme we have in mind and shows the exact time evolution of the population transfer between the two levels of $F = 9/2$ in two neighboring sites. Interestingly enough, we show a flip of the Zeeman spin during the tunneling process, and thus obtain the promised spin-dependent hopping matrix. The parameters of the simulation can be found in table 2.3. The fidelity of the simulated hopping process is $\mathcal{F}^2 > 88\%$. A meaningful estimate is made here difficult by the fast oscillations appearing on top of the slow Rabi oscillations; we give here a lower bound, given by the lower envelope of the curve.

In comparison with figure 2.5, the Rabi oscillations of figure 2.7 present additional fast oscillations of small amplitude; and also do not reach perfect state transfer. The reason can be found in the inset of figure 2.7, which shows that a fraction of the population has been transferred to the states $|F = 9/2; m_F = 7/2; 1\rangle$ and $|F = 9/2; 9/2; 3\rangle$. This is the result of the on-site spin-flipping transitions which have to be avoided using the lattice staggering.

The fact that they are not completely suppressed means that the simulation uses parameters which are not optimal; in particular, the system would benefit from larger staggering values. Finally, we also mention that the lattice staggering introduces an asymmetry between the two sites. As a consequence, the different ac-Stark shifts of the levels with $k = 1$ and $k = 3$ due to the Raman beams must be accounted when selecting the laser frequencies. We note that these corrections turn out to be crucial for achieving an optimal population transfer.

We have demonstrated that the Raman-assisted tunneling scheme leads to both diagonal and non-diagonal tunneling events. Note that the achieved fidelities above $\mathcal{F}^2 > 88\%$ highlight the accuracy of our scheme, and show that only energy-based selection rules, together with lattice staggering, suffice to allow the desired tunneling.

2.4 From a Spin-Dependent Hopping to a Quantum Simulator

In the previous section, we discussed how the superlattice geometry could be used to create non-trivial hopping processes on each link. Here we want to assemble these ingredients and discuss how to use them to engineer a quantum simulator in arbitrary dimensions.

First of all, we stress that the lasers needed to engineer the hopping along one direction must transfer momentum along that same direction (see equation (2.7)). Therefore, just by controlling the beam propagation directions, we can tailor different tunneling processes along each axis. This is an important feature which will be largely exploited in the proposals listed in chapter 3 (see for example tables 3.1 and 3.3, which list the different hopping matrices that must be engineered for each particular model of interest). This kind of *directionality selection rule* is also responsible for avoiding the population of higher-order minima which do not lie on the edges of the unit lattice cell. Since they are not connected to the main minima by a line parallel to a Cartesian axis, we do not consider any momentum transfer along such direction, and thus the formal orthogonality of the Wannier functions localized in those minima is never lifted.

Due to the very general formulation of the superlattice potential, the setup is well-suited also to work in two and one dimensions. Moreover in one dimension it is possible to use polarization selection rules to selectively couple different atomic levels. In order to favor the experimental realization of this setup, it is important to characterize the most interesting simulatable one-dimensional systems, where the presence of more symmetries can lower the experimental intricacies. We partially address this question in chapter 3, where we argue that several one-dimensional topological insulators can be realized. In a three- or two-dimensional case, only energy-based selection rules are reliable; the discussion in section 2.3 already showed that these are enough. Let us stress that if the spin quantization axis $\hat{B}$, given by the external magnetic field, is not chosen along a highly symmetric axis of the lattice, even a Raman coupling polarized with respect to its propagation axis, i.e. one of the axes of the lattice, can contain all the polarizations in the basis of $\hat{B}$. As sketched in figure 2.8, the polarization matching the addressed transition will drive it whereas the other ones, being

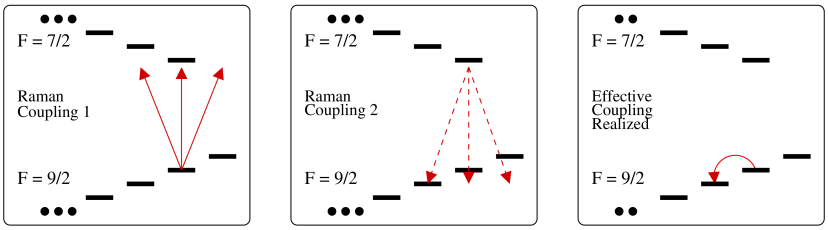

Figure 2.8: The scheme does not rely on any polarization selection rule and therefore does not face any fundamental problem once considered in two and three dimensions. If the Raman coupling is not polarized with respect to the quantization axis of the hyperfine levels, all the polarizations are present, even if with different intensities. The first and second Raman couplings drive therefore an effective population transfer between two states with different hyperfine spin even without engineering polarized couplings; energy detuning is enough. Reproduced from [MBG+12].

detuned, will have negligible effect.

Unfortunately, energy-based selection rules do not prevent, in the case of spin-flipping hopping rates, spurious on-site spin-flipping couplings. We proposed to solve this issue by staggering the optical lattice, i.e. lifting the degeneracy of the lattice sites of some tens of kHz (see also the discussion in reference [GD10]). One should also mention that the diagonal hopping matrix can still be engineered in presence of such staggering, with the only additional issue of using two Raman couplings (as in the non-diagonal case) to match the energy difference between sites.

Regarding the form of the staggering potential, we propose to use a separable one: $V_{\mathrm{st1}}(\mathbf{x}) = V(\mathbf{x}) - V_2 \sum_i \cos^2\left(\frac{qx_i}{2}\right)$. The separability of the potential V_{st1} allows us to apply the developed theory and in particular the directionality selection rule. The absolute value of the energy differences between neighboring sites is $\sim V_2$, which is what we studied in subsection 2.3.5. A calculation done using equation (2.6) shows that given the propagation direction of the Raman couplings, the effective hopping does not depend on whether the initial site was the staggered one or not. Alternatively, we also considered explicitly the case of a two-dimensional lattice staggered by a non-separable potential: $V_{\mathrm{st2}}(\mathbf{x}) = V(\mathbf{x}) - V_2 \cos^2\left(\frac{qx_1+qx_2+qx_3}{2}\right)$, which may be of some experimental relevance. The corresponding two- and three-dimensional Wannier functions are not anymore a product of one-dimensional ones and a Raman coupling can induce hopping in the direction transverse to its propagation. We computed numerically the band-structure and Bloch functions of the staggered two-dimensional system for the proposed lattice parameters. The wavefunctions differ from those of the case $V_2 = 0.0$ by less than 1% of the averaged maxima of the wavefunctions. This leads us to the conclusion that they can be nicely approximated by product wavefunctions, for which the directionality selection rule applies. Spurious couplings in the orthogonal directions introduce noise which is negligible with respect to the fidelity of the non-diagonal hopping discussed in section 2.3.5.

Each of the matrix elements of the hopping matrix is realized via an effective

four-photon process. This means that the spin of the atom can be flipped of at most $|\Delta m_F| = 4$: a careful analysis is needed in case one is interested in simulating a theory with more than 4 fields, because some hopping matrix elements might be not engineerable.

Finally, the description given in this proposal is essentially at the single-particle level where no many-body effects have been used. As a consequence, the proposal works both for bosons and fermions.

Before concluding, we would like to mention some possible technical issues which should be addressed before running an experiment. First, in the absence of an efficient taming of the atomic interactions, which has been assumed through the whole chapter, the gas could be collisionally unstable; spin exchange and dipolar relaxation could indeed populate non-physical states or even lead to losses. A quantification of such effects strongly depends on the chosen atomic system and goes therefore beyond the scope of this chapter. Such an estimate would also identify the regime of controlled interactions in which the quantum simulator would explore interacting relativistic field theories and interacting topological insulators (chapter 3). We leave this topic for future work.

Second, in the previous sections the possibility of realizing the needed Raman coupling has been always assumed, this technique being currently developed in cold-atom laboratories. We mention here the lifetime issue which one would face in presence of transitions which are not enough detuned from the excited states. This issue also requires accurate system-dependent quantification before setting up an experiment and goes beyond the scope of this thesis.

* * *

This concludes the description of the optical superlattice proposal. We have provided the relevant results supporting the initial claim that it is indeed possible to realize a system whose low-energy structure is described by Hamiltonian (2.2). In the next two chapters we will discuss some possible applications of the system.

Chapter 3

Non-Interacting Relativistic Theories and Topological Insulators

In this chapter we discuss some applications of the optical superlattice scheme presented in chapter 2 as a quantum simulator [BMR+10, MBG+12]. In particular, we focus on non-interacting lattice field theories for relativistic fermions [Kog83] and topological insulators [HK10, QZ11].

The task of an analog quantum simulator is to engineer a system described by an effective Hamiltonian $\hat{H}_{\text{eff}}$ that reproduces faithfully the properties of the model to be simulated. In our case, this model corresponds to relativistic fermions $\hat{H}_{\text{rel}}$, or topological insulators $\hat{H}_{\text{top}}$. The resource to be used is the control over the setup, which we have argued previously to be described by the Hamiltonian (2.2), rewritten here for reading convenience,

$$\hat{H}_{\text{sys}} = \sum_{\mathbf{r}\boldsymbol{\nu}} \sum_{\tau\tau'} t_\nu \, \hat{a}^\dagger_{\mathbf{r}+\boldsymbol{\nu}\tau'} [U_{\boldsymbol{\nu}}]_{\tau'\tau} \hat{a}_{\mathbf{r}\tau} + \sum_{\mathbf{r}} \sum_{\tau\tau'} \Omega \, \hat{a}^\dagger_{\mathbf{r}\tau'} [\Lambda]_{\tau'\tau} \hat{a}_{\mathbf{r}\tau} + H.c. \tag{3.1}$$

where $\hat{a}^{(\dagger)}_{\mathbf{r},\tau}$ are fermionic operators satisfying canonical anticommutation relations.

The main objective of this chapter is to provide concrete recipes for the values of:

1. the optical lattice dimension D;
2. the tunneling strengths t_ν;
3. the spin-dependent hopping matrices $U_{\boldsymbol{\nu}}$;
4. the on-site Raman transitions Ω, Λ;

such that the Hamiltonian of equation (3.1) simulates the desired physics:

$$\hat{H}_{\text{sys}}(\{t_\nu, U_{\mathbf{r}\boldsymbol{\nu}}, \Lambda, \Omega\}) \;\rightarrow\; \hat{H}_{\text{eff}} \approx \hat{H}_{\text{rel}},\, \hat{H}_{\text{top}}.$$

Phases of matter displaying non-conventional properties are usually associated to interactions. Graphene [CNGP+09] and the integer quantum Hall effect (IQHE) [vK86] are relevant exceptions; they are satisfactorily described by

quadratic, and thus non-interacting, fermionic Hamiltonians and still display characteristics, e.g. transport properties, which deviate from standard solid-state theory. The low-energy excitations of graphene display properties similar to those of massless relativistic fermions, since the Fermi surface is composed of two isolated points and their energy depends linearly on the momentum. In the IQHE, a two-dimensional electron gas subject to a strong magnetic field displays a robust quantization of the transverse conductivity $\sigma_{xy} = n \cdot e^2/h$, where $n \in \mathbb{Z}$.

Graphene and IQHE can be considered as the paradigmatic examples of effective relativistic theories in condensed-matter systems, and of topological insulators, respectively. In this chapter we show that the optical superlattice scheme can be used as a quantum simulator of these phenomena: in section 3.1 we focus on non-interacting relativistic theories; in section 3.2 we address topological insulators.

Even if these models can be solved exactly with classical methods, designing a setup mimicking their properties is the first step towards the use of a quantum simulator to answer related open problems, as for instance that of interacting topological insulators. We elaborate on this in section 3.3.

The work presented in this chapter has significantly benefited from the collaboration with Dr. A. Bermudez and Dr. N. Goldman under the supervision of Prof. M. Lewenstein and Prof. M. A. Martin-Delgado; their contribution is gratefully acknowledged.

3.1 Relativistic Lattice Fermions

The properties of a relativistic spin-1/2 fermion with mass m are described by the Dirac Hamiltonian [PS95]:

$$\hat{H} = \int \mathrm{d}\mathbf{r}\ \hat{\Psi}(\mathbf{r})^\dagger H_{\mathrm{DI}} \hat{\Psi}(\mathbf{r}), \qquad H_{\mathrm{DI}} = c\boldsymbol{\alpha} \cdot \mathbf{p} + mc^2\beta; \tag{3.2}$$

where α_ν, β are the so-called Dirac matrices fulfilling the Clifford algebra:

$$\{\alpha_\nu, \alpha_\mu\} = 2\delta^{\nu\mu}, \qquad \{\alpha_\nu, \beta\} = 0;$$

and c stands for the speed of light. Here, $\hat{\Psi}(\mathbf{r})^{(\dagger)}$ is the N_D-component fermionic field operator satisfying canonical anticommutation relations, where $N_D = 2$ for one and two spatial dimensions, and $N_D = 4$ for three spatial dimensions.

We now consider the Hamiltonian in (3.1) and discuss a tuning of the parameters which let it resemble the field theory in (3.2). It is worth mentioning that the optical superlattice scheme is strictly non-relativistic, being composed of a cold atomic gas, and that its physics is only *effectively* relativistic. For instance, the effective speed of light is $c_{\mathrm{eff}} \approx 5 \cdot 10^{-6} \div 5 \cdot 10^{-5}$ m/s and has therefore no connection with the real one, $c \sim 299 \cdot 10^6$ m/s.

3.1.1 Massless and Massive Dirac Fermions

The number of atomic fermionic species to be considered is N_D. We propose to engineer translationally invariant hopping operators, $U_\nu = e^{\mathrm{i}\phi_\nu \alpha_\nu}$, according

D	α_x	α_y	α_z	β	Γ	Θ_{T}
1	σ_x			σ_z	α_x	$\mathrm{i}\sigma_y$
2	σ_x	σ_y		σ_z		$\mathrm{i}\sigma_y$
3	$\sigma_z \otimes \sigma_x$	$\sigma_z \otimes \sigma_y$	$\sigma_z \otimes \sigma_z$	$\sigma_x \otimes \mathbb{I}_2$	$-\mathrm{i}\alpha_x\alpha_y\alpha_z$	$\mathrm{i}\mathbb{I}_2 \otimes \sigma_y$

Table 3.1: Quantum simulator of Dirac fermions. Hopping matrices of the optical superlattice are defined as $U_\nu = \exp[i\phi_\nu\alpha_\nu]$, and α_ν are listed in the table for different spatial dimensions D. We also list the Dirac matrices β, which are relevant for the massive case, and the matrices Γ and Θ_{T}, useful for discussing the symmetry of the model.

to the SU(N_D) group. For the particular choices specified in table 3.1, the momentum-space representation of Hamiltonian (3.1) is

$$\hat{H} = \sum_{\mathbf{k}\in \mathrm{BZ}} \hat{\Psi}^\dagger_{\mathbf{k}} \left(\sum_\nu 2t_\nu \cos\phi_\nu \cos(k_\nu a)\mathbb{I} + 2t_\nu \sin\phi_\nu \sin(k_\nu a)\alpha_\nu \right) \hat{\Psi}_{\mathbf{k}}; \qquad (3.3)$$

where $\Psi_{\mathbf{k}}$ is the multicomponent fermionic operator comprising the atomic levels involved in the simulation, $\mathbf{k}$ is defined within the first Brillouin zone (BZ) and a is the lattice constant.

For $\phi_\nu = \pi/2$, the energy spectrum develops $\mathcal{N}_D = 2^D$ degeneracy points, $\mathbf{K_d}$, where the energy bands touch: $E(\mathbf{K_d}) = 0$. Around these points $\mathbf{K_d} = (d_x\pi/a, d_y\pi/a, d_z\pi/a)$, where $d_\nu \in \{0, 1\}$ is a binary variable, the low-energy excitations of the atomic gas are described by the effective Hamiltonian:

$$\hat{H}_{\mathrm{eff}} = \sum_{\mathbf{d}} \sum_{\mathbf{p_d}} \hat{\Psi}^\dagger(\mathbf{p_d})\, H^{\mathbf{d}}_{\mathrm{DI}}\, \hat{\Psi}(\mathbf{p_d}), \qquad H^{\mathbf{d}}_{\mathrm{DI}}(\mathbf{p_d}) = c\boldsymbol{\alpha}^{\mathbf{d}} \cdot \mathbf{p_d}; \qquad (3.4)$$

where $\mathbf{p_d} = \mathbf{k} - \mathbf{K_d}$ represents the momentum around the degeneracy points, $(\boldsymbol{\alpha}^{\mathbf{d}})_\nu = (-1)^{d_\nu}\alpha_\nu$ are the Dirac matrices listed in table 3.1. The role of the effective speed of light, $c = 2t_x a = 2t_y a = 2t_z a$, is played by the Fermi velocity; since $a \approx 500$ nm and $t_\nu \approx 10^2 \div 10^3$ Hz we obtain the estimates presented above. Therefore, the Fermi surface of the half-filled gas consists of a set of isolated points, the so-called Dirac points, and the low-energy excitations around those points behave according to the Hamiltonian of massless Dirac fermions in equation (3.4).

The number of relativistic fermionic species is $\mathcal{N}_D$, each located around a different Dirac point, and it is even. The doubling of fermionic species is a well-known phenomenon in lattice gauge theories [Kog83], where the fermions in equation (3.4) are called *naive Dirac fermions* [KS81]. As predicted by the Nielsen-Ninomiya theorem [NN80, NN81], the doubling cannot be avoided without breaking an underlying symmetry of the model.

For D odd, such symmetry is the *chiral symmetry* (see table 3.1 for the definition of the Γ matrix):

$$[\Gamma\,,\, H_{\mathrm{DI}}] = 0. \qquad (3.5)$$

There is no chiral symmetry for D even [Kap09]; let us briefly elaborate on this. The generators of the Lorentz group, i.e. the matrices which leave the Minkowski metric $\eta^{\mu\nu}$ unchanged, can be written in terms of the $D+1$ γ^μ matrices, which

are defined by the following relation: $\{\gamma^\mu, \gamma^\nu\} = 2\eta^{\mu\nu}$. A possible explicit construction is given using the α_ν and β matrices already introduced: $\gamma^0 = \beta$ and $\gamma^j = \beta\alpha_j$. Consistently with the matrices listed in table 3.1, for $D = 2k-1$ and $D = 2k$ the smallest matrix representation has dimension 2^k. Therefore, the matrices γ^μ for $\mu \leq 2k$ can be chosen to be the same in the cases $D = 2k-1$ and $D = 2k$. This implies the existence of one matrix, γ^{2k+1}, which commutes with all the γ^μ matrices needed to generate the Lorentz group in odd spatial dimensions. The matrix Γ is proportional to γ^{2k+1} and commutes by construction with all the α_ν. The proportionality constant is chosen to make Γ Hermitian. Clearly, this construction is impossible for D even.

Let us consider a more general symmetry which protects the presence of an even number of Dirac cones and applies also for D even. It is the *time-reversal symmetry*, which is antiunitary:

$$\Theta_{\mathrm{T}}^\dagger \left[H_{\mathrm{DI}}^{\mathbf{d}}(-\mathbf{p_d})\right]^* \Theta_{\mathrm{T}} = H_{\mathrm{DI}}^{\mathbf{d}}(\mathbf{p_d}). \tag{3.6}$$

In this case, the Kramer's degeneracy theorem forces the presence of Dirac cones in all the highly-symmetric $\mathbf{K_d}$ points[1]. It follows that if we take as Fermi energy the energy which makes the Dirac cone we want to study half filled, the low-energy physics is affected by the presence of other gapless excitations at different momenta.

These results show that the optical superlattice scheme can be used as a quantum simulator of *massless Dirac fermions* in any spatial dimension. It is possible to make these fermions massive, as in Hamiltonian (3.2). We propose to control the on-site Raman transitions such that matrix Λ in (3.1) equals the matrix β listed in table 3.1. In such case, the Rabi frequency plays the role of the mass $mc^2 = 2\Omega$, and the effective Hamiltonian in equation (3.4) becomes

$$H_{\mathrm{DI}}^{\mathbf{d}}(\mathbf{p_d}) = c\boldsymbol{\alpha}^{\mathbf{d}} \cdot \mathbf{p_d} + mc^2\beta. \tag{3.7}$$

Therefore, the quantum simulator can span models from the non-relativistic regime ($pc \ll mc^2$) to the ultra-relativistic limit ($pc \gg mc^2$). Notice that the presence of the mass already breaks the mentioned symmetries but does not solve the doubling problem, since no massless Dirac fermion is left.

3.1.2 Wilson Fermions

From a lattice gauge theory perspective, the additional fermions around $\mathbf{K_d} \neq \mathbf{0}$ are spurious doublers that modify the physics at low energy and prevent the study of a single fermionic species. Among the solutions which have been proposed, it was suggested to give the doublers a very large mass $m_{\mathbf{K_d}}c^2$, so that they effectively decouple from the low-energy physics of the Dirac fermion at $\mathbf{K_d} = \mathbf{0}$, namely $m_{\mathbf{K_d}} \gg m_{\mathbf{K_0}}$.

By combining the laser-assisted tunneling listed in table 3.1 with the additional terms $U'_{\boldsymbol{\nu}} = \mathrm{i}e^{\mathrm{i}\varphi_\nu\beta}$, the Hamiltonian $\hat{H}$ in (3.3) becomes $\hat{H} + \hat{H}'$, where

$$\hat{H}' = \sum_{\mathbf{k}\in \mathrm{BZ}} \hat{\Psi}_{\mathbf{k}}^\dagger \left(\sum_\nu 2t'_\nu \cos\varphi_\nu \sin(k_\nu a)\mathbb{I} - 2t'_\nu \sin\varphi_\nu \cos(k_\nu a)\beta \right) \hat{\Psi}_{\mathbf{k}}, \tag{3.8}$$

[1] Strictly speaking more exotic situations can happen, as for example a quadratic band touching around the highly symmetric points. They do not change the final result of the reasoning.

where t'_ν are the additional laser-assisted tunneling strengths. Once more, for the π-flux phases $\varphi_\nu = \pi/2$, the effective Hamiltonian in equation (3.2) is modified into:

$$H^{\mathbf{d}}_{\mathrm{DI}}(\mathbf{p_d}) = c\boldsymbol{\alpha}^{\mathbf{d}} \cdot \mathbf{p_d} + m_{\mathbf{K_d}} c^2 \beta, \qquad m_{\mathbf{K_d}} = m - \sum_\nu (-1)^{d_\nu} m_\nu, \tag{3.9}$$

where $m_\nu c^2 = 2t'_\nu$.

The optical superlattice scheme provides the control over the different masses, since m depends on the on-site Raman transition strengths, whereas m_ν depends on the assisted-hopping strength, and thus on the laser power. In particular, when these parameters fulfill $\sum_\nu m_\nu = m$ (i.e. $m_x = m$ for $D = 1$, $m_x + m_y = m$ for $D = 2$, and $m_x + m_y + m_z = m$ for $D = 3$), there is a single massless Dirac fermion at $\mathbf{K_d} = \mathbf{0}$, whereas the doublers are massive. This discussion shows that the optical superlattice scheme can be used as a quantum simulator of the so-called *Wilson fermions* in any spatial dimension [Wil77].

The introduced mass terms responsible for the decoupling explicitly break the discussed symmetries, thus there is no violation of the Nielsen-Ninomiya theorem. This is particularly important in odd dimensions, because the Wilson fermion arising from this procedure has not a defined chirality, and thus prevents the study on a lattice of particles, such as neutrinos, which are believed to be chiral and massless.

3.1.3 Kaplan Fermions

In order to preserve the concept of chirality in a lattice with odd spatial dimensions $D = 2k - 1$, Kaplan showed that an embedding in a higher-dimensional system $D = 2k$ can lead to the appearance of chiral massless Dirac fermions bound to a $(2k-1)$-dimensional wall [Kap92, Kap09].

Let us consider even dimensions, $D = 2$, and a mass term whose strength depends on the y coordinate:

$$m(\mathbf{r}) = |m| - 2|m|\,\theta(y - y_0) \tag{3.10}$$

If the space is continuous, there are solutions of the Dirac equation $\psi(x, y, t) = \psi(x, t)\psi(y)$ such that $\psi(y) \propto e^{-|m||y-y_0|}$ and such that $\psi(x, t)$ satisfies the Dirac equation for a chiral one-dimensional fermion. The method works also if the discontinuous $m(\mathbf{r})$ in (3.10) is substituted by a smooth function $m(\mathbf{r}) = f(y)$ such that $f(y) \xrightarrow{y\to\pm\infty} \mp m$ and $f(y_0) = 0$. The wavefunction $\psi(y)$ is still localized around y_0, even if localization properties benefit from the sharp behavior of $m(\mathbf{r})$.

The idea can be translated to a discrete space via the Wilson mechanism explained above. In a lattice situation the idea is to engineer a Wilson mass which is space dependent:

$$m_\nu = |m|\,\theta(y - y_0); \qquad \begin{cases} m_{\mathbf{K_d}=(0,0)} = |m| - 2|m|\,\theta(y - y_0); \\ m_{\mathbf{K_d}=(\pi,0)} = |m|; \\ m_{\mathbf{K_d}=(0,\pi)} = |m|; \\ m_{\mathbf{K_d}=(\pi,\pi)} = |m| + 2|m|\,\theta(y - y_0). \end{cases} \tag{3.11}$$

Only the fermion at $\mathbf{K_d} = (0, 0)$ gets a mass which has opposite sign for $y \to \pm\infty$ and only this fermion behaves along the x direction as a fermion with well-defined chirality.

Kaplan fermions can be realized in a finite system with open boundary conditions making the mass of one of the Wilson fermions negative. Let us provide an intuitive argument for this. In the example of (3.11), the mass of the Wilson fermion is negative in the region $y \in [y_0, +\infty)$, and this was crucial to obtain the localized fermion. Intuitively, we can compactify the y dimension with the point at the infinite and then deform $[0, +\infty]$ into $[0, L_y]$. Let us think at the complementary region as a region with infinite positive mass. Two Kaplan fermions are expected to appear localized at the boundaries $y = 0, L_y$. The fermion at $y = L_y$ corresponds to the solution which in the infinite-space case had to be neglected because non-normalizable $\psi(y) \propto e^{+|m||y-y_0|}$ and which in this case can be retained. We provide numerical evidence of the Kaplan mechanism via mass inversion in section 3.2.3.

Kaplan fermions obtained via mass inversion bring our discussion to the next topic, as it is always possible to find a Kaplan-fermion representative within each class of topological insulators [QHZ08, RSFL10].

3.2 Topological Insulators

The study of topological insulators indirectly dates back to the discovery of the IQHE in 1980 [vK86], but was established as a research field in itself only in the last years [HK10, QZ11]. It is a relatively young research subject and therefore we present here a short review of its most fundamental concept, namely *topological band theory*.

Topological band theory generalizes the usual solid-state band theory, which has successfully been used to classify insulators, semiconductors and metals [AM76]. It has been introduced to characterize materials with an insulating bulk and remarkably robust conducting edge modes, and that therefore elude the standard classification. From the mathematical point of view, it focuses on quadratic fermionic models and sorts them according to a non-trivial topological integral of the bulk spectrum, which also carries information about the edge modes. Let us stress that the framework of this analysis is that of single-particle physics and that the presented topological considerations are different from those discussed in [Wen04] to study topological order in strongly-correlated systems.

3.2.1 A Model for the Integer Quantum Hall Effect

The toy model for a first understanding of topological band theory is the Harper Hamiltonian [Har55, Hof76] describing free fermions in a two-dimensional square lattice subject to an external magnetic field $\mathbf{B} = Be_z$, with $\mathbf{A}(\mathbf{r}) = Bxe_y$ being the corresponding vector potential:

$$\begin{aligned} \hat{H}_{\mathrm{QH}} &= -J \sum_{<\mathbf{m},\mathbf{n}>} \hat{a}^\dagger_{\mathbf{n}}\, e^{-i\frac{2\pi}{\Phi_0}\int_{\mathbf{m}}^{\mathbf{n}} \mathbf{A}(\mathbf{r})\cdot d\mathbf{l}}\, \hat{a}_{\mathbf{m}} = \\ &= -J \sum_{\mathbf{m}} \hat{a}^\dagger_{\mathbf{m}} \hat{a}_{\mathbf{m}+a\hat{e}_x} + \hat{a}^\dagger_{\mathbf{m}+a\hat{e}_x} \hat{a}_{\mathbf{m}} + \\ &\quad -J \sum_{\mathbf{m}} e^{2\pi i \frac{\Phi}{\Phi_0} m_x}\, \hat{a}^\dagger_{\mathbf{m}} \hat{a}_{\mathbf{m}+a\hat{e}_y} + e^{-2\pi i \frac{\Phi}{\Phi_0} m_x}\, \hat{a}^\dagger_{\mathbf{m}+a\hat{e}_y} \hat{a}_{\mathbf{m}}. \end{aligned} \tag{3.12}$$

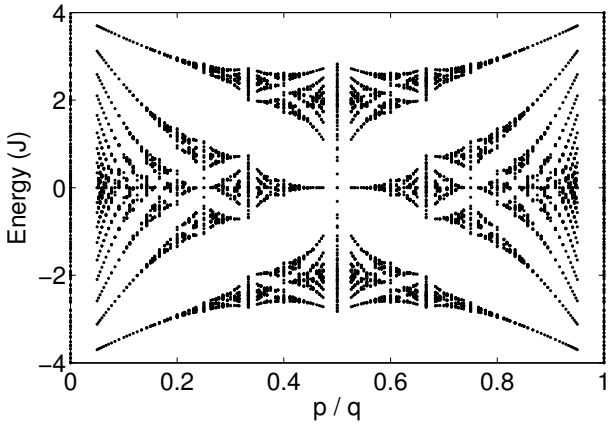

Figure 3.1: The spectrum of Hamiltonian (3.13) studied with periodic boundary conditions with $\Phi/\Phi_0 = p/q$ for $q \leq 20$ and $\gcd(p,q) = 1$. For a given value p/q, the energy spectrum displays q separate bands. This plot is known as the *Hofstadter butterfly* [Hof76].

where $\mathbf{m} = (m_x a, m_y a)$ and a is the lattice spacing. The field operators $\hat{a}^{(\dagger)}_{\mathbf{m}}$ are fermionic, $\Phi_0 = hc/e$ is the quantum of flux and Φ is the flux per plaquette. This model is a topological insulator and it has some relevance in the theory of the IQHE.

Let us start considering periodic boundary conditions, i.e. the bulk properties of the model. We consider a lattice of $L_x \times L_y$ sites; the Hamiltonian can be diagonalized working in momentum space. The reciprocal lattice is spanned by the vectors $\mathbf{g}_1 = \frac{2\pi}{a}(1,0)$ and $\mathbf{g}_2 = \frac{2\pi}{a}(0,1)$. Let's consider a rational magnetic flux through one lattice plaquette $\Phi = p/q\,\Phi_0$, with $p, q \in \mathbb{N}$ and $\gcd(p,q) = 1$. We introduce the Fourier transform of the operators:

$$\hat{a}_{\mathbf{k}} = \frac{1}{\sqrt{L_x L_y}} \sum_{\mathbf{m}} e^{i\mathbf{m}\cdot\mathbf{k}}\, \hat{a}_{\mathbf{m}};$$

The Hamiltonian now reads:

$$\hat{H}_{\mathrm{QH}} = -J \sum_{\mathbf{k}} 2\cos(k_x a)\, \hat{a}^{\dagger}_{\mathbf{k}} \hat{a}_{\mathbf{k}} + e^{ik_y a} \hat{a}^{\dagger}_{\mathbf{k}-\mathbf{w}} \hat{a}_{\mathbf{k}} + e^{-ik_y a} \hat{a}^{\dagger}_{\mathbf{k}+\mathbf{w}} \hat{a}_{\mathbf{k}}; \qquad (3.13)$$

with $\mathbf{w} = p/q\,\mathbf{g}_1$ and can be diagonalized. Figure 3.1 shows the spectrum of the Hamiltonian for different values of p/q; we can recognize q energy bands separated by clear energy gaps. We can therefore affirm that the system displays an insulating bulk for rational filling factors.

Still, Hamiltonian (3.13) is different from that of an ordinary insulator. The difference can be understood in terms of the Berry phase associated with the adiabatic movement of the Bloch eigenstates of $\hat{H}_{\mathrm{QH}}$, which we denote $|m, \mathbf{k}\rangle$, in the Brillouin zone. Let us consider a single band, m, and define the Berry phase γ_m which the state $|m, \mathbf{k}\rangle$ acquires moving around the whole Brillouin

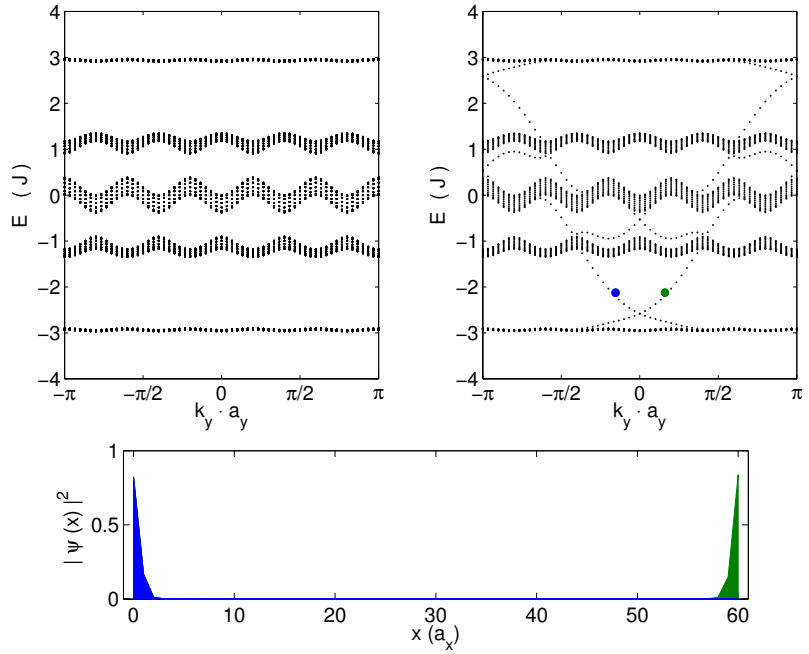

Figure 3.2: (Top, left) Spectrum of Hamiltonian (3.13) with periodic boundary conditions for $p/q = 1/5$. Five bulk bands are clearly recognizable. (Top, right) Spectrum of Hamiltonian (3.13) with cylindrical boundary conditions for $p/q = 1/5$. In addition to the bulk states, mid-gap states appear. (Bottom) The wavefunctions $|\Psi(x)|^2$ of the two mid-gap states highlighted in the top-left plot are clearly localized on the boundaries, motivating the name of *edge-states*.

zone:

$$\mathbf{A}_m(\mathbf{k}) = i \begin{pmatrix} \langle m, \mathbf{k} | \partial_{k_x} | m, \mathbf{k} \rangle \\ \langle m, \mathbf{k} | \partial_{k_y} | m, \mathbf{k} \rangle \end{pmatrix}; \quad \mathcal{F}(\mathbf{k}) = \partial_{k_x} A_{m,2}(\mathbf{k}) - \partial_{k_y} A_{m,1}(\mathbf{k}); \quad (3.14)$$

$$\gamma_m = \oint d\mathbf{k} \cdot \mathbf{A}_m(\mathbf{k}) = \int_{\mathrm{BZ}} d\mathbf{k}\, \mathcal{F}_m(\mathbf{k}). \quad (3.15)$$

It is possible to show[2] that γ_m is an integer multiple of 2π. We define $n_m = \gamma_m/2\pi \in \mathbb{Z}$ and speak of a *topologically non-trivial band* whenever $n_m \neq 0$.

When the energy bands are either completely filled or empty, the transverse conductivity σ_{xy} is related to the values n_m via the TKNN formula [TKNdN82], which is obtained via the application of the Kubo formula for electric conductivity to this problem[3]:

$$\sigma_{xy} = \frac{e^2}{h} N = \frac{e^2}{h} \sum_{\substack{\text{filled} \\ \text{bands } m}} n_m. \quad (3.16)$$

[2]The mathematical details can be found in chapter 10 and 11 of reference [Nak03a].

[3]The Kubo formula for AC electric conductivity can be find in [AM76], equation (13.37). In order to obtain the formula used in [TKNdN82] one has to first take the static limit $\omega \to 0$ and then the zero-temperature limit.

This relation shows the existence of an observable quantity, namely the transverse conductivity, which is quantized, and robust against moderate disorder. Indeed, the values n_m are insensitive to continuous deformations of the band structure which do not close any energy gap; such deformations may arise, as mentioned, in presence of moderate disorder, or, more generally, of local perturbations of the Hamiltonian.

Let us now consider Hamiltonian (3.13) with cylindrical boundary conditions. When we impose open edges only in one direction, the spectrum shows the presence of mid-gap eigenvalues whose eigenfunctions are localized on the open edge (see figure 3.2).

The quantized Hall conductivity can be characterized also using the edge states, as shown in [RTJH83], via the relation:

$$\sigma_{xy} = \frac{e^2}{h} \sum_{\substack{\text{right} \\ \text{edge}}} \operatorname{sgn}\left(\frac{\partial E_{\text{edge}}(k)}{dk}\right). \tag{3.17}$$

The comparison of equation (3.16) with (3.17) highlights a link between the topological invariant N, which is related to the bulk properties of the model, and the edge excitations. We have therefore found a *bulk-boundary correspondence*; the argument which was assuring the robust quantization of σ_{xy} now guarantees the appearance of mid-gap edge states even in presence of local perturbations.

These states are *chiral*, i.e. they have a defined wavevector k_y, and states localized on the same edge share the same propagation direction. Since the backscattering of a conduction electron requires it to jump from one edge to the opposite one, which is macroscopically separated [Hal82], the transport properties of this model are also expected to be robust against disorder.

The IQHE is only one instance of a large list of topological insulators. In general, they are quadratic fermionic models which can be represented by matrices $\mathbb{H}$ and then classified according to their fundamental symmetries: *time-reversal* $\mathcal{T}$, *charge conjugation* $\mathcal{C}$, and the combination of both $\mathcal{S} = \mathcal{T}\mathcal{C}$ [AZ97]. We say that a matrix has one such symmetry if there exists one matrix $\Theta_{\mathrm{T,C,S}}$ such that:

$$\mathcal{T}: \quad \Theta_{\mathrm{T}}\, \mathbb{H}^T\, \Theta_{\mathrm{T}}^{-1} = +\mathbb{H}; \qquad \Theta_{\mathrm{T}}\Theta_{\mathrm{T}}^{\dagger} = \mathbb{I}; \quad \Theta_{\mathrm{T}}^T = \pm\Theta_{\mathrm{T}}; \tag{3.18a}$$

$$\mathcal{C}: \quad \Theta_{\mathrm{C}}\, \mathbb{H}^T\, \Theta_{\mathrm{C}}^{-1} = -\mathbb{H}; \qquad \Theta_{\mathrm{C}}\Theta_{\mathrm{C}}^{\dagger} = \mathbb{I}; \quad \Theta_{\mathrm{C}}^T = \pm\Theta_{\mathrm{C}}; \tag{3.18b}$$

$$\mathcal{S}: \quad \Theta_{\mathrm{S}}\, \mathbb{H}\, \Theta_{\mathrm{S}}^{-1} = -\mathbb{H}; \qquad \Theta_{\mathrm{S}}\Theta_{\mathrm{S}}^{\dagger} = \mathbb{I}; \quad \Theta_{\mathrm{S}}\Theta_{\mathrm{S}} = +\mathbb{I}. \tag{3.18c}$$

The $\mathcal{T}$ and $\mathcal{C}$ symmetries are be labelled by two numbers, ± 1, depending on the value of $\Theta_{\mathrm{T,C}}^T\Theta_{\mathrm{T,C}}^{\dagger}$. The $\mathcal{S}$ symmetry has only one label $S = 1$.

Topological insulators have been classified according to this set of symmetries [SRFL08, Kit09], and a periodic table has been accordingly derived, partially reported in table 3.2. The IQHE model we have studied belongs for example to class A. The table is incomplete because four symmetry classes have been excluded; they correspond to models which do not conserve the number of particles, also named topological superconductors. Their quantum simulation requires a pairing mechanism, which is not provided by Hamiltonian (3.1)[4].

[4] A discussion of one topological superconducting model, the Kitaev chain, is presented in chapter 7.

Class	**Name**	T	C	S	$D=1$	QS	$D=2$	QS	$D=3$	QS
A	Unitary	0	0	0	0		$\mathbb{Z}$	yes	0	
AIII	Chiral unitary	0	0	1	$\mathbb{Z}$	yes	0		$\mathbb{Z}$	yes
AI	Orthogonal	+1	0	0	0		0		0	
BDI	Chiral Orthogonal	+1	+1	1	$\mathbb{Z}$	?	0		0	
AII	Symplectic	−1	0	0	0		$\mathbb{Z}_2$	yes	$\mathbb{Z}_2$	yes
CII	Chiral Symplectic	−1	−1	1	$2\mathbb{Z}$	yes	0		$\mathbb{Z}_2$	yes

Table 3.2: Periodic table of topological insulators [SRFL08, Kit09]. There are six possible symmetry classes for non-interacting fermionic Hamiltonians conserving the number of particles and another four for pairing Hamiltonians, not shown here. The topological insulator is characterized by the *integer* $\mathbb{Z}$ or *binary* $\mathbb{Z}_2$ nature of the topological invariant. Notice that in a given spatial dimension D only some of the classes can appear. In the column QS, we list the particular instances that can be simulated with the superlattice quantum simulator.

We now discuss how the optical superlattice of chapter 2 can reproduce the properties of several classes of topological insulators; we follow two possible strategies.

3.2.2 Bottom-Up Approach

In this case, we propose to identify a specific topological insulator model and to tune the parameters of Hamiltonian (3.1) accordingly. In principle, a different experiment would be required for each simulation.

Two simple one-dimensional examples are the Su-Schrieffer-Hegger model of polyacetilene [SSH79], which is a $D=1$ BDI topological insulator; and the $\pi-$flux phase of the fermionic Creutz ladder [Cre99], which is a $D=1$ AIII topological insulator.

The former is rather simple and can be simulated without the optical superlattice. By using a one-component Fermi gas in a one-dimensional dimerized optical superlattice, one directly obtains:

$$\hat{H}_{\mathrm{BDI}} = \sum_n (t-\delta)\hat{a}^\dagger_{2n-1}\hat{a}_{2n} + (t+\delta)\hat{a}^\dagger_{2n}\hat{a}_{2n+1} + H.c. \tag{3.19}$$

where δ quantifies the different tunneling strength between superlattice sites.

On the other hand, the Creutz ladder is described by

$$\hat{H}_{\mathrm{AIII}} = -K\sum_n \mathrm{e}^{-\mathrm{i}\theta}\hat{a}^\dagger_{n+1}\hat{a}_n + \mathrm{e}^{\mathrm{i}\theta}\hat{b}^\dagger_{n+1}\hat{b}_n + \hat{b}^\dagger_{n+1}\hat{a}_n + \hat{a}^\dagger_{n+1}\hat{b}_n + \frac{M}{K}\hat{a}^\dagger_n\hat{b}_n + H.c.$$

where K, M are tunneling strengths, and θ is a magnetic flux piercing the ladder. This requires two hyperfine levels to be assigned to the fermion species a_n, b_n, and a one-dimensional laser-assisted tunneling $U_{\mathbf{a}_1} = \mathrm{diag}\{\mathrm{e}^{-\mathrm{i}\theta}, \mathrm{e}^{\mathrm{i}\theta}\}$, $\tilde{U}_{\mathbf{a}_1} = \mathrm{i}\sigma_x$, together with the Raman on-site operator of strength M [BPAMD09].

Following this approach, it is possible to proceed to higher dimensions and to different topological classes.

The possibility of engineering topological insulators with cold atoms has already been discussed in the literature and this should not be considered the first

attempt. One of the most relevant examples is the honeycomb time-reversal breaking Haldane model [Hal88], a two-dimensional topological insulator of class A, which has already attracted attention [SZS+08, SGDS10, LLWS10, AFGMP+11]. Our approach is different because whereas usually a model is first identified and then an *ad hoc* setup is proposed, here we provide the general guidelines for a simulation scheme which can address many different models.

3.2.3 Symmetry-Based Approach

We propose a different approach, whose starting point is the quantum simulator of D-dimensional Wilson fermions in (3.9). Depending on the particular choice of Dirac matrices, the inverted-mass regime described in section 3.1.3 corresponds to a different class of topological insulators. Moreover, a dimensional reduction, that experimentally amounts to the increase of the optical lattice depth in one direction, brings the system to a different lower-dimensional class [QHZ08, RSFL10].

Let us explain this in more details. We start from the Hamiltonian (3.9), which we rewrite here for reading convenience:

$$\hat{H}_{\text{eff}} = \sum_{\mathbf{d},\mathbf{p_d}} \hat{\Psi}^\dagger(\mathbf{p_d}) H^{\mathbf{d}}_{\text{DI}} \hat{\Psi}(\mathbf{p_d}); \qquad H^{\mathbf{d}}_{\text{DI}}(\mathbf{p_d}) = c\alpha^{\mathbf{d}} \cdot \mathbf{p_d} + m_{\mathbf{K_d}} c^2 \beta. \tag{3.20}$$

The masses of the Wilson fermions are $m_{\mathbf{K_d}} = m - \sum_\nu (-1)^{d_\nu} m_\nu$, and the Dirac matrices $\alpha^{\mathbf{d}}_\nu, \beta$ are selected depending on the class to be simulated (see table 3.3).

The symmetries $\mathcal{T}, \mathcal{C}, \mathcal{S}$ defined in (3.18) are expressed, in this translationally-invariant case, via unitary matrices $\Theta_{\text{T}}, \Theta_{\text{C}}$ such that:

$$\mathcal{T}: \qquad \Theta^\dagger_{\text{T}} \left[H^{\mathbf{d}}_{\text{DI}}(-\mathbf{p_d})\right]^* \Theta_{\text{T}} = +H^{\mathbf{d}}_{\text{DI}}(\mathbf{p_d}); \tag{3.21a}$$

$$\mathcal{C}: \qquad \Theta^\dagger_{\text{C}} \left[H^{\mathbf{d}}_{\text{DI}}(-\mathbf{p_d})\right]^* \Theta_{\text{C}} = -H^{\mathbf{d}}_{\text{DI}}(\mathbf{p_d}); \tag{3.21b}$$

$$\mathcal{S}: \qquad \left[\Theta^\dagger_{\text{T}}\right]^* \Theta^\dagger_{\text{C}} H^{\mathbf{d}}_{\text{DI}}(\mathbf{p_d}) \Theta_{\text{C}} \Theta^*_{\text{T}} = -H^{\mathbf{d}}_{\text{DI}}(\mathbf{p_d}). \tag{3.21c}$$

In table 3.3, we characterize the symmetry properties of several Hamiltonians $\hat{H}_{\text{eff}}$, for different choices of the Dirac matrices.

It is important to note that these symmetries might or might not correspond to the exact symmetries of nature. For example, when considering the hyperfine levels $\{|F, m_F\rangle, |F, -m_F\rangle\}$, the time-reversal symmetry given by $\Theta_{\text{T}} = \mathrm{i}\sigma_y$ is exactly that of nature. Otherwise, these symmetries are related to the algebraic properties of the effective Hamiltonian. Let us emphasize, however, that as far as the disorder respects such symmetries, the robustness of the edge excitations is guaranteed. It would be interesting to design disorder breaking or preserving such symmetries, generalizing the studies on Anderson localization with cold atoms [BJB+08, GDF+08].

In order to turn the system into a topological insulator, the mass of an *odd* number of Wilson fermions must be inverted. The technique is analogous to that explained in section 3.1.3. This mass-inversion occurs through a gap-closing point, and thus a quantum phase transition between a normal band insulator and a topological one occurs. This new phase is characterized by an *odd* number of massless fermionic excitations (i.e. massless Dirac fermions) bound to the boundaries of the system, and protected by a topological invariant.

Class	D	α_x	α_y	α_z	β	Θ_{T}	Θ_{C}	$T\ C\ S$
CII	3	$\sigma_z \otimes \sigma_x$	$\sigma_z \otimes \sigma_y$	$\sigma_z \otimes \sigma_z$	$\sigma_z \otimes \mathbb{I}_2$	$\mathrm{i}\mathbb{I} \otimes \sigma_y$	$\mathrm{i}\sigma_x \otimes \sigma_y$	-1 -1 1
AIII	3	$\sigma_z \otimes \sigma_x$	$\sigma_z \otimes \sigma_y$	$\sigma_z \otimes \sigma_z$	$\sigma_y \otimes \mathbb{I}_2$	$\mathrm{i}\mathbb{I} \otimes \sigma_y$	$\mathrm{i}\sigma_x \otimes \sigma_y$	0 0 1
AII	3	$\sigma_z \otimes \sigma_x$	$\sigma_z \otimes \sigma_y$	$\sigma_z \otimes \sigma_z$	$\sigma_x \otimes \mathbb{I}_2$	$\mathrm{i}\mathbb{I} \otimes \sigma_y$	$\mathrm{i}\sigma_x \otimes \sigma_y$	-1 0 0
$\hookrightarrow$ AII	2	$\sigma_z \otimes \sigma_x$	$\sigma_z \otimes \sigma_y$		$\sigma_x \otimes \mathbb{I}_2$	$\mathrm{i}\mathbb{I} \otimes \sigma_y$	$\mathrm{i}\sigma_x \otimes \sigma_y$	-1 0 0
A	2	σ_x	σ_y		σ_z	$\mathrm{i}\sigma_y$	$\mathrm{i}\sigma_z$	0 0 0
$\hookrightarrow$ AIII	1	σ_x			σ_z	$\mathrm{i}\sigma_y$	$\mathrm{i}\sigma_z$	0 0 1
CII	1	$\sigma_z \otimes \sigma_x$			$\sigma_z \otimes \mathbb{I}_2$	$\mathrm{i}\mathbb{I} \otimes \sigma_y$	$\mathrm{i}\sigma_x \otimes \sigma_y$	-1 -1 1

Table 3.3: Quantum simulator of topological insulators. We list different realizations of Hamiltonian (3.20) that lead to the realization of several classes of topological insulators. The table shows that each class has a Wilson fermion representative via a different choice of the Clifford algebra α_ν, β. We also highlight the topological insulators that can be obtained by dimensional reduction from a parent Hamiltonian, such as $\mathrm{AII}, D = 3 \hookrightarrow \mathrm{AII}, D = 2$, or $\mathrm{A}, D = 2 \hookrightarrow \mathrm{AIII}, D = 1$. We list the unitary matrices $\Theta_{\mathrm{T}}, \Theta_{\mathrm{C}}$ used to define the symmetries (see equation (3.21)).

Let us consider for example the three-dimensional case of a topological insulator of class AII (see table 3.3). Let us consider the Wilson fermions at $\mathbf{K_d} = (0, 0, 0)$ and $(0, 0, \pi/a)$. If we set $m_y = m/2$ and $m_z = m/4$, for $1/4 < m_x < 3/4$ the mass of the Wilson fermion at $\mathbf{K_d} = (0, 0, 0)$ is negative, whereas for $m_x > 3/4$ both Wilson fermions at $\mathbf{K_d} = (0, 0, 0)$ and $(0, 0, \pi/a)$ have negative masses. Accordingly, if we now set open boundary conditions along z and focus on the states at $(k_x, k_y) = (0, 0)$, we expect zero-energy modes to appear for $1/4 < m_x < 3/4$. The result of the numerical simulation, shown in figure 3.3, confirm that the system displays two in-gap zero-energy modes localized at the edges where open boundary conditions have been imposed. Table 3.3 contains all the relevant information to explore the exotic properties of different topological insulators in a superlattice-based experiment with ultracold atoms.

3.3 Perspectives

In this chapter we have discussed some possible applications of the optical superlattice scheme presented in chapter 2 as a quantum simulator; we have focussed on fermionic non-interacting theories, ranging from relativistic field theories to topological insulators. The discussion has also tried to highlight some of the connections between the two topics.

Because of their mathematical simplicity, these models have already been theoretically understood with classical simulations, and a quantum simulation would not add new information. An experimental realization of these models is anyway mandatory in order to exploit from a more applied point of view the unconventional transport properties of topological insulators. Even if the ultimate goal, in this respect, would be a solid-state realization, contributions from the cold-atoms community are not to be excluded.

Furthermore, the combination of this proposal with the control of atomic interactions via Feshbach resonances might boost experiments into regimes where classical numerical simulations fail. We mention for example the problem of

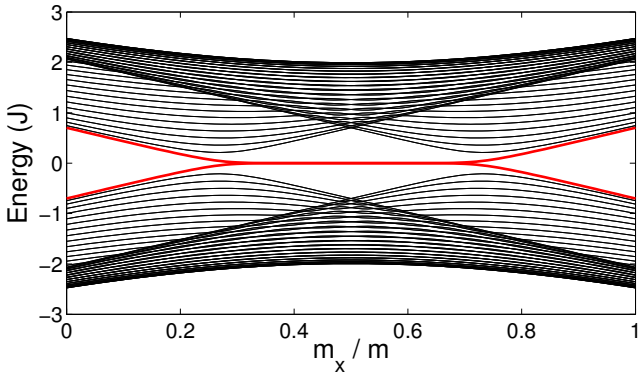

Figure 3.3: Spectrum of a three-dimensional topological insulator of class AII (see table 3.3) studied with open boundary conditions along z. We only plot the modes for $(k_x, k_y) = (0, 0)$. We consider a system of size $41 \times 41 \times 41$. Tuning the parameter m_x it is possible to turn a trivial insulator into a topological one, as it is clearly demonstrated by the presence of zero-energy modes, highlighted in red, which are localized on the boundaries.

generalizing topological insulators to the interacting case, which is recently attracting a lot of attention [WQZ10, RT10, FK11, TPB11, Gur11]. In this respect, the highly-controllable cold gases might provide relevant experimental insights.

From the point of view of the quantum simulation with cold atoms of interacting relativistic field theories, the path has been opened in 2010, with a proposal for interacting one-dimensional Dirac fermions [CMP10]. We envisage the possibility of working in the same direction using the optical superlattice scheme, where as discussed more fermionic models are available, and also in higher dimensions.

Chapter 4

Three-Body Interactions with Spin-1 Atoms

In this chapter we discuss the possibility of using cold atoms in optical lattices to study three-body contact interactions [MRLC10].

Interactions involving more than two particles can give rise to intriguing many-body phenomena. We focus on a particular state of the fractional quantum Hall effect, the so-called Pfaffian wavefunction [MR91, GWW92], which arises in two-dimensional systems subject to a magnetic field in the presence of three-body contact repulsion. Whereas such quantum state was initially proposed for electrons, a bosonic version exists as well, which shares all the interesting features of its fermionic counterpart. Let us mention, for example, that its quasi-excitations are non-Abelian anyons [JSWW03]. Furthermore, states similar to the Pfaffian wavefunction appear also in other models, such as in p-wave superconductors, where the non-Abelian excitations correspond to zero-energy Majorana fermions [RG00, NSS$^+$08, Sch99][1], or even one-dimensional systems [PKC07].

Since significant many-body interactions are rare in nature, in order to observe such phenomenology it is important to be able to externally engineer three-body interactions. Let us briefly list the most relevant proposals which exploit ultracold atomic and molecular gases to achieve this goal. To the best of our knowledge, the earliest attempts exploited higher-order super-exchange interactions on triangular and kagomé lattices [PR04]. Unfortunately, the temperatures required are even lower than those necessary for the observation of quantum magnetism in Mott phases. Super-exchange interactions of the second order involving Raman transitions between atoms and molecules in square lattices have been proposed to realize an effective ring-exchange Hamiltonian for bosons [BHH$^+$05]. A completely different approach has been proposed in [BMZ07], where it was suggested to use polar molecules dressed by laser fields inhibiting two-body interactions. Very recently it has been suggested to use the dissipative dynamics of three-body losses in order to implement an effec-

[1] Systems with zero-energy Majorana modes are the focus of chapter 7. We do not deal explicitly with a two-dimensional system displaying a ground state closely related to the Pfaffian wavefunction [RG00], but rather with the one-dimensional version, the so-called Kitaev chain [Kit01].

tive three-body hardcore constraint [DTD$^+$09, RRC10]. The idea is reminiscent of an experiment where it is shown that dissipation induces strong correlations in molecular gases [SBL$^+$08]. The combination of this dissipative scheme with the rotation of the atomic trap, which simulates an artificial magnetic field, can lead to the formation of the Pfaffian wavefunction [RRC10]. Finally, it has been theoretically shown via a perturbative treatment of higher lattice bands that the dynamics of the optical lattice contains effective many-body interactions, whose effects have also been experimentally observed in the time-evolution of the system [JTPW09, WBS$^+$10].

The aim of this chapter is twofold. On one side, we provide some numerical evidence that in a discrete two-dimensional system, in the presence of a perpendicular magnetic field, the ground state of bosons interacting via three-body contact repulsion corresponds to the lattice version of the bosonic Pfaffian wavefunction. In particular, we discuss the stability of the topological properties of such wavefunction in a non-dilute limit with the magnetic length comparable to the lattice spacing.

On the other one, we show that a spin-1 Mott insulator with one particle per site offers the possibility of studying three-body interactions in an optical lattice. The idea is to map the three internal states of real spin-1 bosons into occupation numbers of some emerging bosons, similarly to the correspondence between spin-1/2 particles and emerging hardcore bosons. An easy generalization to higher-spin atoms can open the route to the simulation of four-, five- and many-body contact infinite repulsions. The versatility of the experimental system presented in chapter 2, which individually tailor the hopping rates of the different spin species, can be used to tune several models characterized by three-body interactions. Unfortunately, the discrete Pfaffian wavefunction is outside the class of models accessible with our proposal.

In section 4.1 we describe how to realize three-body interacting bosons using atoms with three relevant internal states. In section 4.2 we consider the explicit case of atoms with $F = 1$ hyperfine ground manifold trapped in a two-dimensional optical lattice and derive the corresponding super-exchange Hamiltonian. In section 4.3 we focus on the Pfaffian wavefunction, on its lattice version and discuss the difficulties which are still to be overcome in order to engineer it.

4.1 The Mapping

Let us start recalling that particles interacting via three-body infinite repulsion effectively undergo a three-body hardcore constrain, that is, there cannot be more than two particles cannot share the same position. Therefore, in the presence of a spatially discrete setup, the local description of the wavefunction is captured by a finite Hilbert space of dimension three:

$$\mathcal{H}^{\mathrm{loc}}_{\mathrm{3hb}} = \mathrm{Span}\{|n=0\rangle, |n=1\rangle, |n=2\rangle\}. \tag{4.1}$$

We therefore propose to simulate a system subject to three-body infinite interactions using an experimental setup which is discrete and whose local Hilbert space $\mathcal{H}^{\mathrm{loc}}_{\mathrm{real}}$ has dimension three. A unitary mapping between the local Hilbert spaces:

$$\hat{\mathsf{W}} : \mathcal{H}^{\mathrm{loc}}_{\mathrm{real}} \longrightarrow \mathcal{H}^{\mathrm{loc}}_{\mathrm{3hb}}\,, \tag{4.2}$$

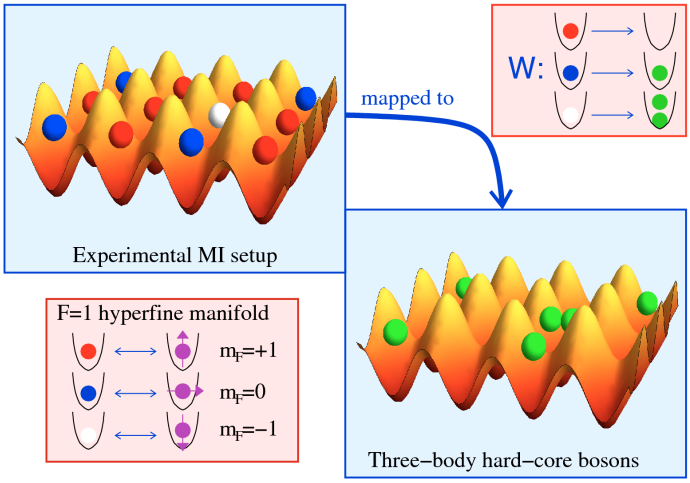

Figure 4.1: Sketch of the proposed mapping. A Mott insulator with one particle per site and whose atoms have three relevant internal states can simulate a system of bosons with an infinite three-body contact repulsion via the mapping $\hat{\mathsf{W}}$. The three relevant states can be identified with a $F = 1$ hyperfine spin. Reproduced from [MRLC10].

allows us to connect the real experimental dynamics to the dynamics of some emerging particles characterized by an infinite three-body interaction living in $\mathcal{H}^{\mathrm{loc}}_{3\mathrm{hb}}$ (see also figure 4.1). When the dynamics of the real system is described by a Hamiltonian $\hat{H}^{\mathrm{eff}}_{\mathrm{real}}$, the corresponding Hamiltonian for the system to be simulated characterized by three-body interactions is:

$$\hat{H}_{3\mathrm{hb}} = \hat{\mathsf{W}}^{\otimes L^2}\ \hat{H}^{\mathrm{eff}}_{\mathrm{real}}\ \hat{\mathsf{W}}^{\dagger\otimes L^2}\ . \tag{4.3}$$

The tuning of the experimental parameters in $\hat{H}^{\mathrm{eff}}_{\mathrm{real}}$ permits in principle the investigation of several "blackboard" models described by $\hat{H}_{3\mathrm{hb}}$.

In the context of ultracold atoms in optical lattices, it is quite natural to consider a Mott insulator with one particle per site and atoms with three internal degrees of freedom. In this chapter we focus our attention on the Zeeman levels of a hyperfine spin $F = 1$, exhibited for instance by ^{87}Rb or ^{23}Na. Such atoms have already been loaded into an optical lattice and cooled to a Mott insulator without freezing the spins [WGF$^+$06]. Because of super-exchange effects, the Mott insulator is characterized by a non-trivial spin dynamics, which, unfortunately, has still to be observed (the spin degrees of freedom have indeed not yet been cooled). This spin physics is characterized by an effective Hamiltonian $\hat{H}^{\mathrm{eff}}_{\mathrm{real}}$ obtained through a second-order perturbative expansion of the kinetic term of the Bose-Hubbard Hamiltonian describing the real atoms on the lattice. The next section is devoted to a derivation of such effective theory.

Let us conclude stressing that other internal degrees of freedom could have been chosen; as proposed in [KS03] for a different purpose, these three local degrees of freedom could even correspond to different spin-polarized atomic species.

4.2 Spin-1 Atoms

We derive the effective Hamiltonian for the spin degrees of freedom of a spin-1 Mott insulator with one particle per site and describe the class of Hamiltonians $\hat{H}_{\rm 3hb}$ which can be effectively mimicked via the proposed mapping (4.2). The analysis we present is valid for systems in one, two and three dimensions.

In order to describe spin-1 atoms in a deep optical lattice, we use the Bose-Hubbard Hamiltonian for spin systems [ILD03]:

$$\begin{aligned}\hat{H}_{\rm real} &= \sum_{<i,j>}\sum_{\alpha}[-t_\alpha \hat{b}^\dagger_{i,\alpha}\hat{b}_{j,\alpha} + H.c.] + \sum_{i,\alpha}\Delta_\alpha \hat{n}_{i,\alpha} + \\ &+\frac{U_0}{2}\sum_i \hat{n}_i(\hat{n}_i - 1) + \frac{U_2}{2}\sum_i(\vec{\hat{S}}_i^2 - 2\hat{n}_i). \end{aligned} \tag{4.4}$$

The bosonic field operators $\hat{b}^{(\dagger)}_{i,\alpha}$ satisfy canonical commutation relations, $\alpha = \{-,\circ,+\}$ runs over the three spin states $\{|m_F=-1\rangle,\ |m_F=0\rangle,\ |m_F=+1\rangle\}$ and:

$$\hat{n}_{i,\alpha} = \hat{b}^\dagger_{i,\alpha}\hat{b}_{i,\alpha}; \qquad \hat{n}_i = \sum_\alpha \hat{n}_{i,\alpha}; \qquad \left(\vec{\hat{S}}_i\right)_{\alpha,\beta} = \hat{b}^\dagger_{i,\alpha}\vec{F}_{\alpha,\beta}\hat{b}_{i,\beta}\,.$$

The operator $\vec{\hat{S}}_i$ is the spin-operator at the site i; the parameters Δ_α represent the energy offset of each of the three states ($\Delta_\circ = 0$). The last two terms of (4.4) describe the local two-body interaction, that due to the spin nature of atoms is characterized by two s-wave scattering lengths, a_0 for the $S^{\rm tot}=0$ channel and a_2 for the $S^{\rm tot}=2$ channel, with the ratio U_2/U_0 given by [ILD03]:

$$\frac{U_2}{U_0} = \frac{a_2 - a_0}{a_2 + 2a_0}.$$

Hamiltonian (4.4) preserves the total magnetization $\hat{M} \equiv \sum_i \hat{S}^z_i$ of the sample, allowing us to work in a convenient block-diagonal representation. Moreover, each energy offset Δ_α plays the role of a chemical potential for the atomic species α. As a consequence, in absence of spin-flipping interactions (n_α conserved), the Δ_α play no role in the dynamics at fixed magnetization. In our case the situation is complicated by the presence, in the atomic Hamiltonian, of terms which flip the atomic spin:

$$|m_F=0\rangle|0\rangle \ \longleftrightarrow\ |+1\rangle|-1\rangle. \tag{4.5}$$

The Δ_α would still not play any role in the dynamics if the following relation holds: $2\Delta_\circ = \Delta_+ + \Delta_-$. In presence of an external magnetic field, only the linear Zeeman shift satisfies this requirement, whereas the quadratic one does not. In this case, the relevant dynamical quantity is $\delta = \Delta_+ + \Delta_- - 2\Delta_\circ$, which quantifies deviations from the linear splitting regime. It is experimentally possible to control small values of δ dressing the system with microwave fields [GWF+06].

When interaction energies are larger than the hopping rates ($U_0+U_2, U_0-2U_2 \gg |t_\alpha|$), the system is in a Mott insulator phase and we compute the super-exchange Hamiltonian $\hat{H}^{\rm eff}_{\rm real}$ with a second-order perturbative expansion of the kinetic term. We provide the explicit expression of such Hamiltonian on one link of the lattice. Let us consider the following basis for the link:

$$\text{Basis}: \{|-\rangle|-\rangle,\ |-\rangle|\circ\rangle,\ |-\rangle|+\rangle,\ |\circ\rangle|-\rangle,\ |\circ\rangle|\circ\rangle, |\circ\rangle|+\rangle, |+\rangle|-\rangle,\ |+\rangle|\circ\rangle, |+\rangle|+\rangle\};$$

where the ket notation stand for $|m_{F,\,\mathrm{site1}}\rangle|m_{F,\,\mathrm{site2}}\rangle$. The zero-th order Hamiltonian in such a basis reads:

$$\hat{H}^{\mathrm{eff}(0)}_{\mathrm{real}} = \mathrm{Diag}\left(2\Delta_-,\, \Delta_-,\, \Delta_+ + \Delta_-,\, \Delta_-,\, 0,\, \Delta_+,\, \Delta_+ + \Delta_-,\, \Delta_+,\, 2\Delta_+\right) \quad (4.6)$$

whereas the second order reads:

$$\hat{H}^{\mathrm{eff}(2)}_{\mathrm{real}} = -\frac{1}{U_0+U_2}\cdot \quad (4.7)$$
$$\cdot \begin{pmatrix}
4|t_-|^2 & 0 & 0 & 0 & 0 & 0 & 0 & 0 & 0 \\
0 & |t_-|^2+|t_\circ|^2 & 0 & 2t^*_\circ t_- & 0 & 0 & 0 & 0 & 0 \\
0 & 0 & (|t_-|^2+|t_+|^2)\mathcal{B} & 0 & -(t^*_\circ t_- + t^*_+ t_\circ)\mathcal{A} & 0 & 2t^*_+ t_- \mathcal{B} & 0 & 0 \\
0 & 2t^*_- t_\circ & 0 & |t_-|^2+|t_\circ|^2 & 0 & 0 & 0 & 0 & 0 \\
0 & 0 & -(t^*_\circ t_+ + t^*_- t_\circ)\mathcal{A} & 0 & |t_\circ|^2\mathcal{C} & 0 & -(t^*_\circ t_- + t^*_+ t_\circ)\mathcal{A} & 0 & 0 \\
0 & 0 & 0 & 0 & 0 & |t_\circ|^2+|t_1|^2 & 0 & 2t^*_+ t_\circ & 0 \\
0 & 0 & 2t^*_- t_+ \mathcal{B} & 0 & -(t^*_- t_\circ + t^*_\circ t_+)\mathcal{A} & 0 & (|t_+|^2+|t_-|^2)\mathcal{B} & 0 & 0 \\
0 & 0 & 0 & 0 & 0 & 2t^*_\circ t_+ & 0 & |t_\circ|^2+|t_+|^2 & 0 \\
0 & 0 & 0 & 0 & 0 & 0 & 0 & 0 & 4|t_+|^2
\end{pmatrix};$$

where

$$\begin{aligned}
\mathcal{A} &= \frac{U_2(U_0+U_2)}{(U_0+U_2)(U_0-2U_2)+\delta U_0} + \frac{U_2(U_0+U_2)}{(U_0+U_2)(U_0-2U_2)+\delta(U_2-U_0)};\\
\mathcal{B} &= \frac{(U_0-\delta)(U_0+U_2)}{(U_0+U_2)(U_0-2U_2)+\delta(U_2-U_0)};\\
\mathcal{C} &= \frac{4(U_0-U_2+\delta)(U_0+U_2)}{(U_0+U_2)(U_0-2U_2)+\delta U_0}.
\end{aligned}$$

Let us now consider a simple class of mappings $\hat{\mathsf{W}}_{\{\varphi\}}$ which will be used in the following, characterized only by a simple phase freedom:

$$\hat{\mathsf{W}}_{\{\varphi\}}|m_F=\alpha\rangle_{\mathrm{real}} = e^{i\varphi_\alpha}|n=\alpha+1\rangle_{\mathrm{3hb}} \quad (4.8)$$

These mappings are characterized by the property that the magnetization of the spin insulator is directly mapped into the density of the three-hardcore bosons. Therefore, since the Hamiltonian in equation (4.7) contains only off-diagonal terms which preserve the total magnetization, we automatically gain the possibility of studying hardcore bosons setups at fixed density.

As far as the interaction strengths are concerned, we report that the scattering lengths a_0 and a_2 have very similar values both in ^{87}Rb and ^{23}Na. This means that the spin-dependent part of the interaction is in natural setups almost negligible, as it becomes clear once the ratio U_2/U_0 is calculated, respectively -0.005 and 0.04 for the two atoms [vKKHV02, WGF$^+$06, TWJ$^+$96]. We do not elaborate further on this issue as the scientific community is working on methods to control independently the two scattering lengths.

The off-diagonal matrix elements in equation (4.7) correspond, via the mappings $\hat{\mathsf{W}}_{\{\varphi\}}$ (4.8), to terms describing the hopping of the emerging particles. In particular, the matrix elements of the second sub-/superdiagonal correspond in $\hat{H}_{\mathrm{3hb}}$ to one-particle hopping terms

$$|0\rangle|1\rangle \leftrightarrow |1\rangle|0\rangle, \quad |1\rangle|1\rangle \leftrightarrow |2\rangle|0\rangle, \quad |1\rangle|2\rangle \leftrightarrow |2\rangle|1\rangle. \quad (4.9)$$

In order to map the spin model into a bosonic model with an effective three-body repulsion, the one-particle hopping rates in (4.9) must be those of a system of bosons. In other words, the rate of the $|1\rangle|2\rangle \leftrightarrow |2\rangle|1\rangle$ process must be twice as large as that of $|0\rangle|1\rangle \leftrightarrow |1\rangle|0\rangle$ and a factor $\sqrt{2}$ larger than that of $|1\rangle|1\rangle \leftrightarrow |2\rangle|0\rangle$.

The matrix elements of the fourth sub-/superdiagonal correspond to a two-particle hopping:

$$|0\rangle|2\rangle \leftrightarrow |2\rangle|0\rangle. \tag{4.10}$$

The relative importance of one- and two-particle hopping rates can be modified just by tuning $|t_\circ|$, a factor which multiplies the second sub-/superdiagonal and is not present in the fourth one. In [MRLC10] we exploit this feature to propose the experimental study a quasi-condensate of pairs of quantum particles.

Finally, let us stress that we have implicitly assumed to have the possibility of tuning independently the three t_α. Indeed, the superlattice scheme of chapter 2 can be used to do this[2].

4.3 The Pfaffian Wavefunction

In this section we analyze the Pfaffian wavefunction [GWW92], an interesting many-body state arising in the presence of three-body interactions. This state has been proposed in the context of the quantum Hall effect (QHE) [Eza00] in order to describe the many-body electron liquid at fractional magnetic filling $\nu = 5/2$. The interest in this wavefunction resides in the predicted property of supporting non-Abelian quasi-excitations [MR91, RR96].

Here we deal with the bosonic version of the Pfaffian state and show that this wavefunction can be studied also in a lattice. Combining exact-diagonalization numerical approaches to some topological benchmark quantities, we show that the ground state of the system features non-trivial topological hallmarks even in the presence of significant magnetic fields. We then employ these tools to discuss the possibility of using a spin-1 Mott insulator to realize such a wavefunction, and underline some problems in this method.

4.3.1 Quantum Hall Effect on a Lattice

We consider a two-dimensional setup with N bosons with charge q interacting via purely three-body repulsion (no two-body term) in presence of an external uniform magnetic field with vector field $\mathbf{A}(\mathbf{r})$. The setup is pierced by a number of magnetic fluxes N_Φ equal to the number of particles N (filling factor $\nu = 1$); a typical length $\ell = \sqrt{\hbar c/qB}$ is induced in the system by the magnetic field itself. The system is ruled by the following many-body Hamiltonian, in which we write the position of the particles with complex coordinates $z = (x + iy)/\ell$:

$$\hat{H}_{\mathrm{Pf}} = \sum_i \frac{\left[\mathbf{p}_i - \frac{q}{c}\mathbf{A}(z_i)\right]^2}{2m} + c_3 \sum_{i<j<k} \delta(z_i - z_j)\delta(z_i - z_k). \tag{4.11}$$

c_3, greater than zero, is the strength of the repulsion. The single particle levels are arranged into a collection of degenerate manifolds, the Landau levels, separated by a gap twice the cyclotron frequency $2\hbar(qB/mc)$; as long as the chemical

[2] See reference [MRLC10] for some specific numerical simulations

N	N_Φ	$L_x \times L_y$	ℓ/a	degen.	overlap	CN	$\dim\mathcal{H}$
4	4	4×4	~ 0.8	3	78%	3	3620

Table 4.1: Exact diagonalization study of the many-body ground state of Hamiltonian (4.14) on a torus. The degeneracy and the Chern number of the ground manifold in the continuum case are respectively 3 and 3. As discussed in Appendix A, the presence of magnetic fields strongly constraints the dimension of the torus to be simulated; the next size would be 5×5, with an Hilbert space of dimension 110000.

potential is smaller than this separation, the particles are confined to the lowest Landau level and are characterized by wavefunctions which are analytical in z (the exponent being the angular momentum). Within this framework, the double-delta potential is properly regularized and the ground state of the Hamiltonian is the Pfaffian wavefunction [GWW92]:

$$\Psi(z_1, ...z_N) \propto \mathrm{Pf}\left[\frac{1}{z_i - z_j}\right] \prod_{i<j}(z_i - z_j)\ e^{-\sum_j |z_j|^2/2}. \tag{4.12}$$

The Slater determinant $\prod_{i<j}(z_i - z_j)$ prevents the coincidence of two or more particles in the same spatial position; the prefactor $\mathrm{Pf}[1/(z_i - z_j)]$ is the Pfaffian of the antisymmetric matrix with elements $A_{ij} = 1/(z_i - z_j)$:

$$\mathrm{Pf}[A] = \frac{1}{2^m m!} \sum_{\pi \in S_{2m}} \mathrm{sgn}(\pi) A_{\pi_1,\pi_2} A_{\pi_3,\pi_4} \ldots A_{\pi_{2m-1},\pi_{2m}}. \tag{4.13}$$

It enables the superposition of two bosons but still forbids that of three. With this construction, the wavefunction is forced to be the lowest angular momentum state in the intersection between lowest Landau level and kernel of the three-body interaction.

In order to discuss the possibility of simulating the Pfaffian state with spin-1 atoms, we have first to discretize the system. The discrete version of a single-particle Hamiltonian with minimal coupling was shown in (3.13). We take into account the presence of a three-body interaction with $c_3 \to \infty$ introducing the three-hardcore bosons operators $\hat{a}_j$ and $\hat{a}_j^\dagger$ satisfying $\hat{a}_j^3 = 0$ and $\hat{a}_j^{\dagger 3} = 0$. The Hamiltonian we are interested in is:

$$\hat{H}_{\mathrm{Pf-lat}} = -J \sum_{<k,j>} e^{i\phi_{k,j}}\, \hat{a}_k^\dagger \hat{a}_j + H.c.; \quad (\hat{a}_j^\dagger)^3 = 0. \tag{4.14}$$

As in every discrete $U(1)$ gauge theory, the magnetic field coupling to the positional degrees of freedom of the particles is represented by a phase $\phi_{k,j} = 2\pi/\Phi_0 \int_k^j \boldsymbol{A} \cdot d\boldsymbol{l}$, where $\Phi_0 = hc/q$ is the quantum of flux.

4.3.2 Topological Properties as a Benchmark

We now investigate to which extent transposing the system into a discrete lattice modifies the nature of the many-body state. The problem arises from the competition of two typical lengths, the magnetic length ℓ and the lattice constant

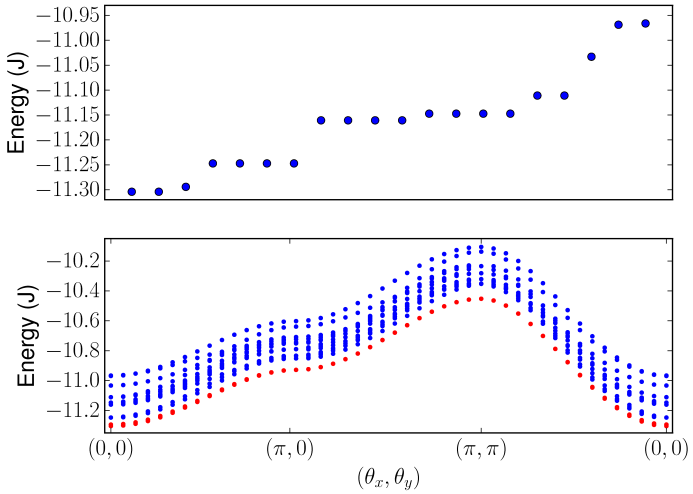

Figure 4.2: (Top) Plot of the first 20 energy levels of the Hamiltonian (4.14) studied on a 4×4 torus with the parameters listed in table 4.1. A threefold quasi-degenerate ground state can be recognized. (Bottom) Cut of the first twenty energy bands in the (θ_x, θ_y) space. The lowest red line, threefold degenerate, does not mix with the higher bands, i.e. the ground state multiplet is always well-defined and separated from higher energy levels. This is a crucial requirement in order to speak of a topological state. Reproduced from [MRLC10].

a. In the small magnetic field limit $\ell \gg a$ (or dilute limit, since the constraint $N = N_\Phi$ must hold), we expect the system to be insensitive to the discrete nature of the space. On the other side, an analysis of what happens when the magnetic field (and the particle density as well) increases is needed to test the robustness of a fully discrete version of the Pfaffian wavefunction.

The characterization of QHE wavefunctions transposed from continuum systems, usually two-dimensional strongly interacting electrons, to discrete optical lattices is a problem that has already been faced in the literature [HSDL07, HSLD08, MC09]. Here we follow the standard approach. We perform an exact diagonalization of the system with periodic boundary conditions (PBC). Three marks are used to test the topological properties of the numerical ground state and its resemblance with the Pfaffian wavefunction:

1. the agreement between the degeneracy of the discrete numerical and continuum analytical ground manifolds (the Pfaffian wavefunction has been generalized on a torus first in [GWW92]);

2. a significant overlap of the discrete numerical wavefunctions with the continuum analytical ones;

3. the agreement between the Chern number [NTW85, Hat04, Hat05] of the discrete numerical and continuum analytical ground manifolds.

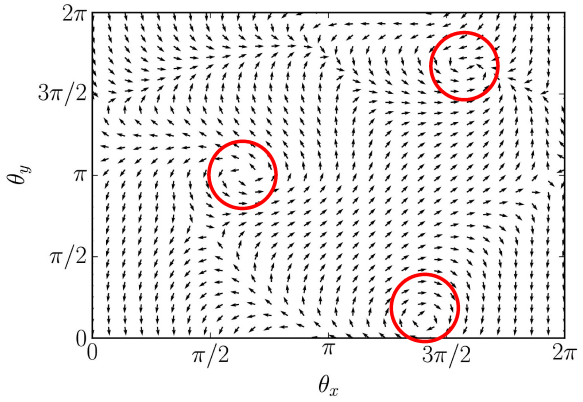

Figure 4.3: Plot of the auxiliary field $\Omega(\theta_x, \theta_y)$ for the system with Hamiltonian (4.14). The parameters of the system are those in table 4.1. The three highlighted vortices mean that the Chern number of the system is equal to 3. The definition of the field $\Omega(\theta_x, \theta_y)$ and the way it can be computed are discussed extensively in [Hat04, HSDL07, HSLD08], to which we refer the interested reader. Reproduced from [MRLC10].

Results are reported in table 4.1. The three-fold degeneracy of the Pfaffian ground state is strictly connected to the properties of the Jacobi theta functions, which are often used to generalize several QHE states on the torus [GWW92].

Chern numbers have already been introduced in section 3.2.1 (see in particular equations (3.14) and (3.15)). Because the considered model was non-interacting, the analysis exploited the properties of a well-defined Brillouin zone. This approach can be generalized to a systems with disorder or with interactions by testing its sensibility towards the twist of the boundary conditions, expressed by two parameters $(\theta_x, \theta_y) \in [0, 2\pi) \times [0, 2\pi)$ [NTW85]. We give here the expression of the Chern number for the simple case of non-degenerate ground state, whereas for more dimensions we refer to [Hat04, HSDL07]:

$$C = \frac{1}{2\pi} \int d\theta_x d\theta_y \left[\partial_{\theta_x} A_y(\theta_1, \theta_2) - \partial_{\theta_y} A_x(\theta_1, \theta_2) \right] \tag{4.15}$$

where $A_i = \langle \Psi(\theta_x, \theta_y) | \frac{\partial}{\partial \theta_i} | \Psi(\theta_x, \theta_y) \rangle$ and $|\Psi(\theta_x, \theta_y)\rangle$ is the ground state with boundary conditions (θ_x, θ_y). As in equation (3.15), C is an integer number. We compute the Chern number with the method provided in [Hat04] which avoids any explicit numerical differentiation and connects the evaluation of C to the number of vortices displayed by a proper auxiliary field $\Omega(\theta_x, \theta_y)$. The fact that $C \in \mathbb{Z}$ motivates its extensive use, since it provides a reliable yes-no benchmark of topological properties which works better than the wavefunction overlap ranging in $[0, 1]$.

In figure 4.2 we show the energy spectrum of the Hamiltonian (4.14) studied on a torus with the parameters listed in table 4.1. The figure highlights also the fact that moving in the (θ_x, θ_y) space the threefold degeneracy of the ground state multiplet is preserved. Figure 4.3 shows the auxiliary field $\Omega(\theta_x, \theta_y)$ in

$U_2 = \sqrt{2}/(2\sqrt{2}+3)U_0 \sim 0.24U_0$		$\delta = -2\lvert t_\circ\rvert^2/(U_0+U_2)$	
$t_\circ = 0.1U_0$	$t_- = 0.1t_\circ e^{i\vartheta}$	$t_+ = 2t_-^*$	
$\lvert 0\rangle\lvert 1\rangle \leftrightarrow \lvert 1\rangle\lvert 0\rangle$	$-0.0016\ U_0$	$\lvert 1\rangle\lvert 1\rangle \leftrightarrow \lvert 2\rangle\lvert 0\rangle$	$-0.0022\ U_0$
$\lvert 1\rangle\lvert 2\rangle \leftrightarrow \lvert 2\rangle\lvert 1\rangle$	$-0.0032\ U_0$	$\lvert 0\rangle\lvert 2\rangle \leftrightarrow \lvert 2\rangle\lvert 0\rangle$	$-0.0006\ U_0$

Table 4.2: Set of parameters used together with the mapping $\hat{\mathsf{W}}_{\mathrm{PF}}$ to recover the model in equation (4.14). The last lines show the amplitudes of the matrix elements representing the hopping of one and two emerging hardcore bosons. The one-particle ones are in a ratio $\{1, \sqrt{2}, 2\}$ whereas the two-particle one is smaller.

this case and the three vortices, which correspond to a Chern number equal to three.

Within the uncertainty given by working with small systems without accessing the thermodynamic limit, we can at least affirm that our results are compatible with the presence of an incompressible liquid with a degenerate ground state on the torus at $\ell \sim 0.8\,a$. Moreover, they also present significant signatures that the nature of the system should be strictly linked to that of the Pfaffian state.

4.3.3 Tentatives Towards an Implementation with Spin-1 Atoms

The previous section shows that if we were able to implement Hamiltonian (4.14) we would access the Pfaffian wavefunction with our quantum simulator. The Hamiltonian for effective bosons obtained in equation (4.7) has to be then compared with the link version of equation (4.14):

$$\hat{H}_{\mathrm{disc}} = -J \begin{pmatrix} 0 & 0 & 0 & 0 & 0 & 0 & 0 & 0 & 0 \\ 0 & 0 & 0 & e^{i\phi_{i,j}} & 0 & 0 & 0 & 0 & 0 \\ 0 & 0 & 0 & 0 & \sqrt{2}e^{i\phi_{i,j}} & 0 & \heartsuit & 0 & 0 \\ 0 & e^{-i\phi_{i,j}} & 0 & 0 & 0 & 0 & 0 & 0 & 0 \\ 0 & 0 & \sqrt{2}e^{-i\phi_{i,j}} & 0 & \spadesuit & 0 & \sqrt{2}e^{i\phi_{i,j}} & 0 & 0 \\ 0 & 0 & 0 & 0 & 0 & 0 & 0 & 2e^{i\phi_{i,j}} & 0 \\ 0 & 0 & \heartsuit & 0 & \sqrt{2}e^{-i\phi_{i,j}} & 0 & 0 & 0 & 0 \\ 0 & 0 & 0 & 0 & 0 & 2e^{-i\phi_{i,j}} & 0 & 0 & 0 \\ 0 & 0 & 0 & 0 & 0 & 0 & 0 & 0 & 0 \end{pmatrix}$$

where the graphic symbols highlight some terms of equation (4.7) which are not present in (4.14).

One of the problems is related to the presence in ♡ of the correlated hopping term (4.10), which is not comprised by the the QHE model. Therefore, we tried to study the model in the regime: $|t_\circ| \gg |t_+|, |t_-|$, which decreases the relevance of correlated hopping. In this case we use a mapping $\hat{\mathsf{W}}_{\mathrm{PF}}$ characterized by the phases: $\{\varphi_- = 0; \varphi_\circ = 0; \varphi_+ = \pi\}$ and set the various parameters to the values listed in table 4.2. This sets the second sub-/superdiagonal to be approximately proportional to $\{1; \sqrt{2}; \sqrt{2}; 2\}$. Unfortunately, this tunes only eight of the terms of the diagonal to an approximate same value: the central

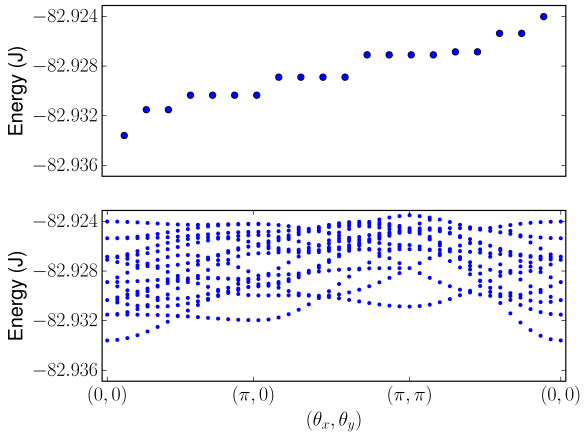

Figure 4.4: (Top) Plot of the first 20 energy levels of the spin-1 based model with the parameters listed in table 4.2, studied on a 4×4 torus as before. No threefold quasi-degenerate ground state can be recognized. Moreover, the gap here is approximately one order of magnitude smaller than in the Pfaffian case (here we take $J = -0.0016\ U_0$). (Bottom) Cut of the first twenty energy bands in the (θ_x, θ_y) space. No definite three-fold ground state multiplet can be recognized. This result strongly tells us that the system is far from featuring a ground state sharing the topological properties of the Pfaffian wavefunction. Reproduced from [MRLC10].

one ♠ is significantly different from the others, leading to a completely different model with an effective nearest neighbours interaction. Moreover, this method has the general disadvantage that the effective hopping rate J would be proportional to $|t_\circ t_-|/(U_0 + U_2)$ and therefore require temperatures even lower than the pure super-exchange effect $|t_\circ|^2/(U_0 + U_2)$. As displayed in figure 4.4, a further numerical analysis shows that the energy spectrum does not exhibit any degenerate ground state and that moving in the (θ_x, θ_y) space many energy bands cross, making the calculation of C meaningless.

As an alternative, we abandon the attempt to exactly recover the model in equation (4.14) and try instead to realize a similar system whose ground state is characterized by the same benchmarks of the Pfaffian wavefunction, i.e. the same degeneracy on the torus and the same Chern number. At low density, the number of global Fock states with more than two particles on one link is lower than that of the other states. Thus, we expect that matrix elements of the link Hamiltonian connecting states with more than two particles per link do not play a relevant role in the global dynamics; even sensible deviations of such terms from the exact values should not change too much the properties of the ground state. Hence, we investigated sets of parameters which could make such matrix elements the only ones sensibly different from the ideal values. We consider the same 4×4 system as before at density $\rho = 1/4$ and magnetic field $N_\Phi = 4$, which we can numerically analyze, but the next considerations could also be generalized to systems with smaller magnetic fields (or more dilute).

Unfortunately, even this turned out to be impossible. We tried to combine a tomographic analysis of the Pfaffian wavefunction with the tuning of all the matrix elements of the link Hamiltonian connecting states with less than three particles. However the numerical simulation of these Hamiltonians gave always as result non-degenerate ground states characterized by no topological properties, i.e. a Chern number equal to zero [Hat05].

Unfortunately we were then not able to find neither a way to get the Hamiltonian in equation (4.14) nor to realize a similar Hamiltonian whose ground state was three-fold degenerate and characterized by a Chern Number equal to three. We think that the Pfaffian wavefunction cannot be readily implemented with the help of a quantum simulator based merely on the ingredients described in this work. It might be nonetheless the case that, with the help of further ideas such as additional ancillary system, it becomes feasible.

4.4 Conclusions and Perspectives

In this chapter we have examined the properties of a discrete bosonic Pfaffian wavefunction, a many-body state arising in presence of contact three-body repulsion, in the non-dilute limit. Our proposal to simulate such interaction relies on a local mapping between the dynamics of a spin-1 Mott insulator and that of emerging bosons characterized by such interaction. Numerical calculations show that the setup is unable to realize the Pfaffian wavefunction, and that additional external control is needed. This result leaves the open perspective of actually solving the encountered problem. In this case, it would also be extremely interesting to develop experimental methods for the manipulation of the non-Abelian excitations of the Pfaffian wavefunction.

Another interesting perspective is the search for systems characterized by three-body interactions which could be simulated with a spin-1 Mott insulator. In [MRLC10] we study a one-dimensional model characterized by a dominating correlated hopping, which can drive a phase transition to a one-dimensional quasi-condensate of pairs without any two-body attraction. Moreover, we show that substituting the three-body interaction with a two-body one, the system becomes unstable toward collapse: this strictly links the quasi-condensate of pairs to the stabilizing effect of the three-body repulsion. We show that this phase transition from a quasi-condensate of atoms to a quasi-condensate of pairs can be studied with the setup explained in this chapter.

Recently, it has been proposed that the spin-1 Mott insulator could be used to simulate compact Quantum Electrodynamics and the effect of confinement between two external static charges [ZCR12].

Chapter 5

Particle-Hole Pairs and String Order in One Dimension

The development of the in-situ measurement technique reviewed in section 1.3 (see references [BGP+09, SWE+10]) has allowed the experimental investigation of several aspects of the Bose-Hubbard model in low dimensions [BPT+10, WSF+11, WES+11, CBP+12, EFP+12]. In this chapter we focus on the observation of correlated particle-hole pairs and of a string order parameter in a one-dimensional bosonic gas [ECF+11].

The quantum phase transition from Mott insulator to superfluid in three-dimensions is characterized by the spontaneous breaking of the $U(1)$ symmetry of the phase of the condensate wavefunction. Due to the Mermin-Wagner theorem [Bog62, MW66], this cannot happen in a one-dimensional optical lattice and no long-range order is expected to set in. Instead, the superfluid shows quasi-long range order with algebraic decay of correlations. This phase is sometimes called *Luttinger liquid*.

In this chapter we discuss how to detect this quantum phase transition by probing local and non-local fluctuations of the atomic density. Moreover, we summarize the results of an experiment aimed at the detection of these quantities carried out in the group of Prof. I. Bloch at the Max-Planck-Institut für Quantenoptik [ECF+11]. The author of this thesis participated at the experiment as theoretical support providing the simulations of an infinite one-dimensional system made with the density matrix renormalization group algorithm (DMRG) [Sch11]. Numerical simulations with Matrix Product States (MPS) have been done by Dr. M. C. Bañuls whereas quantum Monte Carlo (QMC) results have been provided by Prof. L. Pollet.

In the sections 5.1, 5.2 and 5.3 we summarize the experiment and the main results; we support the discussion with the necessary theoretical background. In section 5.4 we focus on the methods used to analyze numerical data and obtain information about the infinite system. Conclusions and perspectives are presented in section 5.5.

5.1 Correlated Particle-Hole Pairs

The physics of an ultracold bosonic gas trapped in a one-dimensional optical lattice is described by the Bose-Hubbard model (see also section 1.2):

$$\hat{H} = -J \sum_i \left[\hat{b}_i^\dagger \hat{b}_{i+1} + H.c. \right] + \frac{U}{2} \sum_j \hat{n}_j (\hat{n}_j - 1) + \sum_j (-\mu + V_0\, j^2) \hat{n}_j \qquad (5.1)$$

where $\hat{b}_i^{(\dagger)}$ are bosonic field operators and $V_0\, j^2$ represents the parabolic confinement.

The Mott insulator phase, which appears for $J \ll U$, is characterized by the squeezing of the number of atoms per site. However, because the operator $\hat{n}_i$ commutes with the Hamiltonian only for $J = 0$, for $J \neq 0$ the eigenstates of $\hat{H}$ do not have a defined number of atoms per site. Intuitively, the ground state can be understood as a fixed-density background on top of which coherent *particle-hole pairs* appear. These are usually referred to as *doublon-holon pairs*; we will not use this convention. The first goal of the experiment is to reveal the existence of such pairs.

A degenerate gas of ^{87}Rb is prepared in a two-dimensional optical lattice. In order to avoid Mott insulators with mean occupation numbers $\bar{n} > 1$, the typical experimental realization has a relatively small number of atoms, comprised between 150 and 200. The setup can be used for studying either a two-dimensional gas, or, by increasing the lattice depth along one dimension, an array of one-dimensional systems. This latter case is considered in this section, in which we primarily deal with one-dimensional physics.

The in-situ measurement technique introduced in section 1.3 enables the measurement of the on-site parity, described by the operator $\hat{s}_j = e^{i\pi(\hat{n}_j - \bar{n})}$, whereas no direct information about $\hat{n}_j$ is accessible. From now on, since the experiments run in a regime where there is in average one atom per site, we set $\bar{n} = 1$, and therefore the eigenstates of $\hat{s}_j$ with eigenvalue $+1$ are those states with an odd number of atoms at site j, whereas states with an even number of atoms have eigenvalue -1.

Let us define the two-site parity correlation function:

$$C_k(d) = \langle \hat{s}_k \hat{s}_{k+d} \rangle - \langle \hat{s}_k \rangle \langle \hat{s}_{k+d} \rangle \qquad (5.2)$$

where d represents the distance between the two sites. The function $C_k(d)$ is expected to detect the presence of correlated particle-hole pairs via the enhancement of $\langle \hat{s}_k \hat{s}_{k+d} \rangle$, because uncoherent excitations (mainly thermal) contribute only to $\langle \hat{s}_k \rangle \langle \hat{s}_{k+d} \rangle$. Experimentally, the average over many realizations and over many sites k yields the quantity $C(d)$, which is used and plotted in the following.

Let us theoretically discuss $C(d)$ for an ideal situation with no parabolic confinement, $V_0 = 0$, and without thermal excitations, $T = 0$. We apply perturbation theory to compute $C(d = 1)$ in the limit of deep Mott insulator with $\bar{n} = 1$, i.e. $J \ll U$ and $0 < \mu < U$. Let us split Hamiltonian (5.1) into an unperturbed term, $\hat{H}_0 = \frac{U}{2} \sum_j \hat{n}_j (\hat{n}_j - 1) - \mu \sum_j \hat{n}_j$, and a perturbation, $\hat{H}_1 = -J \sum_i \hat{b}_i^\dagger \hat{b}_{i+1} + H.c.$.

In case one is interested in intensive properties of the ground state for $T = 0$, such as the energy density, or $C(d = 1)$, the cluster expansion for many-body states developed in [GSH90] is the tool to be used[1]. The computation of

[1] This technique has been applied to the Bose-Hubbard model in [EM99].

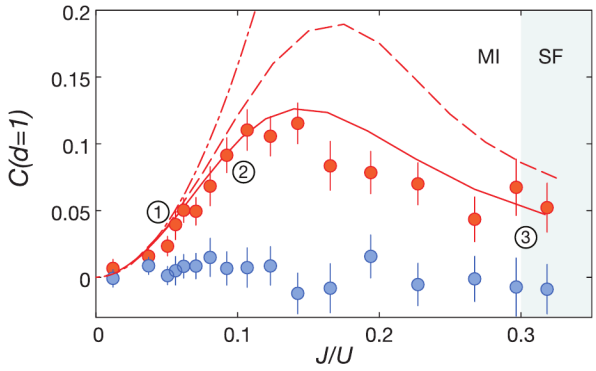

Figure 5.1: Nearest-neighbour correlations $C(d=1)$ for a one-dimensional system as a function of J/U. Red dots: experimental data. Blue dots: measurements of correlations between neighbouring sites belonging to different one-dimensional arrays. They are consistent with zero and show the genuine one-dimensional nature of the experiment. The curves represent theoretical calculations. Those computed via first-order perturbation theory (dashed-dotted line) and via DMRG (dashed line) are for a homogeneous system at $T=0$. Solid line: finite-temperature MPS calculation including temperature $T=0.09\,U/k_B$ and the harmonic confinement. Reproduced from [ECF+11] with permission from AAAS.

such intensive quantities is rewritten in terms of ground state properties of the original Hamiltonian restricted to connected graphs of the lattice. Moreover, low-order contributions require to take into account only small graphs.

In order to compute $C(d=1)$ at the lowest order, it suffices to consider the smallest connected graphs, i.e. those composed of two neighboring sites. The Hamiltonian restricted to two sites is:

$$\hat{H} = -J\hat{b}_1^\dagger \hat{b}_2 - J\hat{b}_2^\dagger \hat{b}_1 + \frac{U}{2}\hat{n}_1(\hat{n}_1-1) + \frac{U}{2}\hat{n}_2(\hat{n}_2-1) - \mu(\hat{n}_1+\hat{n}_2). \tag{5.3}$$

The ground state, computed via standard first-order perturbation theory, is:

$$|\Psi_{J/U\sim 0}\rangle = \frac{1}{\mathcal{N}}\left(|1,1\rangle + \sqrt{2}\frac{J}{U}(|2,0\rangle + |0,2\rangle)\right); \quad \mathcal{N} + \sqrt{1+4\left(\frac{J}{U}\right)^2} \tag{5.4}$$

where $|n,m\rangle$ is the Fock state with n (m) particles in the first (second) site of the link. Applying the definition of $C(d=1)$ to $|\Psi_{J/U\sim 0}\rangle$ and retaining the second order in J/U we obtain $C(d=1) = 16(J/U)^2 + \ldots$.

In order to obtain the full dependence of $C(d=1)$ on J/U, we analyze a homogeneous system at $T=0$ with an open-source DMRG algorithm[2] which implements the conservation of the number of particles and considers open boundary conditions. The computation of $C(d)$ can be done reliably even with relatively small systems, as for example $L=48$. Numerically, $C(d)$ is computed in the center of the system, so that finite-size effects can be neglected. This has been tested by moving k slightly far off from the exact center.

[2]It can be downloaded from `www.dmrg.it`.

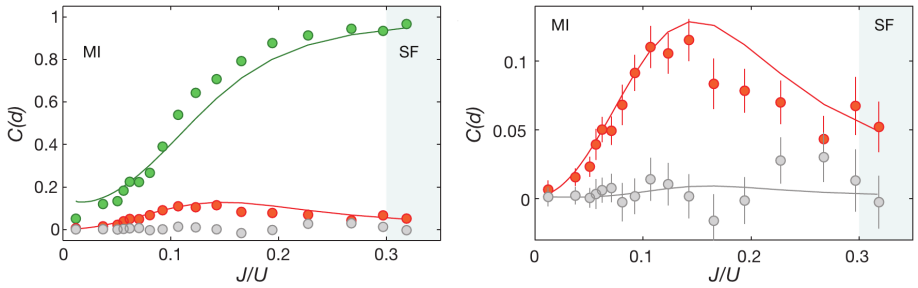

Figure 5.2: Parity correlations for different distances $d = 0$, 1, 2 (respectively in green, red and gray). Dots are experimental measures whereas lines are theoretical simulations via an MPS algorithm including harmonic confinement and temperature $T = 0.09\,U/k_B$. Right panel is a zoom of the left one. Reproduced from the supplementary materials of [ECF+11] with permission from AAAS.

Figure 5.1 shows experimental data and different theoretical calculations. The DMRG calculation, which can be considered exact for any practical purpose, is the dashed red line. The quadratic behaviour predicted via perturbation theory is valid only for an extremely small region $J/U < 0.05$. As expected, at $J = 0$ we get $C(d = 1) = 0$; the signal increases for increasing J/U and reaches a peak for $0.1 < J/U < 0.2$. Moreover, $C(d = 1)$ is not zero at the transition to the superfluid phase, which is at $J/U \sim 0.3$, and therefore it is not a good order parameter for the insulating phase. The measured quantity is a genuine quantum effect and is decreased by incoherent (thermal) fluctuations. This explains why the theoretical prediction at $T = 0$ obtained via DMRG reproduces only qualitatively, but not quantitatively, the experimental data. Thermal effects in the experiment cannot be disregarded and temperature is estimated to $T = 0.09\,U/k_B$. Another source of noise is the fact that experimental realizations differ slightly from each other in the number of atoms. The statistical average needed to compute $C(d)$ includes an average over the chemical potential. The effect is especially severe close to the phase transition, where the Mott lobe becomes narrower.

It is also possible to probe $C(d)$ for $d \neq 1$. For $d = 0$, it is equivalent to probing the on-site variance of the parity operator $\hat{s}_k$. Since the Mott insulator is characterized by the squeezing of the on-site atomic number, we expect also $C(d = 0)$ to be very small for deep Mott insulators, and to reach larger values at the phase transition.

For $d > 1$, the quantity $C(d)$ does not only probe the presence of particle-hole pairs of length d, but also shorter. Nevertheless, the values of $C(d)$ decrease while increasing d; for $d = 2$ the theory predicts a small maximum of 0.01 at $J/U \sim 0.17$ which is experimentally not distinguishable from statistical noise. Experimental and theoretical $C(d)$ for $d = 0$, 1, 2 are shown in figure 5.2.

Finally, the measurement of correlated particle-hole pairs is repeated also for a two-dimensional optical lattice. Theoretical results via quantum Monte Carlo (QMC) and experimental measures clearly highlight the important role of dimensionality, as shown in figure 5.3. In particular, the prominent role of quantum correlations in one dimension is underlined.

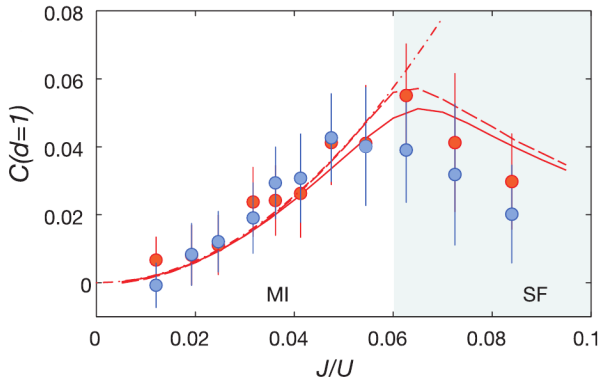

Figure 5.3: Nearest-neighbour correlations $C(d = 1)$ for a two-dimensional system as a function of J/U. Dots: experimental correlations between neighboring sites along the x direction (red) and y direction (blue). The agreement of the data shows the genuine two-dimensionality of the system. The curves represent theoretical calculations for a homogeneous system: first-order perturbation theory (dashed-dotted line) and QMC at $T = 0.01\,U/k_B$ (dashed line) and at $T = 0.1\,U/k_B$ (solid line). Reproduced from [ECF+11] with permission from AAAS.

Correlations are smaller than in the one-dimensional case: the peak values are $C(d = 1) = 0.1$ in one dimension and $C(d = 1) = 0.06$ in two. The superfluid phase sets in for a smaller value of J/U and numerical simulation obtained via extremely different methods (perturbation theory at $T = 0$, exact QMC for $T = 0.01\,U/k_B$ and for $T = 0.1\,U/k_B$, all of them for a homogeneous system) do not significantly disagree, as long as the insulating phase is considered. The good theory-data agreement benefits from the thickness of the Mott lobe in two dimensions, reducing therefore errors due to the average over different chemical potentials.

5.2 A String Order Parameter

The second goal of the experiment is the measurement of the string correlation function

$$\mathcal{O}^2_{\mathrm{P},k}(l) = \left\langle \prod_{j=k}^{k+l} \hat{s}_j \right\rangle \tag{5.5}$$

for a bosonic gas trapped in a one-dimensional optical lattice. Note that once the non-local operator

$$\hat{O}_{\mathrm{P}}(k) = \prod_{j<k} \hat{s}_k \tag{5.6}$$

is defined, the expectation value (5.5) can be rewritten as:

$$\mathcal{O}^2_{\mathrm{P},k}(l) = \langle \hat{O}_{\mathrm{P}}(k)\hat{O}_{\mathrm{P}}(k+l)\rangle. \tag{5.7}$$

The interest of this quantity resides in the fact that:

$$\mathcal{O}_{\mathrm{P}}^2 \doteqdot \lim_{l\to\infty} \mathcal{O}_{\mathrm{P},k}^2(l) \tag{5.8}$$

is a good order parameter for the Mott-insulating phase of a homogeneous Bose-Hubbard model ($V_0 = 0$). For homogeneous systems there is no dependence on the site k, thus it is dropped in the notation when not needed. Let us briefly recall that researchers have already studied string operators as order parameters of one-dimensional quantum systems very similar to the one considered here [dNR89, DTBA06, BDTGA08, PGWS$^+$08].

We now elaborate on the relevance of $\mathcal{O}_{\mathrm{P}}^2$. Up to now, the Mott-superfluid phase transition has been observed via two methods (see also the discussion in section 1.3). The first is the detection of the phase coherence of the superfluid, which is related to the $U(1)$ symmetry breaking appearing in three spatial dimensions, and which strictly speaking only identifies the superfluid phase. The second is the measurement of the excitation spectrum. Since the Mott insulator is gapped and the superfluid is gapless, a measurement of the excitation gap detects the phase transition. The quantity $\mathcal{O}_{\mathrm{P}}^2$ is different from those listed previously in that it is a good order parameter for the Mott insulator in one dimension and it is a function of the ground state only, rather than of the spectrum.

Let us better motivate that $\mathcal{O}_{\mathrm{P}}^2$ is a good order parameter, starting with an intuitive argument. We first consider the global ground state for $J = 0$:

$$|\Psi_{J/U=0}\rangle = \prod_j \hat{b}_j^\dagger |0\rangle. \tag{5.9}$$

For this state, $\mathcal{O}_{\mathrm{P},k}^2(l) = 1$. Now, let us consider $0 < J/U \ll 1$. The state is a linear superposition of Fock states, some of which are characterized by the presence of particle-hole pairs. Notice that Fock states are eigenstates of the string operator $\prod \hat{s}_k$; therefore, the value $\mathcal{O}_{\mathrm{P},k}^2(l)$ is the weighted average of the expectation value of $\prod \hat{s}_k$ over the relevant Fock states. Let us consider a Fock state which locally looks like a state with a single particle-hole pair: $\hat{b}_j^\dagger \hat{b}_{j+1}|\Psi_{J/U=0}\rangle$. The expectation value of $\hat{s}_j$ and of $\hat{s}_{j+1}$ is equal to -1 because sites j and $j+1$ have even occupation number. Fock states with pairs which are entirely within the string $[k, k+l]$ contribute globally to $\mathcal{O}_{\mathrm{P},k}^2$ with a plus one because for a Fock state $\langle \prod \hat{s}_k \rangle = \prod \langle \hat{s}_k \rangle$. There are also Fock states whose pairs are cut, as for example when $j = k + l$: the particle is inside the string and the hole is outside. The expectation value of the string operator on such Fock state yields -1. As a consequence, $\mathcal{O}_{\mathrm{P},k}^2(l) < 1$. In particular, it monotonically decreases with increasing J/U because the probability to cut particle-hole pairs increases with the length of the particle-hole. The length of the correlated pairs increases with J/U, finally reaching the system size at the phase transition. Because in order to probe correctly a particle-hole pair a string longer than the pair is needed, the limit $l \to +\infty$ must be taken. At the phase transition, particles and holes are not anymore nicely coupled, but rather randomly distributed, so that their contributions average to $\mathcal{O}_{\mathrm{P}}^2 = 0$.

The properties of $\mathcal{O}_{\mathrm{P}}^2$ can also be numerically tested with a DMRG simulation. Figure 5.4 shows a numerical calculation of $\mathcal{O}_{\mathrm{P}}^2(l)$ both for finite values of l and for $l \to \infty$. The finite-size scaling procedure used to obtain $\mathcal{O}_{\mathrm{P}}^2$ is presented

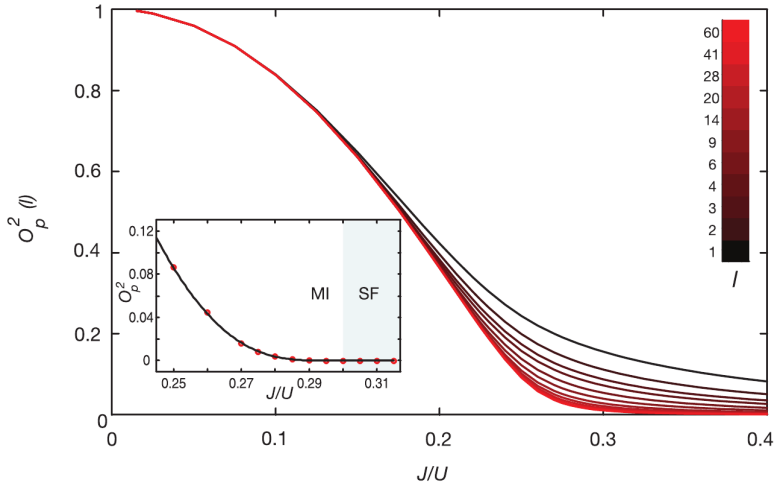

Figure 5.4: Numerical calculation of the string-order parameter $\mathcal{O}_{\mathrm{P}}^2(l)$ via DMRG for a homogeneous system at $T = 0$. $\mathcal{O}_{\mathrm{P}}^2(l)$ is plotted as a function of J/U for different string length l. Inset: the extrapolated value for $l \to \infty$ is a good order parameter for the Mott insulator phase (see section 5.4 for the scaling technique). Reproduced from [ECF+11] with permission from AAAS.

in section 5.4. The figure shows that also for the experimentally relevant case of short strings $l \ll \infty$, $\mathcal{O}_{\mathrm{P}}^2(l)$ has features which make it reminiscent of the insulator-superfluid transition.

Finally, we can also present an analytical analysis of $\mathcal{O}_{\mathrm{P}}^2(l)$. It requires the technique of bosonization of a bosonic gas in a one-dimensional optical lattice[3]. Reference [BBZ03] provides a derivation of the bosonization of a weak optical lattice, which is described by the sine-Gordon Hamiltonian [Gia04, GNT98]:

$$\hat{H} = \frac{\hbar v_S}{2\pi} \int_{-\infty}^{+\infty} dx \left[K \left(\partial_x \hat{\phi}(x) \right)^2 + \frac{1}{K} \left(\partial_x \hat{\theta}(x) \right)^2 + g \cos\left(2\hat{\theta}(x) \right) \right], \quad (5.10)$$

where the two field operators satisfy canonical commutation relations:

$$\left[\partial_x \hat{\theta}(x_1), \hat{\phi}(x_2) \right] = i\pi\delta(x_1 - x_2). \quad (5.11)$$

v_S is the sound velocity of the excitations, K is the dimensionless Luttinger parameter and g is related to the strength of the optical lattice. In particular, for an optical lattice potential $V(x) = V_0/2 \sin(2\pi x/a)$, where V_0 is the strength of the potential and a is the lattice spacing, we get $g = \pi V_0 \bar{n}/(\hbar v_S a)$. Even if we are interested in studying a strong optical lattice, whose best description is accounted by the Bose-Hubbard model, we can obtain qualitative information about the quantum phases of a strong optical lattice also by studying Hamiltonian (5.10), since it describes its low-energy limit. In particular, the superfluid

[3] We do not review the technique of bosonization because it only plays a marginal role in this dissertation and it is reviewed in good textbooks, as for example [Gia04]. Reference [Caz04] studies it with a focus on cold gases.

phase appears for $K > 2$ and the term proportional to g is not relevant. The phase is gapless and displays the same qualitative features of a bosonic gas without optical lattice. The Mott insulator phase appears for $K < 2$ and the term proportional to g is relevant; the phase is gapped.

The bosonized version of the operator $\hat{O}_{\mathrm{P}}(k)$ (5.6) is [Nak03b, DTBA06, BDTGA08]:

$$\hat{O}_{\mathrm{P}}(k) = \prod_{j<k} \hat{s}_k \propto \cos\left(\hat{\theta}(x_k)\right) \tag{5.12}$$

We can estimate the dependence on l of $\mathcal{O}^2_{\mathrm{P},k}(l) = \langle \hat{O}_{\mathrm{P}}(k)\hat{O}_{\mathrm{P}}(k+l)\rangle$ in the two phases. For $K > 2$, the computation can be done setting $g = 0$. We expand: $\cos(\hat{\theta}(x_k)) = \frac{1}{2}\left(e^{i\hat{\theta}(x_k)} + e^{-i\hat{\theta}(x_k)}\right)$. Since the Hamiltonian is quadratic, we make use of the formula: $\langle e^{iA\hat{\theta}(x_k)} e^{iB\hat{\theta}(x_{k+l})}\rangle = e^{-\frac{1}{2}\left\langle (A\hat{\theta}(x_k)+B\hat{\theta}(x_{k+l}))^2\right\rangle}$. Moreover:

$$\left\langle \left(A\hat{\theta}(x_k) + B\hat{\theta}(x_{k+l})\right)^2 \right\rangle \neq 0 \Leftrightarrow A + B = 0. \tag{5.13}$$

Consequently:

$$\langle \hat{O}_{\mathrm{P}}(k)\hat{O}_{\mathrm{P}}(k+l)\rangle \propto e^{-\frac{1}{2}\left\langle (\hat{\theta}(x_k)-\hat{\theta}(x_{k+l}))^2\right\rangle} \sim \left(\frac{l^2+\Lambda^2}{\Lambda^2}\right)^{-\frac{K}{4}} \xrightarrow{l\to+\infty} l^{-\frac{K}{2}} \tag{5.14}$$

The parameter Λ is a cutoff for large momenta which regularizes the expectation value. The correlator decays algebraically to zero and the exponent is easily related to the Luttinger parameter K. The formula used to demonstrate (5.14) can be found in appendix C of reference [Gia04].

Let us consider the Mott insulator, i.e. $K < 2$. Here $g \neq 0$ and the calculation is more complicated. An analytical analysis can be done for $K \sim 0$. Let us start with the canonical transformation: $\hat{\phi}(x) \mapsto \hat{\phi}(x)/\sqrt{K}$ and $\hat{\theta}(x) \mapsto \sqrt{K}\hat{\theta}(x)$. The Hamiltonian turns into:

$$\hat{H} = \frac{\hbar v_S}{2\pi} \int_{-\infty}^{+\infty} dx \left[\left(\partial_x \hat{\phi}(x)\right)^2 + \left(\partial_x \hat{\theta}(x)\right)^2 + g\cos\left(2\sqrt{K}\hat{\theta}(x)\right)\right] \tag{5.15}$$

The term proportional to g can be expanded as:

$$\cos\left(2\sqrt{K}\hat{\theta}(x)\right) \sim 1 - 2K\hat{\theta}(x)^2 + \dots \tag{5.16}$$

The Hamiltonian is again quadratic in the field operators and correlations can be computed [GNT98]:

$$\langle \hat{O}_{\mathrm{P}}(k)\hat{O}_{\mathrm{P}}(k+l)\rangle \propto \left\langle e^{i\hat{\theta}(x_k)} e^{-i\hat{\theta}(x_{k+l})}\right\rangle \xrightarrow{l\to\infty} \left|\left\langle e^{i\hat{\theta}(x_k)}\right\rangle\right|^2 + \Omega\sqrt{l}e^{-\sqrt{4\pi g K}l} \tag{5.17}$$

where Ω is a positive number which we do not better specify. It is also possible to show that $\left\langle e^{i\hat{\theta}(x_k)}\right\rangle \neq 0$ and that, because of homogeneity, the quantity is independent from x_k [LZ97]. This calculation highlights a different decay of the correlation function, which is now exponential. The correlation length depends on the Luttinger parameter K.

Motivated by this analysis, the experimental measurement of $\mathcal{O}^2_{\mathrm{P}}(l)$ is performed. Results are shown in figure 5.5, together with the comparison to MPS

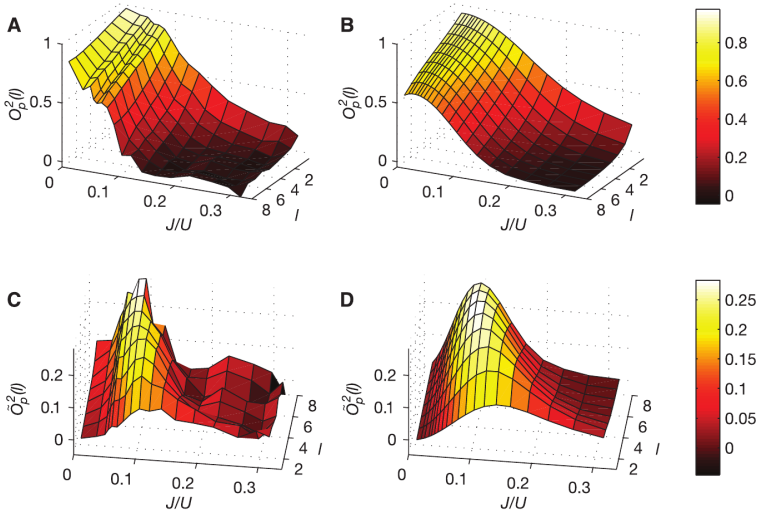

Figure 5.5: Experimental measures and theoretical predictions of string correlators. Experimental values (A) and MPS calculation (B) of $\mathcal{O}^2_{\mathrm{P}}(l)$ for $l \leq 8$. Experimental values (C) and MPS calculation (D) of $\tilde{\mathcal{O}}^2_{\mathrm{P}}(l)$ defined in equation (5.18) for $l \leq 8$. The numerics considers the parabolic confinement and $T = 0.09\,U/k_B$. Reproduced from [ECF+11] with permission from AAAS.

simulations taking into account the presence of the trap and of temperature $T = 0.09\,U/k_B$. There is a qualitative theory-data agreement. As in the homogeneous system, $\mathcal{O}^2_{\mathrm{P}}(l)$ decays with increasing J/U. The decay is significantly enhanced, probably by temperature effects, as it can be observed comparing data for $l = 8$ in figure 5.4 and 5.5 A. The effect of temperature is also revealed by the fact that $\mathcal{O}^2_{\mathrm{P}}(l)$ is significantly smaller than one even at $J/U \sim 0$. We leave as an interesting open problem the theoretical development of quantities which can be extracted from such measurements to be used for better characterizing the quantum state of the system, as for example the determination of the Luttinger parameters of the effective low-energy model, even in presence of non-negligible thermal and finite-size effects.

5.3 Multi-Site Correlations

Finally, we investigate whether the observation of a non-zero string order correlation function can be related to the presence of genuine multi-site correlations.

First, we rule out that the observed state is completely uncorrelated. We define:

$$\tilde{\mathcal{O}}^2_{\mathrm{P}}(l) = \mathcal{O}^2_{\mathrm{P}}(l) - \prod_{j=k}^{k+l} \langle \hat{s}_j \rangle. \tag{5.18}$$

Notice that $\tilde{\mathcal{O}}^2_{\mathrm{P}}(l = 1) = C(d = 1)$. Moreover, since for $J/U \neq 0$ it holds that

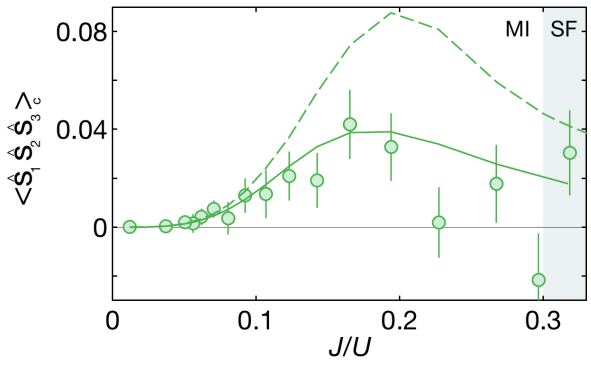

Figure 5.6: Three-site cumulant $\langle \hat{s}_1 \hat{s}_2 \hat{s}_3 \rangle_c$ for three neighbouring site. Dots: experimental data. Dashed line: DMRG calculation for a homogeneous system at $T = 0$. Solid line: MPS calculation including the confining potential and $T = 0.09\, U/k_B$. Reproduced from the supplementary materials of [ECF+11] with permission from AAAS.

$\prod_{j=k}^{k+l} \langle \hat{s}_j \rangle \xrightarrow{l\to\infty} 0$, we have:

$$\lim_{l\to\infty} \tilde{\mathcal{O}}^2_{\mathrm{P}}(l) = \mathcal{O}^2_{\mathrm{P}}(l); \quad J/U \neq 0 \tag{5.19}$$

Figure 5.5 shows the experimental and theoretical results. As expected, the uncorrelated state $J/U = 0$ is not detected by $\tilde{\mathcal{O}}^2_{\mathrm{P}}(l)$. We observe a rapid increase for increasing J/U and then a sudden decrease which resembles the behavior of $\mathcal{O}^2_{\mathrm{P}}(l)$. The experimental data clearly rule out the possibility of an uncorrelated state.

Still, this does not rule out the possibility that the state is characterized by only two-site correlations. Let us consider a string of length $l = 3$ and define a correlator which can detect a genuine three-site correlation, or so-called three-site cumulant:

$$\langle \hat{s}_1 \hat{s}_2 \hat{s}_3 \rangle_c = \langle \hat{s}_1 \hat{s}_2 \hat{s}_3 \rangle - \langle \hat{s}_1 \rangle \langle \hat{s}_2 \rangle \langle \hat{s}_3 \rangle - C_{1,2} \langle \hat{s}_3 \rangle - C_{1,3} \langle \hat{s}_2 \rangle - C_{2,3} \langle \hat{s}_1 \rangle \tag{5.20}$$

with $C_{i,j}$ the two-site cumulant $C_{i,j} = \langle \hat{s}_i \hat{s}_j \rangle - \langle \hat{s}_i \rangle \langle \hat{s}_j \rangle$. Figure 5.6 shows the experimental measure of $\langle \hat{s}_1 \hat{s}_2 \hat{s}_3 \rangle_c$. The experimental data show a clear peak for $0.1 < J/U < 0.2$ which is not compatible with zero and therefore rules out the possibility that the state can be described only in terms of two-site correlations alone.

Finally, let us stress that three-site correlations can arise also from a state as $|\Psi_{J/U\sim 0}\rangle$, where only particle-hole pairs extended on nearest neighboring sites are present.

5.4 Finite-Size Scaling of the String Order Parameter

We describe the DMRG simulations used to obtain the data plotted in figure 5.4.

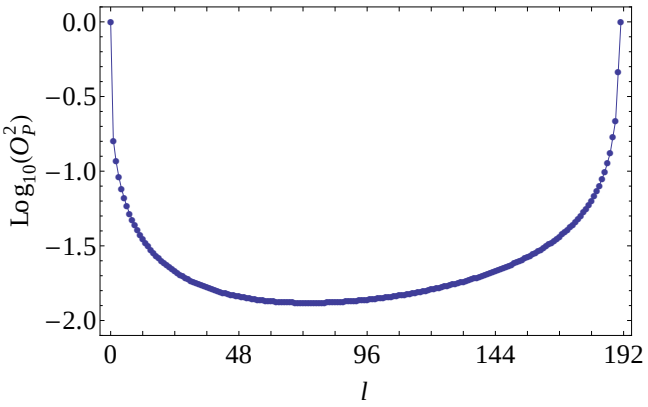

Figure 5.7: Numerical simulation of $\mathcal{O}_{\mathrm{P}}^2(l)$ for a system of length $L = 192$ with $N = 192$ particles via DMRG ($m = 235$). $J/U = 0.33$. The l sites are always taken in the center of the system. Lines connecting the dots are a guideline for the eye. The fact that $\mathcal{O}_{\mathrm{P}}^2(l = 0) = 1$ is a numerical artifact and is not relevant for the future discussion. The fact that $\mathcal{O}_{\mathrm{P}}^2(l = 191) = 1$ is a consequence of the fixed number of particles and is to be considered a finite-size effect, together with the growth which starts even before $l = L/2$.

The numerical simulations span system sizes between $L = 120$ and $L = 256$. The number of states retained in the DMRG calculation, m, has been chosen in order to have a truncation error smaller than 10^{-8}. This results in a relative error for the shown data which is smaller than 10^{-3}, as estimated via comparison of data for different m between 180 and 235.

In figure 5.7 we plot $\mathcal{O}_{\mathrm{P}}^2(l)$ for a system of length $L = 192$. The plot highlights the importance of finite-size effects. Indeed, since the algorithm works with a fixed number of particles, an unphysical growth of the signal sets in at $l < L/2$. Practically speaking, from a system of length $L = 192$ we are able to extract only $30 \div 35$ points which are physically relevant. This emphasizes the importance of an accurate scaling procedure for $l \to \infty$.

We introduce the notation $\mathcal{O}_{\mathrm{P}}^2(J/U, l, L)$ to denote for the expectation value of the string correlator of length l obtained from the numerical simulation of a system of length L. The l sites are always taken in the center of the system in order to minimize finite-size effects.

For the finite-size scaling in the inset of figure 5.4, we analyzed correlators $\mathcal{O}_{\mathrm{P}}^2(J/U, \alpha L, L)$ for a fixed fraction α of the total length L. We extrapolated:

$$\mathcal{O}_{\mathrm{P}}^2 = \lim_{L\to\infty} \mathcal{O}_{\mathrm{P}}^2(J/U, \alpha L, L) \tag{5.21}$$

using a scaling of the form $\mathcal{O}_{\mathrm{P}}^2(J/U, \alpha L, L) = a + bL^{\eta}$ [KT92, UNK08, DDDBO11].

To determine the point of the phase transition, $(J/U)_c$, we fit the extrapolated values with:

$$\mathcal{O}_{\mathrm{P}}^2 \propto e^{-A\sqrt{\left(\frac{J}{U}\right)_c - \frac{J}{U}}} \tag{5.22}$$

The results for $(J/U)_c$ appear to be strongly dependent on the fitting interval $[(J/U)_1, (J/U)_2]$ and α, and are shown in table 5.1. This large systematic error

	$\alpha = 1/4$	$\alpha = 1/3$	$\alpha = 1/2$
$[(J/U)_1, (J/U)_2] = [0.23, 0.37]$	0.303	0.306	0.296
$[(J/U)_1, (J/U)_2] = [0.24, 0.36]$	0.310	0.311	0.299
$[(J/U)_1, (J/U)_2] = [0.25, 0.35]$	0.319	0.318	0.305
$[(J/U)_1, (J/U)_2] = [0.26, 0.34]$	0.321	0.319	0.311
$[(J/U)_1, (J/U)_2] = [0.27, 0.33]$	0.317	0.314	0.309

Table 5.1: Results for $(J/U)_c$ for different relative lengths α and fitting intervals $[(J/U)_1, (J/U)_2]$.

reflects the difficulty of doing reliable numerics in presence of a phase-transition of BKT type.

5.5 Conclusions and Perspectives

In conclusion, we have presented a theoretical and experimental study of the phase transition from Mott insulator to superfluid of the one-dimensional Bose-Hubbard model via local and non-local parity measurements. We have shown that parity-parity correlation functions can be used to probe the presence of correlated particle-hole pairs in the Mott insulator. We have analyzed the properties of the string operator given by the product of parity operators in a string. In particular, it is a non-local order parameter for the Mott-insulating phase. These quantities can be measured experimentally for a bosonic gas trapped in a one-dimensional optical lattice and are compared to finite-size MPS simulations at finite temperature. Finally, the data have been proven to show genuine multi-site correlations.

From the experimental point of view, these results open the way to the experimental revelation of topological phases via probing the non-local order parameter which characterizes them. In particular, the same technique could be applied to one-dimensional spin-1 atoms with long-range interactions to detect the Haldane phase [Hal83, dNR89].

Theoretically, this experiment underlines the interest in pursuing the study of finite-size systems to develop quantities which are experimentally accessible and theoretically relevant. Moreover, the generalization of the string order parameter for higher-dimensional systems to a membrane order parameter could also be interesting [PGWS$^+$08].

Part II

Quantum Information Applications of Topological Superconductors

Chapter 6

Fermionic Gaussian States

In this chapter we present a self-consistent introduction to fermionic Gaussian states. Gaussian states are many-body quantum states which are completely characterized by their covariance matrix.

To the best of our knowledge, comprehensive studies of fermionic Gaussian states have been first presented by Botero and Reznick [BR04] and by Bravyi [Bra05], even if there are earlier studies on closely related problems [Kni01, TD02]. We do not follow the construction of [Bra05], based on the functional integral of Grassmann variables, but rather follow an approach which only relies on matrix analysis, as in [BR04].

Gaussian states are the appropriate instrument for solving problems related to quadratic Hamiltonians, which can be always mapped to non-interacting models. For instance, they can be used to determine the ground state properties and to compute the corresponding time evolution. Since the treatment of a Gaussian state composed of N fermionic modes requires to work with matrices whose size scales linearly in N, they can be efficiently simulated with a classical computer [Kni01, TD02].

Starting from these early works, fermionic Gaussian states have been further developed. We list here some of the most significant recent contributions. In [Hor11] the authors compute the time evolution of a Gaussian state via a master equation with jump operators which are linear and quadratic in the fermionic fields. This method is used to characterize the interplay between dissipation and quantum phase transitions in spin systems. A similar work has been presented in [EP10]. In [KC10] the authors also include the mean-field treatment of interactions within this formalism. The method is used to compute the Gaussian state which optimally approximates the ground state of an interacting model; the time evolution ruled by a quartic Hamiltonian is also discussed. In [BK11a] the authors rigorously demonstrate that the time evolution described by a master equation with jump operators which are linear in the fermionic field maps Gaussian states into Gaussian states.

In this chapter we review some known results and derive some formulas which we could not find in the scientific literature. These tools are used in chapter 7 to answer a physically relevant problem related to fermionic topological quantum memories. In section 6.1 we introduce the Majorana fermions. In section 6.2 we discuss the canonical transformations for such fermions, and in section 6.3 we analyse the properties of fermionic Gaussian states. In section 6.4 we focus on

quadratic Hamiltonians. In section 6.5 we present some forms of time evolution which map Gaussian states to Gaussian states; instead, in section 6.6, we discuss forms of time evolution which do not fulfill such property.

Finally, we would like to thank Prof. Michael M. Wolf and Dr. Géza Giedke for sharing with us some unpublished personal notes on this subject, which have been used as a starting point for understanding fermionic Gaussian states.

6.1 Dirac and Majorana Fermions

Let us consider N fermionic modes, described by $2N$ Dirac fermionic operators $\{\hat{a}_i^{(\dagger)}\}_{i=1\dots N}$ satisfying the canonical anticommutation relations:

$$\{\hat{a}_i, \hat{a}_j\} = 0; \quad \{\hat{a}_i, \hat{a}_j^\dagger\} = \delta_{i,j}. \tag{6.1}$$

We introduce the Majorana operators, i.e. fermionic operators which are real, Hermitian and unitary:

$$\hat{c}_{j,1} = \hat{a}_j + \hat{a}_j^\dagger; \qquad \hat{c}_{j,2} = -i(\hat{a}_j - \hat{a}_j^\dagger). \tag{6.2}$$

They satisfy the following canonical anticommutation relations:

$$\{\hat{c}_{j,\sigma}, \hat{c}_{k,\tau}\} = 2\delta_{j,k}\delta_{\sigma,\tau}. \tag{6.3}$$

Majorana operators are useful because they remove the asymmetry between $\hat{a}_j$ and $\hat{a}_j^\dagger$ operators, which are substituted by a list of $2N$ operators to be treated on an equal footing. This choice has been made because of convenience and in principle the work presented in this chapter could have been derived also using Dirac operators, at the price of more intricate calculations.

Majorana operators are labelled by two indices, $j \in \{1, \dots N\}$ and $\sigma \in \{1, 2\}$. When it is not necessary to distinguish between the two labels, we use one single index $k \in \{(1,1), \dots (N,2)\}$.

We list some useful relations between Majorana and Dirac operators.

$$\begin{array}{cc}
\hat{c}_{j,1} = \hat{a}_j + \hat{a}_j^\dagger; & \hat{c}_{j,2} = -i(\hat{a}_j - \hat{a}_j^\dagger); \\
\hat{a}_j = \frac{1}{2}\left(\hat{c}_{j,1} + i\hat{c}_{j,2}\right); & \hat{a}_j^\dagger = \frac{1}{2}\left(\hat{c}_{j,1} - i\hat{c}_{j,2}\right); \\
\hat{a}_j^\dagger\hat{a}_j = \frac{1}{2}\hat{1} + \frac{i}{4}\left[\hat{c}_{j,1}, \hat{c}_{j,2}\right]; & \hat{c}_{j,1}\hat{c}_{j,2} = i\left[\hat{a}_j, \hat{a}_j^\dagger\right]; \\
\hat{a}_j^\dagger\hat{a}_j = \frac{1}{2}\hat{1} + \frac{i}{2}\hat{c}_{j,1}\hat{c}_{j,2}; & \hat{c}_{j,1}\hat{c}_{j,2} = -i\hat{1} + 2i\hat{a}_j\hat{a}_j^\dagger; \\
\hat{a}_j\hat{a}_j^\dagger = \frac{1}{2}\hat{1} - \frac{i}{2}\hat{c}_{j,1}\hat{c}_{j,2}; & \hat{c}_{j,1}\hat{c}_{j,2} = i\hat{1} - 2i\hat{a}_j^\dagger\hat{a}_j.
\end{array} \tag{6.4}$$

6.2 Canonical Transformations

Canonical transformations of the Majorana operators, i.e. linear transformations preserving the anticommutation relations (6.3), are represented by real orthogonal matrices:

$$\begin{aligned}
&\hat{c}_k \to \hat{c}'_k = \sum_l O_{kl}\hat{c}_l; \\
&\{\hat{c}'_j, \hat{c}'_k\} = 2\delta_{j,k} \;\Rightarrow\; O_{kl} \in \mathbb{R};\; OO^T = O^TO = \mathbb{I}.
\end{aligned} \tag{6.5}$$

All canonical transformations have a unitary representation $\hat{U}$:

$$\hat{c}'_k = \sum_l O_{kl}\hat{c}_l = \hat{U}\hat{c}_k\hat{U}^\dagger; \quad \hat{U}\hat{U}^\dagger = \hat{U}^\dagger\hat{U} = \hat{1}. \tag{6.6}$$

If $\det O = +1$, the unitary $\hat{U}$ is:

$$\hat{U} = \exp\left[-\frac{1}{4}\sum_{\alpha,\beta} A_{\alpha,\beta}\hat{c}_\alpha\hat{c}_\beta\right],\ A \text{ s.t. } O = e^A,\ A = -A^T \tag{6.7}$$

This can be demonstrated rotating O into its canonical form, $\tilde{O}$, using an orthogonal transformation:

$$\tilde{O} = \bigoplus_{\alpha=1}^{\#\text{modes}} \begin{pmatrix} \cos\theta_\alpha & \sin\theta_\alpha \\ -\sin\theta_\alpha & \cos\theta_\alpha \end{pmatrix} \tag{6.8}$$

The unitary representation is not unique: for instance, $\hat{U}$ and $-\hat{U}$ induce the same canonical transformation O.

If $\det O = -1$, the unitary $\hat{U}$ is [BR04]:

$$\hat{U} = \sum_k v_k\hat{c}_k; \quad v_k \text{ s.t. } v_k \in \mathbb{R}, \quad \sum_k v_k^2 = 1, \quad O_{k,l} = 2v_kv_l - \delta_{k,l}. \tag{6.9}$$

From now on, we focus only on canonical transformation with $\det O = +1$.

6.2.1 Single-Mode and Multi-Mode Cases

A canonical transformation for a single mode system depends on only one parameter $\theta \in \mathbb{R}$ (see equation (6.8)). The real skew-symmetric matrix A, defined as the logarithm of O, by definition in its canonical form, is:

$$A = \begin{pmatrix} 0 & \eta \\ -\eta & 0 \end{pmatrix} = \begin{pmatrix} 0 & \theta \\ -\theta & 0 \end{pmatrix} + 2\pi K \begin{pmatrix} 0 & 1 \\ -1 & 0 \end{pmatrix}; \tag{6.10}$$

with $\eta \in [-\pi, \pi)$ and $K \in \mathbb{Z}$. Accordingly, the unitary $\hat{U}$ can be written in one of the equivalent following forms:

$$\begin{aligned} \hat{U} &= \exp\left[-\frac{1}{4}A_{\alpha,\beta}\hat{c}_\alpha, \hat{c}_\beta\right] = e^{-(\frac{\theta}{2}+K\pi)\hat{c}_1\hat{c}_2} = \\ &= \cos\left(\frac{\theta}{2}+K\pi\right)\left[\hat{1} - \tan\left(\frac{\theta}{2}+K\pi\right)\hat{c}_1\hat{c}_2\right] = \\ &= (-1)^K\cos\frac{\theta}{2}\left[\hat{1} - \tan\frac{\theta}{2}\hat{c}_1\hat{c}_2\right] = \cos\frac{\eta}{2}\left[\hat{1} - \tan\frac{\eta}{2}\hat{c}_1\hat{c}_2\right] = \\ &= \cos\frac{\eta}{2}\hat{1} - \sin\frac{\eta}{2}\hat{c}_1\hat{c}_2. \end{aligned} \tag{6.11}$$

The singularity at $\eta = -\pi$ is fictitious since $\tan\eta/2$ is always multiplied by $\cos\eta/2$. Moreover, it happens that $\hat{U}$, as written in (6.11), is a periodic function of θ, with period 4π; on the other hand, the expression of O in equation (6.8) has period 2π. This difference reflects the fact that $\hat{U}$ and $-\hat{U}$ induce the same transformation O.

We explicitly rewrite (6.11) as:

$$\hat{U} = e^{-i\eta/2} e^{i\eta \hat{a}^\dagger \hat{a}} = e^{-i\eta/2} |0\rangle\langle 0| + e^{i\eta/2} |1\rangle\langle 1|;$$

which is the most general canonical transformation for a fermionic single-mode system.

Let us consider the case of N modes. The unitary operator in (6.7) can be easily computed considering the canonical form $\tilde{O}$ in (6.8). In this case, the matrix $\tilde{A}$ reads:

$$\tilde{A} = \bigoplus_{\alpha=1}^{\#\text{modes}} \begin{pmatrix} 0 & \eta_\alpha \\ -\eta_\alpha & 0 \end{pmatrix} = \bigoplus_{\alpha=1}^{\#\text{modes}} \begin{pmatrix} 0 & \theta_\alpha \\ -\theta_\alpha & 0 \end{pmatrix} + 2\pi K_\alpha \begin{pmatrix} 0 & 1 \\ -1 & 0 \end{pmatrix} \quad (6.12)$$

with $\eta_\alpha \in [-\pi, \pi)$ and $K_\alpha \in \mathbb{Z}$. The operator $\hat{U}$ gets a particularly simple expression in this basis:

$$\begin{aligned} \hat{U} &= \left(\prod_\alpha \cos \frac{\eta_\alpha}{2} \right) \cdot \prod_\alpha \left(\hat{1} - \tan \frac{\eta_\alpha}{2} \hat{c}_{\alpha,1} \hat{c}_{\alpha,2} \right) = \\ &= (-1)^{\sum_\alpha K_\alpha} \left(\prod_\alpha \cos \frac{\theta_\alpha}{2} \right) \cdot \prod_\alpha \left(\hat{1} - \tan \frac{\theta_\alpha}{2} \hat{c}_{\alpha,1} \hat{c}_{\alpha,2} \right) \end{aligned} \quad (6.13)$$

The singularities at $\eta_\alpha = -\pi$ are fictitious and there is an intrinsic sign ambiguity, as discussed before.

Finally, $\mathrm{Tr}[\hat{U}] = \prod_\alpha 2\cos(\eta_\alpha/2)$ or $\mathrm{Tr}[\hat{U}] = (-1)^{\sum_\alpha K_\alpha} \prod_\alpha 2\cos(\theta_\alpha/2)$. If there is at least one $\eta_\alpha = -\pi$, then $\mathrm{Tr}[\hat{U}] = 0$.

6.2.2 Covariance Matrix

Let us introduce the covariance matrix of a canonical transformation $\hat{U}$:

$$\Upsilon_{\alpha,\beta} = -\frac{i}{2} \mathrm{Tr} \left[\hat{U} (\hat{c}_\alpha \hat{c}_\beta - \hat{c}_\beta \hat{c}_\alpha) \right] \quad (6.14)$$

For the single mode case of equation (6.11) it looks like:

$$\Upsilon = i\, 2\cos\frac{\eta}{2} \begin{pmatrix} 0 & -\tan\frac{\eta}{2} \\ +\tan\frac{\eta}{2} & 0 \end{pmatrix} = \mathrm{Tr}[\hat{U}] \begin{pmatrix} 0 & -i\tan\frac{\eta}{2} \\ +i\tan\frac{\eta}{2} & 0 \end{pmatrix} \quad (6.15)$$

For the multi-mode case of equation (6.13), it is:

$$\Upsilon = \mathrm{Tr}[\hat{U}] \cdot \bigoplus_\alpha \begin{pmatrix} 0 & -i\tan\frac{\eta_\alpha}{2} \\ +i\tan\frac{\eta_\alpha}{2} & 0 \end{pmatrix} \quad (6.16)$$

The singularities at $\eta_\alpha = -\pi$ are fictitious; because in this case $\mathrm{Tr}[\hat{U}] = 0$, the matrix Υ is almost completely covered with zeros, and loses its importance. In order to deal with such operators, which are not singular, but have a bad-defined matrix representation, we introduce another matrix:

$$\Omega = \bigoplus_\alpha \begin{pmatrix} 0 & -i\cot\frac{\eta_\alpha}{2} \\ i\cot\frac{\eta_\alpha}{2} & 0 \end{pmatrix} \quad (6.17)$$

This matrix is singular whenever there exists one α such that $\eta_\alpha = 0$. Let us assume there is one such η_α. In this case, there are two Majorana modes $\hat{c}_{\alpha,1}$ and $\hat{c}_{\alpha,2}$ which define a two-dimensional Hilbert space: $\mathcal{H}_\alpha = \mathrm{Span}\{|0_\alpha\rangle, |1_\alpha\rangle\}$, with $|0_\alpha\rangle$ defined by $\hat{a}_\alpha|0_\alpha\rangle = 0$ and $|1_\alpha\rangle = \hat{a}_\alpha^\dagger|0_\alpha\rangle$. We observe that the global Hilbert space is partitioned in $\mathcal{H} = \mathcal{H}_\alpha \otimes \mathcal{H}_{\bar{\alpha}}$, such that: $\hat{U} = \hat{\mathbb{I}}_2 \otimes \hat{U}_{\bar{\alpha}}$. In this case, we define the matrix $\Omega_{\bar{\alpha}}$ of the operator $\hat{U}_{\bar{\alpha}}$, which is still Gaussian[1]. This easily generalizes to the presence of many such η_α.

6.3 Fermionic Gaussian States

We introduce the fermionic Gaussian states and discuss some of their most relevant properties.

6.3.1 Single-Mode and Multi-Mode Cases

A single-mode Gaussian state is a one-fermion state which has a density operator of the form:

$$\hat{\rho} \;=\; \frac{e^{-\beta \hat{a}^\dagger \hat{a}}}{1+e^{-\beta}} = \frac{1}{2}\left(\hat{1} - i\tanh\frac{\beta}{2}\hat{c}_1\hat{c}_2\right). \tag{6.18}$$

In the following, we use the notation:

$$\hat{\rho} \;=\; \frac{1}{2}\left(\hat{1} + \lambda\left[\hat{a}, \hat{a}^\dagger\right]\right) \;=\; \frac{1}{2}\left(\hat{1} - i\lambda\hat{c}_1\hat{c}_2\right); \qquad \lambda = \tanh\frac{\beta}{2}. \tag{6.19}$$

The density operator can be equivalently rewritten as:

$$\hat{\rho} = \frac{1}{2}(1+\lambda)\hat{1} - \lambda\hat{n}; \qquad \hat{\rho} = \frac{1}{2}\left[(1+\lambda)|0\rangle\langle 0| + (1-\lambda)|1\rangle\langle 1|\right].$$

One can easily verify that $\mathrm{Tr}\hat{\rho} = 1$, whereas $\mathrm{Tr}\hat{\rho}^2 = (1+\lambda^2)/2$, i.e. the state is pure if and only if $\lambda = \pm 1$. Looking at the eigenvalues, we notice that $\hat{\rho}$ is positive, and thus a well-defined density operator, if and only if $\lambda \in [-1, 1]$. Pure states which are linear superposition of $|0\rangle$ and $|1\rangle$ are not fermionic Gaussian states.

We now take a pragmatic approach and generalize the previous discussion to N modes. A N-modes fermionic Gaussian state is a N-fermions state which has a density operator of the form:

$$\hat{\rho} = \prod_\alpha \frac{1}{2}\left(\hat{1} + \lambda_\alpha\left[\hat{a}_\alpha, \hat{a}_\alpha^\dagger\right]\right) = \prod_\alpha \frac{1}{2}\left(\hat{1} - i\lambda_\alpha\hat{c}_{\alpha,1}\hat{c}_{\alpha,2}\right); \tag{6.20}$$

where $\{\hat{a}_\alpha^{(\dagger)}\}_{\alpha=1\ldots N}$ are Dirac operators and $\hat{c}_{\alpha,\sigma}$ are the corresponding Majorana operators. The $\hat{a}_\alpha^{(\dagger)}$ and $\hat{c}_{\alpha,\sigma}$ are the eigenmodes of the density operator.

Finally, we introduce the number parity operator:

$$\hat{P} = (-1)^{\sum_j \hat{a}_j^\dagger \hat{a}_j} = i^N \prod_k \hat{c}_k. \tag{6.21}$$

[1]Notice that we could have also defined a matrix $\tilde{\Upsilon} = \bigoplus_\alpha \begin{pmatrix} 0 & -i\tan\frac{\eta_\alpha}{2} \\ +i\tan\frac{\eta_\alpha}{2} & 0 \end{pmatrix}$ which would have not been more pathological than Ω. The singular case would have been $\eta_\alpha = -\pi$, corresponding to the decomposition $\hat{U} = \hat{c}_{\alpha 1}\hat{c}_{\alpha 2} \otimes \hat{U}_{\bar{\alpha}}$. We think that the definition presented in the text is more convenient.

This expression is almost invariant under canonical transformations:

$$i^N \prod_k \hat{c}'_k = \det O \; i^N \prod_k \hat{c}_k.$$

Notice the presence of the $\det O$ pre-factor.

Density matrices of fermionic Gaussian states $\hat{\rho}$ commute with the parity operator because they are a linear combination of operators which have an even number of fermionic fields. Therefore, they are the direct sum of an operator living in the even fermionic sector and one living in the odd sector: $\hat{\rho} = \hat{\rho}_{\mathrm{e}} \oplus \hat{\rho}_{\mathrm{o}}$. Fermionic Gaussian states automatically satisfy the superselection rule of the parity of the number of fermions.

6.3.2 Covariance Matrix and Wick's Theorem

Let us introduce the covariance matrix of a Gaussian state $\hat{\rho}$:

$$\Gamma_{\alpha,\beta} = -\frac{i}{2} \mathrm{Tr}\left[\hat{\rho}\,(\hat{c}_\alpha \hat{c}_\beta - \hat{c}_\beta \hat{c}_\alpha)\right]. \tag{6.22}$$

For the single mode case in (6.19) and for the multi-mode case in (6.20) it is:

$$\Gamma = \begin{pmatrix} 0 & \lambda \\ -\lambda & 0 \end{pmatrix}; \qquad \Gamma = \bigoplus_\alpha \begin{pmatrix} 0 & \lambda_\alpha \\ -\lambda_\alpha & 0 \end{pmatrix}. \tag{6.23}$$

Moreover, if we apply the canonical transformation (6.5) to the Majorana operators, O, the covariance matrix in the new basis reads as follows:

$$\Gamma' = O \Gamma O^T. \tag{6.24}$$

Let us write, as an example, the covariance matrix of the following two-modes Gaussian state:

$$|\Psi\rangle = A|g\rangle + B a^\dagger b^\dagger |g\rangle; \qquad \Gamma_\Psi = \begin{pmatrix} 0 & \gamma & i\alpha & \beta \\ -\gamma & 0 & \beta & -i\alpha \\ -i\alpha & -\beta & 0 & \gamma \\ -\beta & i\alpha & -\gamma & 0 \end{pmatrix} \tag{6.25}$$

where $\alpha = A^*B - AB^*$, $\beta = A^*B + AB^*$ and $\gamma = |A|^2 - |B|^2$. This explicit expression will be useful in chapter 7 where we describe the encoding of a qubit into two fermionic modes.

Fermionic Gaussian states are efficiently simulated with classical computers because their covariance matrix completely characterizes their properties. This is elegantly stated by the following relation:

$$(-i)^p \; \mathrm{Tr}[\hat{\rho}\, \hat{c}_{\alpha_1} \dots \hat{c}_{\alpha_{2p}}] = \mathrm{Pf}\left[\Gamma|_{\alpha_1 \dots \alpha_{2p}}\right]; \tag{6.26}$$

which is a consequence of the Wick's theorem[2]. $\Gamma|_{\alpha_1 \dots \alpha_{2p}}$ is the restriction of Γ to the modes $\{\alpha_1 \dots \alpha_{2p}\}$, which is a $2p \times 2p$ matrix. We rewrite the definition of Pfaffian of a $2m \times 2m$ skew-symmetric matrix M:

$$\mathrm{Pf}[M] = \frac{1}{2^m m!} \sum_{\pi \in S_{2m}} \mathrm{sgn}(\pi) M_{\pi_1,\pi_2} M_{\pi_3,\pi_4} \dots M_{\pi_{2m-1},\pi_{2m}}. \tag{6.27}$$

[2] A demonstration of the Wick's theorem applied to Majorana fermions can be found in [TD02]. Moreover, Wick's theorem applies also to the canonical transformations discussed in the previous section, and it can be found in equation (B.5).

6.3.3 Overlap between Gaussian States

In this and in the next subsection we discuss two methods to compare fermionic Gaussian states. We start considering the squared overlap between two N-mode fermionic Gaussian states, $\hat{\rho}$ and $\hat{\sigma}$. It reads [Bra05]:

$$\mathrm{Tr}\left[\hat{\rho}\,\hat{\sigma}\right] = +\sqrt{\det\left[\frac{1-\Gamma_\rho\Gamma_\sigma}{2}\right]} \tag{6.28}$$

The formula is symmetric with respect to exchange of $\hat{\sigma}$ and $\hat{\rho}$, as stated by the Silvester determinant theorem. In appendix B we generalize this formula to the expectation value of a canonical transformation: $\mathrm{Tr}[\hat{\rho}\,\hat{U}]$. Moreover, we also show how to compute $\mathrm{Tr}[\hat{U}'\,\hat{U}'']$.

Proof of equation (6.28)*:* Let us work in the diagonal basis for $\hat{\rho}$, which assumes the form of (6.20). Let's expand the product:

$$\hat{\rho} = \frac{1}{2^N}\cdot\sum_{s=0}^{N}\sum_{\substack{\text{ordered}\\ \text{strings of}\\ \text{length } s\\ \{\alpha_1\ldots\alpha_s\}}}(-i)^s\lambda_{\alpha_1}\ldots\lambda_{\alpha_s}\hat{c}_{\alpha_1,1}\hat{c}_{\alpha_1,2}\ldots\hat{c}_{\alpha_s,1}\hat{c}_{\alpha_s,2} \tag{6.29}$$

where the case $s=0$ yields a $\hat{1}$. Using equation (6.26), after some algebraic manipulation, assuming $\lambda_\alpha \neq 0\ \forall\alpha$, we write:

$$\mathrm{Tr}\left[\hat{\rho}\,\hat{\sigma}\right] = \left(\prod_\alpha\frac{\lambda_\alpha}{2}\right)\sum_{s=0}^{N}\sum_{\text{strings }\ldots}\frac{1}{\prod_{\alpha\notin\text{string}}\lambda_\alpha}\mathrm{Pf}\left[\Gamma_\sigma|_{\alpha\in\text{string}}\right] \tag{6.30}$$

We now notice that $\frac{1}{\prod_{\alpha\notin\text{string}}\lambda_\alpha} = \mathrm{Pf}\left[-\Gamma_\rho^{-1}|_{\alpha\notin\text{string}}\right]$ and obtain:

$$\mathrm{Tr}\left[\hat{\rho}\,\hat{\sigma}\right] = \left(\prod_\alpha\frac{\lambda_\alpha}{2}\right)\sum_{s=0}^{N}\sum_{\text{strings }\ldots}\mathrm{Pf}\left[-\Gamma_\rho^{-1}|_{\alpha\notin\text{string}}\right]\mathrm{Pf}\left[\Gamma_\sigma|_{\alpha\in\text{string}}\right] \tag{6.31}$$

We now make use of the following result from [IW99]: Let A and B be $m\times m$ skew-symmetric matrices. Put $s=[m/2]$, the integer part of $m/2$. Then:

$$\mathrm{Pf}(A+B) = \sum_{t=0}^{s}\sum_{\mathbf{i}\in I_{2_t}^m}(-1)^{|\mathbf{i}|-t}\,\mathrm{Pf}A_{\mathbf{i}}\,\mathrm{Pf}B_{\mathbf{i}^c} \tag{6.32}$$

where we denote by $\mathbf{i}^c$ the complementary set of $\mathbf{i}$ in $[m]$ which is arranged in increasing order, and $|\mathbf{i}| = i_1+\ldots+i_{2_t}$ for $i=(i_1,\ldots,i_{2_t})$.

We can apply equation (6.32) to equation (6.31). Notice that Γ_ρ is in canonical form (6.23) and for all the relevant $\mathbf{i}$ we have $(-1)^{|\mathbf{i}|-t}=1$. We obtain:

$$\mathrm{Tr}\left[\hat{\rho}\,\hat{\sigma}\right] = \left(\prod_\alpha\frac{\lambda_\alpha}{2}\right)\cdot\mathrm{Pf}\left(\Gamma_\sigma-\Gamma_\rho^{-1}\right) = \mathrm{Pf}\left[\frac{\Gamma_\rho}{2}\right]\cdot\mathrm{Pf}\left[\Gamma_\sigma-\Gamma_\rho^{-1}\right] \tag{6.33}$$

Since we know that $\mathrm{Tr}\left[\hat{\rho}\,\hat{\sigma}\right]>0$, exploiting that $(\mathrm{Pf}\,A)^2=\det A$, we can rewrite it as in (6.28). Moreover, formula (6.28) is true even if the covariance matrices

have been computed for the eigenmodes which do not put ρ in form (6.20) because it is invariant under orthogonal transformations.

Let's discuss the case with one $\lambda_\alpha = 0$. This means that the corresponding eigenmodes $\hat{c}_{\alpha,1}$ and $\hat{c}_{\alpha,2}$ define a two-dimensional Hilbert space: $\mathcal{H}_\alpha = \mathrm{Span}\{|0_\alpha\rangle, |1_\alpha\rangle\}$ with $|0_\alpha\rangle$ defined by $\hat{a}_\alpha|0_\alpha\rangle = 0$ and $|1_\alpha\rangle = \hat{a}_\alpha^\dagger|0_\alpha\rangle$ such that: $\mathcal{H} = \mathcal{H}_\alpha \otimes \mathcal{H}_{\bar{\alpha}}$ and

$$\hat{\rho} = \frac{\hat{\mathbb{1}}}{2} \otimes \hat{\rho}'' \tag{6.34}$$

The other density matrix is: $\hat{\sigma} = \sum_\beta \hat{\sigma}'_\beta \otimes \hat{\sigma}''_\beta$. The reduced density matrix $\hat{\sigma}_{\bar{\alpha}}$ is:

$$\hat{\sigma}_{\bar{\alpha}} = \mathrm{Tr}_{\mathcal{H}_\alpha}[\hat{\sigma}] = \sum_\beta \mathrm{Tr}_{\mathcal{H}_\alpha}[\hat{\sigma}'_\beta]\,\hat{\sigma}''_\beta \tag{6.35}$$

We compute $\mathrm{Tr}\,[\hat{\rho}\,\hat{\sigma}]$ and obtain:

$$\mathrm{Tr}\,[\hat{\rho}\,\hat{\sigma}] = \sum_\beta \mathrm{Tr}_{\mathcal{H}_\alpha}\left[\frac{\hat{\mathbb{1}}_2}{2}\hat{\sigma}'_\beta\right] \cdot \mathrm{Tr}_{\mathcal{H}_{\bar{\alpha}}}\left[\hat{\rho}''\,\hat{\sigma}''_\beta\right] = \frac{1}{2}\mathrm{Tr}\,[\hat{\rho}''\hat{\sigma}_{\bar{\alpha}}] \tag{6.36}$$

The operators $\hat{\rho}''$ and $\hat{\sigma}_{\bar{\alpha}}$ are still Gaussian and the corresponding covariance matrix is known, i.e. the restriction of the original ones to the modes of $\mathcal{H}_{\bar{\alpha}}$. In presence of M eigenvalues $\lambda_\alpha = 0$, we define $\tilde{\Gamma}_\rho = \Gamma_\rho|_{\alpha\ \mathrm{s.t.}\lambda_\alpha \neq 0}$ and $\tilde{\Gamma}_\sigma$ correspondingly. Formula (6.33) must be generalized to:

$$\mathrm{Tr}\,[\hat{\rho}\,\hat{\sigma}] = \frac{1}{2^M}\mathrm{Pf}\left[\frac{\tilde{\Gamma}_\rho}{2}\right] \cdot \mathrm{Pf}\left(\tilde{\Gamma}_\sigma - \tilde{\Gamma}_\rho^{-1}\right) \tag{6.37}$$

Notice that formula (6.28) is still valid; indeed the only problem was that Γ_ρ^{-1} was not defined if some α are such that $\lambda_\alpha = 0$. □

6.3.4 Uhlmann Fidelity

In this subsection we consider a second method to compare two Gaussian states $\hat{\rho}$ and $\hat{\sigma}$, i.e. the Uhlmann fidelity:

$$F(\hat{\rho}, \hat{\sigma}) = \mathrm{Tr}\sqrt{\hat{\rho}^{1/2}\hat{\sigma}\hat{\rho}^{1/2}} \tag{6.38}$$

If at least one of the two states is pure, $F(\hat{\rho}, \hat{\sigma}) = +\sqrt{\mathrm{Tr}\,[\hat{\rho}\,\hat{\sigma}]}$. We therefore assume that both states are mixed.

Let us make the stronger assumption that all the λ_α of the covariance matrices of the two states are such that $|\lambda_\alpha| < 1$. In this case, the state $\hat{\rho}$ admits the representation:

$$\hat{\rho} = \frac{\exp\left[-\frac{i}{4}\sum_j \beta_j(\hat{c}_{j,1}\hat{c}_{j,2} - \hat{c}_{j,2}\hat{c}_{j,1})\right]}{\prod_j 2\cosh\beta_j/2}; \qquad \lambda_j^{(\rho)} = \tanh\frac{\beta_k}{2} \tag{6.39}$$

As a consequence, $\hat{\rho}^{1/2}$ has the form:

$$\hat{\rho}^{1/2} = \frac{\exp\left[-\frac{i}{4}\sum_j \frac{\beta_j}{2}(\hat{c}_{j,1}\hat{c}_{j,2} - \hat{c}_{j,2}\hat{c}_{j,1})\right]}{\prod_j (2\cosh\beta_j/2)^{1/2}} \tag{6.40}$$

Let us define the effective Hamiltonian:

$$\hat{H}_\rho = \frac{i}{4}\sum_j \frac{\beta_j}{2}(\hat{c}_{j,1}\hat{c}_{j,2} - \hat{c}_{j,2}\hat{c}_{j,1}); \tag{6.41}$$

and the corresponding imaginary-time evolution of the state $\hat{\sigma}$ [KC10]:

$$\hat{\sigma}_I(\tau) = \frac{e^{-\hat{H}_\rho \tau}\hat{\sigma}e^{-\hat{H}_\rho \tau}}{\mathrm{Tr}\left[e^{-2\hat{H}_\rho \tau}\hat{\sigma}\right]} \tag{6.42}$$

which is a well-defined density matrix. It follows that:

$$\hat{\rho}^{1/2}\,\hat{\sigma}\,\hat{\rho}^{1/2} = \frac{\mathrm{Tr}\left[e^{-2\hat{H}_\rho}\hat{\sigma}\right]}{\prod_j 2\cosh\beta_j/2}\hat{\tilde{\sigma}}(\tau=1) \tag{6.43}$$

Due to the properties of imaginary time evolution, $\hat{\sigma}_I(\tau)$ is still a Gaussian state and its covariance matrix can be efficiently computed [KC10]. It is interesting to observe that:

$$\frac{\mathrm{Tr}\left[e^{-2\hat{H}_\rho}\hat{\sigma}\right]}{\prod_k 2\cosh\beta_k/2} = \mathrm{Tr}[\hat{\rho}\,\hat{\sigma}]. \tag{6.44}$$

The fidelity is therefore:

$$F(\hat{\rho},\hat{\sigma}) = \sqrt{\mathrm{Tr}[\hat{\rho}\,\hat{\sigma}]}\;\mathrm{Tr}\sqrt{\hat{\sigma}_I(\tau=1)}. \tag{6.45}$$

We define the parameters $\{\varphi_\alpha\}_\alpha$ via $\tanh\varphi_\alpha/2 = \Re(\lambda_\alpha^{\sigma_I})$, where λ_α are the eigenvalues of the covariance matrix of $\hat{\sigma}_I(\tau=1)$. We obtain:

$$\sqrt{\hat{\sigma}_I(\tau=1)} = \prod_\alpha \frac{2\cosh\varphi_\alpha/4}{\sqrt{2\cosh\varphi_\alpha/2}}\cdot\frac{\exp\left[-\frac{i}{4}\sum_\alpha \frac{\varphi_\alpha}{2}(\hat{c}'_{\alpha,1}\hat{c}'_{\alpha,2} - \hat{c}'_{\alpha,2}\hat{c}'_{\alpha,1})\right]}{\prod 2\cosh\varphi_\alpha/4}; \tag{6.46}$$

from which follows that

$$\mathrm{Tr}\sqrt{\tilde{\sigma}(\tau=1)} = \prod_\alpha \frac{\sqrt{2}\cosh\varphi_\alpha/4}{(\cosh\varphi_\alpha/2)^{1/2}}. \tag{6.47}$$

Putting together formula (6.45) with (6.28) and (6.47) one finds a computable expression for the Uhlmann fidelity $F(\hat{\rho},\hat{\sigma})$.

6.4 Quadratic Hamiltonians

A general Hamiltonian operator quadratic in the fermionic fields can be written as:

$$\hat{H} = \frac{i}{4}\sum_{\alpha,\beta} T_{\alpha,\beta}\hat{c}_\alpha\hat{c}_\beta \tag{6.48}$$

The matrix $T_{\alpha,\beta}$ is real and skew-symmetric. There exists an orthogonal transformation O which rotates T into the canonical form:

$$T = O^T\cdot\bigoplus_\alpha\begin{pmatrix}0 & \varepsilon_\alpha\\ -\varepsilon_\alpha & 0\end{pmatrix}\cdot O\,; \qquad \varepsilon_\alpha \geq 0. \tag{6.49}$$

Therefore, there is a basis $\hat{c}'_i = \sum_j O_{i,j}\hat{c}_j$ such that:

$$\hat{H} = \frac{i}{4}\sum_{\alpha=1}^{N} 2\varepsilon_\alpha \hat{c}'_{\alpha,1}\hat{c}'_{\alpha,2} = -\sum_\alpha \frac{\varepsilon_\alpha}{2} + \sum_\alpha \varepsilon_\alpha \hat{a}'^{\dagger}_\alpha \hat{a}'_\alpha \tag{6.50}$$

where the Dirac modes are defined as: $\hat{a}'_\alpha = \frac{1}{2}(\hat{c}_{\alpha,1} + i\hat{c}_{\alpha,2})$. We automatically obtain the energy of the ground state: $E_0 = -\sum_\alpha \varepsilon_\alpha/2$.

The ground state of $\hat{H}$ is defined by the property:

$$\hat{a}'_\alpha|g\rangle = 0; \quad \forall\alpha. \tag{6.51}$$

Using this property, we can derive the covariance matrix of $|g\rangle$ in the basis $\hat{c}'_k$:

$$\Gamma'_g = \bigoplus_\alpha \begin{pmatrix} 0 & 1 \\ -1 & 0 \end{pmatrix}. \tag{6.52}$$

Using (6.24), we can obtain the covariance matrix of $|g\rangle$ in the initial basis $\hat{c}_k$ using the orthogonal transformation O of equation (6.49). It is easy to generalized these results to compute the covariance matrix of any eigenstate of $\hat{H}$.

The ground state $|g\rangle$ is a well-defined Gaussian state by construction:

$$\hat{\rho}_g = \prod_\alpha \hat{a}_\alpha \hat{a}^\dagger_\alpha = \prod_\alpha \frac{1}{2}\left(\hat{1} - i\hat{c}_{\alpha,1}\hat{c}_{\alpha,2}\right) \tag{6.53}$$

The same holds for all the eigenstates of $\hat{H}$.

Finally, the expectation value of the Hamiltonian $\hat{H}$ on any Gaussian state $\hat{\rho}$ is given by:

$$\mathrm{Tr}\left[\hat{H}\hat{\rho}\right] = \mathrm{Tr}\left[T\,\Gamma\right]. \tag{6.54}$$

A similar relation can be worked out for every quadratic operator.

6.5 Gaussian Time Evolution

We now start focussing on the time evolution of Gaussian states. In this section, we consider two particular cases which are important because they map Gaussian states into Gaussian states.

6.5.1 Hamiltonian Evolution

The dynamics induced by an Hamiltonian $\hat{H}$ is described by the unitary operator:

$$\hat{U}(t) = \exp\left[-\frac{i}{\hbar}\hat{H}t\right] = \exp\left[\frac{t}{4\hbar}\sum_{\alpha,\beta} T_{\alpha,\beta}\,\hat{c}_\alpha\,\hat{c}_\beta\right] \tag{6.55}$$

By comparison with (6.7) we find that the time evolution induced by a Hamiltonian is a canonical transformation of the Majorana modes.

All the results derived in section (6.2) for canonical transformations apply therefore to Hamiltonian time evolutions. Clearly, the time evolution maps

Gaussian states to Gaussian states. The covariance matrix of the time evolved state can be obtained from that of the initial one via:

$$\Gamma(t) = O(t)^T \, \Gamma(0) \, O(t); \qquad O(t) = \exp\left[-\frac{T}{\hbar}t\right] \tag{6.56}$$

The time-dependent covariance matrix satisfies the following differential equation:

$$\partial_t \Gamma(t) = \frac{1}{\hbar}\left[T(t), \Gamma(t)\right]. \tag{6.57}$$

6.5.2 Master Equation with Linear Jump Operators

The time evolution of a system coupled to an environment is usually described, under the Markov and Born approximations, by the Lindblad master equation reads:

$$\partial_t \hat{\rho} = -\frac{i}{\hbar}\left[\hat{H}, \hat{\rho}\right] + \sum_{\alpha}^{n_\alpha}\left(\hat{\mathcal{L}}_\alpha \hat{\rho} \hat{\mathcal{L}}_\alpha^\dagger - \frac{1}{2}\{\hat{\mathcal{L}}_\alpha^\dagger \hat{\mathcal{L}}_\alpha, \hat{\rho}\}\right) \tag{6.58}$$

where $\hat{H}$ is the Hamiltonian of the system and $\hat{\mathcal{L}}_\alpha$ are the the jump operators describing the decoherence process.

It has recently been proved that the time evolution governed by a master equation with jump (Lindblad) operators which are linear in the fermionic fields, maps Gaussian states into Gaussian states [BK11a].

We therefore restrict our study to quadratic fermionic Hamiltonians (6.48), and to Lindblad operators linear in the fermionic fields:

$$\hat{\mathcal{L}}_\alpha = \sum_k (L_{k,\alpha,\mathbb{R}} + iL_{k,\alpha,\mathbb{I}})\, \hat{c}_k = \vec{L}_{\alpha,\mathbb{R}} \cdot \vec{\hat{c}} + i\vec{L}_{\alpha,\mathbb{I}} \cdot \vec{\hat{c}} \tag{6.59}$$

Let us write the time dependence of the covariance matrix Γ of a Gaussian state obeying (6.58). The $2n_\alpha$ vectors $\vec{L}_{\alpha,\sigma} \in \mathbb{R}^{2N}$, ($\sigma \in \{\mathbb{R}, \mathbb{I}\}$) can be put together to build the $2N \times 2n_\alpha$ matrix $\tilde{L}$:

$$\tilde{L} = \left(\vec{L}_{1,\mathbb{R}}; \vec{L}_{1,\mathbb{I}}; \vec{L}_{2,\mathbb{R}}; \vec{L}_{2,\mathbb{I}} \ldots \vec{L}_{n_\alpha,\mathbb{R}}; \vec{L}_{n_\alpha,\mathbb{I}}\right) \tag{6.60}$$

The time evolution of the covariance matrix is given by [Hor11, EP10]:

$$\partial_t \Gamma = \frac{1}{\hbar}[T, \Gamma] - \{L_1, \Gamma\} - 2iL_2 \tag{6.61}$$

where L_1 and L_2 are defined as follows:

$$L_1 = 2\tilde{L}\tilde{L}^T; \qquad L_2 = 2i\tilde{L} \cdot \bigoplus_{k=1}^{n_\alpha} \begin{pmatrix} 0 & 1 \\ -1 & 0 \end{pmatrix} \cdot \tilde{L}^T \tag{6.62}$$

6.6 Non-Gaussian Time Evolution

It is also interesting to study time evolutions which do not map Gaussian states into Gaussian states. In some physically relevant cases, it is still possible to compute some properties of the time evolved state, as, for instance, its covariance matrix.

6.6.1 Master Equation with Quadratic Jump operators

Let us consider the Lindblad master equation in (6.58); we focus here to the case of jump operators which are quadratic and Hermitian:

$$\hat{\mathcal{L}}_\alpha = \frac{i}{4}\sum_{k,l} M^\alpha_{kl}\,\hat{c}_k\,\hat{c}_l. \tag{6.63}$$

The time evolution does not map Gaussian states into Gaussian states because the action of the jump operators (6.63) on $\hat{\rho}$ in the master equation (6.58) is quartic in the fermionic fields. Nevertheless, because of the specific properties of the $\hat{\mathcal{L}}_\alpha$, it is possible to write the time evolution of the covariance matrix of the initial Gaussian state. The time evolution of the covariance matrix is given by [Hor11]:

$$\partial_t\Gamma = \frac{1}{\hbar}[T,\Gamma] + \frac{1}{2}\sum_\alpha [M^\alpha,[M^\alpha,\Gamma]] \tag{6.64}$$

The case of Lindblad operators which are quadratic but not Hermitian does not yield a closed differential equation as in (6.64).

6.6.2 Convex-Combination of Hamiltonian Time Evolutions

Let us consider another situation in which the time evolution is not mapping a Gaussian state to a Gaussian state, and namely, the convex combination of several different Hamiltonian time evolutions. As we discuss in chapter 7, such a time evolution describes a form of Hamiltonian perturbation, in that there is no environment but, for example, an experimental setup which is not fully controlled and that yields for every realization a slightly different system, e.g. with a different number of particles.

We consider a quadratic Hamiltonian $\hat{H}_0$ (6.48) and a set of quadratic Hermitian perturbations $\{\hat{V}_j\}_{j=1}^{N_d}$; we define a set of evolution operators $\hat{U}_j(t) = \exp[-\frac{i}{\hbar}(\hat{H}_0+\hat{V}_j)t]$. Given an initial state $\hat{\rho}(0)$, the time evolved state is defined by:

$$\hat{\rho}(t) = \frac{1}{N_d}\sum_{j=1}^{N_d}\hat{U}_j(t)\,\hat{\rho}(0)\,\hat{U}_j(t)^\dagger \tag{6.65}$$

The final state is a well-defined density operator; this time evolution does not preserve purity. Moreover, $\hat{\rho}(t)$ is not Gaussian because in general the convex combination of Gaussian states is not a Gaussian state. Nevertheless, using (6.56) we can derive the covariance matrix of the state $\hat{\rho}(t)$:

$$\Gamma(t) = \frac{1}{N_d}\sum_{j=1}^{N_d} O_j(t)^T\,\Gamma(0)\,O_j(t); \qquad O_j(t) = \exp\left[-\frac{T_0+T_j^{(V)}}{\hbar}t\right] \tag{6.66}$$

where T_0 is the skew-symmetric matrix associated to $\hat{H}_0$ and $T_j^{(V)}$ that associated to $\hat{V}_j$.

We can access another important property of the time evolved states, that is, the distance between two of them. To make this more quantitative, let us consider two orthogonal initial states $|\Phi\rangle$ and $|\Psi\rangle$ and let us introduce the notation

$|\Phi_j(t)\rangle = \hat{U}_j(t)|\Phi\rangle$ (the same for $|\Psi_j(t)\rangle$). If we define $\hat{\rho}_j^{\Phi}(t) = |\Phi_j(t)\rangle\langle\Phi_j(t)|$ (the same for $\hat{\rho}_j^{\Psi}(t)$), the following distance can be computed:

$$\left\|\hat{\rho}^{\Phi}(t) - \hat{\rho}^{\Psi}(t)\right\|_{\mathrm{tr}} = \left\| \frac{1}{N_d}\sum_{j=1}^{N_d} \hat{\rho}_j^{\Phi}(t) - \frac{1}{N_d}\sum_{j=1}^{N_d} \hat{\rho}_j^{\Psi}(t) \right\|_{\mathrm{tr}} \tag{6.67}$$

The distance we consider here is induced by the *trace norm*, or *Shatten* 1-norm, which is defined as the sum of the singular values of the operator representing the difference of the two states. The explicit procedure to evaluate (6.67) is in appendix B; we do not report it here because it is not a simple self-contained formula.

6.6.3 Interactions

We now consider an interacting Hamiltonian:

$$\hat{H} = \frac{i}{4}\sum_{\alpha,\beta} T_{\alpha,\beta}\hat{c}_\alpha\hat{c}_\beta + \sum_{\alpha,\beta,\gamma,\epsilon} U_{\alpha,\beta,\gamma,\epsilon}\hat{c}_\alpha\hat{c}_\beta\hat{c}_\gamma\hat{c}_\epsilon \tag{6.68}$$

In order to have an Hermitian Hamiltonian, the tensor $U_{\alpha,\beta,\gamma,\epsilon}$ is real and skew-symmetric with respect to the exchange of neighbouring indexes. The time evolution ruled by Hamiltonian (6.68) does not map Gaussian states to Gaussian states; moreover, it is not possible to explicitly derive a closed expression for the time evolution of the covariance matrix of the initial state $\hat{\rho}(0)$.

However, it has been recently shown that one can study such time evolution using the generalized Hartree-Fock theory [KC10]. The main idea is to project at each time step the time evolved state onto the closest fermionic Gaussian state. This approximation is equivalent, roughly speaking, to a mean field approach, as high-order correlations of the approximate state are trivial. The explicit formula for the time evolution of the covariance matrix are formally similar to (6.57), although the matrix $T_{\alpha,\beta}$ is state-dependent:

$$\partial_t\Gamma(t) = [\bar{T}(\Gamma(t)), \Gamma(t)]; \qquad \bar{T}(\Gamma(t))_{\alpha,\beta} = T_{\alpha,\beta} + 24\sum_{\gamma,\epsilon} U_{\alpha,\beta,\gamma,\epsilon}\Gamma_{\epsilon,\gamma}. \tag{6.69}$$

Let us consider the following nearest-neighbour interaction, which is going to be relevant in the next chapter:

$$\hat{U} = U\sum_{<i,j>}\left(\hat{n}_i - \frac{1}{2}\right)\left(\hat{n}_j - \frac{1}{2}\right) \tag{6.70}$$

This is the most simple interaction one can write for lattice spin-polarized fermions. The Majorana representation is:

$$\hat{U} = U\sum_{<i,j>}\left(\frac{1}{2} + \frac{i}{2}\hat{c}_{i1}\hat{c}_{i2} - \frac{1}{2}\right)\left(\frac{1}{2} + \frac{i}{2}\hat{c}_{j1}\hat{c}_{j2} - \frac{1}{2}\right) = -\frac{U}{4}\sum_{<i,j>}\hat{c}_{i1}\hat{c}_{i2}\hat{c}_{j1}\hat{c}_{j2} \tag{6.71}$$

The 4-indexes tensor $U_{\alpha,\beta,\gamma,\epsilon}$ defined in (6.68) is:

$$\begin{aligned} U^{(4)}_{\alpha,\beta,\gamma,\epsilon} = -\frac{U}{4}\frac{1}{24}\sum_{<i,j>} (& [\delta_{\alpha,i1}\delta_{\beta,i2} - \delta_{\alpha,i2}\delta_{\beta,i1}]\,[\delta_{\gamma,j1}\delta_{\epsilon,j2} - \delta_{\gamma,j2}\delta_{\epsilon,j1}] + \\ & - [\delta_{\alpha,i1}\delta_{\beta,j1} - \delta_{\alpha,j1}\delta_{\beta,i1}]\,[\delta_{\gamma,i2}\delta_{\epsilon,j2} - \delta_{\gamma,j2}\delta_{\epsilon,i2}] + \\ & + [\delta_{\alpha,i1}\delta_{\beta,j2} - \delta_{\alpha,j2}\delta_{\beta,i1}]\,[\delta_{\gamma,i2}\delta_{\epsilon,j1} - \delta_{\gamma,j1}\delta_{\epsilon,i2}] + \\ & - [\delta_{\alpha,i2}\delta_{\beta,j2} - \delta_{\alpha,j2}\delta_{\beta,i2}]\,[\delta_{\gamma,i1}\delta_{\epsilon,j1} - \delta_{\gamma,j1}\delta_{\epsilon,i1}] + \\ & + [\delta_{\alpha,i2}\delta_{\beta,j1} - \delta_{\alpha,j1}\delta_{\beta,i2}]\,[\delta_{\gamma,i1}\delta_{\epsilon,j2} - \delta_{\gamma,j2}\delta_{\epsilon,i1}] + \\ & - [\delta_{\alpha,j1}\delta_{\beta,j2} - \delta_{\alpha,j2}\delta_{\beta,j1}]\,[\delta_{\gamma,i2}\delta_{\epsilon,i1} - \delta_{\gamma,i1}\delta_{\epsilon,i2}]) \end{aligned} \tag{6.72}$$

Notice that, due to the fermionic anticommutation relations, the tensor $U_{\alpha,\beta,\gamma,\epsilon}$ is completely skew-symmetric.

The quantity we are interested in is:

$$\sum_{\gamma,\epsilon} U^{(4)}_{\alpha,\beta,\gamma,\epsilon}\Gamma_{\epsilon,\gamma} = -\sum_{\gamma,\epsilon} U^{(4)}_{\alpha,\beta,\gamma,\epsilon}\Gamma_{\gamma,\epsilon}; \tag{6.73}$$

which reads:

$$\begin{aligned} -\sum_{\gamma,\epsilon} U^{(4)}_{\alpha,\beta,\gamma,\epsilon}\Gamma_{\gamma,\epsilon} = \frac{U}{4}\frac{1}{24}\sum_{<i,j>} (& 2[\delta_{\alpha,i1}\delta_{\beta,i2} - \delta_{\alpha,i2}\delta_{\beta,i1}]\Gamma_{j1,j2} + \\ & -2[\delta_{\alpha,i1}\delta_{\beta,j1} - \delta_{\alpha,j1}\delta_{\beta,i1}]\Gamma_{i2,j2} + \\ & +2[\delta_{\alpha,i1}\delta_{\beta,j2} - \delta_{\alpha,j2}\delta_{\beta,i1}]\Gamma_{i2,j1} + \\ & +2[\delta_{\alpha,j1}\delta_{\beta,j2} - \delta_{\alpha,j2}\delta_{\beta,j1}]\Gamma_{i1,i2} + \\ & -2[\delta_{\alpha,i2}\delta_{\beta,j2} - \delta_{\alpha,j2}\delta_{\beta,i2}]\Gamma_{i1,j1} + \\ & +2[\delta_{\alpha,i2}\delta_{\beta,j1} - \delta_{\alpha,j1}\delta_{\beta,i2}]\Gamma_{i1,j2}) \end{aligned} \tag{6.74}$$

* * *

This concludes the technical chapter on fermionic Gaussian states; we reviewed the instruments which we are going to use in chapter 7 to characterize topological memories based on zero-energy Majorana modes.

Chapter 7

On a Quantum Memory Encoded with Zero-Energy Majorana Modes Subject to External Perturbations

In this chapter we address the following question: How long can we reliably store quantum information in a topological superconductor subject to perturbations?

Topological superconductors are quadratic fermionic models which do not conserve the number of particles and which have a band structure, obtained via the solution of the Bogoliubov-de Gennes equation, with non-trivial topological properties (see section 3.2.1 and references [HK10, QZ11]). We consider the subclass of such models which exhibit a ground space that can be described in terms of several spatially-localized zero-energy Majorana modes [Kit01, RG00]. This property and therefore also the degeneracy of the ground space are unaffected by local Hamiltonian perturbations, e.g. weak disorder.

Following the original idea by Kitaev, we encode one (or many, depending on the degeneracy) qubit with such Majorana modes [Kit97, DKLP02]. Because of the mentioned robustness, the dephasing time of the qubit, related to the degeneracy of the ground space, benefits from the topological properties of the model and is insensitive to local Hamiltonian perturbations. However, the aforementioned constitute only a restricted subclass of the wider set of disturbances which could appear in a realistic experiment. A complete characterization of the stability properties of such qubit is still missing. Recent results, which we are now going to briefly summarize, suggest that there are important cases, such as thermal environments [AFH09], which could significantly reduce the storage time of these systems.

To the best of our knowledge, the problem of the stability of a topological memory encoded with Majorana modes has been first addressed in [GC11][1]. The

[1] If we do not consider only topological superconductors, but also other kinds of topological models, the scientific literature on the stability of the corresponding quantum memories is larger. References [AFH09, Yos11, CLBT10] nicely review the problem of thermal instability, the topic on which most of the researchers have focussed, although other perturbations have also been considered, such as the depolarizing noise [PKSC10].

authors develop a formalism which quantifies the decoherence of the qubit via the two-time correlations of the Majorana fermions in which the information is stored. Among the different forms of perturbations considered, time-dependent perturbations are shown to be especially severe for the memory properties.

Similar conclusions, although obtained from a different point of view and with a different approach, are presented in [BWT12]. Using two different toy models which describe the interaction between the topological system and the environment, the authors show that the Majorana qubit is susceptible to decoherence because of particle losses.

In a a more recent work [RL12], it is even argued that the proposals for a solid state implementation of topological superconductors could lead to the fast decoherence of any encoded qubit because of intrinsic instability. Indeed, the mechanism used to turn a trivial semiconducting wire into a topological one is expected to provide other non-negligible competing effects which destroy the topological memory.

Among all these negative results, let us mention reference [CLDS12], where the authors state that braiding operations, corresponding to the manipulation of quantum information with a topological system, should not be significantly sensitive to thermal environments.

Because these results are often strictly related to the physics of solid-state systems, it is often difficult to understand which results have a more general validity and which ones do not translate to other alternative implementations. We therefore choose an alternative approach, mainly shaped by a quantum information background, which is more abstract and focuses only on *size scalings*. We consider a topological superconductor consisting of N fermionic modes and use two of them, that is the zero-energy modes, to store the qubit. All modes are exposed to small perturbations and interactions with the external environment. We are interested in determining the longest time at which it is still possible to restore, at least approximately, the initial state of the qubit. Furthermore, we investigate the extent to which this time may increase as a function of N, the size of the system. Our method is different from the previous ones in that the memory stability is defined by the scaling with the size N of the memory time. When this is the case, the system as a whole is actively collaborating to the protection of the qubit; otherwise, other memory schemes could be equivalent or even better.

Moreover, we consider the possibility that after the time evolution a *recovery operation* is applied to the system. We do not restrict to a specific error correcting code but rather identify the optimal recovery operation, and its relative fidelity. This approach therefore quantifies how much of the information initially put in the system has not been lost after the time evolution. In [BK11b] the authors present a similar analysis, but discuss only one specific correcting code. They consider a one-dimensional Kitaev chain, for which zero-energy Majorana modes appear at the two edges. The possibility of writing the Hamiltonian as a sum of commuting local operators allows for the application of the correcting codes which have been developed in the context of stabilizer theory [Got97, NC04]. The authors show that the presence of an additional random potential can exponentially improve the memory properties of the Kitaev chain in presence of external perturbations.

This chapter is organized as follows. In section 7.1 we overview all the results, avoiding technical details and demonstrations. In section 7.2 we review

the properties of the Kitaev chain, a specific example of a Hamiltonian with zero-energy Majorana modes. The following three sections 7.3, 7.4 and 7.5 are devoted to technical results related to the optimal recovery operation, to the Gaussian optimal recovery operation and to the case of a Gaussian decoherence channel, respectively. The reader not interested in mathematical details can skip these chapters without prejudicing the understanding of the subsequent results. In section 7.6 we discuss the action on the memory of a master equation with linear Lindblad operators, whereas in section 7.7 we focus on quadratic and Hermitian Lindblad operators. We devote section 7.8 to the discussion of the presence of a small non-Markovian fermionic environment whereas in section 7.9 we consider Hamiltonian perturbations. Finally, our conclusions are presented in section 7.10.

7.1 Summary of the Main Results

We consider a system consisting of N fermionic modes. We assume the presence of a Hamiltonian $\hat{H}$ with several zero-energy localized Majorana modes and use four of them, $\hat{c}_1$, $\hat{c}_2$, $\hat{c}_3$ and $\hat{c}_4$, to construct two Dirac modes, $\hat{a}^{(\dagger)}$ and $\hat{b}^{(\dagger)}$:

$$\hat{a} = \frac{1}{2}\left(\hat{c}_1 + i\hat{c}_2\right); \qquad \hat{a}^\dagger = \frac{1}{2}\left(\hat{c}_1 - i\hat{c}_2\right); \tag{7.1a}$$

$$\hat{b} = \frac{1}{2}\left(\hat{c}_3 + i\hat{c}_4\right); \qquad \hat{b}^\dagger = \frac{1}{2}\left(\hat{c}_3 - i\hat{c}_4\right). \tag{7.1b}$$

One such Hamiltonian is described in section 7.2. We call A_0 and B_0 these modes and use them to construct a qubit; we define the corresponding representation of the Pauli operators in the even parity sector of the two-modes Hilbert space:

$$\hat{\sigma}'_x = -(\hat{a}\hat{b} + \hat{b}^\dagger\hat{a}^\dagger); \qquad \hat{\sigma}'_y = i(\hat{a}\hat{b} - \hat{b}^\dagger\hat{a}^\dagger); \qquad \hat{\sigma}'_z = \hat{1} - \hat{a}^\dagger\hat{a} - \hat{b}^\dagger\hat{b}. \tag{7.2}$$

Even if the Pauli operators characterizing the qubit are defined in terms of fermionic operators, they always appear in pairs, so that the fermionic character (e.g. superselection rules) is not relevant.

We denote by $\hat{\rho}(t)$ the state of the system at time t, and by $\hat{\rho}_q$ the initial state of the qubit:

$$\hat{\rho}_q = \frac{\hat{1}}{2} + \frac{1}{2}\sum_{\alpha=x,y,z} \hat{\sigma}'_\alpha \operatorname{tr}\left[\hat{\sigma}'_\alpha \hat{\rho}(0)\right]. \tag{7.3}$$

We assume the qubit to be initially in a pure state, i.e. $\hat{\rho}_q = |\varphi\rangle\langle\varphi|$. The map:

$$\hat{\rho}_q \to \hat{\rho}(t) \doteqdot \mathcal{D}_t(\hat{\rho}_q) \tag{7.4}$$

describes the decoherence process of the qubit for a time t. It is a quantum channel, i.e. a linear, trace-preserving, and completely-positive map; we thus call $\mathcal{D}_t$ the *decoherence channel*. We stress that it also takes into account the action of the Hamiltonian which is supposed to protect the state of the qubit.

The quantum information stored in the qubit can only be recovered if we can find a physical procedure to undo the decoherence channel. If realized, such a procedure is mathematically described by another quantum channel, the *recovery channel* $\mathcal{R}_t$, such that the composite channel $\mathcal{T}_t \doteqdot \mathcal{R}_t \circ \mathcal{D}_t$ is approximately the identity channel for all $\hat{\rho}_q$. Note that $\mathcal{D}_t$ maps one qubit to

N fermionic modes, whereas $\mathcal{R}_t$ does the opposite. In order to quantify this statement, we define the usual channel fidelity [BOS$^+$02]:

$$F(\mathcal{R}_t) = \int d\mu_\varphi \langle\varphi| \mathcal{T}_t \left(|\varphi\rangle\langle\varphi|\right) |\varphi\rangle; \tag{7.5}$$

where the integral is over the Haar measure corresponding to the pure qubit states[2].

The optimal storage fidelity, F_t^{opt}, is the maximum value of $F(\mathcal{R}_t)$ with respect to all channels $\mathcal{R}_t$. The evaluation of F_t^{opt} can be simplified if one assumes that the decoherence channel does not affect the fermionic mode A_0. In that case, the optimal fidelity can be determined without any maximization, but just by computing the appropriate properties of the decoherence channel. Specifically, in section 7.3 we show that:

$$F_t^{\text{opt}} = \frac{2}{3} + \frac{1}{6}\|\hat{\rho}_{x,+}(t) - \hat{\rho}_{x,-}(t)\|_{\text{tr}}; \tag{7.6}$$

where $\hat{\rho}_{x,\pm}(t) = \mathcal{D}_t(\hat{\Psi}_{x,\pm})$, $\hat{\Psi}_{x,\pm} = (\hat{1} \pm \hat{\sigma}'_x)/2$, and $\|\cdot\|_{\text{tr}}$ denotes the trace norm. Thus, in order to determine the fidelity, it suffices to study the evolution of two specific states of the qubit, $\hat{\Psi}_{x,\pm}$. The quantity F_t^{opt} can also be interpreted as a measure of the amount of information put initially in the system (the state of the qubit $\hat{\rho}_q$) which has not been destroyed by the action of the decoherence for a time t.

If we drop the simplified assumption that the fermionic mode A_0 is not affected by the decoherence channel, an upper bound to the optimal fidelity is provided by equation (7.21). Results obtained under the assumption of a decoherence-free mode can only be better than those obtained in the more general case. This, in particular, increases the importance of the negative results we are deriving. Moreover, we expect the obtained results to qualitatively apply also to the situation in which the mode A_0 is substituted by a subsystem subject to dissipation, which is not interacting with the subsystem of B_0.

The quantity F_t^{opt} does not provide any information regarding the optimal recovery operation, which may be difficult to implement in practice. From the experimental point of view, it is interesting to restrict the optimization of $F(\mathcal{R}_t)$ to those physical actions that can be operatively realized. Those actions depend on the specific experimental setup and thus should be independently considered for each physical implementation.

In this work, we consider as experimentally relevant recovery operations those which are a fermionic Gaussian channel, which map Gaussian states into Gaussian states (see chapter 6 and [Bra05]). They comprise the linear optics

[2] In mathematical analysis, the Haar measure is introduced in order to assign an invariant measure to compact groups and to subsequently define an integral for functions on those groups. In quantum information theory it is often needed to integrate over all the pure states of a system and the measure to be used must be uniformly distributed over the quantum states. For example, let us consider a two-level system (qubit), for which the space of all the pure states is isomorphic to the surface of a sphere (the Bloch sphere). Intuitively, the measure we need must be invariant under all rotations of the Bloch sphere, and can be thought of as a "constant density distribution" over the surface of the sphere. Mathematically, one requires the measure to be invariant with respect to the group SU(2), which describes all the pure state of the system, and then consider the Haar measure of SU(2). For all practical purposes, we follow the intuitive approach. See also equation (7.20) and reference [BOS$^+$02].

operations applied to fermions, i.e. the evolution under a Hamiltonian or Liouvillian which is quadratic in the fermionic modes, and the addition or the discard of ancillary modes. In general these operations do not involve the simultaneous manipulation of more than two fermionic modes. This choice arises naturally as in this work we consider decoherence channels which are either fermionic Gaussian channels or convex combinations thereof.

Thus, we define the optimal fidelity with respect to recovery operations which are Gaussian channels, $F^{\text{opt}}_{\text{G},t}$. In section 7.4 we show that the optimal fidelity is given by:

$$F^{\text{opt}}_{\text{G},t} = \frac{2}{3} + \frac{1}{6}\|\Gamma_{x,+}(t) - \Gamma_{x,-}(t)\|_{\text{op}}. \tag{7.7}$$

Here, $\Gamma_{x,\pm}(t)$ are the covariance matrices of $\rho_{x,\pm}(t)$. Note that in general $F^{\text{opt}}_{\text{G},t}$ provides a lower bound to the general optimal recovery strategy. Furthermore, a recovery operation which is a convex combination of trace-preserving Gaussian channels cannot overcome such optimal value. This is not the case of the recovery operation considered in [BK11b], which is based on measurements, and therefore is not described by a convex combination of trace-preserving Gaussian channels.

In section 7.5 we show there are some decoherence channels, $\mathcal{D}_t$, which are Gaussian channels and for which the Gaussian recovery operation is optimal: $F^{\text{opt}}_{\text{G},t} = F^{\text{opt}}_{t}$. These channels are characterized by the fact that $(\hat{\rho}_{x,+}(t) - \hat{\rho}_{x,-}(t))/2$ is a Gaussian operator. Unfortunately, this is in not what happens in general.

We study some specific kinds of decoherence maps. For each one, once the optimal fidelity is determined as a function of time and of the number of fermions, $F^{\text{opt}}_{t,N}$, we identify the minimal time, t_N, at which it reaches a given fidelity $F_0 < 1$. Subsequently, the dependence of t_N on N is computed. If it is an increasing function, we conclude that the qubit is protected. Ideally, we would like it to grow exponentially with N, as it happens in the case for the noise models considered in fault-tolerant quantum computing.

We start considering decoherence maps which account for the interaction of the topological system with an environment described by a master equation. In section 7.6 we consider a master equation with jump operators which are linear in the fermionic fields, whereas in section 7.7 the jump operators are quadratic and Hermitian. We show that under the reasonable assumption that the whole system is affected by dissipation, both master equations have one unique steady state. We also show that for almost every master equation, the topological Hamiltonian cannot slow down the decay process to the steady state, and that in general the typical decay time does not depend on the size of the system. A similar result is obtained in section 7.8 for the case of a small non-Markovian environment, which we treat exactly. This is a negative result which is qualitatively similar to those obtained in [AFH09, CLBT10, Yos11] for other topological systems.

A different phenomenology is displayed by a decoherence map which describes the convex combination of several time evolutions ruled by slightly different topological Hamiltonians. In section 7.9, we show that there exists an optimal recovery operation which significantly benefits from considering larger systems. Interestingly, we show that the fidelity of the Gaussian recovery operation cannot overcome a critical value which is smaller than one even for $N \to \infty$.

This result is partially positive and opens the road towards the development of topologically protected memories in closed systems.

The results presented here extend naturally to the situation in which the decoherence-free mode is substituted by an independent system hosting two zero-energy Majorana modes. In this case we expect essentially the same results, with the difference that the recovery operation has to act on both subsystems, rather than on only one. This situation has practical relevance, since there are proposals to realize topological qubits via two disconnected topological one-dimensional systems.

7.2 The Kitaev Chain: a 1D Topological Superconductor

We start discussing a specific example of a one-dimensional topological superconductor, the Kitaev chain [Kit01]. This is the simplest model featuring all the properties we are interested in, and it will be used in the following for some specific numerical simulations. The Hamiltonian of the model, written for open boundary conditions, reads as follows:

$$\hat{H}_{\mathrm{KC}} = -\mu \sum_{j=1}^{N} \hat{n}_j - J \sum_{j=1}^{N-1} \left[\hat{a}_j^\dagger \hat{a}_{j+1} + H.c. \right] + \Delta \sum_{j=1}^{N-1} \left[\hat{a}_j \hat{a}_{j+1} + H.c. \right] \tag{7.8}$$

where $\hat{a}_j^{(\dagger)}$ are fermionic modes satisfying canonical anticommutation relations:

$$\{\hat{a}_k, \hat{a}_l\} = 0; \quad \{\hat{a}_k, \hat{a}_l^\dagger\} = \delta_{k,l}. \tag{7.9}$$

The parameter Δ can be chosen to be real by an appropriate redefinition of the Dirac modes. Hamiltonian (7.8) does not conserve the number of fermions but does conserve the parity of the number of fermions. Moreover, since it is quadratic in the fermionic fields, it can be easily treated with the fermionic Gaussian states presented in chapter 6 (see in particular section 6.4).

Let us begin the discussion considering a special point of the phase diagram, $\mu = 0$ and $\Delta = J$. We introduce the Majorana fermionic operators (see section 6.1) and rewrite the Hamiltonian as:

$$\hat{H}_{\mathrm{KC}} = -iJ \sum_{j=1}^{N-1} \hat{c}_{j+1,1} \hat{c}_{j,2}; \quad \text{with} \quad \hat{c}_{j,1} = \hat{a}_j + \hat{a}_j^\dagger; \;\; \hat{c}_{j,2} = -i(\hat{a}_j - \hat{a}_j^\dagger). \tag{7.10}$$

This writing highlights the fact that the Hamiltonian is the sum of commuting operators which are local in space. This point of the phase diagram is therefore called *frustration-free* and *commuting point*. Let us introduce the Dirac eigenmodes of the system:

$$\hat{d}_j = \frac{1}{2}(\hat{c}_{j,2} + i\hat{c}_{j+1,1}), \qquad j \in \{1, 2, \dots N-1\}; \tag{7.11}$$

which diagonalize the Hamiltonian:

$$\hat{H}_{\mathrm{KC}} = -J(N-1)\hat{1} + 2J \sum_{i=1}^{N-1} \hat{d}_j^\dagger \hat{d}_j. \tag{7.12}$$

The ground space is two-fold degenerate. Indeed, let us consider the additional operator $\hat{d}_0 = \frac{1}{2}(\hat{c}_{1,1} + i\hat{c}_{N,2})$, which commutes with the Hamiltonian. We define the ground state $|g\rangle$ via the property:

$$\hat{d}_\alpha |g\rangle = 0; \quad \forall \alpha \in \{0, 1, \dots N-1\} \tag{7.13}$$

Additionally, $\hat{d}_0^\dagger |g\rangle$ is also an eigenstate of the Hamiltonian with the same energy of $|g\rangle$; the ground space is twofold degenerate and is spanned by $\{|g\rangle; \hat{d}_0^\dagger |g\rangle\}$. The two states belong to different parity sectors of the theory. It is reasonable to include in the discussion of this model the superselection rule on the parity of the fermionic number typical of fermionic systems. Such rule forbids the existence of linear superpositions of states with different parity and therefore $\{|g\rangle; \hat{d}_0^\dagger |g\rangle\}$ cannot be used to store a qubit. In order to construct a well-defined qubit, it is customary to consider a separated fermionic auxiliary mode, $\hat{a}_a^{(\dagger)}$, with trivial dynamics. If we denote $|g_a\rangle$ the ground state of this ancilla, we can encode a well-defined qubit into the subspace spanned by: $\{|g\rangle \otimes |g_a\rangle, \hat{d}_0^\dagger |g\rangle \otimes \hat{a}_a^\dagger |g_a\rangle\}$.

In reference [BK11b] the authors proof that even if a local Hermitian perturbation is added to Hamiltonian (7.8), it is always possible to find an operator $\hat{d}_0$ such that the energy difference between $|g\rangle$ and $\hat{d}_0^\dagger |g\rangle$ closes exponentially with the system size. Moreover, an energy gap above these two states persists in the thermodynamic limit. No local observable can distinguish between $|g\rangle$ and $\hat{d}_0^\dagger |g\rangle$. The two states can be identified by looking at the parity of the global number of fermions $i^N \prod_k \hat{c}_k$ (6.21). Notice that this is a string operator, formally similar to that considered in chapter 5.

A similar situation happens for a larger region of the phase diagram, characterized by $|\mu/J| < 2$ and $\Delta \neq 0$. A non-rigorous demonstration of this fact relies on the interpretation of the model as a topological insulator (see section 3.2 and [HK10, QZ11]). Let us therefore consider periodic boundary conditions and write the Hamiltonian in Fourier space:

$$\hat{H}_{\mathrm{KC}} = \sum_{k \in \mathrm{BZ}} \begin{pmatrix} \hat{a}_k^\dagger; & \hat{a}_{-k} \end{pmatrix} \begin{pmatrix} \xi_k & \Delta_k \\ \Delta_k^* & -\xi_k \end{pmatrix} \begin{pmatrix} \hat{a}_k \\ \hat{a}_{-k}^\dagger \end{pmatrix}; \quad \begin{matrix} \xi_k = -J\cos(ka) - \mu/2; \\ \Delta_k = -i\Delta \sin(ka). \end{matrix} \tag{7.14}$$

where a is the lattice spacing. The spectrum is $E(k) = \sqrt{\xi_k^2 + \Delta_k^2}$. The fact that the gap closes at $\mu = \pm 2J$ for $k = \{0, \pi\}$ is an indicator that all the points of the phase diagram such that $|\mu/J| < 2$ share the same properties (notice that the frustration-free point is one of them). This can be put on a more solid ground by considering the topological invariant of this topological insulator.

Let us first discuss the symmetry class of the model. Hamiltonian (7.8) is characterized by the particle-hole symmetry. Regarding the time-reversal symmetry, from a purely mathematical point of view, $\hat{H}_{\mathrm{KC}}$ possesses such symmetry, although this is not true when Δ is complex. In the former case, more symmetric, the Kitaev chain is of class BDI; in the latter, of class D.

Let us consider the first case, which is characterized by a $\mathbb{Z}$ topological invariant. The Hamiltonian $\hat{H}_{\mathrm{KC}}$ is represented a list of 2×2 matrices, which we write as $\mathbb{H}_{\mathrm{KC}}(k) = \vec{h}(k) \cdot \vec{\sigma}$, with $\vec{h}(k)^T = (0, \Delta \sin(ka), \xi_k)$. The topological integral is defined in terms of $\vec{n}_k = \vec{h}_k / |\vec{h}_k|$:

$$\nu = \frac{1}{2\pi} \int_{-\pi}^{\pi} \hat{e}_x \cdot (\vec{n}_k \wedge \partial_k \vec{n}_k)\, dk \ \in \ \mathbb{Z} \tag{7.15}$$

The region $|\mu/J| \leq 2$, $\Delta \neq 0$ is characterized by $\nu = 1$, which confirms that we are in presence of a topologically non-trivial state. Zero-energy Majorana modes appearing on the edges of the open chain are the gapless edge modes which characterize every model which is a topological insulator (see section 3.2).

Let us mention that there exists a two-dimensional model with very similar properties, the so-called $p_x + ip_y$ model. In this case, zero-energy Majorana modes appear in the core of vortices of a space dependent pairing term $\Delta(\mathbf{r})$. The adiabatic interchange of these vortices realizes a representation of the non-Abelian braid group, and therefore these defects behave effectively as non-Abelian anyons [Iva01][3]. It has recently been demonstrated that also the edge modes of the Kitaev chain can display non-Abelian statistics [AOR+11]. The interchange, in this one-dimensional case, can be realized using a T-shaped system.

Let us conclude this section with a connection to the first part of the thesis by mentioning two recent proposals for the experimental realization of a Kitaev chain with cold atoms. In [DRBZ11] the authors propose to realize the ground state of a Kitaev chain in a one-dimensional fermionic gas with a technique based on engineered dissipation. In [JKA+11] the authors propose to couple a one-dimensional gas to a molecular Bose-Einstein condensate. Finally, in [GR07] the authors discuss the possibility of observing a $p_x + ip_y$ superfluid in fermionic gases in presence of a p-wave Feshbach resonance; other proposals have been also developed using s-wave resonances [STF09, LCS11].

7.3 Optimal Recovery Operation

Let us start the presentation of the original results of this chapter with the derivation of the fidelity of the optimal recovery operation acting after a given decoherence map. Its value is reported in equation (7.6), which we rewrite here for reading convenience:

$$F_t^{\text{opt}} = \frac{2}{3} + \frac{1}{6}\|\hat{\rho}_{x,+}(t) - \hat{\rho}_{x,-}(t)\|_{\text{tr}};$$

where $\hat{\rho}_{x,\pm}(t) = \mathcal{D}_t(\hat{\Psi}_{x,\pm})$, $\hat{\Psi}_{x,\pm} = (\hat{1} \pm \hat{\sigma}'_x)/2$.

We first show that the fidelity of any recovery operation is upper bounded:

$$F(\mathcal{R}_t) \leq \frac{2}{3} + \frac{1}{6}\|\hat{\rho}_{x,+}(t) - \hat{\rho}_{x,-}(t)\|_{\text{tr}}, \quad \forall \mathcal{R}_t. \tag{7.16}$$

In order to simplify the notation, we drop the dependence of F on $\mathcal{R}_t$. We then construct an explicit recovery operation, $\mathcal{R}_t^{\text{opt}}$, which achieves the upper bound and is of the following form:

$$\mathcal{R}_t^{\text{opt}}(\hat{\rho}(t)) = \frac{\hat{1}}{2}\,\text{tr}\left[\hat{\rho}(t)\right] + \frac{1}{2}\sum_{\alpha=\{x,y,z\}} \hat{\sigma}'_\alpha\,\text{tr}\left[\hat{H}_\alpha\,\hat{\rho}(t)\right]; \tag{7.17}$$

with the $\hat{H}_\alpha$ to be specified.

[3]The ground state of the $p_x + ip_y$ model shares a number of properties with the Pfaffian wavefunction discussed in chapter 4. The explicit discussion of this similarity goes beyond the purpose of this chapter and it is nicely reviewed in [GR07].

7.3.1 Properties of the Trace Norm

Let us recall some simple properties of the trace norm. For a bounded Hermitian operator $\hat{X}$, one defines

$$\|\hat{X}\|_{\mathrm{tr}} = \max_{\hat{H}} \mathrm{tr}(\hat{H}\hat{X}); \tag{7.18}$$

The maximization is restricted to operators fulfilling

$$\hat{H} = \hat{H}^\dagger, \quad \|\hat{H}\|_{\mathrm{op}} \leq 1, \tag{7.19}$$

where the operator norm is the maximum absolute value of the eigenvalues. This last condition can be replaced by $\hat{H}^2 \leq \hat{1}$. It is called trace norm because it is equal to the sum of singular values of $\hat{X}$. This norm is contractive under the action of any quantum channel $\mathcal{E}$, i.e. $\|\mathcal{E}(\hat{X})\|_{\mathrm{tr}} \leq \|\hat{X}\|_{\mathrm{tr}}$; it is unitarily invariant, i.e, $\|\hat{U}\hat{X}\hat{V}\|_{\mathrm{tr}} = \|\hat{X}\|_{\mathrm{tr}}$ for any $\hat{U}$, $\hat{V}$ unitary; and subadditive, i.e. $\|\hat{X} + \hat{Y}\|_{\mathrm{tr}} \leq \|\hat{X}\|_{\mathrm{tr}} + \|\hat{Y}\|_{\mathrm{tr}}$.

7.3.2 Derivation of the Upper Bound

The fidelity defined in equation (7.5) can be rewritten as [BOS+02]:

$$F = \frac{1}{2} + \frac{1}{12} \sum_{\alpha=x,y,z} \mathrm{tr}[\hat{\sigma}'_\alpha \mathcal{T}_t(\hat{\sigma}'_\alpha)]. \tag{7.20}$$

This follows by writing $|\varphi\rangle\langle\varphi| = \left(\hat{1} + \vec{n}_\varphi \cdot \vec{\hat{\sigma}}\right)/2$ in (7.5), where $\vec{n}_\varphi$ is a unit vector, and performing the integration over $\vec{n}_\varphi$ on the unit sphere.

We derive the upper bound. Because

$$\mathrm{tr}\left[\hat{\sigma}'_\alpha \mathcal{T}_t(\hat{\sigma}'_\alpha)\right] \leq \|\hat{\sigma}'_\alpha\|_{\mathrm{op}} \|\mathcal{T}_t(\hat{\sigma}'_\alpha)\|_{\mathrm{tr}} = \|\mathcal{T}_t(\hat{\sigma}'_\alpha)\|_{\mathrm{tr}} \leq \|\mathcal{D}_t(\hat{\sigma}'_\alpha)\|_{\mathrm{tr}}$$

we obtain

$$F \leq \frac{1}{2} + \frac{1}{12} \sum_{\alpha=x,y,z} \|\hat{\rho}_{\alpha,+}(t) - \hat{\rho}_{\alpha,-}(t)\|_{\mathrm{tr}}. \tag{7.21}$$

Here, $\hat{\rho}_{\alpha,\pm}(t) = \mathcal{D}_t(\hat{\Psi}_{\alpha,\pm})$, where $\hat{\Psi}_{\alpha,\pm} = (\hat{1} \pm \hat{\sigma}'_\alpha)/2$ are projectors onto pure states of the qubit pointing in different directions in the Bloch sphere. Moreover, we have used the linearity of $\mathcal{D}_t$ and that $\mathcal{D}_t(\hat{\sigma}'_\alpha) = \hat{\rho}_{\alpha,+}(t) - \hat{\rho}_{\alpha,-}(t)$.

Let us now specify (7.21) to the case of $\mathcal{D}_t$ not acting on the fermionic mode A_0. The operator $\hat{H}_z \doteqdot \hat{a}\hat{a}^\dagger - \hat{a}^\dagger\hat{a}$ fulfills the requirements (7.19), and

$$\mathrm{tr}[\hat{H}_z\, \hat{\rho}_{z,+}(t)] = -\mathrm{tr}[\hat{H}_z\, \hat{\rho}_{z,-}(t)] = 1. \tag{7.22}$$

Thus we have:

$$2 = \mathrm{tr}[\hat{H}_z(\hat{\rho}_{z,+}(t) - \hat{\rho}_{z,-}(t))] \leq \|\hat{\rho}_{z,+}(t) - \hat{\rho}_{z,-}(t)\|_{\mathrm{tr}} \leq ||\hat{\Psi}_{z,+} - \hat{\Psi}_{z,+}||_{\mathrm{tr}} = 2$$

so that $\|\hat{\rho}_{z,+}(t) - \hat{\rho}_{z,-}(t)\|_{\mathrm{tr}} = 2$. Furthermore, since $\mathcal{D}_t$ does not act on the ancilla, we can write $\hat{\rho}_{y,\tau}(t) = \hat{V}\hat{\rho}_{x,\tau}(t)\hat{V}^\dagger$, where $\hat{V} = e^{-i\pi\hat{a}^\dagger\hat{a}/2}$ is a unitary operator. Therefore:

$$\frac{1}{2}\|\hat{\rho}_{x,+}(t) - \hat{\rho}_{x,-}(t)\|_{\mathrm{tr}} = \frac{1}{2}\|\hat{\rho}_{y,+}(t) - \hat{\rho}_{y,-}(t)\|_{\mathrm{tr}} \tag{7.23}$$

The bound in (7.16) follows from the combination of (7.21) with these considerations.

7.3.3 Explicit Construction of a Recovery Map

We now explicitly construct a recovery map which achieves the upper bound in (7.16). To do that, we need to introduce three operators $\hat{H}_x$, $\hat{H}_y$, $\hat{H}_z$; the operator $\hat{H}_z$ has already been defined: $\hat{H}_z = \hat{a}\hat{a}^\dagger - \hat{a}^\dagger\hat{a}$.

Let us rewrite

$$\hat{\rho}_{x,+}(t) - \hat{\rho}_{x,-}(t) = \hat{a}\hat{R} + \hat{R}^\dagger\hat{a}^\dagger; \quad \hat{R} = \mathcal{D}_t(-\hat{b})$$

We compute $\|\hat{a}\hat{R} + \hat{R}^\dagger\hat{a}^\dagger\|_{\text{tr}}$ using the definition in (7.18) and name $\hat{H}_x$ the operator that achieves the maximum. We write the most general Hermitian operator:

$$\hat{H}_x = \hat{a}\hat{S}_1 + \hat{S}_1^\dagger\hat{a}^\dagger + \hat{a}^\dagger\hat{a}\hat{S}_2 + \hat{a}\hat{a}^\dagger\hat{S}_3$$

which must satisfy $\hat{H}_x^\dagger\hat{H}_x \leq \mathbb{I}$. We get

$$\text{tr}\left[\hat{H}_x\left(\hat{a}\hat{R} + \hat{R}^\dagger\hat{a}^\dagger\right)\right] = \text{tr}\left[\left(\hat{S}_1\hat{R}^\dagger + \hat{R}\hat{S}_1^\dagger\right)\hat{a}^\dagger\hat{a}\right]$$

Using the left polar decomposition $\hat{R} = \hat{P}\hat{U}$, where $\hat{P} = \sqrt{\hat{R}\hat{R}^\dagger}$ is positive semi-definite and $\hat{U}$ is unitary, we have that the maximum is attained when $\hat{S}_1 = \hat{U}$, and $\hat{S}_2 = \hat{S}_3 = 0$. Therefore, combining these results with (7.23), we obtain:

$$\|\hat{\rho}_{\alpha,+}(T) - \hat{\rho}_{\alpha,-}(T)\|_{\text{tr}} = 2\text{tr}[\hat{P}]; \quad \alpha = x, y; \tag{7.24}$$

where the trace is taken on the $N-1$ modes subjected to decoherence. The operators achieving the maximum, according to the definition of the trace norm in (7.18), are:

$$\hat{H}_x = \hat{a}\hat{U} + \hat{U}^\dagger\hat{a}^\dagger; \qquad \hat{H}_y = -i\hat{a}\hat{U} + i\hat{U}^\dagger\hat{a}^\dagger.$$

Furthermore, since both $\hat{a}$ and $\hat{R}$ change the fermionic parity, $\hat{H}_{x,y}$ do not. They also fulfill:

$$\text{tr}\left[\hat{H}_\alpha\hat{\rho}_{\alpha,+}(t)\right] = -\text{tr}\left[\hat{H}_\alpha\hat{\rho}_{\alpha,-}(t)\right] = \frac{1}{2}\|\hat{\rho}_{x,+}(t) - \hat{\rho}_{x,-}(t)\|_{\text{tr}} \tag{7.25}$$

for $\alpha = x, y$.

Now that we have defined $\hat{H}_{x,y,z}$, we construct the optimal recovery map:

$$\mathcal{R}_t^{\text{opt}}(\hat{\rho}(t)) = \frac{1}{2}\hat{1}\,\text{tr}\left[\hat{\rho}(t)\right] + \frac{1}{2}\sum_\alpha \hat{\sigma}'_\alpha\,\text{tr}\left[\hat{H}_\alpha\hat{\rho}(t)\right]. \tag{7.26}$$

It is linear, trace preserving, and it also preserves the fermionic parity, since $\hat{H}_\alpha$ do. For it to be a valid quantum channel we have to show that it is completely positive. We construct a unitary operator acting on all the fermionic modes, $\hat{W}$, such that $\mathcal{R}_t^{\text{opt}}(\hat{\rho}) = \text{tr}\left[\hat{W}\hat{\rho}\hat{W}^\dagger\right]$, where the trace is taken over the fermionic degrees of freedom which are not part of the qubit. The operator is:

$$\hat{W} = \frac{1}{8}\left[\hat{1} + \sum_{\alpha=x,y,z}\hat{\sigma}'_\alpha\hat{H}_\alpha\right]. \tag{7.27}$$

Using that $\hat{H}_\alpha^2 = \hat{1}$ and $\hat{H}_\alpha\hat{H}_\beta = i\epsilon_{\alpha,\beta,\gamma}\hat{H}_\gamma$, where $\epsilon_{\alpha,\beta,\gamma}$ is the Levi-Civita tensor, one can show that $\hat{W}$ is unitary and that it defines the recovery map (7.26). Furthermore, using (7.22) and (7.25) it follows that $F(\mathcal{R}_t^{\text{opt}})$ saturates the bound in (7.16).

7.4 Optimal Gaussian Recovery Operation

Let us now study the case of a Gaussian recovery operation. In this section we derive the optimal fidelity achievable with such an operation, as it is expressed in equation (7.7), which we rewrite here for reading convenience:

$$F_{\mathrm{G},t}^{\mathrm{opt}} = \frac{2}{3} + \frac{1}{6}\|\Gamma_{x,+}(t) - \Gamma_{x,-}(t)\|_{\mathrm{op}}.$$

We also show that a recovery operation which is a convex combination of Gaussian recovery operation cannot overcome the bound $F_{\mathrm{G},t}^{\mathrm{opt}}$.

The proof is similar to that in section 7.3, although here we restrict the study to Gaussian recovery operations, i.e. channels that map Gaussian states into Gaussian states. They include, for instance, operations which involve the addition of ancillas to the Gaussian state, the evolution under a Hamiltonian or a Liouvillian that is quadratic in the creation and annihilation operators, and the discard of the ancillas.

7.4.1 Definition of "New" Pauli Operators

In this case, we need to explicitly consider the fact that the qubit is composed of fermions. In particular, we have to consider what happens if the decoherence channel changes the parity of the state. This occurs, for instance, when decoherence is caused by the interchange of particles with a reservoir, as described by $\mathcal{D}_t(\hat{\rho}) = (\hat{b} + \hat{b}^\dagger)\hat{\rho}(\hat{b} + \hat{b}^\dagger)$. The final state contains all the information about the initial state of the qubit, even if now it has odd parity. The problem, that could be overlooked in section 7.3, arises in this section because the Gaussian recovery operation cannot act independently on the different parity sectors of the state, whereas a general recovery operation can.

Consider a fermionic system composed of N modes, and the respective $2N$ Majorana modes $\hat{c}_n$ fulfilling anticommutation relations $\{\hat{c}_n, \hat{c}_m\} = 2\delta_{n,m}$. We denote $\hat{c}_1$, $\hat{c}_2$, $\hat{c}_3$ and $\hat{c}_4$ the zero-energy modes of the Hamiltonian (see section 7.1). We define the covariance matrix of an operator $\hat{X}$ the $2N \times 2N$ matrix Γ_X, with element:

$$(\Gamma_X)_{n,m} = -\frac{i}{2}\mathrm{tr}\left[\hat{X}(\hat{c}_n\hat{c}_m - \hat{c}_m\hat{c}_n)\right]. \tag{7.28}$$

We express the Pauli operators of the qubit as:

$$\hat{\sigma}_x'' = (\hat{a}^\dagger - \hat{a})(\hat{b}^\dagger + \hat{b}) = i\hat{c}_3\hat{c}_2; \tag{7.29}$$

$$\hat{\sigma}_y'' = -i(\hat{a}^\dagger + \hat{a})(\hat{b}^\dagger + \hat{b}) = i\hat{c}_3\hat{c}_1; \tag{7.30}$$

$$\hat{\sigma}_z'' = \hat{a}^\dagger\hat{a} - \hat{a}\hat{a}^\dagger = i\hat{c}_1\hat{c}_2. \tag{7.31}$$

where the modes $\hat{a}^{(\dagger)}$ and $\hat{b}^{(\dagger)}$ have been defined in equations (7.1a) and (7.1b). Note the difference with the $\hat{\sigma}_\alpha'$ in equations (7.2). Since the $\hat{\sigma}_\alpha''$ act on both the parity sectors of the qubit, they allow the recovery operation independently of whether the parity has been changed or not.

7.4.2 Generalities of Gaussian Channels and Notation

The action of a general Gaussian channel transforms a Gaussian M-modes state with covariance matrix Γ into a N-modes state with covariance matrix Γ'. In

particular, $\Gamma' = B\Gamma B^T + A$ where B (A) is a $2N \times 2M$ ($2N \times 2N$) matrix. A is skew-symmetric and the $2(M+N) \times 2(M+N)$ matrix

$$Q = \begin{pmatrix} A & B \\ -B^T & 0 \end{pmatrix} \tag{7.32}$$

satisfies $Q^T Q \leq \mathbb{I}$ [Bra05].

We denote $\mathcal{R}_{\mathrm{G},t}$ the Gaussian recovery operation, whereas $\mathcal{T}_{\mathrm{G},t} = \mathcal{R}_{\mathrm{G},t} \circ \mathcal{D}_t$. Moreover, we define:

$$\Delta_\alpha = \Gamma_{\mathcal{D}_t(\hat{\Psi}_{\alpha,+})} - \Gamma_{\mathcal{D}_t(\hat{\Psi}_{\alpha,-})}, \tag{7.33}$$

$$\Delta_\alpha^{\mathrm{out}} = \Gamma_{\mathcal{T}_{\mathrm{G},t}(\hat{\Psi}_{\alpha,+})} - \Gamma_{\mathcal{T}_{\mathrm{G},t}(\hat{\Psi}_{\alpha,-})}, \tag{7.34}$$

the difference of covariance matrices corresponding to the states after the decoherence channel and after the recovery operation, respectively. Note that the matrices Δ_α are $2N \times 2N$ matrices, whereas the matrices $\Delta_\alpha^{\mathrm{out}}$ are 4×4 matrices. The assumption that the decoherence channel does not act on the first two Majorana modes $\hat{c}_{1,2}$ is reflected by some properties of Δ_α even if $\mathcal{D}_t$ is not a Gaussian channel and $\mathcal{D}_t(\hat{\Psi}_\alpha)$ is not a Gaussian state. Let us consider the block structure of Δ_α:

$$\Delta_\alpha = \begin{pmatrix} K'_\alpha & -L_\alpha^T \\ L_\alpha & K''_\alpha \end{pmatrix}, \tag{7.35}$$

where K', L and K'' are 2×2, $2(N-1) \times 2$, and $2(N-1) \times 2(N-1)$ matrices, respectively. We obtain:

$$\begin{aligned} K'_z &= \begin{pmatrix} 0 & 2 \\ -2 & 0 \end{pmatrix}; \quad L_x = \begin{pmatrix} \vec{l}_1, & \vec{l}_2 \end{pmatrix}; \\ L_y &= \begin{pmatrix} \vec{l}_2, & -\vec{l}_1 \end{pmatrix} = L_x J; \quad J = \begin{pmatrix} 0 & -1 \\ 1 & 0 \end{pmatrix}; \end{aligned} \tag{7.36}$$

where $\vec{l}_{1,2}$ are column vectors. Additionally, L_z, $K'_{x,y}$ and $K''_{x,y}$ are zero matrices. Thus:

$$\|\Delta_x\|_{\mathrm{op}} = \|\Delta_y\|_{\mathrm{op}} = \|L_x\|_{\mathrm{op}} \leq 2 \tag{7.37}$$

where $\|X\|_{\mathrm{op}}$ is the maximum singular vaulue of the matrix X.

7.4.3 Derivation of the Upper Bound

We can now show that for any Gaussiann recovery operation, $\mathcal{R}_{\mathrm{G},t}$, the fidelity is upper bounded as follows,

$$F_{\mathrm{G},t}(\mathcal{R}_{\mathrm{G},t}) \leq \frac{2}{3} + \frac{1}{6}\|\Delta_x\|_{\mathrm{op}} \tag{7.38}$$

As before, we will drop the dependence of $F_{\mathrm{G},t}$ on $\mathcal{R}_{\mathrm{G},t}$. Our starting point is equation (7.20), modified as follows:

$$F_{\mathrm{G},t} = \frac{1}{2} + \frac{1}{12} \sum_{\alpha=x,y,z} \mathrm{tr}[\hat{\sigma}''_\alpha \mathcal{T}_{\mathrm{G},t}(\hat{\sigma}'_\alpha)]. \tag{7.39}$$

Noting that the $\hat{\sigma}''_\alpha$ are quadratic in the Majorana operators and recalling the definition of covariance matrix (7.28), we obtain:

$$\mathrm{tr}\,[\hat{\sigma}''_\alpha \mathcal{T}_{\mathrm{G},t}(\hat{\sigma}'_\alpha)] = \left(\Delta_\alpha^{\mathrm{out}}\right)_{\beta_1,\beta_2} \leq \|\Delta_\alpha^{\mathrm{out}}\|_{\mathrm{op}}, \tag{7.40}$$

where $(\beta_1,\beta_2) = (1,2)$, $(3,2)$, and $(3,1)$ for $\alpha = x,y,z$, respectively. The most general Gaussian recovery operator $\mathcal{R}_{\mathrm{G},t}$ yields:

$$\|\Delta_\alpha^{\mathrm{out}}\|_{\mathrm{op}} = \|B_{\mathcal{R}}\,\Delta_\alpha\,B_{\mathcal{R}}^T\|_{\mathrm{op}} \leq \|\Delta_\alpha\|_{\mathrm{op}}$$

given that $Q^TQ \leq \mathbb{I}$. Since $2 \geq \|\Delta_z\|_{\mathrm{op}} \geq (\Delta_z)_{1,2} = (K_z)_{1,2} = 2$, we get that $\|\Delta_z\|_{\mathrm{op}} = 2$. Using (7.37) we obtain the result (7.38). If we do not assume any property of the decoherence channel, a similar reasoning brings us to the bound:

$$F_{\mathrm{G}} \leq \frac{1}{2} + \left(\frac{1}{12}\right) \sum_{\alpha=x,y,z} \|\Delta_\alpha\|_{\mathrm{op}} \tag{7.41}$$

7.4.4 Explicit Construction of a Recovery Map

We now provide an explicit Gaussian recovery operation which attains the bound. The recovery operation consists of the application of a Gaussian unitary operation $\hat{W}_{\mathrm{G}}$ to the the system and in subsequently tracing out $N-2$ modes of the system. To define $\hat{W}_{\mathrm{G}}$, consider the singular value decomposition of $L_x = U\Sigma V^T$, where U (V) is a unitary $2(N-1)\times 2(N-1)$ (2×2) matrix and Σ is a $2(N-1)\times 2$ matrix. Clearly, it is also possible to construct U' and V' such that $L_x = U'\Sigma' V'$ and Σ' has at most two elements different from zero, $\Sigma_{1,2} \geq \Sigma_{2,1} \geq 0$, named the singular values of L_x. We define $\hat{W}_{\mathrm{G}}$ to be the unitary transformation which is represented by an orthogonal transformation $V' \oplus U'$:

$$\hat{W}_{\mathrm{G}}\,\vec{\hat{c}}\,\hat{W}_{\mathrm{G}}^\dagger = (V' \oplus U')\;\vec{\hat{c}} \tag{7.42}$$

Physically, $\hat{W}_{\mathrm{G}}$ rotates all the information between ancilla and system into the first two modes of the system. The other modes can be now traced out. Summarizing:

$$\mathcal{R}_{\mathrm{G},t}^{\mathrm{opt}}(\hat{\rho}) = \mathrm{tr}\left[\hat{W}_{\mathrm{G}}\,\hat{\rho}\,\hat{W}_{\mathrm{G}}^\dagger\right] \tag{7.43}$$

The covariance matrix of $\mathcal{R}_{\mathrm{G},t}^{\mathrm{opt}}(\hat{\rho})$ is:

$$\Gamma_{\mathcal{R}_{\mathrm{G},t}^{\mathrm{opt}}(\hat{\rho})} = \left[(V' \oplus U')\,\Gamma\,(V'^T \oplus U'^T)\right]\big|_{(1-4),(1-4)} \tag{7.44}$$

where Γ is the covariance matrix of $\hat{\rho}$.

Finally, let us prove that $F(\mathcal{R}_{\mathrm{G},t}^{\mathrm{opt}})$ saturates the bound (7.38). Denote $\mathcal{T}_{\mathrm{G},t}^{\mathrm{opt}} = \mathcal{R}_{\mathrm{G},t}^{\mathrm{opt}} \circ \mathcal{D}_t$. Clearly,

$$\sum_{\alpha=x,y,z} \mathrm{tr}\left[\hat{\sigma}''_\alpha \mathcal{T}_{\mathrm{G},t}^{\mathrm{opt}}(\hat{\sigma}'_\alpha)\right] = \left(\Delta_x^{\mathrm{out}}\right)_{3,2} + \left(\Delta_y^{\mathrm{out}}\right)_{3,1} + \left(\Delta_z^{\mathrm{out}}\right)_{1,2}.$$

By construction of $\hat{W}_{\mathrm{G}}$, $(\Delta_x^{\mathrm{out}})_{3,2} = \|\Delta_x\|_{\mathrm{op}}$. Since J commutes with every 2×2 orthogonal matrix, $\left(\Delta_y^{\mathrm{out}}\right)_{3,1} = \|\Delta_y\|_{\mathrm{op}} = \|\Delta_x\|_{\mathrm{op}}$. Finally, $(\Delta_z^{\mathrm{out}})_{1,2} = (\Delta_z)_{1,2} = 2$ because the orthogonal transformation V' leaves the covariance matrix of the fermionic mode A_0 unchanged. Together with equation (7.39), this shows that the recovery operation $\mathcal{R}_{\mathrm{G},T}^{\mathrm{opt}}$ saturates the bound in (7.38).

7.4.5 Convex-Combination of Trace-Preserving Gaussian Recovery Operations

Let us consider a convex combination of trace preserving Gaussian recovery operations:

$$\mathcal{R}_{\mathrm{cc},t}(\hat{\rho}) = \sum_j p_j \, \mathcal{R}_{\mathrm{G},j,t}(\hat{\rho}), \quad \sum_j p_j = 1, \, p_j \geq 0. \tag{7.45}$$

We now claim that a recovery operation of this form cannot overcome the bound (7.38). Indeed, because of linearity:

$$F(\mathcal{R}_{\mathrm{cc},t}) = \sum_j p_j F(\mathcal{R}_{G,j,t}) \leq F^{\mathrm{opt}}_{\mathrm{G},t} \tag{7.46}$$

This is not true when the coefficients p_j depend on the state:

$$\mathcal{R}_{\mathrm{cc},T}(\hat{\rho}) = \sum_j p_j(\hat{\rho}) \, \mathcal{R}_{\mathrm{G},j,t}(\hat{\rho}).$$

This is the case, for example, of a measurement-based recovery operation, as the standard quantum error correction algorithms based on syndrome measurement. These algorithms can beat the bound $F^{\mathrm{opt}}_{\mathrm{G},t}$ but not the most tight F^{opt}_{t}.

7.5 Gaussian Decoherence Channel

Let us consider a decoherence channel $\mathcal{D}_t(\cdot)$ which is a Gaussian channel. We now prove that in some specific cases a Gaussian recovery operation achieves the bound in (7.6), i.e. $F^{\mathrm{opt}}_{\mathrm{G},t} = F^{\mathrm{opt}}_{t}$. Notice that $F^{\mathrm{opt}}_{\mathrm{G},t}$ and F^{opt}_{t} have been derived under the assumption of a decoherence-free mode, which we therefore assume also in this chapter. Comparing equation (7.6) with (7.7), we obtain that we have only to show that:

$$\|\hat{\rho}_{x,+}(t) - \hat{\rho}_{x,-}(t)\|_{\mathrm{tr}} = \|\Gamma_{x,+}(t) - \Gamma_{x,-}(t)\|_{\mathrm{op}} \tag{7.47}$$

Let us consider the parametrization of a fermionic Gaussian channel in equation (7.32) for $\mathcal{D}_t$ which maps $M = 2$ Dirac modes into N modes. We start considering a unital map, i.e. $A_{\mathcal{D}} = 0$, $B_{\mathcal{D}} \neq 0$. Moreover, since the fermionic mode A is decoherence-free, $B_{\mathcal{D}} = \mathbb{I} \oplus \tilde{B}_{\mathcal{D}}$. In order to study the action of $\mathcal{D}_T$ on operators we need another parameter, $C_{\mathcal{D}}$, which is not relevant for covariance matrices. For a trace-preserving quantum operation $C_{\mathcal{D}} = 2^{M-N}$.

Let us recall that:

$$\hat{\rho}_{x,+}(t) - \hat{\rho}_{x,-}(t) = \hat{a}\mathcal{D}_t(-\hat{b}) + \hat{a}^\dagger \mathcal{D}_t(-\hat{b}^\dagger) \tag{7.48}$$

We name $\mathcal{D}_t(-\hat{b}) = \hat{R}$; from equation (7.24) we know that $\|\hat{\rho}_{x,+}(t) - \hat{\rho}_{x,-}(t)\|_{\mathrm{tr}} = 2\mathrm{tr}\left[\hat{P}\right]$, where $\mathrm{tr}\left[\hat{P}\right]$ is the sum of the singular values s_k of $\hat{R}$. Let us compute s_k for this specific case. We observe that:

$$\mathcal{D}_t(\hat{c}_j) = C_{\mathcal{D}} \sum_k B_{j,k} \hat{c}'_k \tag{7.49}$$

Therefore, since $-b = -\frac{1}{2}(c_3 + ic_4)$:

$$\hat{R} = -\frac{C_{\mathcal{D}}}{2}\sum_j (B_{3,j} + iB_{4,j})\,\hat{c}'_j = -\frac{C_{\mathcal{D}}}{2}\left(\vec{l}_1\cdot\vec{\hat{c}}' + i\vec{l}_2\cdot\vec{\hat{c}}'\right).$$

Define

$$\hat{c}''_j = \sum_k B_{j+2,k}\hat{c}'_k/\Lambda_j, \quad \Lambda_j = +\sqrt{(\tilde{B}\tilde{B}^T)_{j,j}} \leq 1 \tag{7.50}$$

so that $c''_j c''_j = \mathbb{I}$. Since the two vectors $\vec{l}'_1 = \vec{l}_1/\Lambda_1$ and $\vec{l}'_2 = \vec{l}_2/\Lambda_2$ can be non-orthogonal, we write $\vec{l}'_2 = \Omega\,\vec{l}'_1 + \sqrt{1-\Omega^2}\,\vec{l}'_\perp$, with $\vec{l}'_\perp$ such that $\vec{l}'_1\cdot\vec{l}'_\perp = 0$. This defines the following expansion $c''_2 = \Omega c''_1 + \sqrt{1-\Omega^2}c''_\perp$. With this notation, we rewrite R as:

$$\hat{R} = -\frac{C_{\mathcal{D}}}{2}\left((\Lambda_1 + i\Lambda_2\Omega)\hat{c}''_1 + i\Lambda_2\sqrt{1-\Omega^2}\hat{c}''_\perp\right) \tag{7.51}$$

The two degenerate singular values of this operator are:

$$s_{1,2} = \frac{C_{\mathcal{D}}}{2}\sqrt{\Lambda_1^2 + \Lambda_2^2 \pm 2\Lambda_1\Lambda_2\sqrt{1-\Omega^2}} \tag{7.52}$$

and the trace (over $N-1$ fermions!) can be computed via the nested radical formula:

$$2\mathrm{tr}[P] = \sqrt{2}\sqrt{\Lambda_1^2 + \Lambda_2^2 + \sqrt{(\Lambda_1^2 - \Lambda_2^2)^2 + 4\Lambda_1^2\Lambda_2^2\Omega^2}} \tag{7.53}$$

Let us now discuss the Gaussian formalism. The action of $\mathcal{D}_T$ on the initial covariance matrix:

$$\Gamma_{x,+}(t) - \Gamma_{x,-}(t) = B_{\mathcal{D}}\begin{pmatrix} 0 & -C^T \\ C & 0 \end{pmatrix}B_{\mathcal{D}}^T \tag{7.54}$$

where the only matrix elements of C different from zero are $C_{1,1} = C_{2,2} = 2$. Since the mode A is decoherence free, $B_{\mathcal{D}} = \mathbb{I}_2 \oplus \tilde{B}_{\mathcal{D}}$, and thus:

$$\|\Gamma_{x,+}(t) - \Gamma_{x,-}(t)\|_{\mathrm{op}} = \|\tilde{B}_{\mathcal{D}}C\|_{\mathrm{op}} \tag{7.55}$$

Using the previous notation, we get that:

$$\tilde{B}_{\mathcal{D}}C = 2\begin{pmatrix} \Lambda_3\vec{l}_1\,; & \Lambda_4\left(\Omega\vec{l}_1 + \sqrt{1-\Omega^2}\vec{l}_\perp\right) \end{pmatrix} \tag{7.56}$$

Consider an orthogonal transformation O which maps $O\vec{l}_1 = e_1$ and $O\vec{l}_\perp = e_2$. Since $\|\cdot\|_{\mathrm{op}}$ is a unitarily invariant norm, we have to study the operator norm of the matrix:

$$O\tilde{B}C\Big|_{1-2,1-2} = 2\begin{pmatrix} \Lambda_1 & \Lambda_2\Omega \\ 0 & \Lambda_2\sqrt{1-\Omega^2} \end{pmatrix} \tag{7.57}$$

The singular values of this matrix are:

$$\tilde{s}_\pm = \sqrt{2}\sqrt{\Lambda_1^2 + \Lambda_2^2 \pm \sqrt{(\Lambda_1^2 - \Lambda_2^2)^2 + 4\Lambda_1^2\Lambda_2^2\Omega^2}} \tag{7.58}$$

and $\tilde{s}_+$ is the sought norm. Moreover, $\tilde{s}_+ = 2\mathrm{tr}[P]$. This demonstrates equation (7.47).

Let us work out two easy examples, i.e. $\Omega = \{0, 1\}$. For the best case situation $\Omega = 0$ the optimal fidelity of the channel is given by $F_t^{\text{opt}} = 2/3 + \max(\Lambda_1, \Lambda_2)/3$. For $\Omega = 1$, the fidelity is lower: $F_t^{\text{opt}} = 2/3 + \sqrt{\Lambda_1^2 + \Lambda_2^2}/3$. This section shows us that in presence of a Gaussian decoherence channel a relatively small number of parameters can characterize the fidelity of the system.

Let us now relax the assumption of $\mathcal{D}$ being a unital map, i.e. $A_{\mathcal{D}} \neq 0$. Recalling that the action on a covariance matrix is $\Gamma' = B_{\mathcal{D}} \Gamma B_{\mathcal{D}}^T + A_{\mathcal{D}}$, equation (7.54) is not changed and we expect therefore the result to be independent of $A_{\mathcal{D}}$. Since the first mode is decoherence free, the matrix A must have the following form: $A = 0_2 \otimes \tilde{A}$, where 0_2 represents a 2×2 zero matrix. For a general matrix A of this form, equation (7.47) is not true. A sufficient condition for equation (7.47) to be true is that $O\tilde{A}O^T = A' \oplus A''$, where the action of O is defined in equation 7.57 and in the text before. A' (A'') is a 2×2 ($N - 4 \times N - 4$) skew-symmetric matrix. Physically, this means that A does not have correlations between the modes $\{\hat{c}_1'', \hat{c}_\perp''\}$ and all the other modes of the system.

In this case, the operator $\hat{R}$ in equation (7.51) takes the form:

$$\hat{R} = -\frac{1}{2}\left((\Lambda_1 + i\Lambda_2\Omega)\hat{c}_1'' + i\Lambda_2\sqrt{1-\Omega^2}\hat{c}_\perp''\right)\hat{\rho}_{A''} \tag{7.59}$$

where $\hat{\rho}_{A''}$ is a well-defined density operator written in terms of Majorana modes represented by vectors $\vec{l}_j''$ orthogonal to $\{\vec{l}_1, \vec{l}_\perp'\}$. Exploiting the fact that $\hat{\rho}_{A''}$ is a positive operator with $\text{tr}[\hat{\rho}_{A''}] = 1$ one can demonstrate equation (7.47).

Let us finally notice that in the two cases for which we have found equation (7.47) true, the operator $\hat{\rho}_{x,+}(t) - \hat{\rho}_{x,-}(t)$ is a Gaussian operator. We leave as conjecture that (7.47) is true if and only if $\hat{\rho}_{x,+}(t) - \hat{\rho}_{x,-}(t)$ is Gaussian.

7.6 Master Equation with Linear Jump Operators

In the three previous sections we have focussed on the development of theoretical tools for the quantification of the memory properties of a Kitaev chain. We now switch our focus to the use of these tools. We discuss several kinds of decoherence maps $\mathcal{D}_t(\cdot)$ and characterize their effect on a fermionic topological memory.

The most natural way to construct a decoherence map $\mathcal{D}_t$ is to consider a time evolution governed by a Lindblad master equation, which can be derived under the assumptions: i) system and environment are initially uncorrelated, ii) the coupling between system and environment is weak (Born approximation) and iii) the environment equilibrates fast (Markov approximation). One obtains:

$$\partial_t \hat{\rho} = -\frac{i}{\hbar}\left[\hat{H}, \hat{\rho}\right] + \sum_\alpha^{n_\alpha}\left(\hat{\mathcal{L}}_\alpha \hat{\rho} \hat{\mathcal{L}}_\alpha^\dagger - \frac{1}{2}\{\hat{\mathcal{L}}_\alpha^\dagger \hat{\mathcal{L}}_\alpha, \hat{\rho}\}\right) \tag{7.60}$$

where $\hat{H}$ is the Hamiltonian of the system and $\hat{\mathcal{L}}_\alpha$ are the the jump operators describing the decoherence process.

The differential equation can be formally integrated introducing the superoperator $\mathcal{S}_t$ such that $\hat{\rho}(T) = \mathcal{S}_t(\hat{\rho}_0)$. This defines our decoherence channel:

$$\mathcal{D}_t(\hat{\rho}_q) = \mathcal{S}_t(\hat{\rho}_q \otimes \hat{\rho}'); \tag{7.61}$$

where $\hat{\rho}'$ is the density operator of the $N-2$ fermion modes which are not used to define the qubit. Different $\hat{\rho}'$ define different decoherence channels, as well as different ways of encoding the qubit define different channels. In the following, we encode $\hat{\rho}_q$ into the zero-energy modes of the Hamiltonian $\hat{H}$, and $\hat{\rho}'$ is, for example, the ground state with respect to $\hat{H}$.

We can restrict our study to quadratic fermionic Hamiltonians,

$$\hat{H} = \frac{i}{4}\sum_{\alpha,\beta} T_{\alpha,\beta}\hat{c}_\alpha\hat{c}_\beta,$$

because they entail the class of topological models hosting localized Majorana zero-energy modes we are interested in. The evolution is a Gaussian channel and therefore we can work with covariance matrices rather than with density operators. The time evolution of the covariance matrix is given by (see section 6.5.2 and [Hor11, BK11a]):

$$\partial_t\Gamma = \frac{1}{\hbar}[T,\Gamma] - \{L_1,\Gamma\} - 2iL_2 \tag{7.62}$$

where L_1 and L_2 are defined in section 6.5.2.

In this section we concentrate only on the Gaussian recovery operation. We cannot analytically quantify the value of F_t^{opt} in (7.6). We know that $F_{\text{G},t}^{\text{opt}} < F_t^{\text{opt}}$. Moreover, the value $\|\hat{\rho}_{x,+}(t) - \hat{\rho}_{x,-}(t)\|_{\text{tr}}/2$ is upper bounded by $\sqrt{1-F(\hat{\rho}_{x,+}(t),\hat{\rho}_{x,-}(t))^2}$, where $F(\hat{\rho},\hat{\sigma})$ is the Uhlmann fidelity (see section 6.3.4) [NC04]. Even if we can make precise statements only about the lower bound $F_{\text{G},t}^{\text{opt}}$, the upper bound is also a function of the covariance matrices $\Gamma_{x,\pm}(t)$ and we do not expect a significantly different qualitative behaviour between the upper and the lower bound.

7.6.1 Uniqueness of the Steady State

We study the time evolution of the difference of two given covariance matrices $\Gamma_1(t) - \Gamma_2(t)$ using (7.62):

$$\partial_t(\Gamma_1-\Gamma_2) = (T-L_1)(\Gamma_1-\Gamma_2) + (\Gamma_1-\Gamma_2)(-T-L_1)$$

Let us consider for simplicity the case of T and L_1 not depending on time. We obtain:

$$\Gamma_1(t) - \Gamma_2(t) = e^{(T-L_1)t}(\Gamma_1(0)-\Gamma_2(0))e^{(-T-L_1)t} \tag{7.63}$$

According to the results in appendix C, under the assumption that $\vec{w}^\dagger L_1\vec{w} > 0$ for all the $\vec{w}$ eigenvectors of T, the two matrices $\pm T - L_1$ have eigenvalues with strictly negative real part. Consequently, the operator norm of $\exp((\pm T - L_1)t)$ decays exponentially in time. Therefore, defined $\Lambda = \|\Gamma_1(0)-\Gamma_2(0)\|_{\text{op}} > 0$:

$$\begin{aligned}\|\Gamma_1(t)-\Gamma_2(t)\|_{\text{op}} &\leq \Lambda\|e^{(T-L_1)t}\|_{\text{op}}\|e^{(-T-L_1)t}\|_{\text{op}} \leq \\ &\leq \Lambda\Omega\,\text{poly}(t)e^{\Re(\lambda_+)t}e^{\Re(\lambda_-)t} \xrightarrow{t\to\infty} 0\end{aligned}$$

where $\lambda_\pm$ are the largest negative real parts of the eigenvalues of $\pm T - L_1$. Because $\vec{w}^\dagger L_1\vec{w} = \|\sqrt{2}\tilde{L}^T\vec{w}\|_2$, with $\tilde{L}$ defined in (6.60), the assumption done

is equivalent to asking for a non-trivial action of the Lindblad operators on all the eigenstates of the Hamiltonian.

Under this condition, this demonstrates the uniqueness of the steady state, which is approached exponentially in time. We leave for the next sections the study of the dependence of the typical decay time on the system size N, which can be easily adapted to this case via a similar reasoning.

We can estimate the upper bound on the fidelity using equation (7.41), and considering that $\|\Gamma_{\alpha,+}(0) - \Gamma_{\alpha,-}(0)\|_{\text{op}} = 2$, with $\alpha = \{x, y, z\}$:

$$F_{\text{G},t}^{\text{opt}} \leq \frac{1}{2} + \frac{\Omega}{2}\text{poly}(t)e^{\Re(\lambda_+)t}e^{\Re(\lambda_-)t} \tag{7.64}$$

This rules out the possibility of any recovery operation for $t \to \infty$.

7.6.2 One Decoherence-Free Fermionic Mode

We make use of the assumption introduced in section 7.1 of a qubit composed of two modes A_0 and B_0, with A_0 decoherence-free. We parametrize the covariance matrices as follows:

$$\Gamma = \begin{pmatrix} \Gamma_A & -C^T \\ C & \Gamma_s \end{pmatrix} \tag{7.65}$$

where Γ_A is a 2×2 matrix representing the decoherence-free mode A_0, Γ_s is the $2(N-1) \times 2(N-1)$ covariance matrix of both the B_0 and the remaining modes, and C is $2(N-1) \times 2$ representing correlations.

With similar notation, the matrices T, L_1 and L_2 read:

$$T = \begin{pmatrix} 0 & 0 \\ 0 & T_s \end{pmatrix}, \quad L_1 = \begin{pmatrix} 0 & 0 \\ 0 & L_{1s} \end{pmatrix}, \quad L_2 = \begin{pmatrix} 0 & 0 \\ 0 & L_{2s} \end{pmatrix}.$$

Note that this this choice does not satisfy $\vec{w}_\beta^\dagger L_1 \vec{w}_\beta > 0 \ \forall \beta$ and there can be multiple steady states.

We want to study $F_{\text{G},T}^{\text{opt}}$ using equation (7.7) and observe that:

$$\Gamma_{x,+}(0) - \Gamma_{x,-}(0) = \begin{pmatrix} 0 & -\bar{C}^T \\ \bar{C} & 0 \end{pmatrix}; \tag{7.66}$$

Moreover, using equation (7.62), one obtains: $\partial_t C(t) = (T_s - L_{1s})C(t)$. which implies:

$$C(t) = e^{(T_s - L_{1s})t}C(0) \tag{7.67}$$

One can also show that $\Gamma_{s,x,+}(t) - \Gamma_{s,x,-}(t) = 0$ and that $\Gamma_{A,x,\pm}(t) = \Gamma_A(0)$.

Combining the results of appendix C to a reasoning similar to that used in the previous section, one gets:

$$\|\Gamma_{x,+}(t) - \Gamma_{x,-}(t)\|_{\text{op}} = \|C(t)\|_{\text{op}} \leq \|\bar{C}\|_{\text{op}}\, \Omega\, \text{poly}(t)e^{\Re(\lambda_1)t} \xrightarrow{t\to\infty} 0$$

where λ_1 is the eigenvalue with largest (negative) real part of $T_s - L_{1s}$. If $\Re(\lambda_1) < 0$, $\Gamma_{x,\pm}$ evolve towards the same covariance matrix, which does not have any correlation between modes A and B. Furthermore, $F_{\text{G},T}^{\text{opt}} \to 2/3$ exponentially in time.

The non-trivial action of L_{1s} on all the eigenstates of T_s is necessary (and sufficient) condition in order to have $\Re(\lambda_1) < 0$. We accept this assumption,

because otherwise there would be a decoherence free mode, which is the best candidate for a protected qubit, which would however not be the consequence of the topological properties of T_s. Notice that such a decoherence-free mode is not related to the mode auxiliary mode A which we use to define the qubit.

7.6.3 Dependence on the System Size

Let us study the scaling with the number of modes N of the bound on $\|C(t)\|_{\text{op}}$. We will assume L_{1s} to be positive definite. In this case, as explained in appendix C, the bound can be improved to:

$$\|\Gamma_{x,+}(t) - \Gamma_{x,-}(t)\|_{\text{op}} \leq \|\bar{C}\|_{\text{op}} e^{-\lambda_1 t} \tag{7.68}$$

where λ_1 is the eigenvalue of D with smallest (positive) real part. Since $\|\bar{C}\|_{\text{op}} = 2$ does not depend on N, only the size-scaling of the eigenvalues of L_{1s} must be studied. This depends on the model. Notice that at this stage the Hamiltonian has completely disappeared from our discussion. Even if we find an exponential scaling of F_T^{opt} with the size of the system, it is not an effect of Hamiltonian protection.

We start with a general consideration. We know that the best fidelity of a recovery operation $F_{\text{G},T}^{\text{opt}}$ with N fermionic modes can be bounded as follows:

$$F_{\text{G},T}^{\text{opt}} \leq \frac{2}{3} + \frac{1}{3} e^{-\lambda_{1,N} T} \tag{7.69}$$

We define $T_{0,N}$ as the minimum time for which a fidelity F_0 is reached (from above) in a system of size N. It follows:

$$T_{0,N} \leq \frac{1}{\lambda_{1,N}} \log\left(\frac{1}{3F_0 - 2}\right) \tag{7.70}$$

For an exponential scaling of $T_{0,N} \sim e^{cN}$, $c \in \mathbb{R}^+$, the following must hold:

$$\lambda_{1,N} \leq -A \log(3F_0 - 2)\, e^{-cN}, \quad A, c \in \mathbb{R}^+ \tag{7.71}$$

Therefore, if $\lambda_{1,N}$ decays with N slower than exponentially the qubit is not protected.

7.6.4 Translationally-Invariant Lindblad Operators

Let us now consider some explicit models for $\hat{\mathcal{L}}_\alpha$. We start with Lindblad operators $\hat{\mathcal{L}}_j$ localized on only one lattice site, j. The corresponding vectors $\vec{L}_{j,\mathbb{R}}$ and $\vec{L}_{j,\mathbb{I}}$ have at most only two elements different from zero and $\tilde{L}$ assumes the form:

$$\tilde{L} = \begin{pmatrix} B_1 & 0 & & & \\ 0 & B_2 & 0 & & \\ & \ddots & \ddots & \ddots & \\ & & 0 & B_{N-1} & 0 \\ & & & 0 & B_N \end{pmatrix} \tag{7.72}$$

where B_j are 2×2 matrices. In this case, the matrix L_{1s} is positive definite if and only if $\tilde{L}$ has no singular value equal to zero. $\tilde{L}$ in (7.72) has a zero singular

value if and only if there are two columns which are linearly dependent, i.e. if and only if there is a site, j, such that $\hat{\mathcal{L}}_j$ is as follows:

$$\hat{\mathcal{L}}_j = \nu_1 \xi \hat{c}_{j,1} + \nu_2 \xi \hat{c}_{j,2} = \xi(\nu_1 - i\nu_2)\hat{a}_j + \xi(\nu_1 + i\nu_2)\hat{a}_j^\dagger \tag{7.73}$$

with $\xi \in \mathbb{C}$, $\nu_i \in \mathbb{R}$. Let us assume that this is not the case and that the system is translationally invariant. If all the Lindblad operators are identical, L_1 is positive and the spectrum of L_1 is highly degenerate and composed of at most two fixed values λ_1 and λ_2, larger than zero. Considering a larger system only increases the degeneracy of the spectrum, ruling out the scaling of equation (7.71).

We can generalize the previous discussion to Lindblad operators which are local and localized on l neighboring sites. We assume translational invariance and a one-dimensional system. For a general l, $\tilde{L}$ is a $2(N-1) \times 2(N+l-2)$ real matrix and takes the following form:

$$\tilde{L} = \begin{pmatrix} B_l & B_{l-1} & \dots & B_1 & 0 & \dots & & 0 \\ 0 & B_l & B_{l-1} & \dots & B_1 & 0 & & \vdots \\ \vdots & \ddots & \ddots & \ddots & & \ddots & \ddots & \vdots \\ & & 0 & B_l & B_{l-1} & \dots & B_1 & 0 \\ & & & 0 & B_l & B_{l-1} & \dots & B_1 \end{pmatrix} \tag{7.74}$$

where each B_j is a 2×2 matrix.

Consequently, L_1 is a real symmetric positive semi-definite banded block-Toeplitz matrix:

$$L_1 = 2\tilde{L}\tilde{L}^T = \begin{pmatrix} A_0 & \dots & A_{l-1} & 0 & 0 \\ \vdots & \ddots & \ddots & \ddots & 0 \\ A_{-l+1} & \ddots & \ddots & \ddots & A_{l-1} \\ 0 & \ddots & \ddots & \ddots & \vdots \\ 0 & 0 & A_{-l+1} & \dots & A_0 \end{pmatrix} \tag{7.75}$$

The relation between the A_j and B_k matrices is the following:

$$j \geq 0 \qquad A_j = 2\sum_{k=1}^{l-j} B_k B_{k+j}^T \tag{7.76}$$

$$j < 0 \qquad A_j = A_{-j}^T \tag{7.77}$$

We exploit now one property of Toeplitz matrices in [Ser98]. Consider the matrix-valued generating function $f(x)$ with $x \in [-\pi, \pi]$:

$$f(x) = \sum_{j=-l+1}^{l-1} e^{ijx} A_j \tag{7.78}$$

The theorem states that the eigenvalues of L_1 are in the range $[\sigma_{\min}(f), \sigma_{\max}(f)]$, where the notation $\sigma(f)$ refers to the singular values of f and the min (max) is taken over $x \in [-\pi, \pi]$. Therefore we can simply study a 2×2 matrix to

get eigenvalues of the $2(N-1)\times 2(N-1)$ matrix. Moreover, the eigenvalues are bound from below $\forall N$. The only way to get a zero eigenvalue is that $\sigma_{\min}(f)=0$; in that case the exponential scaling with N is not ruled out by the theorem. It would be interesting to understand what are the conditions on B_k in order to have $\sigma_{\min}(f)=0$, and we leave it for future work. Notice that this formalism allows also the study of the case $l=1$ which we discussed at the end of the previous subsection.

7.6.5 Impossibility of Protection via Engineered Dissipation

Assume to have a matrix L_1 whose eigenvalues are not scaling exponentially with N to zero. Adding an engineered dissipation in the form of a list of new operators $\hat{\mathcal{J}}_\alpha$ on top of the system cannot improve the memory properties. Indeed, one can write the global $L_1^{\rm tot}$ matrix as L_1+J_1 where J_1 accounts for the contribution of the engineered dissipation. Since L_1 is positive and J_1 is positive semidefinite, the spectrum of $L_1^{\rm tot}$ is bounded from below by $\min_{\lambda\in {\rm Sp}L_1}\lambda$.

7.7 Master Equation with Quadratic Lindblad Operators

We consider now the action of a generic master equation with Hermitian jump operators which are quadratic in the fermionic fields:

$$\hat{\mathcal{L}}_\alpha=\frac{i}{4}\sum_{k,l}M^\alpha_{kl}\,\hat{c}_k\,\hat{c}_l. \tag{7.79}$$

The time evolution of the covariance matrix is given by (see section 6.6.1):

$$\partial_t\Gamma=\frac{1}{\hbar}[T,\Gamma]+\frac{1}{2}\sum_\alpha[M^\alpha,[M^\alpha,\Gamma]] \tag{7.80}$$

7.7.1 Uniqueness of the Steady Covariance Matrix

We now proof that under some reasonable assumptions the master equation (7.80) has a unique steady state. We exploit the canonical isomorphism between $2n\times 2n$ covariance matrices and vectors of length $4n^2$ and between the superoperators and $4n^2\times 4n^2$ matrices. Equation (7.80) can be rewritten as:

$$\begin{aligned}\mathcal{T}&=T\otimes\mathbb{I}-\mathbb{I}\otimes T\\ \mathcal{M}&=\sum_\alpha(M^\alpha)^2\otimes\mathbb{I}+\mathbb{I}\otimes(M^\alpha)^2-2M^\alpha\otimes M^\alpha\\ \partial_t\vec{\Gamma}&=(\mathcal{T}+\mathcal{M})\,\vec{\Gamma}\end{aligned} \tag{7.81}$$

We apply, as above, the theorem in appendix C. $\mathcal{T}$ is a $4n^2\times 4n^2$ skew-symmetric matrix; $\mathcal{M}$ is a negative semidefinite matrix. This last fact can be proven by working in the basis diagonalizing $\sum_\alpha M^\alpha$; in particular one can show that given the $2n$ eigenvalues of $\sum_\alpha M^\alpha$, $\{\pm i\lambda_\beta\}_{\beta=1}^n$, $\lambda_\beta\in\mathbb{R}^+$, the eigenvalues of $\mathcal{M}$ are $\{-(\lambda_\beta\pm\lambda_\delta)^2\}_{\beta,\delta=1}^n$, each one being twofold degenerate. The condition

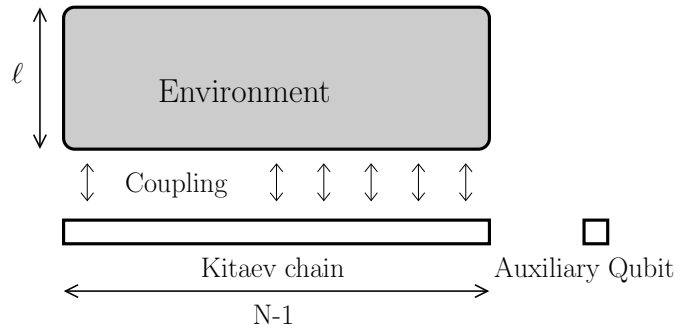

Figure 7.1: Sketch of the system considered: one Kitaev chain of length N coupled to a fermionic reservoir; the initial state of the Kitaev chain is entangled with the auxiliary qubit.

$\vec{w}^\dagger(-\mathcal{M})\vec{w} > 0$ implies that the action of the dissipation $\sum_\alpha M^\alpha$ is not trivial on every eigenstate of the T matrix. Under this assumption there is only one steady covariance matrix, which is equal to zero:

$$\|\Gamma(t)\|_{\text{op}} \xrightarrow{t\to\infty} 0, \quad \forall\, \Gamma(0). \tag{7.82}$$

Note that the asymptotic state is not Gaussian, but a linear combination thereof.

Using equation (7.41) one can put an upper bound to the fidelity of a Gaussian recovery operation, which decays exponentially in time. On the other hand, there is no way of using the covariance matrices to extract information about the general recovery operation because the states are not Gaussian. Finally, all the results derived in the previous section for linear jump operators can be extend also to this case via a suitable adaptation of the reasoning.

7.8 Kitaev Chain Coupled to a Small Fermionic Environment

According to the previous sections, it is problematic to use a fermionic system coupled to an environment described by a master equation as a quantum memory. In this section we explicitly consider a small fermionic environment; we exactly compute the correlations which arise between the system and the environment and study whether they improve the memory properties of the topological system. With the help of a numerical simulation we show that even in this case the information stored in the system is not protected.

We consider a Kitaev chain of N sites as in (7.8) and an auxiliary fermionic ancilla with trivial dynamics. Additionally, we consider a two-dimensional fermionic environment of size $N \times \ell$ ruled by a simple hopping dynamics:

$$\hat{H}_{\text{env}} = -K \sum_{<k,l>} \hat{f}_k^\dagger \hat{f}_l; \tag{7.83}$$

where $\hat{f}_k$ are fermionic operators. The coupling between the chain and the edge

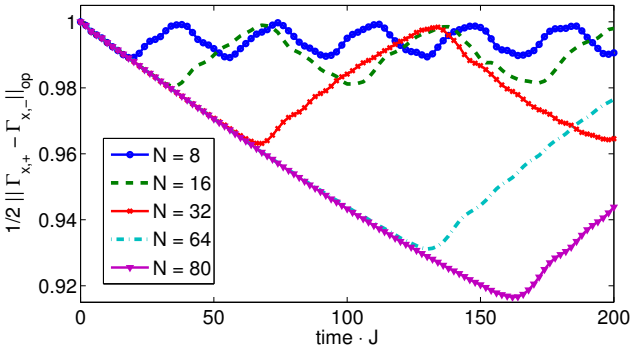

Figure 7.2: Plot of $\frac{1}{2}\|\Gamma_{x,+}(t) - \Gamma_{x,-}(t)\|_{\text{op}}$ for $\ell = 1$ for different chain lengths N. The shared initial decay implies that the qubit is not protected by the chain length.

of the environment is modelled by the Hamiltonian (see figure 7.1 for a sketch):

$$\hat{H}_{\text{K}-\text{e}} = -J_{\text{env}} \sum_j \hat{c}_j^\dagger \hat{f}_j + H.c. \tag{7.84}$$

We define the time-evolution operator for the global system:

$$\hat{U}(t) = e^{-\frac{i}{\hbar}(\hat{H}_{\text{KC}} + \hat{H}_a + \hat{H}_{\text{env}} + \hat{H}_{\text{K}-\text{e}})t}. \tag{7.85}$$

The decoherence map we consider is:

$$\mathcal{D}_t(\hat{\rho}_q) = \text{tr}_{\text{env}} \left[\hat{U}(t) \left(\hat{\rho}_q \otimes \hat{\rho}_{\text{GS}} \right) \hat{U}(t)^\dagger \right]; \tag{7.86}$$

where $\hat{\rho}_q$ is the (pure) state of the qubit, built with $\hat{a}_a$ and $\hat{d}_0$. $\hat{\rho}_{GS}$ represents the ground state (vacuum) of the theory described by $\hat{H}_{\text{KC}} + \hat{H}_{\text{env}}$. Notice that $\hat{\rho}_q \otimes \hat{\rho}_{\text{GS}}$ is not an eigenstate of $\hat{U}(t)$ and thus the action of the map is not trivial. Moreover, $\mathcal{D}_t$ in (7.86) is a Gaussian channel and we study the optimal recovery fidelity via equation (7.7).

We first consider the case $\ell = 1$, which is the case with the smallest environment. We set $\mu = J$, $\Delta = J$, $K = J$ and $J_{\text{env}} = 0.05J$. The behaviour of $1/2\|\Gamma_{x,+}(t) - \Gamma_{x,-}(t)\|_{\text{op}}$ for different N is shown in figure 7.2. We observe fluctuations due to fermions which are coherently entering and leaving the system. Remarkably, the initial decay behaviour is shared by systems with different sizes. We conclude that the size of the chain is not protecting the qubit.

It is interesting to observe that one would obtain the same plot substituting $\hat{\rho}_{\text{GS}}$ with any other $\hat{\rho}'$, e.g. a thermal state. Consider the general Gaussian channel:

$$\mathcal{D}'_t(\hat{\rho}_q) = \text{tr}_{\text{env}} \left[\hat{U}(t) \left(\hat{\rho}_q \otimes \hat{\rho}' \right) \hat{U}(t)^\dagger \right].$$

The covariance matrix of $\mathcal{D}'_t(\hat{\rho}_q)$ is:

$$\Gamma(t) = O(t)(\Gamma_q \oplus \Gamma')O(t)^T\big|_{\text{chain+ancilla}} \tag{7.87}$$

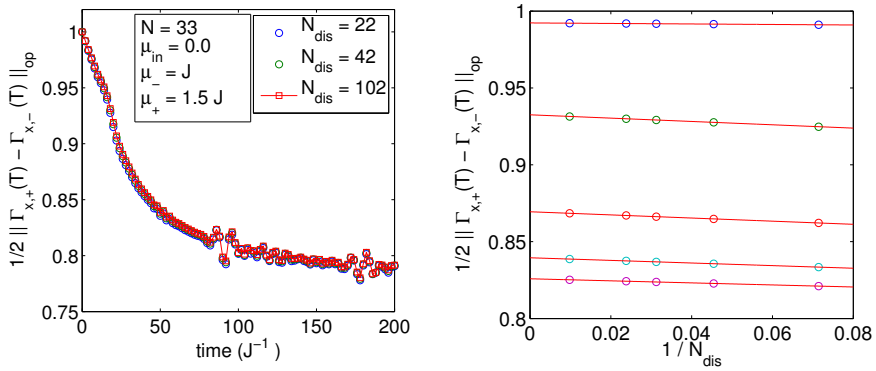

Figure 7.3: Study of the discretization of the interval $[\mu_-, \mu_+]$. We consider a Kitaev chain with 32 sites and a decoherence-free auxiliary mode; initially, the chain is at the frustration-free point ($\mu = 0$, $J = \Delta$). Left: we plot the quantity $1/2\|\Gamma_{x,+} - \Gamma_{x,-}\|_{\rm op}$ for different values of $N_{\rm dis}$, the number of discretizations of the interval. Plots display extremely similar behaviours. Right: we show that the the data scale linearly in $1/N_{\rm dis}$. We consider $N_{\rm dis} = \{14, 22, 32, 42, 102\}$. For the sake of clarity, we show the scaling only for five different times; from top to bottom: $2J^{-1}$, $18J^{-1}$, $34J^{-1}$, $50J^{-1}$ and $66J^{-1}$. Red lines are linear fits. Similar results are obtained for $1/2\|\hat{\rho}_{x,+} - \hat{\rho}_{x,-}\|_{\rm tr}$ (not shown).

where Γ' is the covariance matrix of $\hat{\rho}'$ and $O(t)$ is the orthogonal transformation which represents the unitary time evolution $\hat{U}(t)$. The action of tracing out the environment is performed by restricting the covariance matrix only to the physical modes of the Kitaev chain and of the ancilla. Clearly, the quantity:

$$\Gamma_{x,+}(t) - \Gamma_{x,-}(t) = O(t)\,(\Gamma_{x,+} \oplus \Gamma' - \Gamma_{x,-} \oplus \Gamma')\,O(t)^T \tag{7.88}$$

does not depend on Γ'. Therefore, the fidelity of the recovery operation does not depend on $\hat{\rho}'$.

Finally, we obtain a similar behaviour for $\ell > 1$ (not shown).

7.9 Convex-Combination of Hamiltonian Time Evolutions

Until now we have assumed to be able to precisely encode the qubit $\hat{\rho}_q$ in the zero-energy Majorana modes $\{\hat{c}_1 \dots \hat{c}_4\}$ of the system; in other words, we have assumed to be able to exactly address the ground space of the system. In reality, more complicated situations can appear, because it is often experimentally challenging to be able to control all the parameters of the quantum system. In cold atoms experiments, for example, the number of atoms varies for every different realization. Therefore, every measurement is the expectation value of the corresponding observable over a mixed state which is the convex combination of the different experimental realizations.

This kind of problems motivates the study of decoherence maps which are convex-combinations of Hamiltonian time evolutions. Specifically, let us imagine

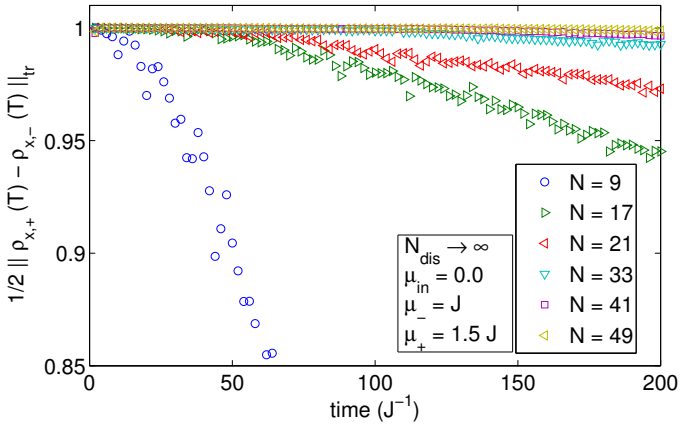

Figure 7.4: Dependence on the length of the Kitaev chain N of $\frac{1}{2}\|\rho_{x,+}-\rho_{x,-}\|_{\mathrm{tr}}$ under the action of the map in equation (7.90) for the parameters described in section 7.9.1. The curves are obtained by the extrapolation procedure to $N_{\mathrm{dis}}\to\infty$ described in the text and in figure 7.3.

to be able to initialize the global system composed of the Kitaev chain and of the ancilla in a given state $\hat{\rho}_q\otimes\hat{\rho}'$, which is not necessarily the ground state of the experimental realization. The assumption of a tensor form for $\hat{\rho}(0)$ is justified by the fact that in order to store information in the system one has to develop an experimental protocol which can freely access the zero-energy modes A_0 and B_0 and whose action is independent from the state of the other modes.

The time evolution is described by the following decoherence map:

$$\hat{U}_\mu(t) = e^{-i(\hat{H}_{\mathrm{KC}}(\mu)+\hat{H}_{\mathrm{a}})t} \tag{7.89}$$

$$\mathcal{D}_T(\hat{\rho}_q) = \frac{1}{\mu_+-\mu_-}\int_{\mu_-}^{\mu_+} d\mu\,\hat{U}_\mu(t)\,(\hat{\rho}_q\otimes\hat{\rho}'(\mu))\,\hat{U}_\mu(t)^\dagger \tag{7.90}$$

We write explicitly the dependence of Hamiltonian $\hat{H}_{\mathrm{KC}}$ on the chemical potential μ, even if every other quadratic perturbation could have been considered. The map accounts for several time evolutions ruled by Hamiltonians characterized by different μ, and then considers the convex combination of the outcomes. The initial state may or may not depend on the specific chemical potential μ of the time-evolution. Even if each time-evolved state is Gaussian, their convex combination is not and the map in (7.90) is not a Gaussian channel. We exploit equations (7.6) and (7.7) to characterize the fidelity of the optimal recovery operation and of the optimal Gaussian one; in general, they do not coincide. This comparison is possible because, as explained in section 6.6.2 and in appendix B.3, we have access not only to $\Gamma_{x,\pm}(t)$, but also to $\hat{\rho}_{x,\pm}(t)$ (this last only in a specific basis), so that both F_t^{opt} and $F_{\mathrm{G},t}^{\mathrm{opt}}$ can be computed.

7.9.1 The Case of $\hat{\rho}'$ Independent from μ

Let us consider the frustration-free point of the Kitaev chain, $\mu=0$ and $J=\Delta$; we use the corresponding zero-energy mode $\hat{d}_0^{(\dagger)}$ and the decoherence-free ancilla

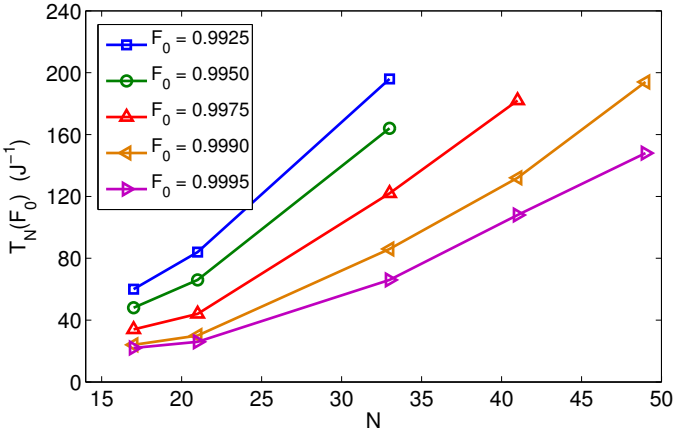

Figure 7.5: Dependence on the length of the Kitaev chain N of the time $T_N(F_0)$ at which a prescribed fidelity F_0 is reached. The semi-logarithmic scale highlights a superlinear scaling. The procedure relies on a parabolic fit of the data shown in figure 7.3, whose oscillating behaviour makes otherwise this analysis impossible.

$\hat{a}_a^{(\dagger)}$ to encode the qubit state $\hat{\rho}_q$. The other modes are in the ground state with respect to the frustration-free $\hat{H}_{\mathrm{KC}}$: $\hat{\rho}' \equiv \hat{\rho}_{\mathrm{GS}}$. Regarding the strength of the perturbation, we take $\mu_- = J$ and $\mu_+ = 1.5J$. According to the characterization given in [BK11b], this is a strong perturbation, because the strength parameter $N\|V\|_{\mathrm{op}}^2$ is much larger than one ($1 < \|V\|_{\mathrm{op}} < 1.5$ and $8 < N < 48$).

Because in the numerical simulations we cannot study a continuum of time evolutions as in equation (7.90), we discretize the integral with a sum over N_{dis} perturbation realizations which are equispaced in the interval $[\mu_-, \mu_+]$. Figure 7.3 shows that the procedure is sound, and that the data show a linear scaling in $1/N_{\mathrm{dis}}$, so that an extrapolation for $N_{\mathrm{dis}} \to +\infty$ is possible.

Let us now study the scaling with $N \to +\infty$ of $\frac{1}{2}\|\rho_{x,+}(t) - \rho_{x,-}(t)\|_{\mathrm{tr}}$, the quantity which characterizes the fidelity of the optimal recovery operation. Figure 7.4 shows that the fidelity of the optimal recovery operation increases as the size N of the system increases. In order to better quantify this form of protection, we fix a value $F_0 < 1$. We define $T_N(F_0)$ as the first time at which $\frac{1}{2}\|\rho_{x,+}(t) - \rho_{x,-}(t)\|_{\mathrm{tr}}$, computed with a system of size N, reaches such value. The scaling of $T_N(F_0)$ with N is shown in figure 7.5 for several values of F_0. The scaling is superlinear and can be identified with a form of protection by the Hamiltonian.

The result is related to the Hamiltonian protection of the zero-energy space. Indeed, it is possible to observe a completely different behaviour both in case in which the perturbation happens in the gapless region at $\Delta = 0$ or outside the topological region, $|\mu/J| > 2$ (not shown).

Let us now concentrate on the optimal Gaussian recovery operation. Our numerics, shown in figure 7.6, shows that $\frac{1}{2}\|\Gamma_{x,+}(t) - \Gamma_{x,-}(t)\|_{\mathrm{op}}$ saturates to a finite value $F_{\mathrm{G}}(T) < 1$ in the limit $N \to \infty$. Therefore, whereas the previous

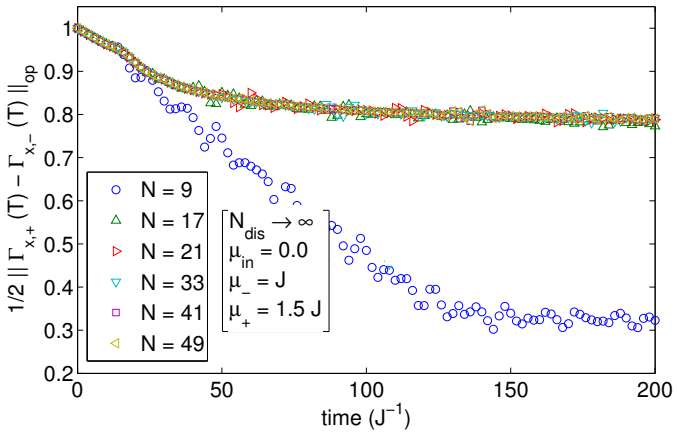

Figure 7.6: Dependence on the length of the Kitaev chain N of $\frac{1}{2}\|\Gamma_{x,+}(T) - \Gamma_{x,-}(T)\|_{\text{op}}$ under the action of the map in equation (7.90) for the parameters described in section 7.9.1. The curves are obtained by the extrapolation procedure to $N_{\text{dis}} \to \infty$ described in the text and in figure 7.3.

analysis shows that the information is not lost and is protected by the topological nature of the Hamiltonian, it cannot be recovered with the simplest class of quantum operations, namely the Gaussian ones. This is a direct consequence of the fact that the final state $\mathcal{D}_T(\hat{\rho}_q)$ is not Gaussian.

Let us provide an intuitive argument for this. Consider a situation with four Dirac modes, and let us consider the following Gaussian states:

$$|\Psi_1\rangle = |0000\rangle; \quad |\Psi_2\rangle = |1111\rangle; \quad |\Psi_3\rangle = |0011\rangle; \quad |\Psi_4\rangle = |1100\rangle. \tag{7.91}$$

We define the following non-Gaussian mixed states:

$$\hat{\rho}_a = \frac{1}{2}\left(|\Psi_1\rangle\langle\Psi_1| + |\Psi_2\rangle\langle\Psi_2|\right); \qquad \hat{\rho}_b = \frac{1}{2}\left(|\Psi_3\rangle\langle\Psi_3| + |\Psi_4\rangle\langle\Psi_4|\right). \tag{7.92}$$

The two states are orthogonal: $\text{tr}[\hat{\rho}_a\hat{\rho}_b] = 0$; still, an easy computation shows that they have the same covariance matrix, the zero-matrix. Even if it is possible to distinguish the two states, this cannot be done just by looking at their covariance matrices.

We now analyze the relation of these results to those presented in [BK11b]. It is shown that in presence of a homogeneous perturbation the memory properties of the Kitaev chain scale only logarithmically with the system size. The discussion is strongly connected to the use of the standard quantum error correction code for frustration-free models. Here we show that such algorithm is not the most efficient. Indeed, our results show that the information is not lost and that it can benefit from increasing the length of the system.

7.9.2 The Case of $\hat{\rho}'$ Dependent on μ

We now study the case of a state $\hat{\rho}_q \otimes \hat{\rho}'(\mu)$ depending on the chemical potential of the Hamiltonian ruling the time evolution. Let us consider in particular the

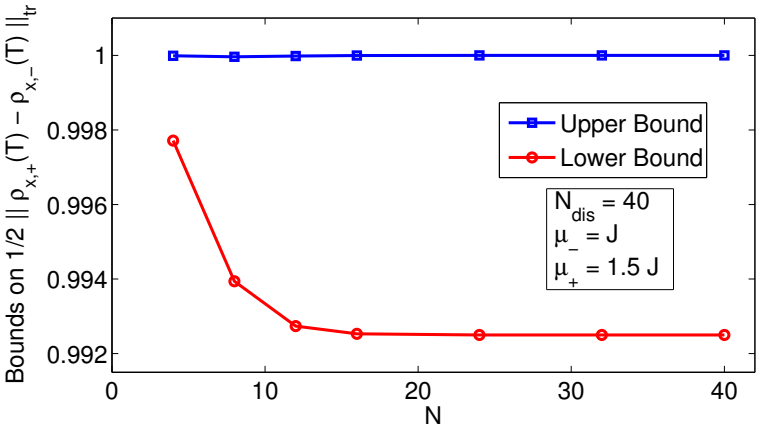

Figure 7.7: Study of the decoherence map (7.90) in the case of a state depending on μ (see section 7.9.2). The definition of the two bounds is in the text.

situation in which the qubit $\hat{\rho}_q$ is encoded with the zero-energy mode $\hat{d}_0^{(\dagger)}(\mu)$ of the Hamiltonian $\hat{H}_{\mathrm{KC}}(\mu)$. Moreover, we also consider the other modes to be in the ground state with respect to $\hat{H}_{\mathrm{KC}}(\mu)$, i.e. $\hat{\rho}' \equiv \hat{\rho}_{\mathrm{GS}}(\mu)$.

Clearly, the action of each time evolution $\hat{U}_\mu(t)\ (\hat{\rho}_q \otimes \hat{\rho}'(\mu))\ \hat{U}_\mu(t)^\dagger$ is trivial because the state is an eigenstate of the operator $\hat{U}_\mu(t)$. This statement hides the assumption of perfect degeneracy of the ground state, i.e. that the energy ε_0 of the modes $\hat{d}_0^{(\dagger)}(\mu)$ is zero. This is in general not true. Still, in [BK11b] it is demonstrated that $\varepsilon_0 \xrightarrow{N\to\infty} 0$ exponentially in the system size, and thus that it is possible to control the dephasing arising from this issue, which we therefore neglect.

The decoherence map (7.90) reduces to the computation of the overlap between the ground spaces of the difference points of the phase diagram of the Kitaev chain. In figure 7.7 we provide an upper bound and a lower bound to $\|\hat{\rho}_{x,+} - \hat{\rho}_{x,-}\|_{\mathrm{tr}}$, which clearly does not depend on time. The upper bound is computed as follows:

$$\begin{aligned}
\|\hat{\rho}_{x,+} - \hat{\rho}_{x,-}\|_{\mathrm{tr}} &= \left\| \frac{1}{N_{\mathrm{dis}}} \sum_{\alpha}^{N_{\mathrm{dis}}} \hat{\rho}_{x,+}^{(\alpha)} - \frac{1}{N_{\mathrm{dis}}} \sum_{\alpha}^{N_{\mathrm{dis}}} \hat{\rho}_{x,-}^{(\alpha)} \right\|_{\mathrm{tr}} \leq \\
&\leq \min_{\pi\in S(\alpha)} \frac{1}{N_{\mathrm{dis}}} \sum_{\alpha} \left\| \hat{\rho}_{x,+}^{(\alpha)} - \hat{\rho}_{x,-}^{(\pi(\alpha))} \right\|_{\mathrm{tr}} \\
&\leq \min_{\pi\in S(\alpha)} \frac{1}{N_{\mathrm{dis}}} \sum_{\alpha} 2\sqrt{1 - F\left(\hat{\rho}_{x,+}^{(\alpha)}, \hat{\rho}_{x,-}^{(\pi(\alpha))}\right)}
\end{aligned}$$

where $F(\hat{\rho}, \hat{\sigma})$ is the Uhlmann fidelity between the two states (see section 6.3.4). The minimization can be easily computed with an optimization algorithm known as the *Munkres-Hungarian method*.

The lower bound is computed via the covariance matrices. Let us consider equation (7.6) and (7.7). Because $F_t^{\mathrm{opt}} \leq F_{\mathrm{G},t}^{\mathrm{opt}}$, we obtain:

$$\|\Gamma_{x,+}(t) - \Gamma_{x,-}(t)\|_{\mathrm{op}} \leq \|\hat{\rho}_{x,+}(t) - \hat{\rho}_{x,-}(t)\|_{\mathrm{tr}} \tag{7.93}$$

The high values of the upper and lower bounds presented in figure 7.7 are compatible with the intuitive idea that the memory should effectively protect the information in this case. We leave for future work the exact quantification of $\|\hat{\rho}_{x,+} - \hat{\rho}_{x,-}\|_{\mathrm{tr}}$.

7.10 Conclusions and Perspectives

In this chapter we study the stability against perturbations of a quantum memory encoded with zero-energy Majorana modes. We discuss the possibility of applying a recovery operation after a noisy or perturbed time evolution; in particular, we identify the recovery operation which yields the maximum recovery fidelity, which is therefore a measure of the information which is still present in the system. We also focus on the class of recovery operations which are most easily implemented, i.e. the Gaussian ones.

We concentrate on several types of perturbed time evolutions. When the system is interacting with an environment whose action can be described with a master equation, we show that the topological Hamiltonian is not able to protect the system. The key assumption to derive this result is that the dissipation is acting on every eigenstate of the protecting Hamiltonian. We find this assumption reasonable, as in the presence of decoherence-free modes, the encoding of the information in such modes would be the best protecting method.

The case of a time evolution which is a convex combination of several Hamiltonian time evolutions is more interesting. Since the final state is not Gaussian, we find that a Gaussian recovery operation cannot achieve a fidelity larger than a critical value, which is stable in the thermodynamic limit. On the other side, a more general recovery operation could obtain fidelity 1 in the thermodynamic limit, as the topological Hamiltonian protects the system against this form of perturbation.

This work can be considered as the initial work of a more general program aimed at probing the feasibility of topological fermionic systems for quantum information applications. The natural next step is, in this respect, to probe the stability against perturbations of the braiding operations in a two-dimensional setup, which will be the target of future work.

Appendix A

Magnetic Flux Quantization Condition

In section 4.3 we deal with a discretely translational invariant two dimensional lattice pierced by an external homogeneous magnetic field. In this appendix we provide more details on the study of such a system via a finite lattice with periodic boundary conditions (PBC). In particular, we show that because the Hamiltonian and the discrete translation operators must commute, one obtains non-trivial conditions on the dimension of the sample.

A.1 Infinite System

We start discussing the Hamiltonian and the discrete translation operator in the bulk. We consider the Landau gauge: $\mathbf{A} = B(0, x)$ and introduce the number of fluxes crossing each plaquette $\alpha = Ba^2/\Phi_0$ where Φ_0 is the flux quantum and a is the dimensional lattice constants. From now on x and y will just be adimensional integer numbers labelling the sites of the lattice.

The standard generalization of the Bose-Hubbard Hamiltonian in presence of an external magnetic field is the Harper Hamiltonian (see [Har55] and section 3.2.1):

$$\hat{H} = -J \sum_{x,y} \left[e^{-2\pi i \alpha x} \hat{a}^\dagger_{x,y+1} \hat{a}_{x,y} + \hat{a}^\dagger_{x+1,y} \hat{a}_{x,y} \right] + H.c. \tag{A.1}$$

where $\hat{a}_{x,y}$ and $\hat{a}^\dagger_{x,y}$ are boson annihilation and creation operators satisfying $[\hat{a}_{x,y}, \hat{a}^\dagger_{x',y'}] = \delta_{xx'}\delta_{yy'}$.

The action of the standard discrete translation operator $\hat{T}_{m,n} = \hat{T}(ma_x + na_y)$ $(m, n \in \mathbb{N})$ on the field operators is the following:

$$\begin{aligned} \hat{T}_{1,0}\ \hat{a}^{(\dagger)}_{x,y}\ \hat{T}^\dagger_{1,0} &= \hat{a}^{(\dagger)}_{x+1,y} \\ \hat{T}_{0,1}\ \hat{a}^{(\dagger)}_{x,y}\ \hat{T}^\dagger_{0,1} &= \hat{a}^{(\dagger)}_{x,y+1} \\ \hat{T}_{m,n} &= \hat{T}^m_{1,0}\ \hat{T}^n_{0,1} = \hat{T}^n_{0,1}\ \hat{T}^m_{1,0} \end{aligned}$$

Because these $\hat{T}_{m,n}$ operators do not commute with the Hamiltonian in equation (A.1), we need a "magnetic" translation operator $\hat{M}_{m,n}$ commuting with

the Hamiltonian, which are the discrete version of the continuum case discussed in [Zak64]:

$$\begin{aligned}
\hat{M}_{1,0}\ \hat{a}^{(\dagger)}_{x,y}\ \hat{M}^{\dagger}_{1,0} &= e^{+(-)2\pi i\alpha y}\ \hat{a}^{(\dagger)}_{x+1,y} \\
\hat{M}_{0,1}\ \hat{a}^{(\dagger)}_{x,y}\ \hat{M}^{\dagger}_{0,1} &= \hat{a}^{(\dagger)}_{x,y+1} \\
\hat{M}_{m,n}\hat{a}^{(\dagger)}_{x,y}\hat{M}^{\dagger}_{m,n} &= e^{-(+)i\pi\alpha mn}\ \hat{M}^{m}_{1,0}\ \hat{M}^{n}_{0,1}\hat{a}^{(\dagger)}_{x,y}\hat{M}^{\dagger n}_{0,1}\ \hat{M}^{\dagger m}_{1,0} \\
&= e^{+(-)i\pi\alpha mn}\ \hat{M}^{n}_{0,1}\ \hat{M}^{m}_{1,0}\hat{a}^{(\dagger)}_{x,y}\hat{M}^{\dagger m}_{1,0}\ \hat{M}^{\dagger n}_{0,1}
\end{aligned}$$

Last equation indicates clearly the peculiarity of the magnetic translations which leads to the Aharonov-Bohm effect: the result of a translation from one point to another one strongly depends on the followed path and eventually, moving along a closed loop, gives to the state a phase proportional to the encircled magnetic flux.

We can verify the commutativity of the magnetic translation operator with the Hamiltonian just by checking $\hat{M}_{1,0}$ because translations along other directions commute straightforwardly:

$$\begin{aligned}
\hat{M}_{1,0}\ e^{-2\pi i\alpha x}\hat{a}^{\dagger}_{x,y+1}\hat{a}_{x,y}\ \hat{M}^{\dagger}_{1,0} &= e^{-2\pi i\alpha x}e^{-2\pi i\alpha(y+1)}e^{+2\pi i\alpha y}\hat{a}^{\dagger}_{x+1,y+1}\hat{a}_{x+1,y} = \\
&= e^{-2\pi i\alpha(x+1)}\hat{a}^{\dagger}_{x+1,y+1}\hat{a}_{x+1,y} \qquad \text{(A.2)}
\end{aligned}$$

$$\hat{M}_{1,0}\ \hat{a}^{\dagger}_{x+1,y}\hat{a}_{x,y}\ \hat{M}^{\dagger}_{1,0} = \hat{a}^{\dagger}_{x+1,y}\hat{a}_{x,y} \qquad \text{(A.3)}$$

Therefore:

$$\hat{M}_{1,0}\ \hat{H}\ \hat{M}^{\dagger}_{1,0} = \hat{H}$$

where we exploit the sum over x in H and change variables to $x' = x+1$, always possible in the bulk.

A.2 Finite System with Periodic Boundary Conditions

We now discuss the possibility of studying the previous infinite system with a finite system of dimension $L_x \times L_y$ with PBC. $L_{x,y}$ are here adimensional numbers which can be used to define the total number of fluxes crossing the finite system: $N_\Phi = L_x L_y \alpha$. In order to be able to identify the bosonic operators residing on sites whose distance is $mL_x a + nL_y a$, with $m, n \in \mathbb{N}$, we must require the total number of fluxes N_Φ to be an integer number. This can be proven simply translating the field operator around one plaquette $L_x \times L_y$. As before, we also require the Hamiltonian and the "magnetic" translation operators to commute; in particular, we discuss in detail the interesting case of translation along $\hat{x}$: $M_{1,0}\ H\ M^{\dagger}_{1,0} = H$.

We separately analyze this equation on each link of the finite lattice. In particular, when considering the links oriented along the $\hat{y}$ direction, it reduces to the following equality:

$$e^{-2\pi i\alpha\, x}\ e^{-2\pi i\alpha\,[\overline{y+1}-y]}\ \cdot \hat{a}^{\dagger}_{\overline{x+1},\overline{y+1}}\hat{a}_{\overline{x+1},y} = e^{-2\pi i\alpha\,\overline{x+1}}\ \hat{a}^{\dagger}_{\overline{x+1},\overline{y+1}}\hat{a}_{\overline{x+1},y} \qquad \text{(A.4)}$$

where $\overline{x+1}$ denotes the modulus count (same for y):

$$\overline{x+1} = (x+1)\,\mathrm{mod} L_x.$$

We distinguish four cases:

1. $x \in [0, L_x - 2] \ \wedge \ y \in [0, L_y - 2]$: Eq. A.4 is automatically satisfied, as it happens in the bulk;
2. $x = L_x - 1 \wedge y \in [0, L_y - 2]$: Eq. A.4 is fulfilled only if $e^{-2\pi i\alpha(L_x-1)}e^{-2\pi i\alpha} = 1$, which implies $\alpha L_x \in \mathbb{N}$;
3. $x \in [0, L_x - 2] \ \wedge \ y = L_y - 1$: Eq. A.4 is fulfilled only if $e^{+2\pi i\alpha(L_y-1)} = e^{-2\pi i\alpha}$, which implies $\alpha L_y \in \mathbb{N}$;
4. $x = L_x - 1 \wedge y = L_y - 1$: Eq. A.4 is fulfilled only if $e^{-2\pi i\alpha(L_x-1)}e^{+2\pi i\alpha(L_y-1)} = 1$, which implies $\alpha(L_y - L_x) \in \mathbb{N}$.

The double constraint $N_\Phi/L_x,\ N_\Phi/L_y \in \mathbb{N}$ and the desired magnetic filling one $N_\Phi = N$ strongly reduces the number of finite size systems numerically treatable with moderate effort. The Hilbert space for the examined 4×4 lattice with 4 particles consists of 3.620 states, but already 5 three-hardcore bosons on a 5×5 grid need 110.630 to be described. Such strict constraints could be circumvented if one introduces proper singularities of the magnetic field to fulfill the correct translational and periodic conditions; however, any spurious correction introduced by hand would strongly affect the numerics on the small scales treatable. Therefore we decided to stay stuck to the strictest version given above. An extensive numerical study of this problem is left for future investigations.

Appendix B

Some Additional Results on Fermionic Gaussian States

In this appendix we discuss some technical results about fermionic Gaussian states which have been mentioned in chapter 6. In section B.1 and B.2 we present two results which generalize equation (6.28): the computation of $\mathrm{Tr}[\hat{\rho}\,\hat{U}]$ and of $\mathrm{Tr}[\hat{U}\,\hat{V}]$ for $\hat{\rho}$ Gaussian state and $\hat{U}$, $\hat{V}$ canonical transformations. The aim of section B.3 is to present an explicit procedure to evaluate the quantity in equation (6.67), i.e. the distance between two mixed states which are convex combinations of pure Gaussian states. The reading of section 6.6.2 is preliminary, as we use the notation introduced there.

B.1 Expectation Value of a Canonical Transformation

We are interested in $\mathrm{Tr}\left[\hat{U}\,\hat{\rho}\right]$. This is completely related to the covariance matrices of the two operators, Υ (here we rather use Ω) and Γ. In the simplest case with $\eta_\alpha \neq 0$, it reads:

$$\mathrm{Tr}\left[\hat{U}\,\hat{\rho}\right] = \left(\prod_\alpha i \sin\frac{\eta_\alpha}{2}\right) \mathrm{Pf}\left[\Omega - \Gamma\right] \tag{B.1}$$

The derivation of this formula goes as the one for $\mathrm{Tr}\left[\hat{\rho}\,\hat{\sigma}\right]$. We take $\hat{U}$ in its standard form (6.13) and expand the product:

$$\begin{aligned}\hat{U} \;=\; & \left(\prod_\alpha \cos\frac{\eta}{2}\right) \cdot \sum_{s=0}^{N} \sum_{\substack{\text{ordered}\\ \text{strings of}\\ \text{length } s\\ \{\alpha_1 \ldots \alpha_s\}}} \left[(-1)^s \cdot\right. \\ & \left. \cdot \tan\frac{\eta_{\alpha_1}}{2} \ldots \tan\frac{\eta_{\alpha_s}}{2}\; \hat{c}_{\alpha_1,1}\hat{c}_{\alpha_1,2} \ldots \hat{c}_{\alpha_s,1}\hat{c}_{\alpha_s,2}\right]\end{aligned}$$

where the case for $s = 0$ yelds a $\hat{1}$. Using equation (6.26), after some algebraic

manipulation, assuming $\eta_\alpha \neq 0\ \forall\alpha$, we write:

$$\mathrm{Tr}\left[\hat{\rho}\,\hat{U}\right] = \left(\prod_\alpha \sin\frac{\eta}{2}\right)\sum_{s=0}^{N}\sum_{\text{strings}}\left(\prod_{\alpha\notin\text{string}}(-i)\cot\frac{\eta_\alpha}{2}\right)\frac{\mathrm{Pf}\left[\Gamma|_{\alpha\in\text{string}}\right]}{i^{2s-N}}$$

We observe that

$$\left(\prod_{\alpha\notin\text{string}}(-i)\cot\frac{\eta_\alpha}{2}\right) = \mathrm{Pf}\left[\Omega|_{\alpha\notin\text{string}}\right]$$

and obtain:

$$\mathrm{Tr}\left[\hat{\rho}\,\hat{U}\right] = \left(\prod_\alpha i\sin\frac{\eta_\alpha}{2}\right)\sum_{s=0}^{N}\sum_{\text{strings...}}\mathrm{Pf}\left[\Omega|_{\alpha\notin\text{string}}\right]\mathrm{Pf}\left[-\Gamma|_{\alpha\in\text{string}}\right]$$

We can now apply the theorem in equation (6.32) and obtain the formula (B.1).

Unlike formula (6.33), the result can have a non-zero imaginary part because Υ is an imaginary matrix. Furthermore, one cannot reduce this calculation to the computation of a determinant as in (6.28), whose square root returns the absolute value of the pfaffian, because we do not have any *a priori* knowledge of the sign of $\mathrm{Tr}\left[\hat{U}\,\hat{\rho}\right]$.

Let us now consider the case of one $\eta_\alpha = 0$. Comparing with the original definition, this means that the Hilbert space can be splitted into a tensor product $\mathcal{H} = \mathcal{H}_\alpha \otimes \mathcal{H}_{\bar{\alpha}}$ (see the corresponding discussion in section ???) and that in this representation:

$$\hat{U} = \hat{\mathbb{I}}_2 \otimes \hat{U}'' \tag{B.2}$$

The density matrix can be written as $\hat{\rho} = \sum_\beta \rho'_\beta \otimes \rho''_\beta$. Defining $\hat{\rho}_{\bar{\alpha}} = \sum_\beta \mathrm{Tr}[\hat{\rho}'_\beta]\,\hat{\rho}''_\beta$, we obtain:

$$\mathrm{Tr}[\hat{U}\,\hat{\rho}] = \sum_\beta \mathrm{Tr}[\hat{\mathbb{I}}_2\,\hat{\rho}'_\beta]\cdot\mathrm{Tr}[\hat{U}''\,\hat{\rho}''_\beta] = \mathrm{Tr}\left[\hat{U}''\hat{\rho}_{\bar{\alpha}}\right] \tag{B.3}$$

Equation (B.1) is not invariant with respect to orthogonal transformations. We know that after a canonical transformation $\hat{c}_i \to \hat{c}'_i = \sum_j O_{i,j}\hat{c}_j$ covariance matrices in the $\hat{c}'_i$ basis are $\Gamma' = O\Gamma O^T$ (the same holds for Υ). The evaluation of $\mathrm{Tr}[\hat{U}\,\hat{\rho}]$ in a basis different from that diagonalizing $\hat{U}$ requires the knowledge of the transformation O:

$$\mathrm{Tr}\left[\hat{U}\,\hat{\rho}\right] = \det[O]\left(\prod_\alpha i\sin\frac{\eta_\alpha}{2}\right)\mathrm{Pf}\left[O\Omega O^T - \Gamma'\right]$$

B.2 Trace of the Product of Two Unitary Operators

We now compute the trace of a product of two Gaussian N-modes unitary operators, which in the case $\eta_\alpha^{(U)} \neq 0 \wedge \eta_\alpha^{(V)} \neq \pi$ reads:

$$\mathrm{Tr}[\hat{U}\,\hat{V}] = \mathrm{Tr}[\hat{V}]\left(\prod_\alpha i\sin\frac{\eta_\alpha^{(U)}}{2}\right)\mathrm{Pf}\left[\Omega_U - \frac{\Upsilon_V}{\mathrm{Tr}[\hat{V}]}\right] \tag{B.4}$$

The derivation of the formula goes as before for formulas (6.28) and (B.1). We take $\hat{U}$ in its standard form and expand the product:

$$\begin{aligned}\hat{U} &= \left(\prod_{\alpha}\cos\frac{\eta_\alpha^{(U)}}{2}\right)\cdot\sum_{s=0}^{N}\sum_{\substack{\text{ordered}\\ \text{strings of}\\ \text{length } s\\ \{\alpha_1\ldots\alpha_s\}}}[(-1)^s\cdot \\ &\cdot\tan\frac{\eta_{\alpha_1}}{2}\ldots\tan\frac{\eta_{\alpha_s}}{2}\;\hat{c}_{\alpha_1,1}\hat{c}_{\alpha_1,2}\ldots\hat{c}_{\alpha_s,1}\hat{c}_{\alpha_s,2}\Big]\end{aligned}$$

We use a slight modification of (6.26) for unitary operators such that $\forall\alpha\ \eta_\alpha \neq -\pi$:

$$(-i)^p\ \mathrm{Tr}[\hat{V}\,\hat{c}_{\alpha_1}\ldots\hat{c}_{\alpha_{2p}}] = \mathrm{Tr}[\hat{V}]\cdot\mathrm{Pf}\left[\left.\frac{\Upsilon_V}{\mathrm{Tr}[\hat{V}]}\right|_{\alpha_1\ldots\alpha_{2p}}\right] \tag{B.5}$$

We obtain:

$$\begin{aligned}\mathrm{Tr}[\hat{U}\,\hat{V}] &= \mathrm{Tr}[\hat{V}]\left(\prod_{\alpha=1}^{N} i\sin\frac{\eta_\alpha^{(U)}}{2}\right)\cdot \\ &\cdot\ \sum_{s=0}^{N}\sum_{\text{strings}\ldots}\left(\prod_{\alpha\notin\text{string}}(-i)\cot\frac{\eta_\alpha^{(U)}}{2}\right)\left[-\left.\frac{\Upsilon_V}{\mathrm{Tr}[\hat{V}]}\right|_{\alpha\in\text{string}}\right]\end{aligned}$$

We can sum this expression and obtain equation (B.4). The presence of eigenvalue $\eta_\alpha^{(U)} = 0$ is not a problem: being the action of the unitary trivial on one subspace, formula (B.4) must be applied only to the unitary $\hat{U}$ reduced to the subspace where its action is not trivial. We still have to find a formula for the case $\eta_\alpha^{(V)} = -\pi$, i.e. at the moment we would not be able to compute $\mathrm{Tr}[\hat{U}\hat{V}]$ of two operators both containing eigenvalues $\eta = -\pi$. This does not seem to be a big drawback, since the case looks rather unlikely.

For the evaluation of $\mathrm{Tr}[\hat{U}\,\hat{V}]$ in a basis different from that diagonalizing $\hat{U}$, the determinant of the transformation mapping the basis to the diagonal one is required, as in the case of $\mathrm{Tr}[\hat{U}\,\hat{\rho}]$.

Formula (B.4) is not clearly symmetric under exchange of $\hat{U}$ and $\hat{V}$, as it should be. We show this in the single mode case. In this case:

$$\begin{aligned}\mathrm{Tr}[\hat{U}\,\hat{V}] &= 2i\cos\frac{\eta^{(V)}}{2}\sin\frac{\eta^{(U)}}{2}\left(\frac{1}{i\tan\frac{\eta^{(U)}}{2}}+i\tan\frac{\eta^{(V)}}{2}\right) = \\ &= 2\cos\left(\frac{\eta^{(U)}+\eta^{(V)}}{2}\right)\end{aligned} \tag{B.6}$$

B.3 Distance between Convex-Combinations of Gaussian States

Let us consider the subspace of the global Hilbert space defined as

$$\mathcal{H} = \mathrm{Span}\left\{|\Phi_j(t)\rangle, |\Psi_j(t)\rangle\right\}_{j=1}^{N_d}.$$

The operators $\hat{\rho}^{\Phi}(t)$ and $\hat{\rho}^{\Psi}(t)$ act non-trivially only in $\mathcal{H}$. Once an orthonormal basis of $\mathcal{H}$ is identified, the computation of $\left\|\hat{\rho}^{\Phi}(t) - \hat{\rho}^{\Psi}(t)\right\|_1$ can be carried out.

We define the Hermitian matrix (the time dependence is not explicitely written):

$$M = \left(\begin{array}{c|c} \langle\Phi_j|\Phi_k\rangle & \langle\Phi_j|\Psi_k\rangle \\ \hline \langle\Psi_j|\Phi_k\rangle & \langle\Psi_j|\Psi_k\rangle \end{array}\right) \tag{B.7}$$

A matrix Y such that $Y^* Y^T = M$ represents the desired basis change:

$$|\Phi_k\rangle = Y_{k,j}|x_j\rangle; \qquad |\Psi_k\rangle = Y_{N_d+k,j}|x_j\rangle.$$

The matrix Y can be constructed via the unitary W which diagonalizes M: $WDW^\dagger = M$; we define $Y^* = W\sqrt{D}$. The representation of $\hat{\rho}^{\Phi}(t) - \hat{\rho}^{\Psi}(t)$ in the $|x_j\rangle$ basis is given by:

$$Y^T \left(\begin{array}{c|c} \mathbb{I} & 0 \\ \hline 0 & -\mathbb{I} \end{array}\right) Y^* \tag{B.8}$$

and $\left\|\hat{\rho}^{\Phi}(t) - \hat{\rho}^{\Psi}(t)\right\|_1$ is the trace-norm of matrix (B.8).

The result is invariant under phase multiplication $e^{i\phi}|\Psi_k\rangle$ because these state are represented by the same density operator $\hat{\rho}^{\Psi}_k$. We can neglect additive constant terms of each Hamiltonian $\hat{H}_0 + \hat{V}_j$ which would just introduce a phase in the time evolution.

The computation of M is involved. For simplicity, let us consider only two disorder realizations $j = 1, 2$: we have $\hat{H}_1 = \hat{H}_0 + \hat{V}_1$ and $\hat{H}_2 = \hat{H}_0 + \hat{V}_2$, the corresponding time evolution operators $\hat{U}_1(t)$ and $\hat{U}_2(t)$, and the skew-symmetric matrices $T^{(1)}$ and $T^{(2)}$. We are interested in the operator $\hat{U}_{1,2}(t) = \hat{U}_2^\dagger(t)\hat{U}_1(t)$, or more precisely in its matrix elements $\langle\Phi_2|\Phi_1\rangle = \langle\Phi|\hat{U}_{1,2}(t)|\Phi\rangle$ and $\langle\Psi_2|\Phi_1\rangle = \langle\Psi|\hat{U}_{1,2}(t)|\Phi\rangle$.

For diagonal matrix elements:

$$\langle\Phi|\hat{U}_{1,2}(t)|\Phi\rangle = \mathrm{Tr}\left[\hat{\rho}_\Phi \hat{U}_{1,2}(t)\right] \tag{B.9}$$

This can be evaluated using formula (B.1), which gives the result in terms of the covariance matrices of the state $\hat{\rho}_\Phi$ and of the unitary $\hat{U}_{1,2}$. Unfortunately, this formula cannot be used because the covariance matrices of $\hat{U}_{1,2}(t)$, Υ_U and Ω_U, are not known. The problem arises because it is impossible to compute directly the matrix A such that

$$\hat{U}_{1,2} = \exp\left[-\frac{1}{4}\sum A_{\alpha,\beta}\hat{c}_\alpha\hat{c}_\beta\right]$$

from $T^{(1)}$ and $T^{(2)}$. Indeed, the Baker-Campbell-Hausdorff formula requires in general the summation of an infinite series.

We therefore compute $B = \log\left[e^{-T^{(2)}t}e^{T^{(1)}t}\right]$. The principal-part logarithm is not a continuous function; accordingly we only know that $\hat{U}_{1,2} = \tau\hat{W}_{1,2}$, with $\hat{W}_{1,2} = \exp[-\frac{1}{4}\sum B_{\alpha,\beta}\hat{c}_\alpha\hat{c}_\beta]$ and $\tau = \pm 1$ to be determined. As discussed in equation (6.7), the principal-part logarithm ensures that $\mathrm{Tr}[\hat{W}_{1,2}] > 0$. Therefore:

$$\tau = \mathrm{sgn}\left(\mathrm{Tr}[\,\hat{U}_2^\dagger(t)\,\hat{U}_1(t)\,]\right) \tag{B.10}$$

This can be evaluated using equation (B.4), which expresses it as a function of the covariance matrices of the two unitary operators. Contrary to the previous case, the computation of Υ_{U_1} from $T^{(1)}$ and of $\Upsilon_{U_2^\dagger}$ from $T^{(2)}$ is possible. Finally:

$$\langle\Phi|\hat{U}_{1,2}(t)|\Phi\rangle = \mathrm{sgn}\left(\mathrm{Tr}[\hat{U}_2^\dagger(t)\hat{U}_1(t)]\right)\cdot \mathrm{Tr}\left[\hat{\rho}_\Phi \hat{W}_{1,2}(t)\right] \tag{B.11}$$

The second factor $\mathrm{Tr}\left[\hat{\rho}_\Psi \hat{W}_{1,2}(t)\right]$ can be computed with Γ_Ψ and Υ_W and (B.1).

For the non-diagonal case we introduce one Gaussian unitary operator $\hat{Z}$ satisfying the only property: $|\Psi\rangle = \hat{Z}|\Phi\rangle$. We obtain:

$$\langle\Psi|\hat{U}_{1,2}(t)|\Phi\rangle = \tau\langle\Phi|\hat{Z}^\dagger\hat{W}_{1,2}(t)|\Phi\rangle = \tau\mathrm{Tr}\left[\hat{\rho}_\Phi\hat{Z}^\dagger\hat{W}_{1,2}(t)\right]$$

We do not know $\hat{Z}$, but we can compute the transformation O_Z such that $O_Z\Gamma_\Phi O_Z^T = \Gamma_\Psi$. We compute $D = \log O_Z$ and build up $\hat{X} = \exp[-\frac{1}{4}\sum D_{\alpha,\beta}\hat{c}_\alpha\hat{c}_\beta]$; as before $\hat{X}$ and $\hat{Z}$ differ for an unknown ± 1 sign. We do not know how to overcome this ignorance. Anyway, it is not a problem because the final result does not depend on whether we consider as initial state $|\Psi\rangle$ or $-|\Psi\rangle$.

The computation of $\tau\mathrm{Tr}\left[\hat{\rho}_\Phi\hat{X}^\dagger\hat{W}_{1,2}(t)\right]$ can be done as before:

$$\langle\Psi|\hat{U}_{1,2}(t)|\Phi\rangle = \mathrm{sgn}\left(\mathrm{Tr}[\hat{U}_2^\dagger(t)\hat{U}_1(t)]\right)\cdot\mathrm{sgn}\left(\mathrm{Tr}[\hat{X}^\dagger\hat{W}_{1,2}(t)]\right)\cdot\mathrm{Tr}\left[\hat{\rho}_\Phi\hat{Y}_{1,2}(t)\right] \tag{B.12}$$

where $\hat{Y}_{1,2} = \exp\left[-1/4\sum_{\alpha,\beta}\log(e^De^B)\hat{c}_\alpha\hat{c}_\beta\right]$

Appendix C

An Eigenvalue Result

We discuss the properties of the exponential of the sum of a skew-symmetric matrix and a negative semidefinite symmetric matrix.

We start with a useful result.

Proposition 1 *Assume J is a real, square, skew-symmetric $2n \times 2n$ matrix and D is a real, square, symmetric, positive semidefinite $2n \times 2n$ matrix. Consider $A = J - D$. Suppose that $\vec{v}^\dagger D\vec{v} > 0 \ \forall$ eigenvectors $\vec{v}$ of J. Then all the eigenvalues λ of A have strictly negative real part, $\Re(\lambda) < 0$.*

Let us note that in general A is not a normal matrix, i.e. it is not related via an orthogonally transformation to a diagonal matrix; there exist a basis transformation which puts it in a Jordan normal form.

Proof Consider λ and $\vec{w}$ that satisfy the eigenvalue problem:

$$(J - D)\vec{w} = \lambda\vec{w} \tag{C.1}$$

We claim that there is no imaginary eigenvalue. Indeed:

$$\vec{w}^\dagger J\vec{w} - \vec{w}^\dagger D\vec{w} = \lambda \tag{C.2}$$

Since $\vec{w}^\dagger J\vec{w}$ is purely imaginary, and since $\vec{w}^\dagger D\vec{w}$ is real and larger or equal than zero, we obtain:

$$\Re(\lambda) = -\vec{w}^\dagger D\vec{w} \leq 0 \tag{C.3}$$

We can rule out the case $\Re(\lambda) = 0$ because this implies that $\vec{w}^\dagger D\vec{w} = 0$ and since D is positive semidefinite that $D\vec{w} = 0$. Therefore, eigenvalues of A which are purely imaginary are at the same time eigenvalues of J on which the action of D is trivial. This is in contradiction with the hypothesis. □

We can now study the operator norm of e^{At}. Let us start with the following property:

$$\|e^{At}\|_{\text{op}} \leq \|e^{(A+A^T)t/2}\|_{\text{op}} \leq 1 \tag{C.4}$$

where the first inequality comes from [Bha96] and the second from the negative semidefiniteness of $A + A^T = -2D$.

In general, the logarithmic norm $\mu_{\text{op}}(A)$ of a matrix A is the smallest element of $M = \{\xi \,|\, \|e^{At}\|_{\text{op}} \leq e^{\xi t}, t \geq 0\}$ [Str75]. Notice that the logarithmic norm is not a norm. For a finite dimensional space it holds:

$$\mu_{\text{op}}(A) = \max\{\lambda \,|\, \det(A + A^\dagger - 2\lambda\mathbb{I}) = 0\} \tag{C.5}$$

We use (C.5) in our case and obtain that $\mu_{\text{op}}(A) = \max_{\lambda \in \text{Spectrum}(-D)} \lambda$. Therefore, only in the case of D positive definite we can have an exponential bound on $\|e^{At}\|_{\text{op}}\ \forall t \geq 0$.

In case D is positive semidefinite we can rely on the following bound. We write A in its Jordan canonical form:

$$A = P \bigoplus_k (\lambda_k \mathbb{I}_{d_k} + N_{d_k})\ P^{-1} \tag{C.6}$$

where $\mathbb{I}_{d_k}$ is the d_k-dimensional identity and N_{d_k} is the d_k-dimensional nilpotent operator with only the first off-diagonal equal to 1. This form is convenient for taking the matrix exponential:

$$e^{At} = P \bigoplus_k e^{\lambda_k t} e^{N_{d_k} t}\ P^{-1} = P \bigoplus_k e^{\lambda_k t} \left(\sum_{p=0}^{d_k - 1} \frac{N_{d_k}^p\, t^p}{p!} \right) P^{-1} \tag{C.7}$$

Take λ_1, the eigenvalue with largest (negative) real part and $\bar{d_k}$ the largest dimension of a Jordan block. It is true that:

$$\|e^{At}\|_{\text{op}} \leq \|P\|_{\text{op}} \|P^{-1}\|_{\text{op}} e^{\Re(\lambda_1) t} \sum_{p=0}^{d_k - 1} \frac{t^p}{p!} \xrightarrow{t \to \infty} 0 \tag{C.8}$$

where the sum is used to majorize via the triangular inequality $\|e^{N_{d_k} t}\|_{\text{op}}$.

Finally, a comment on the possible dimensions of the Jordan blocks. Consider the family of matrices:

$$A(\tau) = (1 - \tau) A - \tau D; \qquad \tau \in [0, 1] \tag{C.9}$$

We know that the number of different eigenvalues is constant apart from a finite number of τ. Therefore, if we assume that J is non degenerate, the dimension of the eigenvalues is equal to $2n$ for almost all the τ. In these cases the dimension of the Jordan blocks is $d_k = 1\ \forall k$.

Conclusions and Perspectives

This thesis focuses on topological phases of matter, which, broadly speaking, are quantum states characterized by a non-local order parameter. The unusual features which result from this property make these states interesting both *per se* and because of some intriguing possible applications, such as fault-tolerant quantum computation schemes. The research community is currently devoting a significant effort in trying to completely characterize the properties of these states, and despite the many relevant achievements, such as the periodic table of topological insulators, there are still important open problems, such as the exhaustive classification of the effects of interactions.

We approach the subject from the point of view of quantum simulators, i.e. we propose to address the mentioned problems using highly controlled experiments. Because there are still many issues to be solved before reaching such an ambitious goal, we have identified three important research directions to pursue. The first one concerns the engineering of Hamiltonians of topological models. The second one is related to the measurement of non-local observables which can unravel the presence of topological order. The third one is related to the possibility of using topological phases of matter for quantum information schemes, in particular for the problem of its storing.

The discussion of the first two aspects is grounded on the perspective that cold atoms trapped in optical lattices are an excellent candidate for an analog quantum simulator. The precise control on a quantum many-body system featured in these setups is foreseen to be the key for successfully using experiments to answer unsolved theoretical questions. The third problem is considered from a more abstract point of view and our discussion can be applied to implementations based both on solid-state systems and on cold atoms.

Regarding the first investigation direction, we develop a proposal for a new technique to create a spin-independent, and thus potentially long-lived, optical lattice, in which an atom hopping to a neighbouring site can change its internal hyperfine state. The method exploits an unconventional use of bi-chromatic optical superlattices. We provide the discussion with numerical simulations which show the high fidelity of the coherent population transfer between two neighbouring sites of the optical lattice, both for the case in which the spin is unchanged and for the case in which it is flipped.

We elaborate on the idea and discuss some systems which could be simulated with this superlattice-based scheme. We start with non-interacting relativistic theories and give a list of the hopping matrices to be implemented in order

to study several kinds of massive and massless fermions. We next move to topological insulators; we discuss their relation to Kaplan fermions and provide explicit recipes for the realization of several classes of their periodic table. It would be interesting to quantify issues which could hinder the effectiveness of the superlattice scheme, such as the collisional stability of the atomic cloud. Such study is preliminary to a discussion of additional ingredients, such as atomic interactions or three-body losses, which could introduce non-linear effects in the model.

Finally, we consider the Pfaffian wavefunction of the fractional quantum Hall effect, which is known to host non-Abelian anyons as quasi-excitations. It is the ground state of a many-body bosonic system characterized by a three-body contact repulsion. We propose an effective realization of the three-body infinite repulsion using spin-1 atoms and discuss the properties of the Pfaffian wavefunction on a lattice structure. Unfortunately, the extreme sensibility of such state to even small changes of the Hamiltonian prevents its simulation with the developed technique, even if we cannot exclude that more sophisticated simulation schemes could accomplish the task.

Regarding the second investigation direction, we report on an experiment, to which we contributed some theoretical support, in which the measurement of a string operator for an ultracold bosonic gas trapped in an optical lattice is demonstrated. The developed experimental protocol is expected to be relevant for future investigations of topological phase transitions, such as that from the Mott insulator to the Haldane phase in spin-1 systems. The measurement of a string operator for a one-dimensional Mott insulator raises the problem of its theoretical generalization to higher dimensions, which has not yet been discussed. Moreover, the comparison between data and theory shows the importance of the development of a theoretical toolbox for the analysis of such quantity in finite and small systems.

The third line of investigation is motivated by the need for a better understanding of the properties of quantum memories encoded in topological states. Despite great expectations related to the robustness of topologically protected ground spaces with respect to local noise or disturbances, we show that there are many physically relevant cases in which a topological Hamiltonian does not protect the system from the action of an environment.

We study the stability of a quantum memory encoded with zero-energy Majorana fermions, which appear as quasi-excitation of the ground state of some topological superconductors. We develop several theoretical quantities which characterize the loss of the initially encoded information and use them to quantify the effect of various specific examples of perturbations. We show that the topological Hamiltonian does not protect the system in presence of an environment whose action can be described by a master equation. We obtain similar results also for a small non-Markovian environment, whose time-evolution is treated exactly. We consider another class of perturbations, i.e. the convex combination of several Hamiltonian time evolutions. In this case, the phenomenology is more interesting. Whereas we show that the Hamiltonian is indeed protecting the information stored in the system from this kind of decoherence, we also show that the class of the most simple quantum operations, the so-called Gaussian channels, cannot retrieve such information with the maximal precision.

The work will be further expanded into a more general analysis of the suit-

ability of topological fermionic systems for quantum information applications. For instance, many of the developed theoretical tools could be used for the characterization of the stability of braiding operations of Majorana fermions in perturbed systems.

As this summary clearly shows, this thesis ranges over a large variety of topological models. However, notwithstanding this large phenomenology, we have tried to rather highlight the numerous properties which are shared by the different models. The topological superconductors considered for the quantum memory problem are just one more example of the topological insulators introduced for the superlattice-scheme. We have also shown that researchers have developed some generalized Chern numbers to be used in the presence of interactions, which extend the topological invariants introduced for topological insulators. Moreover, when dealing with the parity of the fermionic number for the one-dimensional topological superconductor, we have found one example of the string order which was discussed in the experiment with the Mott insulator.

Concluding, we have addressed three relevant aspects of the problem of realizing and using a quantum simulator of topological phases of matter.

Acknowledgements

My grateful thank to Prof. J. I. Cirac, the supervisor of this thesis, is twofold. On the one side, it has been extremely exciting to work with such an outstanding physicist, and I hope to be able, in my future career, to profit from his example. On the other side, he gave me the possibility to work in an intellectually sparkling environment such as the Max-Planck-Institute of Quantum Optics, and I really enjoyed to be a part of it.

I am also deeply indebted to Dr. M. Rizzi, who has formed me as a researcher. His deep understanding of physics, his desire for having always a clear picture of the problems and his ordered work method will hopefully become part of my scientific background. Moreover, I really appreciate all the time he has devoted to my projects, and his valuable efforts to make difficult problems understandable even for a beginner.

It has been a pleasure to interact with the post-docs of my research group. In particular, I would like to thank, in alphabetical order, Dr. M. Aguado, Dr. M. C. Bañuls, Dr. G. Giedke and Dr. H.-H. Tu for invaluable discussions and help on several topics of my thesis.

As the work presented in this thesis is also the result of many collaborations, I would like to thank all the coauthors of my articles. Working together with Prof. M. Lewenstein is great: his almost unconditioned support helped me a lot. I also enjoyed working with Dr. A. Bermudez, who first introduced me to the topic of topological insulators, and whose patience in explaining me new concepts I really appreciate. Together with Dr. N. Goldman and Prof. M. A. Martin-Delgado, they suggested the applications of the superlattice proposal discussed in chapter 3.

Collaborating with Mr. M. Endres has been a scientifically productive experience. I would like to thank Prof. I. Bloch for the interesting discussions, his research group for the measurements presented in chapter 5, and Prof. L. Pollet for the quantum Monte Carlo data for the two dimensional system in figure 5.3. The figures of chapter 5 have been realized by Mr. M. Endres. I give my thanks also to Dr. U. Schneider, with whom the idea of the superlattice was actually conceived.

It is a pleasure to thank Prof. K. Krischer and Prof. W. Zwerger, who kindly accepted to be part of the commision of my Ph.D. exam.

More generally, I would like to thank all the people from my research group and more generally from the Max-Planck-Institute, with whom I discussed about physics, future, and also other topics.

Officemates are an important part of a Ph.D. and I was lucky enough to share my space with Dr. M. Eckolt-Perotti, with Dr. B. Horstmann and with Ms. Anika Pflanzer, whom I consider good friends of mine. It is remarkable

how personally richer I have become just by interacting with them on a daily basis.

Finally, I thank my parents and my brother for having always been on my side: without them I would never have arrived at this point. I also want to thank Gaia for her extraordinary support in this enterprise.

Bibliography

[AAN+11] M. Aidelsburger, M. Atala, S. Nascimbène, S. Trotzky, Y.-A. Chen, and I. Bloch, *Phys. Rev. Lett.* **107** (2011), 255301.

[AFGMP+11] E. Alba, X. Fernandez-Gonzalvo, J. Mur-Petit, J. K. Pachos, and J. J. Garcia-Ripoll, *Phys. Rev. Lett.* **107** (2011), 235301.

[AFH09] R. Alicki, M. Fannes, and M. Horodecki, *Jour. Phys. A:Math. Theor.* **42** (2009), 065303.

[AM76] N. W. Ashcroft and N. D. Mermin, *Solid state physics*, Brooks Cole, 1976.

[AOR+11] J. Alicea, Y. Oreg, G. Refael, F. von Oppen, and M. P. A. Fisher, *Nat. Phys.* **7** (2011), 412.

[AZ97] A. Altland and M. R. Zirnbauer, *Phys. Rev. B* **55** (1997), 1142.

[BBZ03] H. P. Büchler, G. Blatter, and W. Zwerger, *Phys. Rev. Lett.* **90** (2003), 130401.

[BC11] B. Béri and N. R. Cooper, *Phys. Rev. Lett.* **107** (2011), 145301.

[BDN12] I. Bloch, J. Dalibard, and S. Nascimbène, *Nature Phys.* **8** (2012), 267.

[BDTGA08] E. Berg, E. G. Dalla Torre, T. Giamarchi, and E. Altman, *Phys. Rev. B* **77** (2008), 245119.

[BDZ08] I. Bloch, J. Dalibard, and W. Zwerger, *Rev. Mod. Phys.* **80** (2008), 885.

[BGP+09] W. S. Bakr, J. I. Gillen, A. Peng, S. Fölling, and M. Greiner, *Nature* **462** (2009), 74.

[Bha96] R. Bhatia, *Matrix analysis*, Springer Verlag, 1996.

[BHH+05] H.-P. Büchler, M. Hermele, S.D. Huber, M.P.A. Fisher, and P. Zoller, *Phys. Rev. Lett.* **95** (2005), 040402.

[BJ83] B. H. Bransden and C. J. Joachain, *Physics of atoms and molecules*, Longman, 1983.

[BJB+08] J. Billy, V. Josse, A. Bernard, Hambrecht B., P. Lugan, D. Clément, L. Sanchez-Palencia, P. Bouyer, and A. Aspect, *Nature* **453** (2008), 891.

[BK11a] S. Bravyi and R. Koenig, *Classical simulation of dissipative fermionic linear optics*, arXiv:1112.2184v1, 2011.

[BK11b] ———, *Disorder-assisted error correction in majorana chains*, arXiv:1108.3845v1, 2011.

[BMR+10] A. Bermudez, L. Mazza, M. Rizzi, N. Goldman, M. Lewenstein, and M. A. Martin-Delgado, *Phys. Rev. Lett.* **105** (2010), 190404.

[BMZ07] H.-P. Büchler, A. Micheli, and P. Zoller, *Nature Phys.* **3** (2007), 726.

[BN09] I. Buluta and F. Nori, *Science* **326** (2009), 5949.

[Bog62] N. N. Bogoliubov, *Phys, Abh. SU* **6** (1962), 1.

[BOS+02] M. D. Bowdrey, D. K. L. Oi, A. J. Short, K. Banaszek, and J. A. Jones, *Phys. Lett. A* **294** (2002), 258.

[BPAMD09] A. Bermudez, D. Patane, L. Amico, and M. A. Martin-Delgado, *Phys. Rev. Lett.* **102** (2009), 135702.

[BPT+10] W. S. Bakr, A. Peng, M. E. Tai, R. Ma, J. Simon, J. I. Gillen, S. Fölling, L. Pollet, and M. Greiner, *Science* **329** (2010), 547–550.

[BR04] A. Botero and B. Reznik, *Phys. Lett. A* **331** (2004), 39.

[Bra05] S. Bravyi, *Quantum Info. Comput.* **5** (2005), 216.

[BWT12] J. C. Budich, S. Walter, and B. Trauzettel, *Phys. Rev. B* **85** (2012), 121405.

[CA80] D. M. Ceperley and B. J. Alder, *Phys. Rev. Lett.* **45** (1980), 566.

[Caz04] M. A. Cazalilla, *J. Phys. B: At. Mol. Opt. Phys.* **37** (2004), S1.

[CBP+12] M. Cheneau, P. Barmettler, D. Poletti, M. Endres, P. Schauß, T. Fukuhara, C. Gross, I. Bloch, C. Kollath, and S. Kuhr, *Nature* **481** (2012), 484.

[CGJT10] C. Chin, R. Grimm, P. Julienne, and E. Tiesinga, *Rev. Mod. Phys.* **82** (2010), 1225.

[CLBT10] S. Chesi, D. Loss, S. Bravyi, and B. M. Terhal, *New J. Phys.* **12** (2010), 025013.

[CLDS12] M. Cheng, R. M. Lutchyn, and S. Das Sarma, *Phys. Rev. B* **85** (2012), 165124.

[CMP10] J. I. Cirac, P. Maraner, and J. K. Pachos, *Phys. Rev. Lett.* **105** (2010), 190403.

[CNGP+09] A. H. Castro Neto, F. Guinea, N. M. R. Peres, K. S. Novoselov, and A. K. Geim, *Rev. Mod. Phys.* **81** (2009), 109.

[Coo11] N. R. Cooper, *Phys. Rev. Lett.* **106** (2011), 175301.

[Cre99] M. Creutz, *Phys. Rev. Lett.* **83** (1999), 2636.

[CTDRG98] C. Cohen-Tannoudji, J. Dupont-Roc, and G. Grynberg, *Atom-photon interactions: Basic processes and applications*, John Wiley & Sons, 1998.

[CZ12] J. I. Cirac and P. Zoller, *Nat. Phys* **8** (2012), 264.

[DDDBO11] M. Dalmonte, M. Di Dio, L. Barbiero, and F. Ortolani, *Phys. Rev. B* **83** (2011), 155110.

[DGJO11] J. Dalibard, F. Gerbier, J. Juzeliūnas, and P. Öhberg, *Rev. Mod. Phys.* **83** (2011), 1523.

[DKLP02] E. Dennis, A.Y. Kitaev, A. Landahl, and J. Preskill, *J. Math. Phys* **43** (2002), 4452.

[DLM+11] B. Deissler, E. Lucioni, M. Modugno, G. Roati, L. Tanzi, M. Zaccanti, M. Inguscio, and G. Modugno, *New J.Phys.* **13** (2011), 023020.

[dNR89] M. den Nijs and K. Rommelse, *Phys. Rev. B* **40** (1989), 4709.

[DRBZ11] S. Diehl, E. Rico, M. Baranov, and P. Zoller, *Nat. Phys.* **7** (2011), 971.

[DTBA06] E. G. Dalla Torre, E. Berg, and E. Altman, *Phys. Rev. Lett.* **97** (2006), 260401.

[DTD+09] A. J. Daley, J. M. Taylor, S. Diehl, M. Baranov, and P. Zoller, *Phys. Rev. Lett.* **102** (2009), 040402.

[DZR+10] B. Deissler, M. Zaccanti, G. Roati, C. D'Errico, M. Fattori, M. Modugno, G. Modugno, and M. Inguscio, *Nat. Phys.* **6** (2010), 354.

[ECF+11] M. Endres, M. Cheneau, T. Fukuhara, C. Weitenberg, P. Schauß, C. Gross, L. Mazza, M. C. Bañuls, L. Pollet, I. Bloch, and S. Kuhr, *Science* **334** (2011), 200–203.

[EFP+12] M. Endres, T. Fukuhara, D. Pekker, M. Cheneau, P. Schauß, C. Gross, E. Demler, S. Kuhr, and I. Bloch, *The "higgs" amplitude mode at the two-dimensional superfluid-mott insulator transition*, arXiv:1204.5183, 2012.

[EHSP+10] A. Eckardt, P. Hauke, P. Soltan-Panahi, C. Becker, K. Sengstock, and M. Lewenstein, *Europhys. Lett.* **89** (2010), 10010.

[EM99] N. Elstner and H. Monien, *Phys. Rev. B* **59** (1999), 12184, arXiv:cond-mat/9905367v1.

[EP10] J. Eisert and T. Prosen, *Noise-driven quantum criticality*, arXiv:1012.5013v1, 2010.

[EWH05] A. Eckardt, C. Weiss, and M. Holthaus, *Phys. Rev. Lett.* **95** (2005), 260404.

[Eza00] Z. Ezawa, *Quantum Hall Effects: Field Theoretical Approach and Related Topics*, World Scientific, Singapore, 2000.

[Fey82] R. P. Feynman, *International Journal of Theoretical Physics* **21** (1982), 467.

[FK11] L. Fidkowski and A. Kitaev, *Phys. Rev. B* **83** (2011), 075103.

[FTC+07] S. Fölling, S. Trotzky, P. Cheinet, M. Feld, R. Saers, A. Widera, T. Müller, and I. Bloch, *Nature* **448** (2007), 1029.

[FWGF89] M. P. A. Fisher, P. B. Weichman, G. Grinstein, and D. S. Fisher, *Phys. Rev. B* **40** (1989), 546.

[GC11] G. Goldstein and C. Chamon, *Phys. Rev. B* **84** (2011), 205109.

[GD10] F. Gerbier and J. Dalibard, *New J. Phys.* **12** (2010), 033007.

[GDF+08] R. Giacomo, C. D'Errico, L. Fallani, M. Fattori, C. Fort, M. Zaccanti, G. Modugno, M. Modugno, and M. Inguscio, *Nature* **453** (2008), 895.

[Gia04] T. Giamarchi, *Quantum physics in one dimension*, Oxford University Press, 2004.

[GME+02] M. Greiner, O. Mandel, T. Esslinger, T. W. Hänsch, and I. Bloch, *Nature* **415** (2002), 39.

[GNT98] A. O. Gogolin, A. A. Nersesyan, and A. M. Tsvelik, *Bosonization and strongly correlated systems*, Cambridge University Press, 1998.

[Got97] D. Gottesmann, *Stabilizer codes and quantum error correction*, Ph.D. thesis, Caltech, 1997.

[GR07] V. Gurarie and L. Radzihovsky, *Ann. Phys* **322** (2007), 2.

[GSH90] M. P. Gelfand, R. R. P. Singh, and D. A. Huse, *Journ. Stat. Phys.* **59** (1990), 1093.

[GSN+10] N. Goldman, I. Satija, P. Nikolic, A. Bermudez, M. A. Martin-Delgado, M. Lewenstein, and I. B. Spielman, *Phys. Rev. Lett.* **105** (2010), 255302.

[Gur11] V. Gurarie, *Phys. Rev. B* **83** (2011), 085426.

[GWF+06] F. Gerbier, A. Widera, S. Fölling, O. Mandel, and I. Bloch, *Phys. Rev. A* **73** (2006), 041602.

[GWO00] R. Grimm, M. Weidemüller, and Y. B. Ovchinnikov, *Adv. At., Mol., Opt. Phys.* **42** (2000), 95.

[GWW92] M. Greiter, X. G. Wen, and F. Wilczek, *Nucl. Phys. B* **374** (1992), 567.

[Hal82] B. I. Halperin, *Phys. Rev. B* **25** (1982), 2185.

[Hal83] F. D. M. Haldane, *Phys. Rev. Lett.* **50** (1983), 1153.

[Hal88] ———, *Phys. Rev. Lett.* **61** (1988), 2015.

[Har55] P. G. Harper, *Proc. Phys. Soc. A* **68** (1955), 874.

[Hat04] Y. Hatsugai, *J. Phys. Soc. Jpn.* **73** (2004), 2604.

[Hat05] ———, *J. Phys. Soc. Jpn.* **74** (2005), 1374.

[HCT+11] P. Hauke, F. M. Cucchietti, L. Tagliacozzo, I. Deutsch, and M. Lewenstein, *Can one trust quantum simulators?*, arXiv:1109.6457, 2011.

[HK10] M. Z. Hasan and C. L. Kane, *Rev. Mod. Phys.* **82** (2010), 3045.

[Hof76] D. R. Hofstadter, *Phys. Rev. B* **14** (1976), 2239.

[Hor11] B. Horstmann, *Quantum simulation of out-of-equilibrium phenomena*, Ph.D. thesis, Technische Universität München, 2011.

[HQW+08] D. Hsieh, D. Qian, L. Wray, Y. Xia, Y. S. Hor, R. J. Cava, and M. Z. Hasan, *Nature* **452** (2008), 970.

[HSDL07] M. Hafezi, A. S. Sørensen, E. Demler, and M. D. Lukin, *Phys. Rev. A* **76** (2007), 023613.

[HSLD08] M. Hafezi, A. S. Sørensen, M. D. Lukin, and E. Demler, *Europhys. Lett.* **81** (2008), 10005.

[ILD03] A. Imambekov, M. Lukin, and E. Demler, *Phys. Rev. A* **68** (2003), 063602.

[Iva01] D. A. Ivanov, *Phys. Rev. Lett.* **86** (2001), 268.

[IW99] M. Ishikawa and M. Wayama, *Journ. Comb. Theory A* **88** (1999), 136.

[JBC+98] D. Jaksch, C. Bruder, J. I. Cirac, C. W. Gardiner, and P. Zoller, *Phys. Rev. Lett.* **81** (1998), 3108.

[JKA+11] L. Jiang, T. Kitagawa, J. Alicea, A. R. Akhmerov, D. Pekker, G. Refael, J. I. Cirac, E. Demler, M. D. Lukin, and P. Zoller, *Phys. Rev. Lett.* **106** (2011), 220402.

[JSG+08] R. Jördens, N. Strohmaier, K. Günter, H. Moritz, and T. Esslinger, *Nature* **455** (2008), 204.

[JSWW03] L. Jacak, P. Sitko, K. Wieczorek, and A. Wójs, *Quantum hall systems : Braid groups, composite fermions and fractional charge*, Oxford University Press, Oxford, 2003.

[JTPW09] P. R. Johnson, E. Tiesinga, J. V. Porto, and C. J. Williams, *New J. Phys.* **11** (2009), 093022.

[JZ03] D. Jaksch and P. Zoller, *New J. Phys.* **5** (2003), 56.

[JZ05] ———, *Ann. Phys.* **315** (2005), 52.

[Kap92] D. B. Kaplan, *Phys. Lett. B* **288** (1992), 342.

[Kap09] ———, *Chiral symmetry and lattice fermions*, arXiv:0912.2560v2, 2009.

[KBM+07] M. König, H. Buhmann, W. Molenkamp, T. Hughes, C. X. Liu, X. L. Qi, and S. C. Zhang, *Science* **318** (2007), 766.

[KC10] C. Kraus and J.I. Cirac, *New J. Phys* **12** (2010), 113004.

[KFC+09] M. Karski, L. Förster, J.-M. Choi, A. Steffen, W. Alt, D. Meschede, and A. Widera, *Science* **325** (2009), 174.

[Kit97] A. Y. Kitaev, *Fault-tolerant quantum computation by anyons*, arXiv:quant-ph/9707021v1, 1997.

[Kit01] ———, *Physics-Uspekhi* **44** (2001), 131.

[Kit09] ———, *AIP Conf. Proc.* **1134** (2009), 22.

[KM05] C. L. Kane and E. J. Mele, *Phys. Rev. Lett.* **95** (2005), 226801.

[KMS+05] M. Köhl, H. Moritz, T. Stöferle, K. Günter, and T. Esslinger, *Phys. Rev. Lett.* **94** (2005), 080403.

[Kni01] E. Knill, *Fermionic linear optics and matchgates*, arXiv:quant-ph/0108033v2, 2001.

[Kog83] J. B. Kogut, *Rev. Mod. Phys.* **55** (1983), 775.

[Koh59] W. Kohn, *Phys. Rev.* **115** (1959), 809.

[KS81] L.-H. Karsten and J. Smit, *Nuc. Phys. B* **183** (1981), 103.

[KS03] A. B. Kuklov and B. V. Svistunov, *Phys. Rev. Lett.* **90** (2003), 100401.

[KT92] T. Kennedy and H. Tasaki, *Phys. Rev. B* **45** (1992), 304.

[LCS11] J. Levinsen, N. R. Cooper, and G. V. Shlyapnikov, *Phys. Rev. A* **84** (2011), 013603.

[Llo96] S. Lloyd, *Science* **273** (1996), 1073.

[LLWS10] X.-J. Liu, X. Liu, C. Wu, and J. Sinova, *Phys. Rev. A* **81** (2010), 033622.

[LM77] J. M. Leinaas and J. Myrheim, *Il Nuovo Cimento B* **37** (1977), 1.

[LSA+07] M. Lewenstein, A. Sanpera, V. Ahufinger, B. Damski, A. Sen, and U. Sen, *Adv. Phys.* **56** (2007), 243.

[LSC+07] H. Lignier, C. Sias, D. Ciampini, Y. Singh, A. Zenesini, O. Morsch, and E. Arimondo, *Phys. Rev. Lett.* **99** (2007), 220403.

[LZ97] S. Lukyanov and A. Zamolodchikov, *Nucl. Phys. B* **493** (1997), 571.

[MBG+12] L. Mazza, A. Bermudez, N. Goldman, M. Rizzi, M. A. Martin-Delgado, and M. Lewenstein, *New J. Phys.* **14** (2012), 015007.

[MBH+11] S. Müller, J. Billy, E. A. L. Henn, H. Kadau, A. Griesmaier, M. Jona-Lasinio, L. Santos, and T. Pfau, *Phys. Rev. A* **84** (2011), 053601.

[MC09] G. Möller and N. R. Cooper, *Phys. Rev. Lett.* **103** (2009), 105303.

[MD10] D. McKay and B. DeMarco, *New J. Phys.* **12** (2010), 055013.

[MGW+03a] O. Mandel, M. Greiner, A. Widera, T. Rom, T. W. Hänsch, and I. Bloch, *Phys. Rev. Lett.* **91** (2003), 010407.

[MGW+03b] ———, *Nature* **425** (2003), 937.

[MR91] G. Moore and N. Read, *Nucl. Phys. B* **360** (1991), 362.

[MRLC10] L. Mazza, M. Rizzi, M. Lewenstein, and J. I. Cirac, *Phys. Rev. A* **82** (2010), 043629.

[MW66] N. D. Mermin and H. Wagner, *Phys. Rev. Lett.* **17** (1966), 1133.

[MZF+12] V. Mourik, K. Zuo, S. M. Frolov, S. R. Plissard, E. P. A. M. Bakkers, and L. P. Kouwenhoven, *Science* **336** (2012), 1003.

[Nak03a] M. Nakahara, *Geometry, topology and physics*, Taylor & Francis, 2003.

[Nak03b] M. Nakamura, *Phys. A* **329** (2003), 1000.

[NC04] M. A. Nielsen and I. L. Chuang, *Quantum computation and quantum information*, Cambridge University Press, 2004.

[NCA+12] S. Nascimbène, Y-A. Chen, M. Atala, M. Aidelsburger, S. Trotzky, B. Paredes, and I. Bloch, Preprint (2012), arXiv:1202.6361.

[NN80] H. B. Nielsen and M. Ninomiya, *Nuc. Phys. B* **185** (1980), 20.

[NN81] ———, *Nuc. Phys. B* **193** (1981), 173.

[NSS+08] C. Nayak, S. H. Simon, A. Stern, M. Freedman, and S. Das Sarma, *Rev. Mod. Phys.* **80** (2008), 1083.

[NTW85] Q. Niu, D. J. Thouless, and Y.-S. Wu, *Phys. Rev. B* **31** (1985), 3372.

[OBS+05] K. Osterloh, M. Baig, L. Santos, P. Zoller, and M. Lewenstein, *Phys. Rev. Lett.* **95** (2005), 010403.

[PBM+11] B. Pasquiou, G. Bismut, E. Maréchal, P. Pedri, L. Vernac, O. Gorceix, and B. Laburthe-Tolra, *Phys. Rev. Lett.* **106** (2011), 015301.

[PGVWC07] D. Pérez-García, F. Verstraete, M. M. Wolf, and J. I. Cirac, *Quant. Inf. Comp.* **7** (2007), 401.

[PGWS+08] D. Pérez-García, M. M. Wolf, M. Sanz, F. Verstraete, and J. I. Cirac, *Phys. Rev. Lett.* **100** (2008), 167202.

[PKC07] B. Paredes, T. Keilmann, and J. I. Cirac, *Phys. Rev. A* **75** (2007), 053611.

[PKSC10] F. Pastawski, A. Kay, N. Schuch, and J. I. Cirac, *Quant. Inf. Comp.* **10** (2010), 580.

[PR04] J. K. Pachos and E. Rico, *Phys. Rev. A* **70** (2004), 053620.

[PS95] M. E. Peskin and D. V. Schroeder, *An Introduction to Quantum Field Theory*, (Westview Press), 1995.

[PS01] C. J. Pethick and H. Smith, *Bose-einstein condensation in dilute gases*, Cambridge University Press, 2001.

[PS03] L. Pitaevskii and S. Stringari, *Bose-einstein condensation*, Clarendon Press, 2003.

[QHZ08] X.-L. Qi, T. L. Hughes, and S.-C. Zhang, *Phys. Rev. B* **78** (2008), 195424.

[QZ11] X.-L. Qi and S.-C. Zhang, *Rev. Mod. Phys.* **83** (2011), 1057.

[RDJ02] J. Ruostekoski, G. V. Dunne, and J. Javanainen, *Phys. Rev. Lett.* **88** (2002), 180401.

[RG00] N. Read and D. Green, *Phys. Rev. B* **61** (2000), 10267.

[RL12] D. Rainis and D. Loss, *Majorana qubit decoherence by quasiparticle poisoning*, arXiv:1204.3326v1, 2012.

[RR96] N. Read and E. Rezayi, *Phys. Rev. B* **54** (1996), 16864.

[RRC10] M. Roncaglia, M. Rizzi, and J. I. Cirac, *Phys. Rev. Lett.* **104** (2010), 096803.

[RSFL10] S. Ryu, A. P. Schnyder, A. Furusaki, and A. W. W. Ludwig, *New J. Phys.* **12** (2010), 065010.

[RT10] S. Ryu and T. Takayanagi, *Phys. Rev. D* **82** (2010), 086014.

[RTJH83] R. Rammal, G. Toulouse, M. T. Jaekel, and B. I. Halperin, *Phys. Rev. B* **27** (1983), 5142.

[SBL+08] N. Syassen, D. M. Bauer, M. Lettner, T. Volz, D. Dietze, J. J. Garcia-Ripoll, J. I. Cirac, G. Rempe, and S. Dürr, *Science* **320** (2008), 1329.

[Sch99] J. Robert Schrieffer, *Theory of superconductivity*, Advanced Book Classics, 1999.

[Sch11] U. Schollwöck, *Ann. Phys.* **326** (2011), 96.

[Ser98] S. Serra, *Lin. Alg. and its Appl.* **270** (1998), 109.

[SGDS10] T. D. Stanescu, V. Galitski, and S. Das Sarma, *Phys. Rev. A* **82** (2010), 013608.

[SGKDS11] K. Sun, Z. Gu, H. Katsura, and S. Das Sarma, *Phys. Rev. Lett.* **106** (2011), 236803.

[SHW+08] U. Schneider, L. Hackermüller, S. Will, T. Best, I. Bloch, T. A. Costi, R. W. Helmes, D. Rasch, and A. Rosch, *Science* **322** (2008), 1520.

[SOLT+11] J. Struck, C. Ölschläger, R. Le Targat, P. Soltan-Panahi, A. Eckardt, M. Lewenstein, P. Windpassinger, and K. Sengstock, *Science* **333** (2011), 996.

[SPLS+12] P. Soltan-Panahi, D.-S. Lühmann, J. Struck, P. Windpassinger, and K. Sengstock, *Nat. Phys.* **8** (2012), 71.

[SPSH+11] P. Soltan-Panahi, J. Struck, P. Hauke, A. Bick, W. Plenkers, G. Meineke, C. Becker, P. Windpassinger, M. Lewenstein, and K. Sengstock, *Nat. Phys.* **7** (2011), 434.

[SRFL08] A. P. Schnyder, S. Ryu, A. Furusaki, and A. W. W. Ludwig, *Phys. Rev. B* **78** (2008), 195125.

[SSH79] W. P. Su, J. R. Schrieffer, and A. J. Heeger, *Phys. Rev. Lett.* **42** (1979), 1698.

[STF09] M. Sato, Y. Takahashi, and S. Fujimoto, *Phys. Rev. Lett.* **103** (2009), 020401.

[Str75] T. Strom, *SIAM Jour. Math. An.* **12** (1975).

[SWE+10] J. F. Sherson, C. Weitenberg, M. Endres, M. Cheneau, I. Bloch, and S. Kuhr, *Nature* **467** (2010), 68.

[SZS+08] L. B. Shao, S.-L. Zhu, L. Sheng, D. Y. Xing, and Z. D. Wang, *Phys. Rev. Lett.* **101** (2008), 246810.

[TCF+12] S. Trotzky, Y-A. Chen, A. Flesch, I. P. McCulloch, U Schollwöck, J. Eisert, and Bloch I., *Nat. Phys.* **8** (2012), 325.

[TD02] B. M. Terhal and D. P. DiVincenzo, *Phys. Rev. A* **65** (2002), 032325.

[TGU+12] L. Tarruell, D. Greif, T. Uehlinger, G. Jotzu, and T. Esslinger, *Nature* **483** (2012), 302.

[TKNdN82] D. J. Thouless, M. Kohmoto, M. P. Nightingale, and M. den Nijs, *Phys. Rev. Lett.* **49** (1982), 405.

[TPB11] A. M. Turner, F. Pollmann, and E. Berg, *Phys. Rev. B* **83** (2011), 075102.

[TPG+10] S. Trotzky, L. Pollet, F. Gerbier, U. Schnorrberger, I. Bloch, N. V. Prokof'ev, B. Svistunov, and M. Troyer, *Nat. Phys.* **6** (2010), 998.

[TWJ+96] E. Tiesinga, C.J. Williams, P.S. Julienne, K.M. Jones, P.D. Lett, and W.D. Phillips, *J. Res. Natl. Inst. Stand. Technol.* **101** (1996), 582.

[UNK08] H. Ueda, H. Nakano, and K. Kusakabe, *Phys. Rev. B* **78** (2008), 224402.

[VBR+11] M. Viteau, M. G. Bason, J. Radogostowicz, N. Malossi, D. Ciampini, O. Morsch, and E. Arimondo, *Phys. Rev. Lett.* **107** (2011), 060402.

[VC04] F. Verstraete and J.I. Cirac, *Renormalization algorithms for quantum-many body systems in two and higher dimensions*, arXiv:cond-mat/0407066v1, 2004.

[vK86] K. von Klitzing, *Rev. Mod. Phys.* **58** (1986), 519.

[vKKHV02] E. G. M. van Kempen, S. J. J. M. F. Kokkelmans, D. J. Heinzen, and B. J. Verhaar, *Phys. Rev. Lett.* **88** (2002), 093201.

[WBS+10] S. Will, T. Best, U. Schneider, L. Hackermüller, D.-S. Lühmann, and I. Bloch, *Nature* **465** (2010), 197.

[Wen04] X.-G. Wen, *Quantum field theory of many-body systems*, Oxford University Press, 2004.

[WES+11] C. Weitenberg, M. Endres, J. F. Sherson, M. Cheneau, P. Schauß, T. Fukuhara, I. Bloch, and S. Kuhr, *Nature* **471** (2011), 319.

[WGF+06] A. Widera, F. Gerbier, S. Fölling, T. Gericke, O. Mandel, and I. Bloch, *New J. Phys.* **8** (2006), 152.

[Wil77] K. Wilson, *New Phenomena in Subnuclear Physics* (A Zichichi, ed.), Plenum, New York, 1977, p. 69.

[Wil82] F. Wilczek, *Phys. Rev. Lett.* **49** (1982), 957.

[WOH11] G. Wirth, M. Ölschläger, and A. Hemmerich, *Nat. Phys.* **7** (2011), 147.

[WPW09] R. L. Willett, L. N. Pfeiffer, and K. W. West, *Proc. Natl. Acad. Sci. U.S.A.* **106** (2009), 8853.

[WPW10] ———, *Phys. Rev. B* **82** (2010), 205301.

[WQZ10] Z. Wang, X. L. Qi, and S. C. Zhang, *Phys. Rev. Lett.* **105** (2010), 256803.

[WSF+11] C. Weitenberg, P. Schauß, T. Fukuhara, M. Cheneau, M. Endres, I. Bloch, and S. Kuhr, *Phys. Rev. Lett.* **106** (2011), 215301.

[Yos11] B. Yoshida, *Ann. Phys.* (2011), 2566.

[Zak64] J. Zak, *Phys. Rev.* **134** (1964), A1607.

[ZCR12] E. Zohar, J. I. Cirac, and B. Reznik, *Simulating compact quantum electrodynamics with ultracold atoms: Probing confinement and nonperturbative effects*, arXiv:1204.6574v1, 2012.